Universidade de Aveiro Departamento de Química
Ano 2013

Samuel Venâncio de Sousa Freitas

Produção de Biodiesel a partir de Recursos Endógenos de Timor Leste

Production of Biodiesel from the Resources Endogeneous of Timor Leste

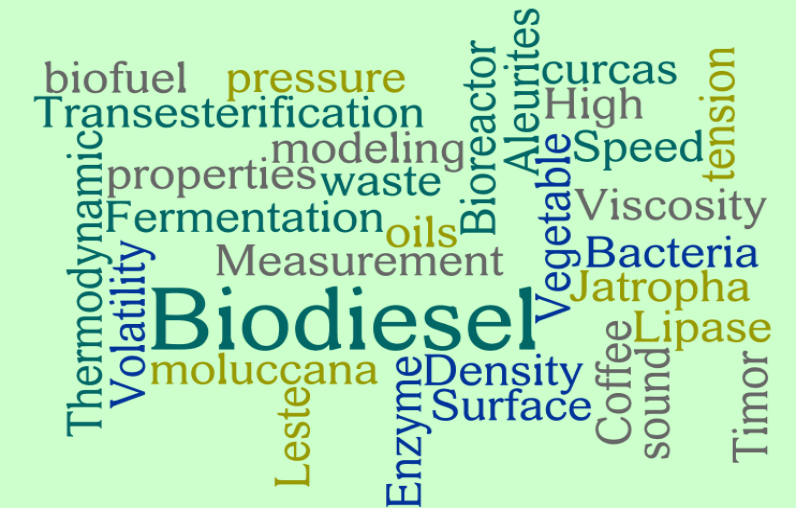

Universidade de Aveiro Departamento de Química
Ano 2013

Samuel Venâncio de Sousa Freitas

Produção de Biodiesel a partir de Recursos Endógenos de Timor Leste

Production of Biodiesel from the Resources Endogeneous of Timor Leste

Universidade de Aveiro Departamento de Química
Ano 2013

Samuel Venâncio de Sousa Freitas

Produção de Biodiesel a partir de Recursos Endógenos de Timor Leste

Production of Biodiesel from the Resources Endogeneous of Timor Leste

Tese apresentada à Universidade de Aveiro para cumprimento dos requisitos necessários à obtenção do grau de Doutor em Engenharia Química, realizada sob a orientação científica do Professor Doutor João Manuel da Costa Araújo Pereira Coutinho, Professor Associado com Agregação do Departamento de Química da Universidade de Aveiro e do Doutor Álvaro Silva Lima, Professor da Universidade Tiradentes, Brasil.

Apoio financeiro do POCTI no âmbito do III Quadro Comunitário de Apoio.

O doutorando agradece o apoio financeiro da FCT no âmbito do III Quadro Comunitário de Apoio (SFRH/BD/51476/2011).

Dedico este trabalho aos meus pais (Venâncio de Sousa Freitas e Anastácia de Sousa Freitas) e a todos os meus irmãos Freitas que suportaram a minha ausência durante muitos anos. Também o dedico a todos os que sempre me apoiaram de perto nos momentos que eu precisei.

o júri

presidente

Prof. Doutor Fernando Manuel dos Santos Ramos
professor Catedrático da Universidade do Aveiro

Prof. Doutor João Manuel da Costa e Araújo Pereira Coutinho
professor Associado com Agregação da Universidade do Aveiro

Prof. Doutor Luís Manuel das Neves Belchior Faia dos Santos
professor associado do Departamento de Química e Bioquímica da Faculdade de Ciências da Universidade do Porto

Prof. Doutor Abel Gomes Martins Ferreira
professor auxiliar do Departamento de Engª Química da Faculdade de Ciências e Tecnologia da Universidade de Coimbra

Prof. Doutor Nuno Clemente Oliveira
professor auxiliar do Departamento de Engª Química da Faculdade de Ciências e Tecnologia da Universidade de Coimbra

Prof. Doutora Maria Clara Ferreira Magalhães
professora auxiliar com agregação da Universidade de Aveiro

Prof. Doutor Álvaro Silva Lima
professor da Universidade Tiradentes

Doutora Mariana Oliveira Belo
Estagiária de Pós doutoramento da Universidade de Aveiro

agradecimentos

A conclusão desta tese não foi um trabalho solitário. Contei com o apoio de muitos profissionais, amigos e colegas. No topo da lista está o meu orientador Prof. João Coutinho. Agradeço-lhe imenso por tudo que fez por mim ao longo do meu doutoramento. Obrigado por ter despertado em mim a paixão pela ciência e proporcionado a possibilidade para eu crescer profissionalmente na Universidade de Aveiro sob a sua supervisão. Sem sua confiança e sua constante orientação, eu não poderia chegar aonde cheguei. Muito obrigado pelo apoio e pelos conhecimentos transmitidos.

Em segundo lugar, agradeço ao Dr. Álvaro Lima, pela co-orientação deste trabalho e pelos conhecimentos partilhados. Obrigado também pela sua amizade e pelo bom acolhimento que me proporcionou na Universidade Tiradentes.

Em terceiro lugar, agradeço à Irmã Juvita da Costa que me arranjou todo o material endógeno de Timor Leste, necessário para concluir a minha tese.

Em quarto lugar, obrigado à Alexandrina Conceição por ter estado sempre comigo durante o período de doutoramento sobretudo nos momentos mais difíceis.

Em quinto lugar, agradeço aos amigos que intervieram directamente na execução experimental e no enriquecimento dos meus trabalhos. Obrigado Mariana Belo, Maria Jorge, Pedro Carvalho, Jorge Pereira e Sónia Ventura.

Em sexto lugar, a todos os membros do PATh, aos mais antigos até aos mais novos muito obrigado por terem sido meu muito bons AMIGOS ao longo destes anos. Aos amigos da UNIT, agradeço pela amizade e alegria que me proporcionaram no Brasil durante os seis meses da minha estadia.

Em sétimo lugar, agradeço à Ana Caço, pelas ajudas diversas que me proporcionou no laboratório de Engenharia Química. Obrigado também pelo carinho e amizade. Obrigado também aos amigos Sónia, Belinda, Rui Duarte e Vânia pelo apoio.

Em oitavo lugar, agradeço aos Serviços Acção Social da Universidade de Aveiro através da pessoa do Mestre Hélder Castanheira por me ter ajudado bastante nos assuntos de alojamento durante o meu doutoramento.

Em nono lugar, um muito obrigado ao Departamento de Química e à Reitoria da Universidade de Aveiro por me terem auxiliado na resolução dos problemas de propina nos anos iniciais do meu doutoramento.

Finalmente, agradeço à Fundação Oriente e à FCT pelo apoio financeiro.

.

palavras-chave

Timor-Leste, biocombustivel, biodiesel, ésteres, propriedades termodinámicas, lipase, *Jatropha curcas, Aleurites moluccana*, borras de café, CPA, SAFT

resumo

Os biocombustíveis têm estado na linha da frente das políticas energéticas mundiais visto que as suas vantagens conseguem colmatar as incertezas e resolver alguns dos problemas associados aos combustíveis fósseis. O biodiesel tem provado ser um combustível muito fiável, alternativo ao petrodiesel. É uma mistura de ésteres alquílicos produzidos a partir de óleos vegetais e gorduras animais através de uma reacção de transesterificação. Como combustível, o biodiesel é economicamente viável, socialmente responsável, tecnicamente compatível e ambientalmente amigável. O principal desafio associado ao seu desenvolvimento tem a ver com a escolha de matéria-prima para a sua produção. Nos países do terceiro mundo, óleos alimentares são mais importantes para alimentar pessoas do que fazer funcionar carros.

Esta tese tem como objectivos produzir/processar biodiesel a partir de recursos endógenos de Timor-Leste e medir/prever as propriedades termodinâmicas do biodiesel, a partir das dos esteres alquílicos. A síntese do biodiesel a partir dos óleos de *Aleurites moluccana, Jatropha curcas* e borras de café foram aqui estudados. As propriedades termodinâmicas como densidade, viscosidade, tensão superficial, volatilidade e velocidade do som também foram medidas e estimadas usando modelos preditivos disponíveis na literatura, incluindo as equações de estado CPA e soft-SAFT.

Timor-Leste é um país muito rico em recursos naturais, mas a maioria da população ainda vive na pobreza e na privação de acesso a serviços básicos e condições de vida decentes. A exploração de petróleo e gás no mar de Timor tem sido controlado pelo Fundo Petrolífero. O país ainda carece de electricidade e combustíveis que são cruciais para materializar as políticas de redução da pobreza. Como solução, o governo timorense criou recentemente o Plano Estratégico de Desenvolvimento a 20 anos cujas prioridades incluem trazer o desenvolvimento do petróleo do mar para a costa sul de Timor-Leste e desenvolver as energias renováveis. É neste último contexto que o biodiesel se insere. O seu desenvolvimento no país poderá ser uma solução para o fornecimento de electricidade, a criação de empregos e sobretudo o combate contra a pobreza e a privação. Para ser usado como combustível, no entanto, o biodiesel deve possuir propriedades termodinâmicas coerentes com as especificadas nas normas da ASTM D6751 (nos Estados Unidos) ou EN 14214 (na Europa) para garantir uma adequada ignição, atomização e combustão do biodiesel no motor.

keywords

Timor-Leste, biofuel, biodiesel, esters, thermodynamic properties, lipase, *Jatropha curcas, Aleurites moluccana*, cofee waste, CPA , SAFT

abstract

The biofuels have been at the forefront of global energy policies as their advantages can overcome the uncertainties of fossil fuels. Biodiesel has proven to be a very reliable fuel alternative to petrodiesel. It is a mixture of fatty acid alkyl esters obtained by the transesterification of vegetable oils and animal fat. As fuel, biodiesel is economically viable, socially responsible, technically compatible and environmentally friendly. The main challenge associated to its development concerns the choice of raw materials for its production. In third world countries, edible oils are more important for feeding people than for running cars.

This thesis aims to produce / process biodiesel from resources endogenous of Timor-Leste and to measure/predict the thermodynamic properties of biodiesel, from those of alkyl esters. The synthesis of biodiesel from oils of *Aleurites moluccana, Jatropha curcas* and coffee waste were here studied. The thermodynamic properties such as density, viscosity, surface tension, volatility and speed of sound were also measured and estimated using predictive models available in the literature including some equations of state like CPA and soft-SAFT.

Timor Leste is a country rich in natural resources, but the majority of the population still lives in poverty and deprivation of access to basic services and decent living conditions. The exploitation of oil and gas in the Timor Sea has filled only the Oil Fund. The country still lacks electricity and fuels that are crucial to materialize policies for poverty reduction. As a solution, the Timorese government has recently established the Strategic Development Plan of 20 years whose priorities include bringing the development of oil from the sea to the south coast of Timor-Leste and developing renewable energy sources. It is in this latter context that biodiesel should be considered. Its development in the country will be contextually an appropriate solution for electricity supply, job creation and especially combat against poverty and deprivation. To be used as fuel, however, biodiesel must possess thermodynamic properties consistent with those specified in the standards of ASTM D6751 (in USA) or EN 14214 (in Europe) to ensure proper ignition, atomization and combustion in diesel engines.

Contents

List of Figures

List of Tables

Nomenclature

List of Abbreviations

Abs = Absorbance
Am = Aleurites moluccana
ARD (s) = Average relative deviation (s)
ASTM = American Society of Testing and Materials
C = castor oil
CH_3ONa = Sodium methoxide
CMAT = Certain Maritime Arrangements in the Timor Sea
CPA = cubic-plus- association
CW = coffee waste
CO_2 = Carbon dioxide
C10F18 = Perfluorodecalina
$C_{12}H_{26}$ = Dodecane
$C_{x:y}$ = ester means the alkyl ester of fatty acid with x carbons and y unsaturations
DHA = Docosahesaenoic acid
DGT = Density gradient theory
EEAI = ethyl esters from *Azadinachta indica*
EEBA = ethyl esters from *Balanites aegyptica*
EDA = Enviroenergy Developments Australia
EEJC = ethyl esters from Jatropha oil
EEWCO = ethyl esters from waste cooking oil
EoS = Equation of state
FA = Fatty acid
FAEE (s) = Fatty acid ethyl ester (s)
FFA = Free fatty acids
FAME (s) = Fatty acid methyl ester (s)
FT = Friction theory
FVT = Free volume theory
GC = group-contribution
GC-FID = gas chromatography flame ionization detector
GCVOL = group contribution method for the prediction of liquid densities
GDP = Gross Domestic product
GH = Gross heat
GHGs = Greenhouse gases
GMSME = genetically modified soy methyl esters
GP = biodiesel from Galp (Soybean +Rapeseed)
GT = Gradient theory
HHV = Higher heating value
HID = Human Index Development

HP = High pressure
H_2SO_4 = Sulphuric acid
H_3PO_4 = Phosphoric acid
Jc = *Jatropha curcas*
JPDA = Joint Petroleum development area
KH_2PO_4 = Potassium hydrogen phosphate
KOH = Potassium hydroxide
LA = Lipase activity
LJ = Lennard Jones
Mb/d = Million barrels per day
$MgSO_4.7H_2O$ = Magnesium sulfate heptahydrate
MJ = Megajoule
MPa = Megapascal
ML = Methyl Linoleate
MO = Methyl oleate
$NaNO_3$ = Sodium nitrate
NaOH = Sodium hydroxide
NOx = Nitrogen oxides
Np = Number of experimental points
Ns = Number of systems
OARDs = Overall Average relative deviation (s)
OECD = Organization for economic cooperation and development
OPEC = Organization of the Petroleum Exporting countries
P = Palm
PFC = Perfluorocarbon
PR = Palm + rapeseed
R = Rapeseed
RD (s) = Relative deviation (s)
Rel-LA = Relative lipase activity
RPM = Rotation per menit
S = Soybean
SAFT = Statistical associating fluid theory
S+B = Beef + tallow
SDP = Strategic Development Plan
Sf = Sunflower
SME = Soybean oil methyl esters
SoyA = Soybean type A
SO_2 =Sulphur dioxide
SP = soybean + palm
SR = Soybean +Rapeseed
SRK = Soave-Redlich-Kwong
SRP = Soybean + rapeseed +palm

TAGs = Triacylglycerides
U = Unit of enzyme activity
VTF = Vogel−Tammann−Fulcher
YGME = Yellow grease methyl esters

List of Symbols

A, B, C – fitting parameter of GCVOL method or for Antoine equation
Ai = site A in molecule *i*
a, b, c, d = fitting parameters for Krisnangkura's model
a = energy parameter in the physical term of the CPA EoS ($J.m^3.mol^{-2}$)
a0 = parameter for calculating *a* ($J.m^3.mol^{-2}$)
b = co-volume parameter in the physical term of the CPA EoS ($m^3.mol^{-1}$)
c = fitting parameter for Gardas' approach or gradient theory influence parameter ($J.m^5.mol^{-2}$)
C1 = Concentration of perfluorodecaline (%)
C2 =Agitation rate (RPM)
c1 = parameter for calculating *a*
Cp = calorific capacity (J.mol-1.K-1)
*C*V = the isochoric heat capacity (Jmol-1K-1)
Fc =correction factor
f0 = Helmholtz free energy density (J.m-3)
g = radial distribution function
H = enthalpy (J.mol-1)
k_b = Bolztman constant
k_d = Decay constant (h^{-1})
k_La = Volumetric mass transfer coefficient (s^{-1})
Km =Molecular compressibility
*k*T = isothermal compressibility coefficient (MPa^{-1})
L = viscosity parameter for SAFT
LA = lipase activity (U/mL)
Mw = molecular weight (mol/g)
m = molecular parameter for SAFT EoS
n = number of groups
P = Pressure (MPa) or protein (g)
Pch =parachor
q_s = Specific rate of substrate consumption ($g.\ g^{-1}\ h^{-1}$)
q_p = Specific rate of product formation ($g.\ g^{-1}\ h^{-1}$)
R = gas constant ($J.mol^{-1}.K^{-1}$)
S = Entrophy ($J.m^{-2}.K^{-1}$) or substrate (g)
T = temperature (K)
u = Speed of sound (m/s)

V =molar volume (mol /L)
X = dry cell biomass (g)
x = liquid phase mole fraction
XA = fraction of molecule not bonded at site A
$Y_{X/S}$= Yield factor of dry cell biomass
$Y_{X/P}$ = Yield factor of protein
Z= Total number of carbon in the molecule used in Krisnangkura's model
Z =compressibility factor
ZRA = racket parameter

Greek Symbols

α = fitting parameter of mixed model Luedeking or the thermal expansion coefficient (K^{-1})
Or viscosity parameters *for SAFT*
β = Association volume in the association part of the CPA EoS or fitting parameter of mixed model Luedeking or viscosity parameters for SAFT
χ = Constant parameter used to take into account the influence of temperature.
Δ = Variation of parameter
$\Delta AiBj$ = association strength between site A in molecule *i* and site B in molecule *j* in the association part of the CPA and SAFT EoS ($m^3.mol^{-1}$)
$\Delta\eta$= Dense-state correction term of free volume theory
$\Delta\nu$ = molar volume for a group
ε = Association energy in the association part of the CPA and SAFT EoS ($J.mol^{-1}$) or molecular parameters for SAFT EoS
γ =surface tension (mN/m)
η = Dynamic viscosity (mPa.s)
μ = kinematic viscosity (mm2/s) or Specific rate of growth (h^{-1})
ρ = Density ($kg.m^{-3}$)
σ = Standard deviation or molecular parameters for SAFT EoS

Subscripts

b = boiling
BD =biodiesel
c = critical
c, mix = critical of mixture
calc. = calculated
exp. = experimental
I = component
j = component
l = liquid

lit = literature
o = initial or atmospheric pressure
m = mixture
r = reduced
X/S = biomass /substrate
X/P =biomass /protein

Superscripts

v = vapor
calc. = calculated
exp. = experimental
lit = literature

CHAPTER 1

General Introduction

This introductory chapter highlights globally the current framework of biodiesel fuels in the international fuel market and specifically their development and prospects in Timor Leste for the projects of alleviating poverty and deprivation.

1.1. The rising trend of biofuel

Nowadays, since «energy & fuel» becomes a frequent matter of worldwide concern and discussion, «sustainability» becomes a buzzword on everyone's lips. Given the scarcity of petroleum resources, the oil-importing countries (e.g., the OECD members) are constantly worrying about their energy security whereas the oil-exporting countries (i.e., the OPEC countries) are apprehensive about the impact of global energy demand on their petroleum resources. The truth is that the existing petroleum resources will not be always available at reliable prices for the non-OPEC countries much less in the circumstances of financial or economy crisis. Moreover, their use is not only costly but also is rigorously controlled by the existing international environmental regulations like Kyoto and Montreal protocols to avoid the emissions of greenhouse gases (GHGs) such as carbon dioxide (CO_2), sulphur dioxide (SO_2) and nitrogen oxides (NOx)[1, 2] that are the main causative of global warming and consequent climate changes. It is noted, for example, that the overall CO_2 emissions from petroleum fuels were 30.3 $GtCO_2$ in 2010 and are foreseen to be 37.0 $GtCO_2$ in 2035[3].

This disquieting scenario can be a picture of contrasts in the coming decades. On the one hand, due to the increase of global population (will reach 9 billion in 2040) and to the growth of global economy (an annual average rate of 2.8 % from 2010 to 2040), the worldwide energy demand will be redoubling until 2040 particularly in Africa and Asia pacific like China and India [4].The demand for oil will be more noticeable in the sector of transportation than other sectors in 2035 (**Figure1.1**). On the other hand, the offer of crude oil for the non-OPEC countries will be in continuous decrement until being negative (-4 mb/d) in the period between 2020 to 2035 comparing to that of non-crude oil (9 mb/d)[5]. This situation has forced governments, civil societies and industries to develop energy from renewable resources aiming at reducing the petroleum dependency and mainly at providing reliable, affordable and clean energy.

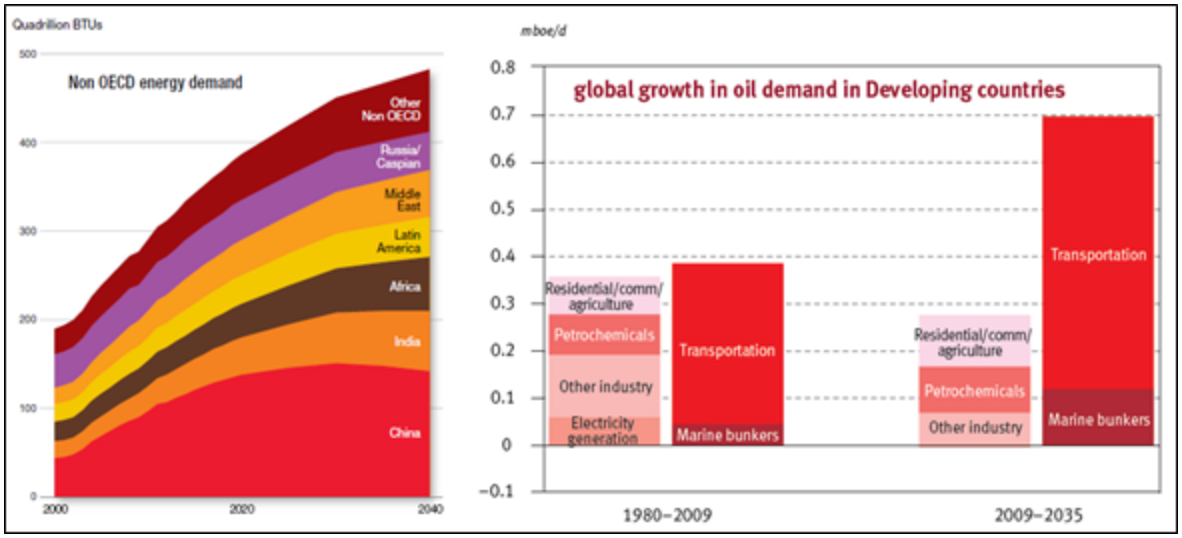

Figure 1 1. Forecast of global energy demand [4]

In this perspective, biofuels have been already at the forefront of alternative fuels to petroleum fuels. Ethanol and biodiesel are able to replace totally or to be blended at any proportion with gasoline and petrodiesel respectively to be used in the conventional engines as they offer several benefits that can override many uncertainties of petroleum-based fuels. Beyond renewable and clean, they are domestically produced from agricultural products such as sugarcane, oleaginous plants, forest biomass and other sources of organic matter[6]. Their production will achieve circa 4.1 Mb/d by 2035[7]especially when the governments also have decided to support financially their development. For example, on 18th December 2012, five advanced biofuels projects and three bioenergy projects, to be hosted in Zone Euro member states, received funding of over €1.2 billion from the European Commission[8]. In the United States of America, the administration of president Barack Obama also announced in 2012 up to $35 million over three years to support research and development in advanced biofuels, bioenergy and high-value bio-based products[9]. Shortly, biofuel is now popular in the arena of energy.

Ethanol is a biocomponent for gasoline produced from sugarcane, sugar beet and cereals. Its average annual growth is 12.8% from 2010 to 2020 [10] and will represent 73% of biofuel demand in 2020[11]. In Brazil, ethanol fuel has been sold as a low blend with gasoline (which varies between 18 to 25% in volume) and also in a pure version (E100)[12, 13]. The high level mixture of ethanol with gasoline like E85 is foreseen to be available worldwide only in 2035 where circa 37 % of domestic ethanol will be used[14].

Biodiesel is a biocomponent for petrodiesel obtained from lipid feedstocks like vegetable oils, greases and animal fats [15, 16]. Its average annual growth is 28.2% from 2010 to 2020 [11] whose supply and demand are foreseen to continuously increase until 2020 as illustrated by **Figure 1.2** with the European Union being the protagonist of this increase (44% of share). The smaller contribution comes from the North America. In Portugal, there is already available in the market petrodiesel with 7% of biodiesel (B7) since January 2010 [17].

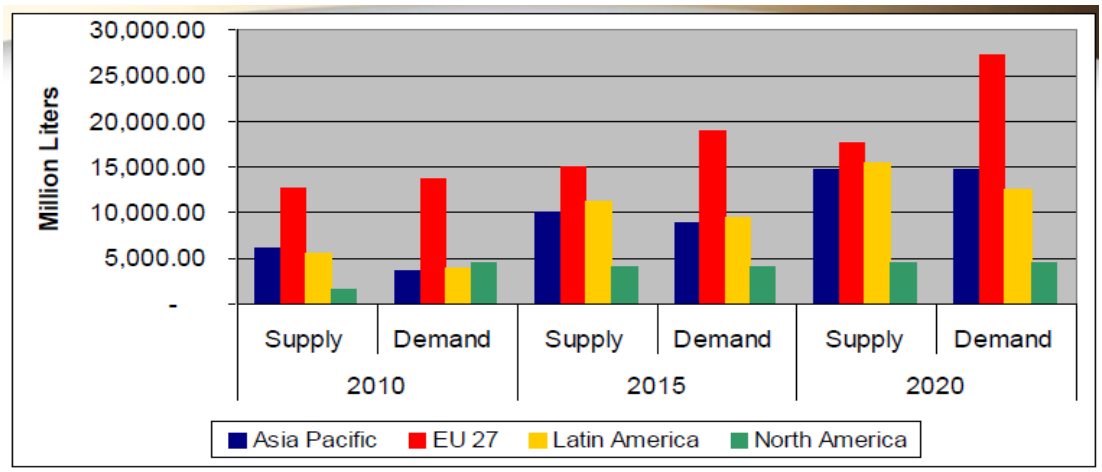

Figure 1 2. World biodiesel supply and demand **[11]**

1.2. Biodiesel as an alternative fuel for diesel engines

1.2.1. Theoretical Concepts

1.2.1.1. Compositional profile and synthesis of biodiesel

Chemically, biodiesel is a fuel composed of monoalkyl esters of long-chain fatty acids produced from the lipid feedstocks like vegetable oils, grease or animal fats [15, 16]. These feedstocks are commonly known as triacylglycerides (TAGs) and the common fatty acid groups in biodiesel are described in **Table 1.1** where the C16:0 and C18:0 fatty acids with unsaturation bond up to three are the most common.

Table 1 1. Typical fatty acid (FA) groups in biodiesel [18]

Common name[n1]	Common acronyms	Formal name	CAS. No.	Molecular formula	Mw ($g.mol^{-1}$)
Lauric acid	C12:0	Dodecanoic acid	143-07-7	C12H24O2	200.32
Myristic acid	C14:0	Tetradecanoic acid	544-63-8	C14H28O2	228.38
Myristoleic acid	C14:1	cis-9-Tetradecenoic acid	544-64-9	C14H26O2	226.26
Palmitic acid	C16:0	Hexadecanoic acid	57-10-3	C16H32O2	256.43
Palmitoleic acid	C16:1	cis-9-Hexadecanoic acid	373-49-9	C16H30O2	254.42
Stearic acid	C18:0	Octadecanoic acid	57-11-4	C18H36O2	284.48
Oleic acid	C18:1	cis-9-Octadecenoic acid	112-80-1	C18H34O2	282.47
Linoleic acid	C18:2	cis-9,12-Octadecadienoic acid	60-33-3	C18H32O2	280.46
Linolenic acid	C18:3	cis-9,12,15-Octadecatrienoic acid	463-40-1	C18H30O2	278.44
Arachidic acid	C20:0	Eicosanoic acid	506-30-9	C20H40O2	312.54
Gadoleic acid	C20:1	cis-11-Eicosenoic acid	5561-99-9	C20H38O2	310.53
Behenic acid	C22:0	Docosanoic acid	112-85-6	C22H44O2	340.6
Erucic acid	C22:1	cis-13-Docosenoic acid	112-86-7	C22H42O2	338.58

[n1]Some oils contain other fatty acids like caprilic acid (C8:0), capric acid (C10:0), lignoceric acid (C24:0) and ricinoleic acid (C18:1OH). To term these fatty acids as fatty acid esters, one just changes the termination *ic* in the nomenclature of fatty acids with *ate* in that of esters (example from laur*ic* to laur*ate*). The common acronyms here presented will be used throughout this thesis.

Biodiesel is usually synthesized from the transesterification reaction between the triglycerides and short-chain alcohol such as methanol or ethanol in the presence of catalysts such as an alkali. This reaction is reversible, although the back reaction is largely negligible because the glycerol formed is not miscible with the product, leading to a two-phase system[19]. If methanol is used for the reaction, then the biodiesel produced is composed of fatty acids methyl esters (FAME). **Equation 1.1** expresses the global transesterification of triglycerides, where R1, R2, R3 are fatty acid chains.

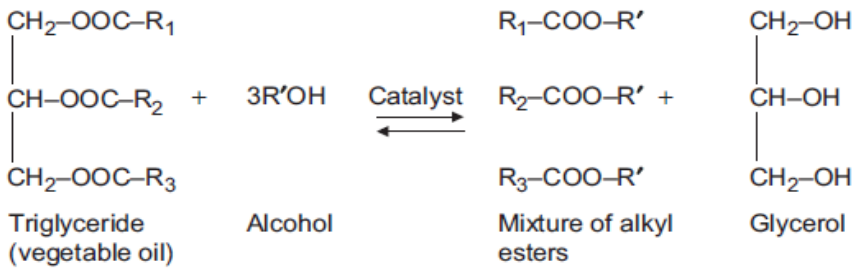

(1.1)

There are several basic factors that affect the efficiency of the transesterification reaction such as free fatty acids (FFA), water content and proportion of alcohol to oil, amount and type of catalyst, reaction temperature and stirring rate. Each factor is equally important to achieve a high quality biodiesel which meets the regulatory standards[20]. The effect of feedstocks on the efficiency of transesterification reaction is normally assessed through FFA level and water content. FFA level is the percentage of saturated or unsaturated monocarboxylic acids that occurs naturally in oils but are not attached to glycerol backbones[21]. They can be removed in an acid-catalysed transesterification. Alkaline transesterification only tolerates oils with less than 3 % of FFA [20] because these can react with the catalyst to form soaps that reduce the catalytic efficiency, as well as causing an increase in viscosity, the formation of gels and difficulty in achieving separation of glycerol [21, 22]. Water content must be as low as 0.1% to prevent the hydrolysis of oils and decrease the conversion of ester[23]. Thus, the removal of the moisture content by heating the oil before starting the transesterification reaction is recommended.

1.2.1.2.Type of catalysts

According to the type of catalyst used in the process, transesterification reaction can be **alkali-catalysed, acid-catalysed or enzyme-catalysed**. Each catalyst has its own suitability for the reaction, depending on the quality of feedstocks.

For an **alkali-catalysed transesterification**, either sodium hydroxide (NaOH), potassium hydroxide (KOH) or sodium methoxide (CH_3ONa) could be used with methanol or ethanol as well as any kind of oils, refined, crude or frying [24]. Although the alkaline catalyst is not corrosive for engine's metallic parts, it does not deal efficiently with oils with high level of FFA and water content. Water retards the transesterification through the hydrolysis reaction. It hydrolyzes triglycerides to form more FFA instead of esters as shown in **equation 1.2**. The risk of FFA or water contamination results in soap formation, making downstream recovery and purification very difficult and expensive [25].

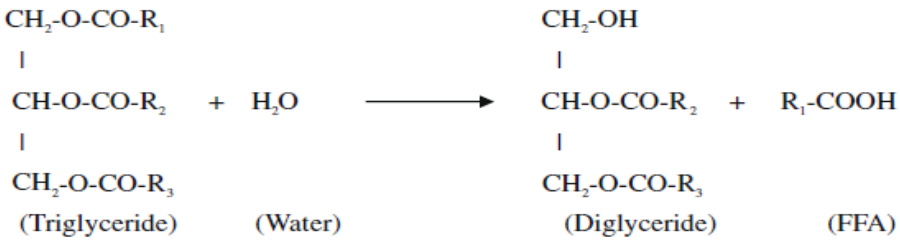

(1.2)

A major advantage of base-catalysed transesterification is the mild reaction conditions, which for the production of methyl esters typically are 1h at 60–65 ºC and ambient pressure, 1% catalyst and a molar ratio of alcohol to oil of 6:1 [21].

Acid catalyst is more tolerant of FFA. So it is more suitable to treat oils with high levels of FFA [26]. Strong acid such as sulfuric acid can catalyze the esterification of the FFA and the transesterification of the triglycerides without formation of soaps. The reaction is shown in **equation 1.3**.

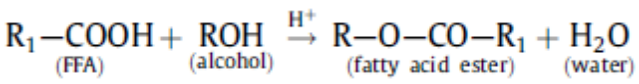

(1.3)

Although the esterification of FFA is relatively fast, proceeding substantially to completion in one hour at 60ºC, the transesterification of the triglycerides is very slow, taking several days to complete. In this case, only an excess of the alcohol solves the problem although hinders the recovery of the glycerol[27]. Another problem with acid

catalysis is that the water production from the following reaction stays in the reaction mixture and ultimately stops the reaction, usually well before reaching completion. Moreover the corrosiveness of the acids may cause damage to the equipment and the reaction rate can also be low, sometimes taking more than a day to finish [25].

Acid catalysis followed by alkali catalysis can improve the transesterification process of low quality feedstocks. Each technique will accomplish the process for which it is best suited. Acid catalysis is relatively fast for esterification of FFA, so it is used as a pretreatment for the high FFA feedstocks to reduce the level of FFA to 0.5-3.0 %, or lower. Then an alkali catalyst is added to convert the triglycerides to biodiesel. Although this process can convert high FFA feedstocks quickly and effectively, water formation is still a problem during the pretreatment phase. An addition of a large excess of methanol during the pretreatment can dilute the water produced to the level where it does not limit the reaction although this approach will still hamper the separation process.

Transesterification can also be carried out enzymatically. Lipases can be used as catalyst in a solvent-free system to produce biodiesel. It is more appropriate for the production of biodiesel from feedstocks containing high FFA and water because the free fatty acids are directly esterified into biodiesel [25]. The immobilization of lipase could enhance the biodiesel yield. Many studies have been focused on optimizing the reaction conditions (solvent, temperature, pH, type of microorganism that generates the enzyme, etc.) in order to establish suitable characteristics for an industrial application[27]. **Table 1.2** shows the comparison of the three different transesterification process here described.

Table 1 2. Comparison of different transesterification process [25]

Variable	Alkali catalysis	Acid catalysis	Lipase catalysis
Reaction temperature, ºC	60-70	55-80	30-40
FFA effect	Saponified products	Esters	Methyl esters
Water effect	Interference with reaction	Interference with reaction	No influence
Yield of esters	Normal	Normal	Higher
Recovery of glycerol	Difficult	Difficult	Easy
Purification of methyl esters	Repeated washing	Repeated washing	None
Production cost of catalyst	Inexpensive	Inexpensive	Relatively expensive
Reaction time	Short	Short (9h)	Long (36 h)

The typical industrial production and purification process of biodiesel is illustrated in **Figure 1.3.** The transesterification reaction occurs in a reactor with the oil reacting with the methanol, in the presence of a catalyst, to produce methyl esters and glycerol. These products then form two phases at the outlet of reactor. The aqueous phase is rich in glycerol and the organic phase in fatty esters. The unreacted methanol is distributed between them. After reaction, the aqueous phase is sent to the alcohol recovery section (**section 1**) to recover and to purify the glycerol for posterior sale in the market (**section 2**). The removal of excess alcohol from the methyl esters stream leaving the transesterification reactor can be performed by flash evaporation or distillation. The organic phase containing methyl esters is washed with acidified water to neutralize the catalyst. The washed product is then dried to reduce the water content to an acceptable value by the biodiesel required standards (**section 3**).

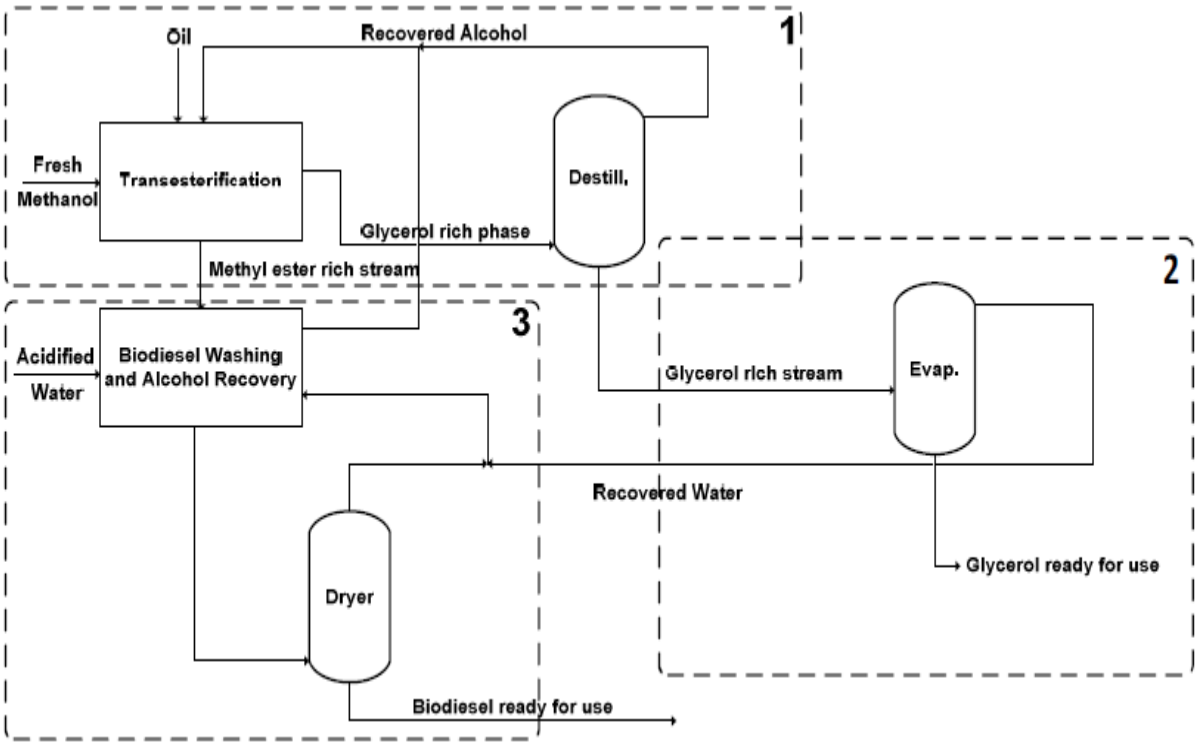

Figure 1 3. Representative flow sheet of an industrial biodiesel production and purification process **[28]**

1.2.2. Practical Concerns: Pros and Cons

1.2.2.1. Pros viewpoints

As a fuel, biodiesel offers several economic, environmental and technical benefits like ready availability, portability, renewability, domestic origin, lower sulfur and aromatic content, biodegradability, better ignition quality, inherent lubricity, higher cetane number, positive energy balance, greater safety, nontoxic character of the exhaust emissions and cleaner burning[15, 23, 29-35]when compared to diesel fuel. Biodiesel degrades, however, four times faster than diesel. In pure state it degrades 80-88 % in water[36]. It is nonflammable and non-explosive; with a flash point of 423 K compared to 337 K for petrodiesel (a higher flash point leads to safe handling and storage). Furthermore, it is miscible with petrodiesel in any proportion and can be used in the conventional diesel engine with no modification [35, 37-40] because of the great molecular similarities of biodiesel to paraffinic diesel fuel compounds [39]. Indeed, biodiesel is most often blended with petroleum diesel in ratios of 2% (B2), 5% (B5), or 20% (B20). It can, nevertheless, also be used as pure biodiesel (B100)[16].

Regarding the emissions, neat biodiesel (B100) reduces carbon dioxide emissions by more than 75% over petroleum diesel, while a B20 reduces carbon dioxide emissions by 15% [41, 42]. Biodiesel also can reduce carbon monoxide by 20%, unburned hydrocarbon by 30% and particulate matter by 40%. Other types of emissions like sulphur dioxide, polycyclic aromatic hydrocarbons and nitric polycyclic aromatic hydrocarbons are also reduced by appreciable magnitudes [1, 42, 43]. Only NOx emissions increase about 10-15 %, compared to that of petrodiesel, because biodiesel contains 10-11 % of oxygen [43-45]. Reductions in NOx tend to be accompanied by increases in particulate emissions and fuel consumption [19]. It can be reduced, however, by retarding the injection time [46] or using exhaust gas recirculation[47].

Beyond the advantages aforementioned, if the development of biodiesel does not harm the ecosystems, it can provide new labor and market opportunities related to production of domestic crops and their further processing into biodiesel and decreases the country's dependence on imported petroleum or refined products[48]. This enables countries with no petroleum resources to join the fuel market, auto sustain their energy needs and reduce unemployment.

1.2.2.2. Cons Viewpoints

Sustainability is the key to the decision. As required for the petroleum fuels, the production of biodiesels must also be sustainable. So far the development of biodiesel, however, is still facing challenges including feedstock bottleneck and quality issues.

First, in most cases, biodiesel production is not truly green, renewable nor environmentally friendly because it still uses methanol derived from petroleum (10% of the feedstock input) and the synthetic catalysts used for the transesterification process are sulfuric acid, sodium or potassium hydroxide, which are highly caustic and toxic[49].

Second, the dilemma *fuel vs. food* always remains alive in the third world countries where the concerns about the risk of diverting farmland or crops for biodiesel production in detriment of the food supply are seriously analysed, namely when the edibles oils are used for the purpose. Many voices claim that edible oils are more important for feeding human than for running vehicles. This reality makes the price of biodiesel feedstocks soaring and the production economically non-viable compared to that of diesel fuel. Note that in recent years about more than 85% of the costs of biodiesel production are field up in feedstock costs [46], placing the marketability of biodiesel in constant equation. Beyond that, ecologically, conversion of natural habitats into monocultures diminishes biodiversity and reduces the natural carbon sink capacity. Converting native ecosystems to biodiesel production frequently causes much greater net green house gas releases over a long period than the combustion of an energy-equivalent amount of petroleum diesel would do [50].

Third, some properties of biodiesel need to be improved to achieve high quality. The higher kinematic viscosity, higher cloud point and pour point [51], lower oxidation stability, hygroscopicity [26], lower calorific value, lower effective engine power, higher emission of NOx, reactivity of unsaturated hydrocarbon chains [52] and greater sensitivity to low temperatures [1] may still compromise the quality of biodiesel and consequently the engine performance and exhaust emissions [53]. These properties are generally influenced by the quality of feedstock (chain length, branching and degree of saturation) and efficiency of biodiesel production and processing. In any situation, the presence of impurities in biodiesel, either due to side-reactions, unreacted feedstock, or non-fatty acid constituents, may increase pollutants[38, 53]. So, the target is to ensure that the neat biodiesel obeys the specifications presented in **Table 1.3** for some properties.

Table 1 3. Biodiesel (B100) standard specifications in several countries [18]

Property	Brazil	China	Colombia	EU	Germany	India	Indonesia	USA	Worldwide
Water and Sediment (% vol., max.)	0.02		0.05	0.05	0.03	0.05	0.05	0.05	0.05
Total Contamination (mg/kg, max.)			500	24	20				24
Kinematic Viscosity @ 40°C (mm^2/s)		1.9 - 6.0	1.9 - 5.0	3.5 - 5.0	3.5 – 5.0	2.5 - 6.0	2.3 - 6.0	1.9 - 6.0	2.0 - 5.0
Flash Point, Closed Cup (°C, min.)	100	130	120	101	110	120	100	93	100
Methanol (wt.%, max.)			0.2	0.2	0.3	0.2		0.2	0.2
Cetane No. (min.)	45	49	47	51	49	48	51	47	51
Sulfated Ash (wt.%, max.)	0.02	0.02	0.02	0.02	0.03	0.02	0.02	0.02	0.005
Total Ash (wt.%, max.)									0.001
Total Sulfur (ppm, max.)	10	50	10	10	10	50	100	15	10
Phosphorous (ppm, max.)	10		10	10	10	10	10	10	4.0
Acid No. (mg KOH/g, max.)	0.8	0.8	0.8	0.5	0.5	0.5	0.8	0.5	0.5
Carbon Residue (wt. %, max)	0.05	0.3[b]	0.3 [b]	0.3 [b]	0.05	0.05	0.05	0.05	0.05
Free Glycerin (wt.%, max.)	0.02	0.02	0.02	0.02	0.02	0.02	0.02	0.02	0.02
Total Glycerin (wt.%, max.)	0.38	0.24	0.25	0.25	0.25	0.25	0.24	0.24	0.24
Mono-Glyceride (wt.%, max.)	1.0			0.8	0.8	0.8			0.8
Di-Glyceride (wt.%, max.)	0.25			0.2	0.4				0.2
Tri-Glyceride (wt.%, max.)	0.25			0.2	0.4				0.2
Distillation (T-90 °C, max.) [a]	360 (T-95)		360				360	360	
Oxidation Stability (hrs @ 110°C, min.)	6	6	6	6		1.5		3	10
Ester Content (wt.%, min.)			96.5	96.5		96.5	96.5		96.5
Iodine Number (g I_2/100g, max.)			120	120	115	115	115		130
Density (kg/m^3)		820 - 900	860 - 900	860 - 900	875 – 900	860 - 900	850 - 890		860 - 900

[a)] Atmospheric equivalent T-90 point

[b)] This limit is based on the bottom 10% fraction of the fuel

In fact, many of the neat biodiesels obtained from different types of oils and fats have indeed magnitudes of viscosity and higher heating value (HHV) concordant with the standard limits as illustrated in **Figures 1.4** and **1.5**, respectively. HHV for biodiesel is only circa 12 % less than that of petrodiesel (46 MJ/kg), meaning that it is worthy to use biodiesel as fuel.

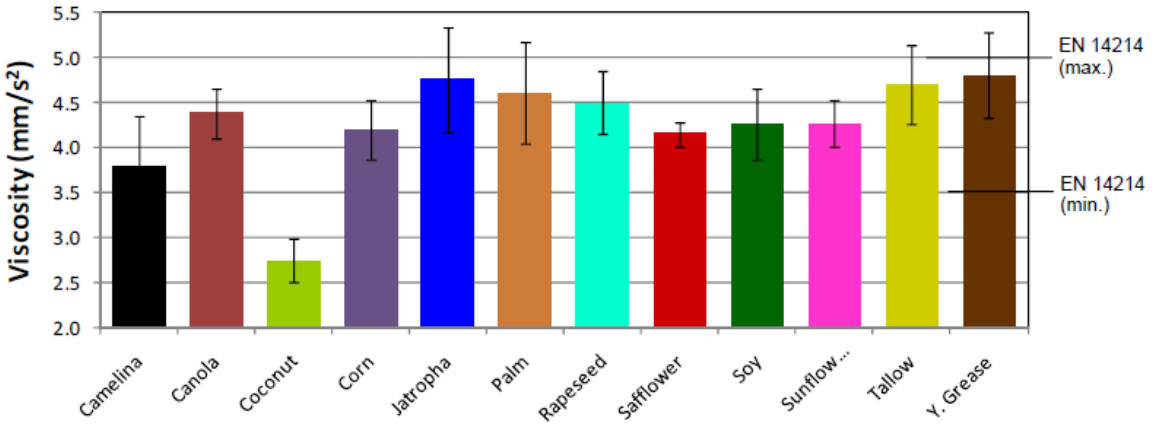

Figure 1 4. Kinematic viscosity for several biodiesel fuels **[18]**

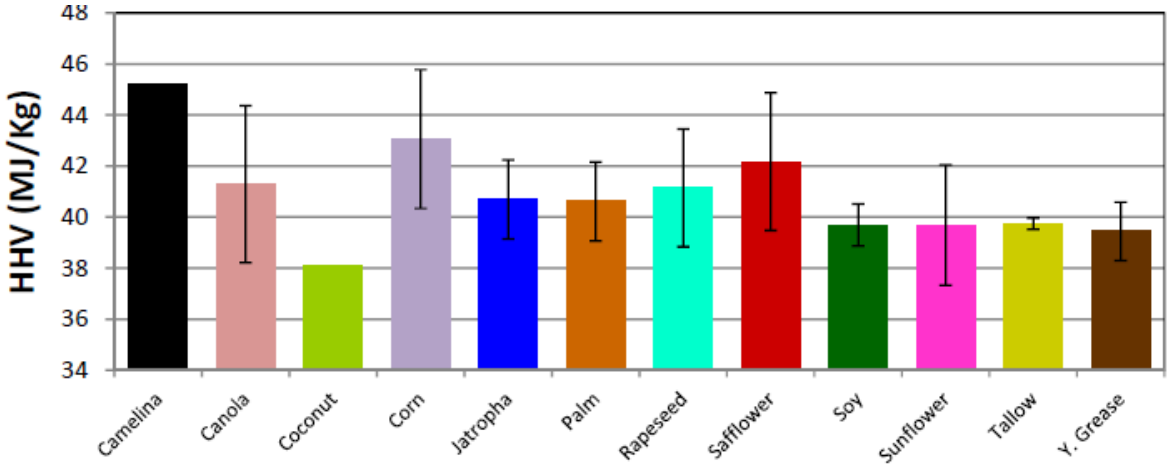

Figure 1 5. Gross heat combustion (GH) of several biodiesel fuels **[18]**

1.2.2.3. Approaches to the challenges

Many efforts have been developed to delineate the beneficial solutions for the challenges of biodiesel development. If the use of virgin edible oils is expensive and competitive with the food supply, then the use of low cost feedstocks and the development of other alternative sources in marginal lands are strongly recommended, not only to increase the economic viability of biodiesel, but also the potential supply of this fuel. In this regard, many researches have been focused on the use of waste frying oils, animal fats, microbial oils and non-edible oils which are not suitable for human consumption and can be developed in nonarable lands [16]. However, given the low cost feedstocks have the relatively higher amounts of free fatty acids and water content, additional processing steps are required to remove any water and either the free fatty acids or soap from the reaction mixture to ensure that the final net biodiesel possess required properties. Only the decrease in the feedstock costs will affirmatively reduce to an acceptable value the great divergence between the prices of biodiesel and diesel fuel.

The choice of source for biodiesel production and also the reagents used in the transesterification process (if they are green or not), however, is made according to the availability and cost in each of the producing countries. Indeed for a given production line, the comparison of the feedstocks should include issues like cultivation practices, availability of land and land use practices, use of resources, soil erosion, contribution to biodiversity and landscape value losses, direct economic value of the feedstocks taking into account the co-products, creation or maintenance of employment and water requirements and water availability among others [51]. In any case the statistics show that today more than 95% of the world biodiesel is produced from edible oils [51].

Countries like USA and those belonging to European Union are self-dependent in production of edible oils and even have surplus amount to export. Hence, edible oils such as soybean and rapeseed are mostly used in USA and European Union, respectively. However the use of edible oils to produce biodiesel in Africa and other developing countries is not feasible because of the huge gap between the demand and the supply of such oils in the developing world [25]. For example India is a net importer of edible oil to meet the food requirements, hence the emphasis of biodiesel is on non-edible oils from plants such as *Jatropha*, karanja, neem, mahua, simarouba, etc.[20, 45].

1.3. Energy Context in Timor Leste

1.3.1. Current Status and development

The provision of reliable, affordable and clean energy is crucial for alleviating poverty and deprivation because energy is the base of human life. This policy is still not easy to implement in Timor Leste, making the country a picture of contrasts during a decade of independence. On the one hand, it has abundant fossil and renewable resources capable of providing fuels and electricity to the whole country like oil, natural gas, water, sun, wind and biomass. If so far the renewable energies are still ongoing projects, the undersea oil and gas have been developed for years by Australia and in return Timor Leste receives the revenues by 90% from the Joint Petroleum Development Area (JPDA) and 50 % from the entire Greater Sunrise field according to the treaty of Certain Maritime Arrangements in the Timor Sea (CMAT) as exemplified in **Figure 1.6** [54]. The revenues made the Timorese Petroleum Fund achieve circa $12 billion in 2012, from which 4.6 % was used to support the 2013 General State Budget, i.e., an amount lower than that used in the 2012 State Budget (6.7 %) but still higher than that of Estimated Sustainable Income (3.0 %)[55].

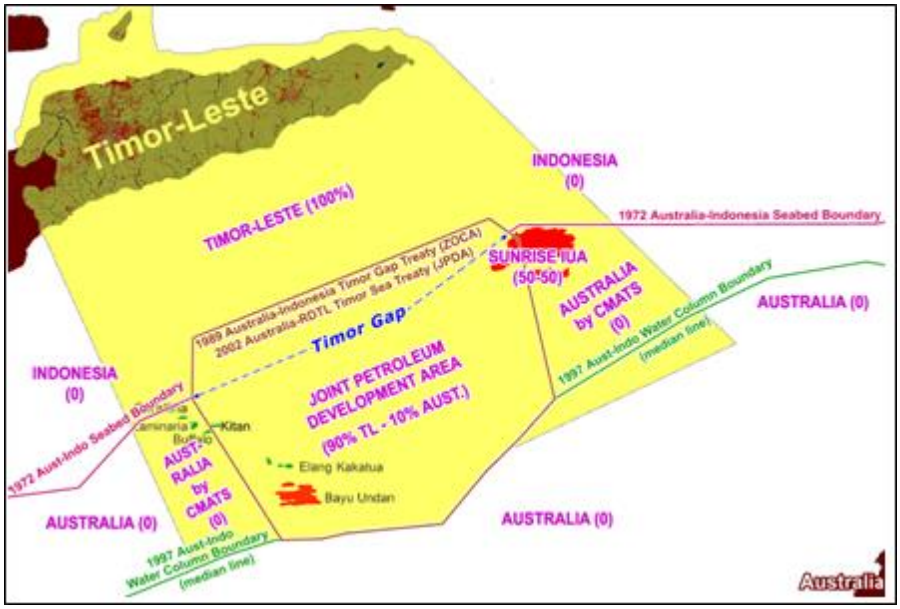

Figure 1 6. Undersea oil and gas resources of Timor Leste [54]

On the other hand, the country still lacks energy and remains a slave to poverty and deprivation. In the sector of electricity generation, the rural territories are not yet electrified as only 58 isolated diesel-powered generators are producing about 40 MWatt of electricity

to the whole country [56]. Moreover, the existing electricity grid continues to use imported fuels. In the sector of transportation, the cars still use Indonesian gasoline and diesel. In the residential sector, most households still use candle, kerosene, battery, solar panel and small gasoline generators to service their energy needs. The poorest households use regularly wood fire as their primary energy for cooking and lighting. For example, in 2006 about 98.3% of households used woods for cooking (**Table1.4**) and only 0.8% got electricity from diesel power generators[57]. In short, it can be said that the struggle for the alleviation of poverty remains so far a complicated mission for Timor Leste, obliging the rural population to live poor and deprived of access to basic services and decent living conditions. It is noted that 49.9 % of population live below the poverty line and 38.7% in the severe poverty [58], despite the Gross Domestic product per capita of $1393 reported in 2011 and the increase of 2.71 % of Human Index Development (HID) in 2012 from 2000 [58], standing this as a proof that economic growth does not always expresses the poverty reduction.

Table 1 4. Source of energy used for cooking in 2006 [57]

Energy source	Urban (%)	Rural (%)	All areas (%)
Fuel-wood	98.3	98.9	98.7
Agricultural residues	0.5	0.4	0.4
Charcoal	0.5	0.7	0.7
Kerosene	9.2	1.6	3.0
Electricity	1.2	0.7	0.8

This controversial scenario happens because of two possible reasons among others. First, the country still has very low social capital, technology and know-how to mine its own resources and revenues without foreign aids. So during the period of independence, Timorese government has been investing intensively on education and skills. The public spending in education was 14% of GDP in 2010 from 2005 [58]. Second, in 1999 the Indonesian troops and pro-integration militia destroyed about 70% of the economic infrastructure including all power sector assets, administrative buildings, power stations, power lines, and associated records and documentation, solar panels and connection boxes at individual home installations, obliging the country to reform all the institutions and infrastructures from the scratch during the period of independence. The truth is that before the independency, 28.7% of all Timorese villages were already electrified and about 70% of the households in the electrified villages were connected to the grid [59].

To remedy the aforementioned challenges, the Timorese government created recently a called Strategic Development Plan (SDP) for 20 years whose priorities also include developing the renewable energy sources like biogas, hydropower, solar panel, wind power and biomass-based energy, beyond bringing the petroleum or natural gas development from the sea, through pipelines, to the south coast of Timor-Leste under the *Tasi Mane (male sea)* project (**Figure1.7**). The target is to improve the electrification rate by 2015 (i.e., everybody will have access to electricity during 24h) and to satisfy by 2020 half of the national energy needs with the renewable energy sources and the energy needs of 100000 families with solar energy as the rates of daily global sunlight in entire territory of Timor Leste are always between 14.85 and 22.33 MJ/m² per day [56].

The *Tasi Mane* Project is planned to start in 2015 and to end in 2030, exactly when the number of Timorese population doubles[58]. The success of this project, however, also depends on the decision of Australia as the Greater Sunrise project is currently operated by Woodside, ConocoPhillips, Royal Dutch Shell and Osaka Gas companies. Anyway, so far, the project continues to be a matter of negotiation between Australia and Timor Leste.

Figure 1 7. Male Sea project [56]

.

1.3.2. Prospect of biodiesel development

Since the fossil projects take time to bring benefits to Timor Leste, the development of renewable energy is at present an urgent mission and an adequate solution to improve the electrification rate and mainly to create jobs for Timorese people. Thereat, among the existing renewable energies, biodiesel production has been widely discussed in the country since 2008. The biggest concern linked to this project is about choosing feedstocks without compromising the food supply as circa 80% of Timorese population is subsistence farmers. Fortunately, the Timorese lands offer solutions to avoid the confrontation between food supply and biodiesel production. Beyond some agroforestry wastes, there are oleaginous plants like *Jatropha curcas* (Ahi oan metan in Tetum and pinhão manso in Portuguese) and *Aleurites moluccana* (Kamí in Tetum and Nogueira de Iguapé in Portuguese) that produce oils useful for biodiesel production without compromising the food security.

Jatropha curcas belongs to the family of *Euforbiaceae (***Figure1.8***)*. It has normally a height not superior to 3 m. It requires little water and fertilizer and can grow in arid, marginal and poor lands, is resistant to pests, produces over 30 to 40 years and the seed has a high oil content (30-40%), which is toxic and may not be suitable for human or animal consumption [60]. It is abundant in the Timorese lands and given the current social and environmental situation, its cultivation could contribute to the reforestation of large areas of the country, reduce soil erosion and allow the economic exploitation of marginal lands useless for conventional agriculture and create jobs.

Figure 1 8. Fruits and seeds of *Jatropha curcas*

Aleurites moluccana also belongs to the family of *Euforbiaceae* (**Figure 1.9**). It is an arborescent plant of 20 *to* 30 feet high, but sometimes as high as 100 feet [61]. It can grow in all kinds of terrain, particularly in tropical climates. Its lipid-containing kernel has

been used for illumination, pharmaceuticals, and seasonings, while its seed covered with a hard shell has been used for children's toys or ritual offerings[62]. The seeds contain about 60% oil. Sulistyo et al.[63] already studied at laboratory scale about the viability of producing biodiesel from the oil of *Aleurites moluccana.*

Figure 1 9. Fruits and seeds of *Aleurites moluccana*

As Timor Leste has adequate lands and good climatic condition to promote the cultivation of these plants to be sources of biodiesel production, Timorese government took on the challenge to explore and strengthen the *Jatropha* production with foreign companies. This effort aimed to set Timor Leste at the forefront of the Southeast Asia biofuel producers and mainly create many jobs in Timor Leste. With this in mind, the Enviroenergy Developments Australia (EDA) Company and Daba-Loqui, a Timorese company, signed in 2005 a deal to develop *Jatropha* plantations in Timor-Leste and other territories aiming at building an oil extraction plant in Timor-Leste to extract oil from seeds of the *Jatropha* plant for biodiesel production. The agreement was again updated in 2008 by Timor Leste, giving to the EDA Company a possibility to access to 59 hectares of industrial land on the waterfront at Carabella (Baucau) and to purchase for a 30 year lease, with options to renew for an additional 60 years. The seeds of *Jatropha* would also be imported from Indonesia, the Philippines, Malaysia, Thailand and India. The installation of Biodiesel Extraction and Refining Facility, Jatropha Pellet Facility and Jatropha Pellet Plant would require an estimated capital investment of $550 million dollars over 10 years. The target was to produce 100 million liters of biodiesel oil per year in Timor and to build a biomass power plant at Carabella, as well as a waste treatment facility and potable water supply plant [64].

Regarding *Aleurites moluccana* there is no plan yet about using its oil to produce biodiesel. The use of the seeds for seasoning is common for Indonesia but it is not for

Timor Leste. So the actual final oil extracted by Acelda Company since 2006 in Baucau is exported to Hawaii for cosmetic purposes.

Timor Leste also has abundant coffee plantations especially in the occidental part of the country. It has been crucial to the country's overall economy and has served as the primary source of income for about 25 % of the country's population [65]. The discovery of Nevada researches about producing biodiesel from the coffee waste oil (10-15%)[66] will value the Timorese coffee in the international market. After all, coffee is not only for beverage but could also be used for biofuel production.

1.4. Scopes, objectives and organization of this thesis

This thesis emphasizes globally the rising trend of biodiesel in the international fuel market as alternative fuel for diesel engines and specifically its prospects in Timor Leste. This biofuel has gained a prominent place in the arena of energy, as already introduced above, because petroleum resources are increasingly limited, constantly soaring and sustainability stays frequently in a complex equation namely for the oil-importing countries. Biodiesel can ensure, to them, energy security, economic growth, environmental safety and human-wellbeing as its benefits constitute a potential therapy for the uncertainties of petroleum fuels. For Timor Leste, the expectation is that, the development of a biodiesel refinery will contribute to the alleviation of poverty and deprivation and possibly will place the country at the forefront of biodiesel producers without jeopardizing the environmental wellbeing. The erection of a biodiesel refinery is adequate to the actual social context of Timor Leste because, the revenues from the undersea fossil resources still do not be a Messiah for the country.

Howsoever, to be used as a fuel, pure or blended with petrodiesel, biodiesel must have good quality. So, the study of thermodynamic properties is important for the optimization of the production and processing of biodiesel. Unfortunately, the exhaustive information about them is still scant much less at the working conditions of the diesel engines. Thereat, the aims of this thesis cover two key-issues: production/processing of biodiesel fuels and measurement/prediction of thermodynamic properties of biodiesel (also feed oils and fatty esters). These key-issues are incorporated in five main chapters:

Chapter 1 is the general introductory chapter that already highlighted the global framework of biodiesel potential in the international fuel market and specifically its prospect in Timor Leste for alleviating poverty and deprivation.

Chapter 2 will focus especially on the importance of lipase as catalyst for the production of biodiesel. It presents mainly the basic informations about improving the lipase production in the fermentation of bacteria *Bacillus* sp. ITP-001 using several oxygen vectors and inducers.

Chapter 3 will address the measurement and prediction of thermodynamic properties of biodiesel, feed oils and fatty esters that compose biodiesel. So it will expose, beyond the experimental data of several properties (such as density, viscosity, surface tension, volatility, speed of sound both at wide range of temperatures and pressures), the predictive models capable of computing the experimental data.

Chapter 4 will concern the use of soft-SAFT Equation of State for prediction of the thermodynamic properties of fatty esters and biodiesels like density, surface tension, speed of sound and viscosity at wide range of temperatures and pressures.

Chapter 5 will report the production of biodiesel from oils endogenous of Timor Leste (*Jatropha curcas, Aleurites moluccana* and coffee waste) and also the evaluation of their thermophysical properties using the models already studied in **Chapter 3**.

Chapter 6 and so on will set out the general conclusions, concluding remarks and future works.

CHAPTER 2

Production of lipase by the fermentation of *Bacillus* sp. ITP-001

This chapter discusses in particular the production of lipase by the submerged fermentation of *Bacillus* sp. ITP-001. The initial goal of this part of work was to produce, separate, purify and immobilize lipase for posterior use as catalyst in the enzymatic synthesis of biodiesel. However, as the processing of lipase did not reach the final stage and the enzymatic transesterification was not performed, this chapter only reports the results linked to the production of lipase namely to the effects of inducers (i.e., vegetable oils) and oxygen vectors (perfluorodecalina, dodecane and particles of silica) on lipase activity.

2.1. Introduction

Enzymes are innovative solutions for many bioconversion processes as they work at expense of mild reaction conditions, low energy demand, decrease in side reactions, high degree of specificity and simplicity of post-recovery [67]. Of all known enzymes, lipases (triacylglycerol acylhydrolase, E.C.3.1.3) have attracted most attention due to their broad industrial applications. They catalyze hydrolysis of carboxylic ester bonds and organic synthesis such as esterification, interesterification, alcoholysis, acidolysis and aminolysis [67-69]. Microbial lipases, mainly bacterial and fungal, represent the most widely used enzymes in biotechnological applications and organic chemistry because of their diversity in catalytic activity, high yield and low cost production, as well as relative ease of genetic manipulation [70]. Moreover, they are stable in organic solvents, do not require cofactors and accept a broad range of substrate (*i.e.,* aliphatic, alicyclic, bicyclic and aromatic esters, thioesters and activated amines) whilst maintaining high regio-, chemo- and enantioselectivity [71]. This versatility makes microbial lipases of choice for potential applications in the food, detergent, pharmaceutical, textile, leather, cosmetic, paper industries (for pitch control), waste treatment (breakdown of fat solids) and biodiesel production [67].

The efficiency of lipase production, in solid state fermentation by fungi or in submerged fermentation by bacteria, depends on strain, nutritional and physico-chemical factors such as growth media composition (nitrogen and carbon sources), presence of lipids, inorganic salts and cultivation conditions (pH, temperature, agitation and dissolved oxygen concentration–for aerobic microorganism) [72]. Since lipases are inducible enzymes, their activity is only known in the presence of inducers like oils, lipids and fatty acids [73-77] In aerobic cultures, i.e., when a supply of oxygen is a limiting factor, a high yield is only achieved with a good aeration, which depends greatly on oxygen solubility in the media and diffusion rate into the broths to satisfy the oxygen demand of microbial population. Unfortunately oxygen, unlike other nutrients, is poorly soluble in aqueous media. The solubility of oxygen in water is just 7.95 $mg.L^{-1}$ at 30 ºC [78].

The conventional approach to overcome this limitation involves improved bioreactor design, agitator and sparger as well as the use of oxygen-enriched air. Other solutions may include the manipulation of microbial metabolism through genetic

engineering [79]. A novel approach is the use of water-insoluble oxygen vectors in which oxygen has a greater solubility such as hydrocarbons [80], perfluorocarbons (PFCs) [81, 82], natural and synthetic oils [83] and functionalized magnetic nanoparticles[84]. Beyond enhancing the oxygen transfer rate, without the need for extra energy supply, and preventing foam formation [85], these can act as surface active agents to lower the surface tension of water and increase the gaseous specific interfacial area[86]. Moreover, oxygen vectors avoid the damage of cells (especially mammalian cells) caused by mechanical agitation and air bubbles.[87] PFCs have been applied very successfully in the culture of *Saccharomyces cerevisiae* [88], immobilized *Streptomycescoelicolor* [89], insect cells and virus-infected insect cells[90] and *Yarrowialypolytica*[82, 91]. They are petroleum-based compounds synthesized by substituting the hydrocarbons hydrogen atoms by fluorine. Due to the presence of very strong carbon-fluorine bonds they are non-toxic towards the cells, stable and chemically inert [82]. Their interesting peculiarity is their high solubility of gases. Oxygen solubility in PFCs is 10-20 times higher than that in pure water. [92, 93] Furthermore due to the low solubility of PFCs in water[94], there is no change in the properties of the aqueous phase, while an increase on the oxygen mass transfer is achieved [95] leading to the enhanced performance of the process with an easy recovery of PFCs at the end of fermentation. Beside PFCs, some immiscible organic solvents have also been used with success in fermentation process as oxygen vectors. N-dodecane has been used in the culture of *Crypthecodiniumcohnii* fermentations and DHA production [96] and in the production of L-asparaginase by *Escherichia coli*[85]. Karimi et al.[97] evaluated the capacity of silicon oil to increase the oxygen transfer coefficient (k_La) in the treatment of gas containing benzene, toluene and xylene and found that silicon oil was only beneficial to the process at low concentration. The ability of some suspended hydrophobic particles to enhance the mass transfer were also tested in the adsorption of surfactants where, at low solid loadings, these particles increased significantly the mass transfer rates [98].

This work aims to evaluate the ability of oils of coconut, *Aleurites moluccana*, *Jatropha curcas* and coffee waste as inducers, and the capability of perfluorodecaline, n-dodecane, silica particles and silicon oil as oxygen vectors, to improve the lipase production by *Bacillus* sp. ITP-001. As aforementioned, so far only two works [76, 77] reported the use of this strain to produce lipase, but without oxygen vectors.

2.2. Materials and methods

2.2.1. Inducers

Oils of *Aleurites moluccana* and *Jatropha curcas* were obtained by solid-liquid extraction of the corresponding seeds in a Soxlet unit with 250 mL of n-hexane. Coffee waste oil was obtained by the same process from the wastes collected at the University of Aveiro while coconut oil was purchased from Brazilian market. These oils were always sterilized in autoclave at 121 ºC before being added in 4 % ($v.v^{-1}$) to the culture media.

2.2.2. Oxygen vectors

Perfluorodecaline was purchased from F2 Chemicals Limited. N-dodecane of 99 % purity and silicon oil were purchased from Sigma. These liquids were always sterilized by filtration through 0.45 μm filters and saturated with oxygen before being added to all experiments at inoculation time. Two types of silica particles were used. Particles of silica A were produced in our laboratory with circa 200 nm of diameter while silica B, nanoparticles of silica with 10 nm of diameter, was purchased from Sigma. The particles of silica A were synthesized following the Stober method that is based on the hydrolysis of tetra-alkyl silicate in homogeneous alcoholic medium using ammonia as a catalyst [99].

2.2.3. Strain and media

Bacillus sp. ITP-001 was isolated from soil with a history of contact with petroleum. It was maintained in nutrient agar tubes and stored at 4 °C. The culture media consisted of (% $w.v^{-1}$): starch (2.0), peptone (0.13), yeast extract (0.6), $MgSO_4.7H_2O$ (0.05), $NaNO_3$ (0.3), KH_2PO_4 (0.1), triton X-100 (2.0). The media was always adjusted to pH 5.0 and then sterilized in the autoclave at 121 °C for 22 minutes.

2.2.4. Cultivation conditions

The experiments were carried out in 250-mL Erlenmeyer flasks on an orbital shaker at 32 °C. Each flask was filled with 100 mL of culture media. To this, a known amount of the oxygen vector was added, before being inoculated with 10 % ($v.v^{-1}$) of an inoculum of 48 h old. At 72 h of fermentation, the inducer was added to the broth and the culture was carried up to 168 h.

2.2.5. Analysis

2.2.5.1. Lipase activity assay

The lipase activity was assayed in accordance with the methodology of Soares *et al*.[100] using olive oil as substrate. This was initially prepared as an emulsion of olive oil and water (50:50) with arabic gum (7 %). Then 2 mL of sodium phosphate buffer (0.1 M, pH 7.0) were added to 5 mL of this emulsion. This mixture was stirred at 100 rpm on an orbital shaker at 37 °C. An aliquot of 1 mL of enzyme solution was added and the reaction occurred for 5 min. A sample of 0.33 mL of reaction solution was withdrawn and added to 2 mL of acetanolic solution (water: ethanol: acetone, 1:1:1) to stop the reaction. This mixture was then titrated with a potassium hydroxide solution using phenolphthalein as indicator. One unit of enzyme activity (U) was defined as the amount of enzyme that liberates one μmol of free fatty acids per minute (μmol.min-1) under the assay conditions.

2.2.5.2. Cell biomass, protein and starch

Cell growth biomass was measured by using centrifugation (2500 rpm, 10 min) followed by drying in the oven (105 ºC) until constant weight. Biomass was expressed as mg of cell dry weight per millilitre. Analyses of protein and starch were performed according to the Bradford method [101] and Soccol method [102] respectively.

2.2.5.3. Emulsion stability

The emulsion stability was measured according to the method of Lima *et al*.[103].The emulsion was prepared by mixing 50 μL of oil with 12.5 mL of the culture media. This mixture was then shaken during two minutes at room temperature and paused for 10 minutes before reading its absorbance at 540 nm over time. The blank contained only the culture media. The decay constant (k_d) is the slope of the ln (Abs) versus time. The lower value of this parameter the higher the stability of the emulsion.

2.2.5.4. Experimental design and statistical analysis

To study the effect of perfluorodecaline concentration and agitation rate on lipase production, an Experimental Design of 2^2 factorial with three replications at the central point was carried. The experimental data were then analyzed with *Statistica*®, version 7.0 to obtain surface response and Pareto diagram.

2.2.5.5. Kinetic parameters

Some kinetic parameters namely the specific rate of growth (μ in h^{-1}); the specific rates of substrate consumption and product formation (*qs* and *qp*in $g.g^{-1}.h^{-1}$) and the yield factors of dry cell biomass and protein ($Y_{X/S}$ and $Y_{P/S}$ in $g.g^{-1}$) were determined at the conditions of maximum productivity of lipase using the Eqs. 2.1- 2.5, where *X, S* and *P* represent biomass, substrate (starch) and product (enzyme) respectively.

$$\mu = \frac{\Delta X}{X \Delta t} \quad (2.1)$$

$$q_S = \frac{\Delta S}{X \Delta t} \quad (2.2)$$

$$q_P = \frac{\Delta P}{X \Delta t} \quad (2.3)$$

$$Y_{X/S} = \frac{\Delta S}{\Delta X} \quad (2.4)$$

$$Y_{P/S} = \frac{\Delta P}{\Delta X} \quad (2.5)$$

2.3. Results and discussion

2.3.1. Effect of inducers

As mentioned above, lipase activity in the fermentation broth is only observed in presence of an inducer that can be oil or a fatty acid. Thereat, many works have studied the influence of vegetables oils and fatty acids in various fermentation processes. Dalmau et al.[73] and Lakshami et al.[74] reported that the highest yields of enzyme were obtained with lipids or fatty acids as carbon sources where the amount of lipase secreted correlated well with the relative percentage of C18:n fatty acid esters, namely oleic acid (C18:1), present in the respective oils. Obradors et al.[75] also observed that C18:1 as inducer was beneficial for lipase production by *Candida rugosa*. Only Makhzoum et al.[104] found a repressing effect of C18:1 on the production of lipase by *Pseudomonas Fluroescens* 2D. These results show that the ability of inducers to improve lipase production depends also on the type of strain used. Certain inducers can be beneficial for a strain but prejudicial for others.

This work evaluated the induction ability of four different oils (coconut oil, coffee waste oil, *Aleurites moluccana* oil and *Jatropha curcas* oil) on lipase production by

Bacillus sp. ITP-001. The cultivation occurred at 200 rpm and the amount of oil used was 4 % ($v.v^{-1}$). The run with coconut oil (without oxygen vector) was used as control. This strain was already used in previous works by Carvalho et al.[76] to evaluate the induction ability of coconut oil, olive oil and castor oil, having obtained the lipase activity of 1675, 1200 and 1400 $U.mL^{-1}$,respectively and by Feitosa et al.[77] that achieved 4370 $U.mL^{-1}$ of lipase activity using palm oil.

In this work, when coconut oil was used as inducer, the maximum lipase activity obtained was 1642 $U.mL^{-1}$ which is consistent with that reported by Carvalho et al. [76] (1675 $U.mL^{-1}$). The corresponding maximum biomass (0.36 $mg.mL^{-1}$), however, was much higher than that of Carvalho (~0.070 $mg.mL^{-1}$), evincing that, although lipase is a growth - associated product, there is no linear correlation between cell growth and lipase production by the strain here used. Using other oils, the lipase activities obtained were 2249, 2112 and 1630 $U.mL^{-1}$, respectively for coffee waste oil, *Aleurites moluccana* oil and *Jatropha curcas* oil. **Figure 2.1** shows the profile of lipase activity over the fermentation time for the four inducers studied. The maximum lipase activity was obtained between 120 and 144 h of fermentation time.

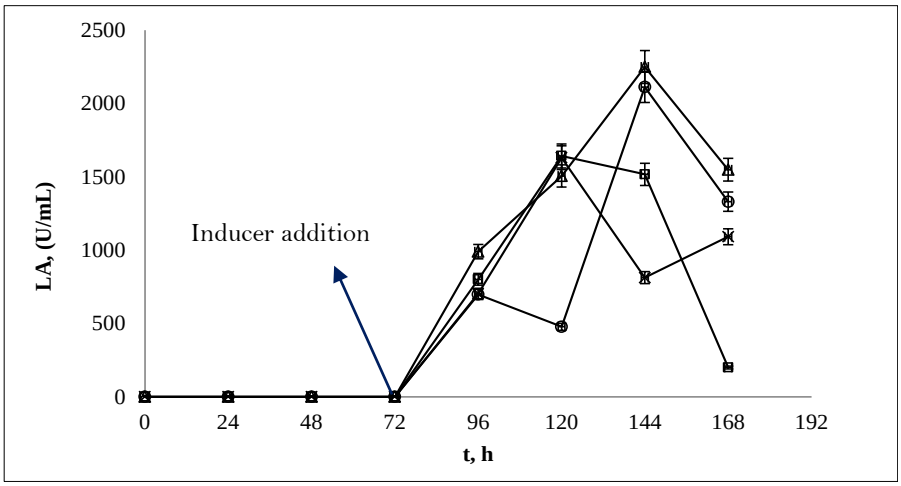

Figure 2 1. Profile of lipase activity for four inducers used in the culture of *Bacillus* sp. ITP-001. Coconut oil, coffee waste oil, Aleurites moluccana oil and Jatropha curcas oil

So far it is known that inducers are important for the production of lipase, some being better than others. Instead of using the oil composition to discuss the results as some works did, in this work we used the emulsion stability, represented by the decay constant (k_d), to justify the discrepancy in lipase activities between the inducers based on the principle that only a stable emulsion reduces the size of oil drops and the respective surface

tension in water-oil to enable the better contact with microorganism and consequently guarantee an easy assimilation of respective oil as carbon source for the bacteria. **Table 2.1** shows that coffee waste oil formed a stable emulsion with the media, presenting a smaller k_d and thus higher lipase activity, followed by *Aleurites moluccana* oil and coconut oil while *Jatropha curcas* oil presented higher k_d and lower relative lipase activity. So, the order of emulsion stability matters for the lipase production. In terms of relative values, coffee waste oil increased the lipase activity about 37 % of the control and *Aleurites moluccana* oil about 29 %.

Table 2 1. Decay constant of different inducers and relative lipase activity

Inducers	Control	σ^b	CW	σ	*Am*	σ	*Jc*	σ
$(k_d \times 10^3)$, min^{-1}	4.14		1.46		1.48		13.17	
LA (U/mL)	1642	145.22	2249	431.79	2112	47.95	1630	429.81
Rel-LA (%)[a]	100		137.0		128.6		85.38	

[a]Ratio of lipase activity in media with other inducers to that with coconut oil. The relative lipase activity (Rel-LA) of the control was regarded as 100%. CW, *Am* and *Jc*refer to coffee waste oil, *Aleurites moluccana* oil and *Jatropha curcas* oil, respectively.[b] = Standard deviation

2.3.2. Effect of oxygen vectors

2.3.2.1. Influence of perfluorodecaline concentration and agitation rate

Several works have reported the potential use of perfluorodecaline as oxygen vector in aerobic cultures. Elibol et al.[79] included 50 % of perfluorodecaline in the culture of *Streptomyces coelicolor* A3(2) to increase the maximum antibiotic concentration by a 5-fold. Amaral et al.[91] enhanced lipase production by *Y. lipolytica* by 23-fold at 250 rpm using 20 % ($v.v^{-1}$) PFC and 2 % ($m.v^{-1}$) of glucose as substrate.

Aiming to evaluate the influence of perfluorodecaline concentration (% $v.v^{-1}$) and agitation rate (rpm) in the culture of *Bacillus* sp. ITP-001, this work used the Experimental Design of 2^2 factorial with three replications at the central point to perform the experiments using coconut oil as inducer. The results from here obtained were used to generate Pareto diagram (**Figure 2.2**) which shows that agitation rate was the more influent parameter than perfluorodecaline concentration and the interaction between the parameters had a negligible effect on lipase production.

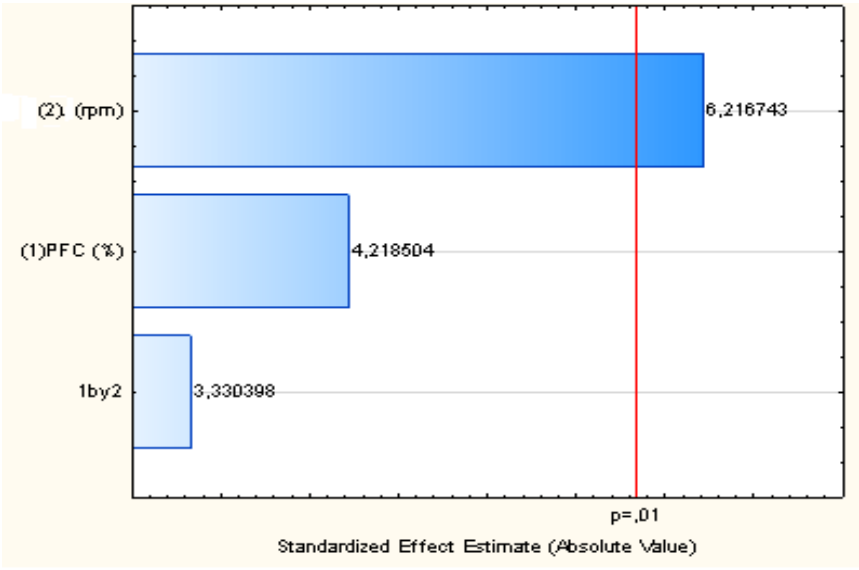

Figure 2 2. Diagram of Pareto for the model tested for lipase activity

The same conclusion was obtained by the ANOVA analysis (**Table 2.2**) through the lower *p*-value for the agitation rate. The response surface curve (**Figure 2.3**) addressed the positive effect of both parameters, i.e., higher lipase activity is obtained at higher concentration of perfluorodecaline and agitation rate.

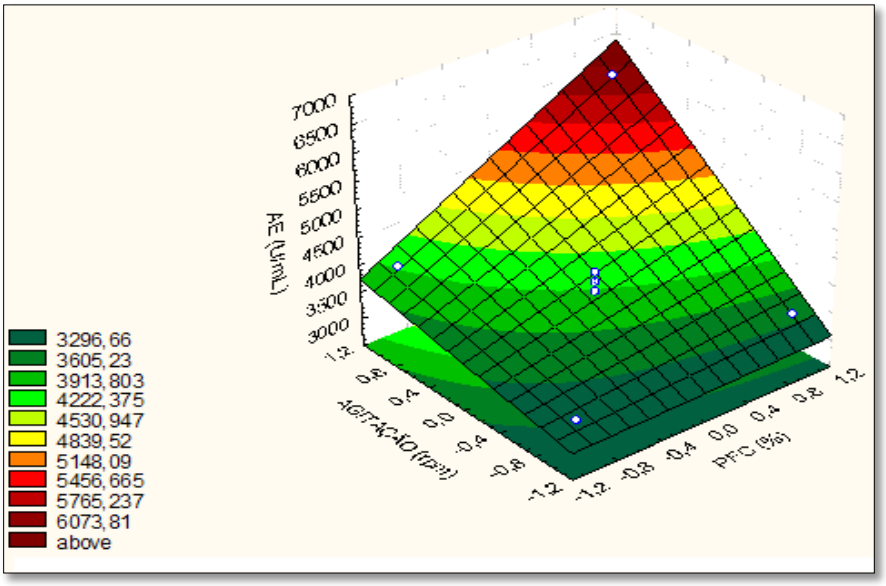

Figure 2 3. Surface curve for the model tested for lipase activity

Table 2 2. Variance analysis (ANOVA)

Factor[c]	SS	df	MS	F	p
Perfluorodecaline (1)	1293713	1	1293713	18.64784	0.022880
Agitation rate (2)	2860039	1	2860039	41.22439	0.007657
1 by 2	791415	1	791415	11.40739	0.043171
error	208132	3	69377		
Total SS	5153299	6			

[c]The correlation factor (R^2) of 0.95961

For an aerobic culture, these results are expected since perfluorodecaline improves the oxygenation of the culture media and higher agitation rate improves the homogeneity of the system, the emulsion stability, the distribution of perfluorodecaline and the bubbles on the system.

The optimal cultivations conditions found for lipase production by *Bacillus* sp. ITP-001 were 20 % ($v.v^{-1}$) of perfluorodecaline and 200 rpm of agitation rate (**Table 2.3**). At this condition, the lipase activity was increased to circa 4-fold of control that is much lower than the value observed by Amaral et al.[90] with *Y. Lipolytica*. This difference shows that the strains have different responses to the oxygen vectors.

Table 2 3. Experimental design for assessing the effect of perfluorodecaline concentration and agitation rate on production of lipase

Experiment[d]	C1 (%)	C2 (rpm)	C1 (code)	C2(code)	LA (U/mL)
1	10	100	-1	-1	3200.7
2	20	100	+1	-1	3448.5
3	10	200	-1	+1	4002.3
4	20	200	+1	+1	6029.3
5	15	150	0	0	4052.3
6	15	150	0	0	3877.4
7	15	150	0	0	3702.5

[d]C_1 is the concentration of perfluorodecaline and C_2 is the agitation rate.

2.3.2.2. Influence of perfluorodecaline in presence of different inducers

Using the optimal operating conditions identified using the Experimental Design described above, the effect of perfluorodecaline on lipase production were also studied in presence of several inducers namely oils of *Aleurites moluccana, Jatropha curcas* and coffee waste. The results, shown in **Table 2.4**, indicate that the inclusion of 20 % ($v.v^{-1}$)

perfluorodecaline in the culture media increased the lipase activity to more than 2-fold of the control, for all inducers.

Table 2 4. Effect of different inducers on lipase production in the presence of 20 % (v/v) perfluorodecaline

Inducer	Control	σ	Coconut	σ	Cw	σ	*Am*	σ	*Jc*	σ
X (mg/mL)	0.36	0.17	1.23	0.16	2.30	0.03	5.75	3.7	1.36	0.23
Rel-LA (%)	100		367.2		284.8		273.4		185.4	

Based on the order of emulsion stability, it was expected that coffee oil would present higher lipase activity than other oils in the presence of perfluorodecaline. The results, however, revealed that, in the presence of perfluorodecaline, coconut oil increased lipase activity to circa 4-fold of the control, even if it formed less stable emulsions when compared with coffee waste oil. In cultures aerated by oxygen vectors the emulsion stability is no longer the only explanatory parameter for the inducer effect. Regarding the cell growth, as shown in **Figure 2.4** below, the results support the absence of dependence between cell growth biomass and lipase activity for the culture of *Bacillus* sp. ITP-001.

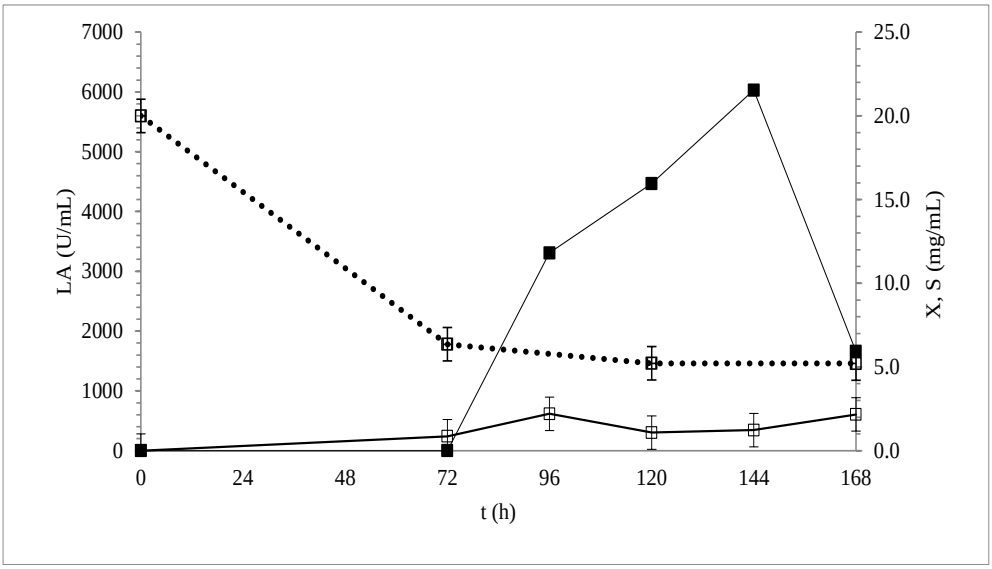

Figure 2 4. Profile of starch, dry cell biomass and lipase activity for the culture of Bacillus sp.ITP-001 at 200 RPM using 20 % C10F18 and 4 % (v/v) of coconut oil. —■— Lipase Activity (LA), —□— Dry cell biomass (X) and ···□··· Starch consumption (S)

The profiles of starch, dry cell biomass and lipase activity for the coconut oil in the presence of 20 % perfluorodecaline are shown in **Figure 2.4**. In general, as expected, there was consumption of starch, increase of biomass and lipase production over the

fermentation time. A situation of diauxia (sequential consumption of two substrates) was observed even with low intensity.

The kinetics parameters for the fermentation with several inducers in presence of perfluorodecaline were determined under conditions of maximum production of lipase and the results are shown in **Table 2.5**.

Table 2 5. Kinetic parameters for different inducers

Parameter	Unit	Coconut	*Am*	*Jc*	CW
μ	h-1	0.007	0.007	0.008	0.007
q_s	g/g.h	0.088	0.022	0.005	0.044
q_p	g/g.h	34.04	5.42	0.96	14.12
Yx/s	g/g	0.079	0.314	1.544	0.157
Yp/s	g/g	387.57	245.13	178.09	319.83

They indicate that the specific rate of growth (***μ)*** is similar for all inducers. The specific rates of substrate consumption (q_s) and product formation (q_p), on the other hand, are dissimilar for the various inducers studied and the higher values were obtained for coconut oil and coffee waste oil. This fact echoed in high yields of lipase (*Yp/s***)** obtained with these oils. Again the results indicate that there is no linear correlation between the cell growth biomass and the lipase production as even though the yield of biomass (*Yx/*s) is low for coconut oil (0.079 $g.g^{-1}$), the production of lipase is high (387.57 $g.g^{-1}$). Theoretically, a linear dependency of lipase production on cell growth biomass can be expressed by the mixed model of Luedeking et al.[105] presented in Eq. (2.6) below, were α and β are the fitting parameters. Many works have reported lipase production to be a microbial growth associated product. Puthli et al.[106], for example, dealt with a linear dependency of lipase production on cell growth in the culture of *Candida rugosa*.

$$q_p = \alpha\mu + \beta \qquad (2.6)$$

However, the non association between cell growth and lipase production observed in this work is not an extraneous case and has been reported by other authors. Deive et al.[107] studied the culture of aerobic *Bacillus* strain and verified that lipase production was found not to be a microbial growth associated product. This situation happened when the lipase activity is detected just at the stationary growth phase.

2.3.2.3. Influence of other oxygen vectors in presence of different inducers

Other oxygen vectors like silica particles, n-dodecane and silicon oil were also evaluated in presence of coconut oil for their ability to improve lipase production by *Bacillus* sp. ITP-001. The runs were carried at 200 rpm. Hydrophobic particles, n-dodecane and silicon oils were previously reported to enhance the mass transfer rates in some fermentation processes[97, 98].

Using silica particles as oxygen vector, two different behaviors were observed. For the larger particles (silica A), lipase activity increased for the lower silica concentrations up to 0.12 g and then decreased with the increasing amount of particles as shown in **Table 2.6**.

Table 2 6. Influence of silica A in Lipase production

Silica A (g)	Control	σ	0.12	σ	0.15	σ	0.30	σ	0.50	σ
X (mg/mL)	0.36	0.17	2.98	0.55	9.63	0.0	6.23	0.05	8.64	0.81
Rel-LA (%)	100		129.2		108.2		102.6		99.5	

For the best conditions an enhancement of about 30% on the lipase production was observed. The opposite effect was observed for the smaller particles (silica B). For these the lipase activity was severely compromised but recovered with the increasing amount of particles in the culture media as shown in **Table 2.7**.

Table 2 7. Effect of silica B on Lipase production

Silica B (g)	Control	σ	0.05	σ	0.10	σ	0.15	σ	0.20	σ
X (mg/mL)	0.36	0.17	3.79	0.75	4.18	1.97	3.09	0.06	7.51	2.80
Rel-LA (%)	100		43.5		47.1		69.6		85.4	

Regarding the n-dodecane and silicon oil, the results are shown in **Table 2.8** for a 20 % ($v.v^{-1}$) and compared with perfluorodecaline. An increase of around 11 % of in the lacase activity was observed with n-dodecane while Silicon oil, had a repressing effect on lipase production. Kaya et al.[98] suggest that only concentrations below 10 % silicon oil are beneficial for increasing oxygen mass transfer. This may explain the poor result observed on this work.

Table 2 8. Effect of other oxygen vectors on Lipase production in presence of coconut oil

Oxygen vector	Control	σ	C10F18	σ	C12H26	σ	Silicon oil	σ
X (mg/mL)	0.36	0.17	1.23	0.16	0.56	0.24	3.29	1.0
Rel-LA(%)	100		367.2		111.1		67.5	

2.4. Conclusions

The influence of various inducers and oxygen vectors on the production of lipase by *Bacillus* sp. ITP-001 was here studied. It is here shown that the production process can be improved by using perfluorodecaline as oxygen vector and the optimal operating conditions here obtained were 20 % ($v.v^{-1}$) of perfluorodecaline concentration and 200 rpm of agitation rate. At this conditions, perfluorodecaline increased the lipase activity to circa 4-fold. Regarding other oxygen vectors, n-dodecane enhanced the lipase activity by about 11 % and silica A by about 29 % while silicon oil and silica B had a repressing influence in lipase production. About the induction ability, without oxygen vectors, coffee waste oil was better than other oils here studied due to its higher emulsion stability. In presence of perfluorodecaline, coconut oil revealed to be the best inducer and the emulsion stability ceases to be the unique explanatory parameter.

In all cases there no direct correlation was observed between the cell growth biomass and lipase activity. The optimal conditions for lipase production seem thus to be using 20 % ($v.v^{-1}$) of perfluorodecalin with coconut oil as inducer.

CHAPTER 3

Thermodynamic properties of biodiesels, fatty esters and feed oils: measurement and prediction

One of the key-challenges linked to the use of biodiesel is that its properties may not be concordant with those established in the standards. The knowledge of thermodynamic properties becomes crucial for process modeling and product design of biodiesel manufacturing. Thereat, this chapter provides experimental data of several properties like density, viscosity, vapor pressure, surface tension and speed of sound for biodiesel, fatty esters and also feed oils as well as methods capable of predicting them at a wide range of temperatures and pressures. The ester nomenclature adopted throughout this chapter is based on the fatty acid chain length. **A $C_{x:y}$ ester means the alkyl ester of fatty acid with x carbons and y unsaturations**.

3.1. Relevance of studying thermodynamic properties

Despite the many promising advantages and merits that biodiesels can offer to override the uncertainties of petrodiesel, to be used in diesel engines, however, their properties must be coherent with those specified in the standards [108, 109] in order to guarantee suitable ignition, atomization and combustion of this fuel in diesel engines. This means that all the steps involved in the manufacturing of biodiesel, since the processing of feedstocks (oils or fats) until the purification of the product, must be always carried out at the optimum conditions. In this regard, the knowledge of the thermodynamic properties of biodiesel, feed oils and fatty esters (that compose biodiesels) become crucial not only for designing the better technology for biodiesel manufacturing but also for enhancing the engine performance.

The knowledge of thermodynamic properties is also relevant for high-pressure technology. This, commonly coupled with thermal processing, has been used in many engineering applications such as in food processing to achieve stable food products, additive free and microbiologically safe, as the constituents and the contaminants of food can be controlled under this condition,[110-114] and in the fuel industry to get low pollutant levels and lower fuel consumption through the enhancement of combustion process using of the common rail fuel injection system [115-117]. High-pressures in the processing of vegetable oils are used for their extraction from the corresponding seeds, the fractionation of their constituents with supercritical fluids [118-120] and also for the production of biodiesels at near or supercritical conditions [121, 122].

The supercritical fluid extraction of oil from seeds, in special, is already considered to be more beneficial than the conventional technology as it does not require the distillation and the solvent removal processes normally involved in the conventional extraction [123]. Moreover, the efficiency of the extraction is simply controlled by the pressure and/or the temperature of operation , the contact time and the solubility of the oil in the extracting fluids[124]. This feature can be also applied for the extraction of oil constituents with supercritical fluids as already addressed elsewhere in the literature[125, 126].

Regarding biodiesel, it is known that transesterification with supercritical alcohol constitutes a better technical approach to the conventional catalytic transesterification of low quality feedstocks [127] as the alkaline-catalyzed transesterification is very sensitive

to the purity of the reactants[128]. Moreover, the injection of biodiesel in diesel engines is usually done at very energetic conditions. This chapter aims to provide experimental data of several properties like density, viscosity, surface tension, vapor pressure and speed of sound either for biodiesel, fatty esters or feed oils and ultimately to recommend methods capable of predicting each property at wide range of temperatures and pressures.

In all studies, the predictive ability of the models studied is evaluated by simply calculating the relative deviations (RDs) between predicted and experimental data according to Eq. (3.1.1). Afterwards, the overall average relative deviation (OARD) was calculated through Eq. (3.1.2), where N_s is the number of systems studied and the average relative deviation (ARD) is the summation of the modulus of RD over N_p experimental data points.

$$RD\,(\%) = \frac{calc_i - \exp_i}{\exp_i} \times 100 \tag{3.1.1}$$

$$OARD(\%) = \frac{\sum_n ARD}{N_s} \tag{3.1.2}$$

3.2. Measurement and prediction of biodiesel density

3.2.1. Density of methylic biodiesels

The production and the measurement of atmospheric density for ten methylic biodiesel samples used in this work were carried out at our Laboratory by Dr. Maria Jorge Pratas. The complete work is already published as paper in the journal of Energy & Fuels [129]. The fitting of the parameters for Revised GCVOL method was also done by her. The measurement of high-pressure density was done in Spain at the University of Vigo by Prof. Manuel Piñeiro and his group. This section only reports my direct contribution to the paper that was the prediction of high-pressure density of biodiesel fuels using **the revised GCVOL group contribution method**.

3.2.1.1. Introduction

Density is an important property for a fuel because injection systems, pumps and injectors must deliver an amount of fuel precisely adjusted to provide proper combustion [130]. So it influences the amount of mass injected in diesel engines [131] [132]. Density data is important in numerous unit operations in biodiesel production and required to be known to properly design reactors, distillation units and separation process, storage tanks and process piping [133, 134]. The magnitude of density depends on the raw materials used for biodiesel fuel production and on the biodiesel alkyl esters profile [135]. So the capacity to correctly predict biodiesel densities from the composition of fatty esters is of major relevance for a correct formulation of an adequate blend of raw materials aiming at producing biodiesel according to the required quality standards [136, 137] with the lowest production costs.

This section used the new experimental density data for ten biodiesel samples measured at temperatures from 278.15 to 373.15 K to assess the adequacy of revised GCVOL group contribution method for predicting the high-pressure densities of biodiesel fuels.

3.2.1.2. Experimental section

3.2.1.2.1. Biodiesel sample synthesis

Ten biodiesel samples were here studied. Two of these samples were obtained from Portuguese biodiesel producers, namely Soy A and GP (Soybean+Rapeseed). Eight biodiesel samples were synthesized at our laboratory by a transesterification reaction of the vegetal oils: Soybean (S), Rapeseed (R), and Palm (P), and their respective binary and ternary mixtures: Soybean+Rapeseed (SR), Rapeseed+Palm (RP), Soybean+Palm (SP), and Soybean+Rapeseed +Palm (SRP) and Sunflower (Sf). The molar ratio of oil/methanol used was 1:5 with 0.5% sodium hydroxide by weight of oil as catalyst. The reaction was performed at 55 ºC during 24 h under methanol reflux. The reaction time chosen was adopted for convenience and to guarantee a complete reaction conversion. Raw glycerol was removed in two steps, the first after 3 h reaction and then after 24 h reaction in a separating funnel. Biodiesel was purified by washing with hot distillated water until a

neutral pH was achieved. The biodiesel was then dried until the EN ISO 12937 limit for water was reached (less than 500 ppm of water). The water content was checked by Karl-Fischer titration.

3.2.1.2.2. Determination of FAME composition

The composition of the fatty acid esters in these biodiesels was analyzed using a capillary gas chromatography flame ionization detector (GC-FID). This equipment is a Varian CP-3800 with a FID in a split injection system with a Varian GC column CP 9080 select biodiesel for fatty acid methyl esters (FAME) column (30 m× 0.32 mm × 0.25 μm). The column temperature was set at 120 ºC and then programmed to increase up to 250 ºC at 4 ºC/min. The detector and injector were set at 250 º C. The carrier gas was helium with a flow rate of 2 mL/min.

3.2.1.2.3. Density measurement

Atmospheric density was measured at our Laboratory in the temperature range of 278.15 to 373.15 K and at atmospheric pressure using an automated SVM 3000 Anton Paar rotational Stabinger Viscometer. The apparatus was equipped with a vibrating U-tube densimeter. The absolute uncertainty of the density is 0.0005 $kg \cdot m^{-3}$. The SVM 3000 uses Peltier elements for fast and efficient thermostability. The temperature uncertainty is ±0.02 K from 288.15 to 378.15 K. The SVM was previously tested for other compounds and presented a very good reproducibility [136, 138]. The instrument was rinsed with ethanol three times and then pumped in a closed circuit at constant flow of the solvent during twenty minutes at 323 K. This cleaning cycle was repeated with acetone and then kept at 343 K for thirty minutes under a stream of air to ensure that the measurement cell was thoroughly cleaned and dried before the measurement of a new sample.

The experimental procedure of high-pressure density measurement is already described elsewhere [139-141]. An Anton Paar 512P vibrating tube densimeter, connected to an Anton Paar DMA 4500 data acquisition unit was used for this purpose. Temperature stability was ensured with a PolyScience 9510 circulating fluid bath, and the temperature value was determined with a CKT100 platinum probe placed in the immediacy of the density measuring cell, with an uncertainty that has been determined to be lower than$5\times10^{-}$

^{2} K. The pressure was generated and controlled using a Ruska 7610 pressure controller, whose pressure stability is 2 $\times 10^{-3}$ MPa. This device determines the vibration period of a metallic U-shape cell filled with the studied fluid, which is directly linked to the sample fluid density. The repeatability in the density values determined from the vibration period measured by the DMA 4500 unit is 10^{-5} g.cm^{-3}. The combinations of density determination repeatability and the accuracies in temperature and pressure measurement lead to an overall experimental density uncertainty value that is lower than 10^{-4} g.cm^{-3}.

3.2.1.3. GCVOL group contribution method

GCVOL method is a group contribution method developed for the prediction of molar volumes of liquids. This method fractionates the molecule into various functional groups and then uses the molar volume of each group to estimate the density of the molecule according to the Eq. (3.2.1) where x is the molar fraction, Mw (g/mol) is the molecular weight and V (g/cm^3) is the molar volume.

$$\rho = \frac{\sum_i x_i Mw_i}{\sum x_i V_i} \tag{3.2.1}$$

The oil molecular weight is calculated from the measured average composition of fatty acids using Eq. (3.7.8) while the molar volume is estimated using the Eq. (3.2.3).

$$V = \sum_i n_i \Delta v_i \tag{3.2.3}$$

In Eq. (3.7.13) n_i is the number of groups i, and the temperature dependency of the molar group, Δvi (cm^3 mol^{-1}), is given by the polynomial function described in Eq. (3.2.4) where T can vary between the melting point and the normal boiling point when the model is used to predict densities of solvents.

$$\Delta v_i = A_i + B_i T + C_i T^2 \tag{3.2.5}$$

According to the parameters Ai, Bi, and Ci used the GCVOL method can be divided in three different versions: The original version uses the parameters reported by Elbro et al.[142] The extended version uses the parameters reported by Ihmels et al.[143] and the revised version use new values for A_i, B_i and C_i for the double bond parameter (–CH=) that were estimated based on the density data for fatty acid esters reported in previous works of

ours [136, 137]. The parameters for the three versions of GCVOL method are presented in **Table 3.2.1**.

Table 3.2 1. Parameters used in GCVOL methods

	GCVOL								
	Original				Extended				Revised
	CH2	CH3	CH=	COO	CH2	CH3	CH=	COO	CH=
A	12.52	18.96	6.761	14.23	12.04	16.43	-1.651	61.15	11.43
B / 10^3	12.94	45.58	23.97	11.93	14.1	55.62	93.42	-248.2	6.756
C / 10^5	0	0	0	0	0	0	-14.39	36.81	0

3.2.1.4. Results and discussion

Table 3.2.2 reports the FAME composition of the studied biodiesels. Palm biodiesel is the most saturated and the sunflower biodiesel the least. New experimental density data for eight biodiesels synthesized in this work and for two industrial biodiesels are reported in **Table 3.2.3**. For palm oil biodiesel, measurements were only carried at temperatures above its cloud point.

Table 3.2 2. FAME Composition of the biodiesels studied, in mass fraction

FAME	S	R	P	SR	PR	SP	SRP	Sf	GP	SoyA
C10:0		0.01	0.03		0.02	0.01	0.01			
C12:0		0.04	0.24	0.03	0.20	0.18	0.14	0.02	0.02	
C14:0	0.07	0.07	0.57	0.09	0.54	0.01	0.38	0.07	0.13	
C16:0	10.76	5.22	42.45	8.90	23.09	25.56	18.97	6.40	10.57	17.04
C16:1	0.07	0.20	0.13	0.15	0.17	0.11	0.14	0.09	0.13	
C18:0	3.94	1.62	4.02	2.76	3.02	4.04	3.28	4.22	2.66	3.73
C18:1	22.96	62.11	41.92	41.82	52.92	33.13	42.51	23.90	41.05	28.63
C18:2	53.53	21.07	9.80	37.51	15.47	31.72	27.93	64.16	36.67	50.45
C18:3	7.02	6.95	0.09	7.02	3.08	3.58	4.66	0.12	7.10	
C20:0	0.38	0.60	0.36	0.46	0.49	0.39	0.45	0.03	0.44	
C20:1	0.23	1.35	0.15	0.68	0.67	0.20	0.52	0.15	0.67	
C22:0	0.80	0.35	0.09	0.46	0.24	0.32	0.33	0.76	0.45	
C22:1	0.24	0.19	0.00	0.12	0.09	0.12	0.14	0.08	0.12	
C24:0		0.22	0.15			0.63	0.53			

Table 3.2 3. Experimental density, in kg·m-³, for methylic biodiesels

T / K	S	R	P	SR	RP	SP	SRP	Sf	GP	SoyA
278.15	894.6	893.3		893.2	889.5		890.4	894.8	891.8	
283.15	890.9	889.6		889.5	885.8	885.7	886.7	890.9	888.0	888.4
288.15	887.3	886.0	877.9	885.7	882.1	882.0	883.0	887.2	884.3	884.7
293.15	883.6	882.3	874.1	882.0	878.4	878.2	879.3	883.5	880.6	881.0
298.15	880.0	878.6	870.4	878.3	874.7	874.5	875.6	879.8	876.9	877.3
303.15	876.3	875.0	866.7	874.7	871.1	870.9	871.9	876.2	873.2	873.6
308.15	872.7	871.3	863.0	871.0	867.4	867.2	868.2	872.6	869.6	870.0
313.15	869.0	867.7	859.4	867.3	863.7	863.5	864.6	868.9	865.9	866.3
318.15	865.3	864.1	855.7	863.7	860.1	859.9	860.9	865.3	862.2	862.7
323.15	861.7	860.4	852.1	860.1	856.5	856.3	857.3	861.6	858.6	859.0
328.15	858.0	856.8	848.5	856.4	852.8	852.6	853.6	858.0	855.0	855.4
333.15	854.3	853.2	844.9	852.8	849.2	849.0	850.0	854.4	851.4	851.8
338.15	850.7	849.5	841.2	849.2	845.5	845.4	846.4	850.7	847.7	848.2
343.15	847.0	845.9	837.6	845.6	841.9	841.8	842.8	847.1	844.1	844.5
348.15	843.4	842.3	834.0	842.0	838.2	838.1	839.2	843.5	840.5	840.9
353.15	839.8	838.7	830.4	838.4	834.6	834.5	835.6	839.9	836.9	837.3
358.15	836.1	835.0	826.8	834.9	830.9	831.0	832.0	836.3	833.3	
363.15	832.5	831.4	823.2	831.3	827.3	827.4	828.4	832.8	829.8	

The experimental data show that the density of biodiesels decreases with increasing temperature and with the level of unsaturation of the FAMEs, as expected from previous works [136, 137] where the same behavior for pure compounds was observed. Pratas et al.[129] used the experimental data to assess the ability of the GCVOL methods to predict atmospheric densities of biodiesel fuels. The results showed that the revised GCVOL method was the most adequate, presenting only an OARD of 0.17 % for ten biodiesel studied as seen in **Table 3.2.4**

Table 3.2 4. ARDs for biodiesels estimated with GCVOL methods

	GCVOL		
Biodiesel	Original	Extension	Revised
S	0.75	4.0	0.039
R	0.79	2.1	0.17
P	0.35	4.0	0.068
SR	0.59	2.8	0.093
RP	0.43	1.2	0.046
SP	1.0	0.54	0.51
SRP	0.96	1.0	0.42
Sf	0.78	4.2	0.043
GP	0.47	2.5	0.24
SoyA	0.52	1.7	0.036
OARD%	**0.66**	**2.4**	**0.17**

The revised GCVOL method was then extended to high pressures using an approach previously proposed by Gardas et al. [144] for ionic liquids and described by Eq. 3.2.6.

$$\rho(T,P) = \frac{Mw}{V(T)\cdot(1+cP)} \tag{3.2.6}$$

where ρ is the density in g/ cm^3, *Mw* the molecular weight in g/mol, *V(T)* the molar volume in cm^3.mol^{-1} predicted by GCVOL, *P* the absolute pressure in MPa and *c* a fitting parameter. Experimental high pressure densities of three methyl esters (laurate, myristate and oleate) reported by us elsewhere[141] were used to estimate the c parameter with a value of -5.7×10^{-4} MPa^{-1}, describing high pressure densities of the methyl esters with average deviations of 0.37 % as reported in **Table 3.2.5**. Equation 3.2.6, using this c value, was then used to predict high pressure densities for seven biodiesel fuels studied by Pratas et al. [141] The relative deviations (RDs) between experimental and predicted densities as function of pressure at 293.15 K are presented in **Figure 3.2.1**. The ARDs for all compounds here studied are presented in **Table 3.2.5**. The OARD of only 0.37 % confirms that the extension to high pressures of the revised GCVOL method here proposed can provide excellent predictions of densities of different biodiesel fuels at high pressure.

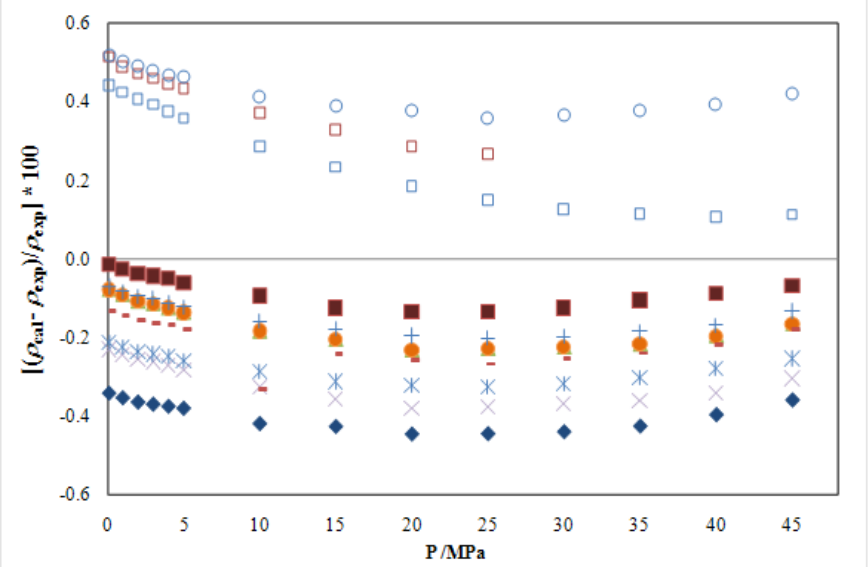

Figura 3.2 1. Relative deviations between experimental and predicted densities as function of pressure at 293.15 K using an extension of GCVOL model for 3 methyl esters and 7 biodiesel fuels [141]. Legend: Legend: ×P, ◆S, ▲R, ✳SR, ●PR, +SP, -SRP, ■Sf, □ MEC12, □ MEC14 and ○ MEC18:1

Table 3.2 5. ARDs for high pressure density of biodiesels and FAME calculated with the revised GCVOL method

Compounds	ARD (%)
C12:0	0.27
C14:0	0.28
C18:1	0.29
P	0.47
S	0.52
R	0.74
Sf	0.23
RP	0.30
SP	0.29
SR	0.40
SRP	0.32
OARD (%)	**0.37**

3.2.2. Density of Ethylic Biodiesels

Two sets of ethylic biodiesels were here studied. The first set includes biodiesels like EEAI (ethyl esters from *Azadinachta indica*), EEJC (ethyl esters from Jatropha oil), EEBA (ethyl esters from *Balanites aegyptica*) and EEWCO (ethyl esters from waste cooking oil). They were produced by Cosseron et al.[145] at the University of Nancy. The second set includes soybean (S), sunflower (Sf), binary mixture of soybean with beef tallow (S+B) and palm (P). These were produced by Prof. Dr. Meirelles and his group at the University of Campinas in Brasil. The measurement of density was done at our Laboratory. This section reports the prediction of density for these fuels using the revised GCVOL group contribution method that already predicted very well the density of methylic biodiesels.

3.2.2.1. Experimental Section

The samples of EEAI (ethyl esters from *Azadinachta indica*), EEJC (ethyl esters from Jatropha oil), EEBA (ethyl esters from *Balanites aegyptica*) and EEWCO (ethyl esters from waste cooking oil) were produced in the LGRP Laboratory (Nacncy, France) by Cosseron et al.[145]. Shortly, they used alkali catalysed-transesterification reaction to convert the oils into biodiesels. The reaction was conducted in a 4-L jacked reactor made of borosilicate glass and equipped with a reflux condenser (operating conditions: 80 °C, 1 wt % EtONa by weight of oil, stirring speed 250 rpm, EtOH :oil molar ratio 6:1). After 2 h of reaction to ensure almost complete conversion of the oil (mass fraction in FAEE of the crude biodiesel obtained at this stage: 91.7 wt %, determined by GC-FID as described in further details below), the reactor was cooled and the two formed layers (a lower phase rich in glycerol and an upper-phase rich in FAEE) were separated by sedimentation and the latter underwent two stages of purification to concentrate the sample. The FAEE composition in biodiesel samples was here analysed again in gas chromatography following the same procedures described in previous **section 3.2.1**.

The samples of soybean (S), sunflower (Sf) and palm (P) were produced by the transesterification of the corresponding oils with ethanol using sodium hydroxide (NaOH) as the catalyst. The amount of NaOH used was 1.0 wt. % of the oil. Oil and ethanol with a mole ratio of 1:6 reacted at 323.15 K for 180 min. A fourth sample consisting of ethylic biodiesel derived from soybean oil and beef tallow (S+B) was supplied by Fertibom (Catanduva, SP, Brazil), a Brazilian company that produces ethylic biodiesel in industrial scale. The fatty acid ethyl esters (FAEE) compositions for all biodiesel samples were determined in triplicate by gas chromatography. The chromatographic analyses were carried out using a GC capillary gas chromatograph system (Agilent, 6850 Series GC System, Santa Clara, CA, USA) under the following experimental conditions: Elite 225 capillary column (PERKIN ELMER, 50% Cyanopropylphenyl-Phenylmethylpolysiloxane, (0.25 μm × 29 m × 0.25 mm); helium as carrier gas at a flow rate of 2.17×10^{-8} m^3/s; injection temperature of 523 K; column temperature of 373 K for 120 s, 373–503 K (rate of 7 K/60 s), 503 K for 600 s; detection temperature of 523 K; and injection volume of 1.0 μL. The fatty acid ethyl esters were identified by comparison with external standards purchased from Nu Check Prep (Elysian, MN, USA). Quantification was done by internal normalization.

The measurement of density was done in the temperature range of 288.15 to 368.15 K and at atmospheric pressure using an automated SVM 3000 Anton Paar rotational Stabinger Viscometer following the same procedure described in **Section 3.2.1.**

3.2.1.1. Results and discussion

The FAEE compositions of the ethylic biodiesels are presented in **Table 3.2.6** where the EEWCO is the most unsaturated biodiesel and P is the less unsaturated one.

Table 3.2 6. FAEE composition of biodiesels in mass percentage

	Mass fraction							
FAEE	EEWCO	EEBA	EEAI	EEJC	S	Sf	S+B	P
C8:0	-	-	-	-	-	-	-	0.03
C10:0	0.11	0.09	0.00	0.00	-	-	-	0.03
C12:0	0.14	0.29	0.42	0.00	-	-	0.03	0.42
C14:0	0.10	0.11	0.48	0.08	0.07	0.09	0.30	0.72
C16:0	6.98	18.22	21.84	23.09	10.92	5.66	11.81	38.67
C16:1	0.16	0.16	0.00	1.32	0.08	0.09	0.16	0.15
C18:0	0.00	8.11	7.21	4.75	2.93	3.11	3.23	4.49
C18:1	84.73	31.37	40.89	41.66	27.45	35.32	27.53	44.51
C18:2	5.53	41.64	29.16	29.10	52.65	54.46	49.90	10.29
C18:3	0.18	0.00	0.00	0.00	4.96	0.28	5.87	0.26
C20:0	0.18	0.00	0.00	0.00	0.29	0.20	0.31	0.25
C20:1	0.38	0.00	0.00	0.00	0.18	0.13	0.20	0.10
C22:0	0.46	0.00	0.00	0.00	0.37	0.49	0.44	0.04
C22:1	0.75	0.00	0.00	0.00	-	0.04	0.08	0.03
C24:0	0.30	0.00	0.00	0.00	0.099	0.14	0.15	0.02

The experimental density and viscosity of the eight biodiesels here studied are presented in **Table 3.2.7** where, as expected, the EEWCO biodiesel, being the highly unsaturated, has higher density than other samples while biodiesel P has lower density as it is more saturated than others.

Table 3.2 7. Experimental density of biodiesel

	ρ, kg. m-3							
T, K	EEWCO	EEJC	EEBA	EEAI	S	Sf	S+B	P
288.15	890.9	878.8	880.0	876.0	881.0	880.2	880.8	871.4
293.15	887.2	875.0	876.2	872.3	877.3	876.5	876.9	867.6
298.15	883.5	871.3	872.5	868.6	873.6	872.8	873.2	863.9
303.15	879.8	867.5	868.8	864.9	870.0	869.1	869.5	860.3
308.15	876.2	863.8	865.2	861.3	866.3	865.4	865.9	856.6
313.15	872.5	860.1	861.5	857.6	862.7	861.7	862.2	852.9
318.15	868.8	856.4	857.8	854.0	859.0	858.1	858.6	849.3
323.15	865.2	852.7	854.1	850.3	855.4	854.5	854.9	845.6
328.15	861.5	849.0	850.5	846.7	851.8	850.8	851.3	842.0
333.15	857.9	845.3	846.8	843.0	848.1	847.2	847.7	838.4
338.15	854.2	841.6	843.2	839.4	844.5	843.6	844.0	834.7
343.15	850.6	837.9	839.5	835.8	840.9	840.0	840.4	831.1
348.15	847.0	834.2	835.9	832.2	837.3	836.4	836.8	827.5
353.15	843.3	830.5	832.2	828.6	833.7	832.8	833.2	823.9
358.15	839.6	826.8	828.6	825.0	830.2	829.2	829.7	820.3
363.15	836.0	823.1	825.0	821.4	826.6	825.6	826.1	816.7
368.15	832.3	819.4	821.4	817.8				

The experimental data here measured were used to evaluate the revised GCVOL method. The model described very well the density of biodiesels here studied, presenting an OARD of only 0.51 % as shown in **Table 3.2.8.** The adequacy of this model can also be seen in **Figures 3.2.2 and 3.2.3** where the deviations are almost stable within the range of temperature studied with a maximum of 0.85 %.

Table 3.2 8. ARDs for density of ethylic biodiesels

Biodiesel	Revised GCVOL
EEWCO	0.12
EEJC	0.49
EEBA	0.31
EEAI	0.76
S	0.49
Sf	0.57
S+B	0.53
P	0.81
OARD, %	**0.50**

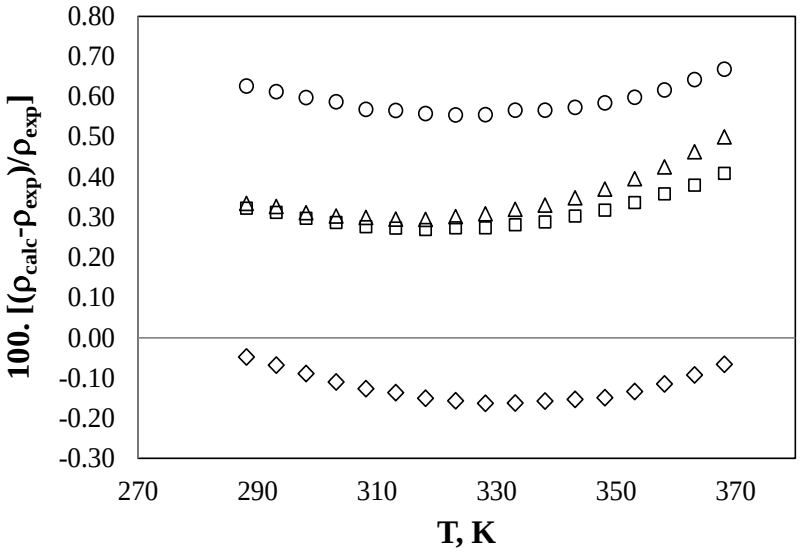

Figura 3.2 2. Relative deviations between experimental and predicted with the revised GCVOL method for ethylic biodiesel: ◇ EEWCO, □ EEBA, △ EEJC and ○ EEAI. Lines are the results of the model

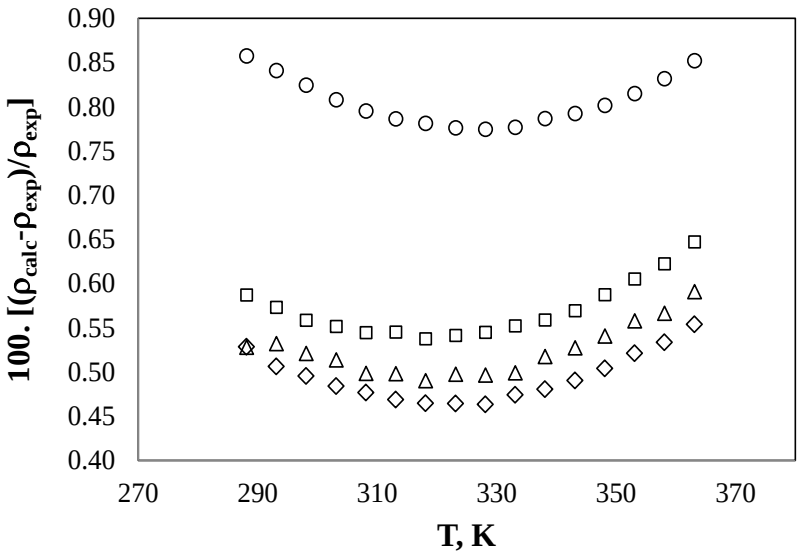

Figura 3.2 3. Relative deviations between experimental and predicted with the revised GCVOL method for ethylic biodiesel: ◇ S, □ Sf, △ S+B and ○ P. Lines are the results of the model

3.2.2. Conclusions

The high-pressure densities of ten methylic biodiesel fuels were here predicted with the revised GCVOL group contribution method. The prediction was excellent with and overall average relative deviations (OARD) of 0.37%. Moreover the deviations over the temperature were almost stable with the maximum of 0.4 %. This model was also applied to predict the atmospheric densities of eight ethylic biodiesels and the prediction was good with and OARD of only 0.51 % and the deviations were stable with a maximum of only 0.85 %. So the revised GCVOL method can be applied for all types of biodiesels since the compositions of fatty esters are known.

3.3. Modeling the viscosity of biodiesel fuels

3.3.1. Viscosity of methylic biodiesels

The measurement of viscosity for seven biodiesel samples used in this work was done at our Laboratory by Dr. Maria Jorge Pratas. The modeling was done by me. The complete work is already published as paper in the journal of Energy & Fuels [129, 146]. So this section is an adapted version of the published paper.

3.3.1.1. Introduction

One of the major problems associated with biodiesel is that its viscosity may be higher than that for diesel fuel. A fuel of high viscosity tends to form larger droplets upon injection, leading to poorer atomization during the spray and creating operation problems, such as increased carbon deposits [147] and may enhance the polymerization reaction, especially for oils of a high degree of unsaturation [148]. It also leads to poor combustion and increased exhaust smoke and emissions, beyond the problems in cold weather because of the increase of viscosity with a decreasing temperature. On the other hand, a fuel with low viscosity may not provide sufficient lubrication for the precision fit of fuel injection pumps, resulting in leakage or increased wear [149].

Thus, the kinematic viscosity of biodiesel at 40°C must be in the range of 3.5-5.0 mm^2/s according to EN-14214 specifications in Europe [108]and 1.9-6.0 mm^2/s in accordance with American Society of Testing and Materials (ASTM) D-6751 specifications in the USA [109], while the limit for diesel fuel is 2.0-4.5 mm^2/s [149]. Nevertheless, in similarity to the feed oils, there is only few information about viscosity of biodiesel blends and biodiesel-diesel mixtures over the whole composition range at different operational conditions of pressure and temperature.

This work evaluated the predictive capabilities of three models developed by Ceriani et al.[150], Krisnangkura et al.[148] and Yuan et al.[151], respectively, for the estimation of the viscosity of several biodiesels and their blends with diesel fuels. A revised version of Yuan's model was also proposed and evaluated.

3.3.1.2. Samples and Viscosity measurement

Seven of ten methylic biodiesel samples already reported in **section 3.2.1** and an additional compound named B1 (methyl oleate of technical grade, 70%) supplied by Sigma were here used.

Measurements of viscosity were performed in the temperature range of 278.15-363.15 K at atmospheric pressure using an automated SVM 3000 Anton Paar rotational Stabinger viscometer. The temperature uncertainty is 0.02 K from 288.15 to 378.15 K. The relative uncertainty of the dynamic viscosity obtained is less than 0.5% for the standard

fluid SHL120 (SH Calibration Service GMbH), in the range of the studied temperatures. This viscometer was previously tested for other compounds and presented a very good reproducibility [152-154].

3.3.1.3. Viscosity Models

The models described here are valid for the estimation of the viscosity of mixtures of fatty acid alkyl esters. The viscosities of biodiesel are calculated using the equation of Grunberg-Nissan, which is known to be the most suitable equation for computing the viscosity of liquid mixtures [147, 151]. Given that biodiesel fuels are non-associated liquids (i.e., they have essentially a dispersive interaction between the individual components), their dynamic viscosity can be estimated using the following equation:

$$\ln \eta_m = \sum_{i=1}^{n} x_i \, ln \, \eta_i \tag{3.3.1}$$

Where η_i is the dynamic viscosity of an individual compound, η_m is the dynamic viscosity of the mixture, and x_i is the mole fraction.

3.3.1.3.1. Ceriani's Model

Ceriani et al.[150] proposed a model to predict the viscosity of fatty acid esters based on a group contribution method, i.e., a compound or a mixture of compounds is considered as a solution of groups, and its properties are the sum of the contributions of each group [150]. The model for the pure compounds is described in Eqs (3.3.2) - (3.3.4)

$$ln(\eta_i/mPa.s) = \sum_k N_k \left(A_{1k} + \frac{B_{1k}}{T/K} - C_{1k} ln\, T/K - D_{1k}\, T/K\right) + \left[M_i \sum_k N_k \left(A_{2k} + \frac{B_{2k}}{T/K} - C_{2k} ln\, T/K - D_{2k}\, T/K\right)\right] + Q \tag{3.3.2}$$

with

$$Q = (f_0 + N_c f_1) q + (s_0 + N_{cs} s_1) \tag{3.3.3}$$

and

$$q = \alpha + \frac{\beta}{T/K} - \gamma \ln(T/K) - \delta\, T/K \tag{3.3.4}$$

where N_k is the number of groups k in the molecule i, M is the component molecular weight that multiplies the "perturbation term", A_{1k}, B_{1k}, C_{1k}, D_{1k}, A_{2k}, B_{2k}, C_{2k}, and D_{2k} are parameters obtained from the regression of the experimental data, k represents the groups of component i, Q is a correction term, f_0, f_1, s_0, and s_1 are optimized constants, α, β, γ, and δ are optimized parameters obtained by regression of the databank as a whole, N_c is the total number of carbon atoms in the molecule, and N_{cs} is the number of carbons of the alcohol side chain. The parameter values were found by Ceriani et al.[150].

3.3.1.3.2. Krisnangkura's model

Krisnangkura et al.[148] fitted Eq. (3.3.5) to an experimental viscosity databank and provided a set of parameters for the description of the viscosity of pure fatty acid methyl esters (FAME) [148].

$$\ln(\mu) = \alpha + bz + \frac{c}{T} + \frac{zd}{T} \tag{3.3.5}$$

This equation was developed by considering the viscosity as the integral of the interaction forces of molecules. On the basis of this approach, the temperature dependency of the viscosity for short-chain methyl esters (C_6-C_{12}) can be estimated by Eq. (3.3.6)

$$\ln(\mu) = -2.915 - 0.158z + \frac{492.12}{T} + \frac{108.35z}{T} \tag{3.3.6}$$

while for longer chain esters ($C_{12:0}$–$C_{18:0}$), the viscosity obeys Eq.(3.3.7).

$$\ln(\mu) = -2.177 - 0.202z + \frac{403.66}{T} + \frac{109.77z}{T} \tag{3.3.7}$$

The viscosity of unsaturated FAME is estimated by Eqs. (3.3.8)-(3.3.11).

$$\ln(\mu)_{18:1} = -5.03 + \frac{2051.5}{T} \tag{3.3.8}$$

$$\ln(\mu)_{18:2} = -4.51 + \frac{1822.5}{T} \tag{3.3.9}$$

$$\ln(\mu)_{18:3} = -4.18 + \frac{1685.5}{T} \tag{3.3.10}$$

$$\ln(\mu)_{22:1} = -5.42 + \frac{2326.2}{T} \tag{3.3.11}$$

In all of these equations, μ is the kinematic viscosity expressed in mm^2/s and T is the absolute temperature in kelvin.

Because Krisnangkura's model does not provide equations for several unsaturated FAME, such as $C_{16:1}$, $C_{20:0}$, $C_{20:1}$, and $C_{22:1}$, to predict the viscosity of biodiesel containing these compounds, it was necessary to resort to a pseudo-component approach, where the biodiesel composition was modified by adding $C_{16:1}$ to $C_{16:0}$, $C_{20:0}$ and $C_{20:1}$ to $C_{18:3}$, and $C_{22:0}$ to $C_{22:1}$.

Beyond that, given that Krisnangkura's model provides only kinematic viscosities, their conversion into dynamic viscosities was performed by considering the density data for pure FAME reported by Pratas et al.[152, 153].

3.3.1.3.3. Yuan's model

Yuan et al. [151] applied the Vogel-Tammann−Fulcher (VTF) equation to describe the viscosity-temperature relationship of pure FAME commonly present in biodiesel fuels

$$\ln \eta/mPa.s = A + \frac{B}{T/K+T_0} \quad (3.3.12)$$

and then to estimate the viscosity of biodiesel fuels based on their FAME composition through the mixture model. In Eq.(3.3.12), A, B, and T_0 are parameters with values determined by fitting experimental viscosity data available and are reported by Yuan et al. [151].

3.3.1.3.4. Revised Yuan's model

In previous works, Pratas et al.[152, 153] reported new and more accurate data for the viscosities of fatty acid methyl and ethyl esters. Revised Yuan's model consists of a version of Yuan's model where the parameters of the VTF model were refitted to the new data. The new parameters for FAME are presented in **Table 3.3.1**.

Table 3.3 1. VTF parameters for the revised Yuan's model

FAME	*A*	*B*	T_0
C8:0	-3.476	859.303	68.948
C10:0	-3.316	814.674	93.317
C12:0	-3.089	767.388	112.267
C14:0	-3.124	837.282	112.358
C16:0	-2.808	746.528	132.676
C16:1	-2.867	748.275	118.441
C18:0	-2.985	876.221	122.303
C18:1	-2.700	748.184	129.249
C18:2	-2.618	733.236	119.641
C18:3	-2.997	904.378	91.882
C20:0	-3.074	967.596	115.000
C20:1	-2.545	733.804	137.194
C22:0	-2.528	768.640	145.057
C22:1	-2.409	715.397	143.268
C24:0	-2.870	951.526	127.000

3.3.1.4. Database of biodiesel viscosities

Although values for the biodiesel viscosity are common in the literature, information concerning the biodiesel composition that is more detailed than the information about the oil used for the biodiesel synthesis is scarce. To apply the models studied here, detailed information about the biodiesel and/or diesel composition is required.

The database for biodiesels used in this work was collected from the literature and supplemented with data for seven new biodiesels measured in our laboratory whose composition is detailed in **Section 3.2**. The compositions in terms of FAME of literature data are reported in **Table 3.3.2**. The biodiesels used in this study cover the most important oils used in biodiesel production, such as soy, palm, canola, rapeseed, and sunflower, but also other oils, such as cotton seed, coconut, and babassu, are relevant because of their singular compositions. In terms of FAME distributions, it addresses both oils rich in short-chain and saturated fatty acids, such as coconut, rich in saturated fractions, such as palm, and rich in unsaturated compounds, such as soy and sunflower.

Table 3.3 2. FAME composition of the biodiesel studied, in mass fraction

		FAME, 100.w														
References	Biodiesel	C8:0	C10:0	C12:0	C14:0	C16:0	C16:1	C18:0	C18:1	C18:2	C18:3	C20:0	C20:1	C22:0	C22:1	C24:0
Yuan *et al.*[151]	Soy	0.02			0.08	10.61		4.27	24.2	51.36	7.48	0.36	0.28	0.4	0.07	0.14
	Palm					40.60		5.10	42.80	11.00	0.50					
	Canola					4.20		1.20	56.80	21.70	15.70					
	Coconut	9.20	6.40	48.70	17.00	7.70		2.20	5.40	2.20						
	YGME[a]				1.70	19.47		14.38	54.67	7.96	0.69	0.25	0.52	0.21		
Yuan *et al.*[155]	SMEA[b]				0.08	10.49	0.12	4.27	24.2	51.36	7.48	0.36	0.28	0.40	0.07	0.14
	SMEB[b]					10.81	0.11	4.54	24.96	50.66	7.27	0.37	0.32	0.42		0.12
	GMSME[c]					3.97	0.13	2.99	82.54	4.98	3.7	0.30	0.50	0.36		0.12
	YGME*				1.27	13.44	2.03	12.38	54.67	7.96	0.69	0.25	0.52	0.21		
Blanginoet *al.[156]*	Soy					9.27		3.77	22.83	57.46	6.67					
Krisnangkura *et al.*[148]	Palm[d]			0.40	1.06	40.05		5.83	42.21	10.46						
	Coconut[d]	4.80	6.20	52.70	17.50	7.40		2.40	7.60	1.40						
Knothe*et al.*[157]	B[g]+Petroleum (B10 to B90)					10.79		4.21	24.41	53.38	7.21					
Feitosa*et al.*[158]	Coconut	4.08	3.65	35.35	19.84	13.83		3.94	14.30	4.73						
Nogueira*et al.*[159]	Babassu		5.10	28.11	25.56	15.41		5.04	20.79							
	Cotton Seed				0.62	24.09		2.56	15.74	56.99						

[a] YGME=yellow grease methyl ester. [b]SMEA and SMEB = soybean oil methyl esters. [c]GMSME = genetically modified soy oil methyl ester. [d]Mol fraction (100.X), [g] B =biodiesel.

The database of blends analyzed in this work was collected from Knothe et al. [157] and Yuan et al.[155] The first author measured the low-temperature kinematic viscosity data of binary blends between methyl oleate, methyl linoleate, and commercial biodiesel and petrodiesel in different mixing ratios, while the last author reported the kinematic viscosities of blending of yellow grease methyl esters (YGME), soybean oil methyl esters (SMEA and SMEB), and genetically modified soy methyl esters (GMSME) with no.2 diesel. The kinematic viscosities of the commercial petrodiesel and the no.2 diesel are listed in **Table 3.3.3**.

Table 3.3 3. Experimental viscosity, in mm^2/s, for petrodiesel and No 2 diesel

T, K	Petrodiesel[157]	No. 2 Diesel[155]
273.15	8.58	
278.15	7.23	
283.15	6.21	
288.15	5.31	
293.15	4.55	3.94
298.15	4.08	
303.15	3.64	
308.15	3.25	
313.15	2.90	2.56
333.15		1.82
353.15		1.35
373.15		1.09

3.3.1.5. Results and Discussion

The viscosities of the seven biodiesel samples measured in this work as function of the temperature are reported in **Table 3.3.4**. The magnitude of the viscosities is in good agreement with other data previously reported in the literature for biodiesel produced from the same oils [148, 151, 155, 156].

Table 3.3 4. Experimental viscosity, in mPa.s, for biodiesel measured in our laboratory

T, K	Biodiesel						
	Soy A	S	B1	Sf	R	P	GP
278.15		8.812			10.33		9.315
283.15	8.016	7.555	9.359	7.940	8.763		7.958
288.15	6.916	6.535	7.998	6.844	7.518	7.814	6.856
293.15	6.021	5.711	6.894	5.965	6.517	6.748	5.971
298.15	5.286	5.033	6.000	5.243	5.701	5.883	5.244
303.15	4.679	4.478	5.271	4.658	5.034	5.152	4.655
308.15	4.170	3.995	4.663	4.143	4.467	4.550	4.137
313.15	3.740	3.548	4.154	3.636	3.942	3.961	3.630
318.15	3.372	3.249	3.722	3.356	3.594	3.632	3.349
323.15	3.057	2.922	3.354	2.988	3.217	3.214	2.981
328.15	2.784	2.697	3.037	2.776	2.955	2.968	2.769
333.15	2.546	2.473	2.767	2.542	2.699	2.702	2.534
338.15	2.338	2.276	2.529	2.337	2.475	2.471	2.329
343.15	2.154	2.102	2.321	2.156	2.278	2.269	2.148
348.15	1.992	1.948	2.138	1.996	2.104	2.091	1.988
353.15	1.848	1.794	1.976	1.831	1.933	1.911	1.823
358.15		1.686		1.726	1.811	1.794	1.718
363.15		1.575		1.612	1.688	1.669	1.604

The ARDs for each biodiesel and biodiesel blend studied are reported in **Table 3.3.5**, while the RDs of the individual data points for the 22 biodiesel samples are shown in **Figures 3.3.1 and 3.3.2**. The results suggest that all of the models tend to underpredict the experimental viscosities. The predictions of Ceriani's and Krisnangkura's models (**Figure 3.3.1**) are systematically larger than the Yuan-type models and temperature-dependent. Note, however, this dependency is opposite in the two cases: while Ceriani's deviations tend to increase with the temperature, the reverse effect is observed for Krisnangkura's model; i.e., the deviations are lower at the higher temperatures, where the viscosities have lower values. In both cases, the deviations at the temperature extremes tend to be very large (up to 25%). The temperature dependency of Ceriani's model seems to be related to the poor description of the viscosity of unsaturated fatty acid esters as discussed in previous works [152, 153]. A re-estimation of the parameters for these compounds should allow for a better description of the experimental viscosities. The temperature dependency of the fatty acid esters is better described in large temperature ranges by a VTF equation as suggested by Yuan et al.[151] than by the Arrhenius type adopted by Krisnangkura. The poor temperature dependency of this model is due to the equation used to describe the temperature dependency of the viscosity of the pure components of the mixture.

Table 3.3 5. ARDs for viscosity of several biodiesel systems

References	Biodiesel	ARD, %			
		Ceriani	Yuan	Revised Yuan	Krisnangkura
Yuan *et al.*[151]	Soy	12	2.4	1.7	4.3
	Palm	8.1	6.2	5.9	6.6
	Canola	12	4.7	3.7	7.2
	Coconut	11	9.1	7.1	14
	YGME	8.5	7.9	6.8	7.4
Yuan *et al.*[155]	SMEA	11	8.7	7.9	7.8
	SMEB	15	9.1	11	8.1
	GMSME	9.8	5.3	4.4	7.7
	YGME*	8.7	8.6	6.9	7.7
Blanginoet *al.[156]*	Soy	9.0	3.3	2.4	5.7
Krisnangkura *et al.*[148]	Palm	1.9	2.4	1.4	2.5
	Coconut	7.7	8.2	6.2	5.9
This work	Soy A	8.1	5.3	4.6	7.0
	S	8.2	3.0	2.5	3.1
	B1	5.4	7.8	6.6	11
	Sf	9.6	5.5	5.6	7.6
	P	4.8	6.2	5.6	2.6
	R	8.9	7.8	6.3	9.1
	GP	6.4	3.6	2.8	3.6
Knothe*et al.*[157]	Blending FAME (14 systems)	6.0	2.4	2.8	8.6
Feitosa *et al.*[158]	Coconut	3.3	0.6	1.9	15
Nogueira *et al.*[159]	Babassu	1.7	1.4	0.4	12
	Cotton seed	9.1	5.4	4.4	3.5
	Cotton seed+Babassu	7.7	3.5	2.5	6.1
OARD, %		**8.1**	**5.3**	**4.7**	**7.3**

Table 3.3 6. ARDs for viscosity of several biodiesel blends with diesel fuel

References	Biodiesel+Diesel	ARD, %			
		Ceriani	Yuan	Revised Yuan	Krisnangkura
Knothe *et al.*[157]	B+Petroleum (B10-B90)	1.8	2.0	1.8	2.2
	MO+petroleum (MO10-MO90)	1.9	3.2	2.5	9.1
	ML+petroleum (ML10-ML90)	7.1	3.8	3.8	7.8
Yuan *et al.*[155]	SMEA (25, 50, 75 %)	10	9.6	9.9	11
	SMEB (25, 50, 75 %)	7.2	5.5	5.3	4.0
	GMSME (25, 50, 75 %)	9.4	6.5	5.5	8.3
	YGME (25, 50, 75 %)	7.8	8.7	7.8	6.9
OARD, %		**6.5**	**5.6**	**5.2**	**7.1**

MO -Methyl Oleate; ML – Methyl Linoleate

Figure 3.3.2 reveal that the RDs obtained with the two versions of Yuan's model are temperature-independent and the maximum deviations observed are in general lower than 10%. They are thus more robust and reliable, producing suitable ARDs in comparison to other models available in the literature. In numbers, both Ceriani's and Krisnangkura's models have global ARDs around 8.0 %, Yuan's original model has ARDs of 5.3%, and the revised version of Yuan's model proposed here has ARDs of just 4.7% that must be close to the experimental uncertainty of many of the experimental data.

The prediction of the viscosities of mixtures of biodiesel with petroleum diesel was also studied here by using eq.3.3.1, where the biodiesel viscosity is estimated using the models studied here, and the petroleum diesel viscosity used was the experimental value (**Figures 3.3.3 and 3.3.4**). The RDs are reported in **Table 3.3.6**. It was found that the deviations observed for the individual mixtures and the global deviations are in good agreement with those observed for the pure biodiesel, showing that their predictive capabilities of the approach used here is not affected by the presence of hydrocarbons in the mixture. Ceriani's model shows an overall deviation of 6.5%, and Yuan's and Krisnangkura's models presented 5.6 and 7.1%, respectively, while revised Yuan's model had the lowest global deviation of just 5.2%, suggesting that the Yuan-type models are also suitable to predict the viscosity data of biodiesel blends with petrodiesel.

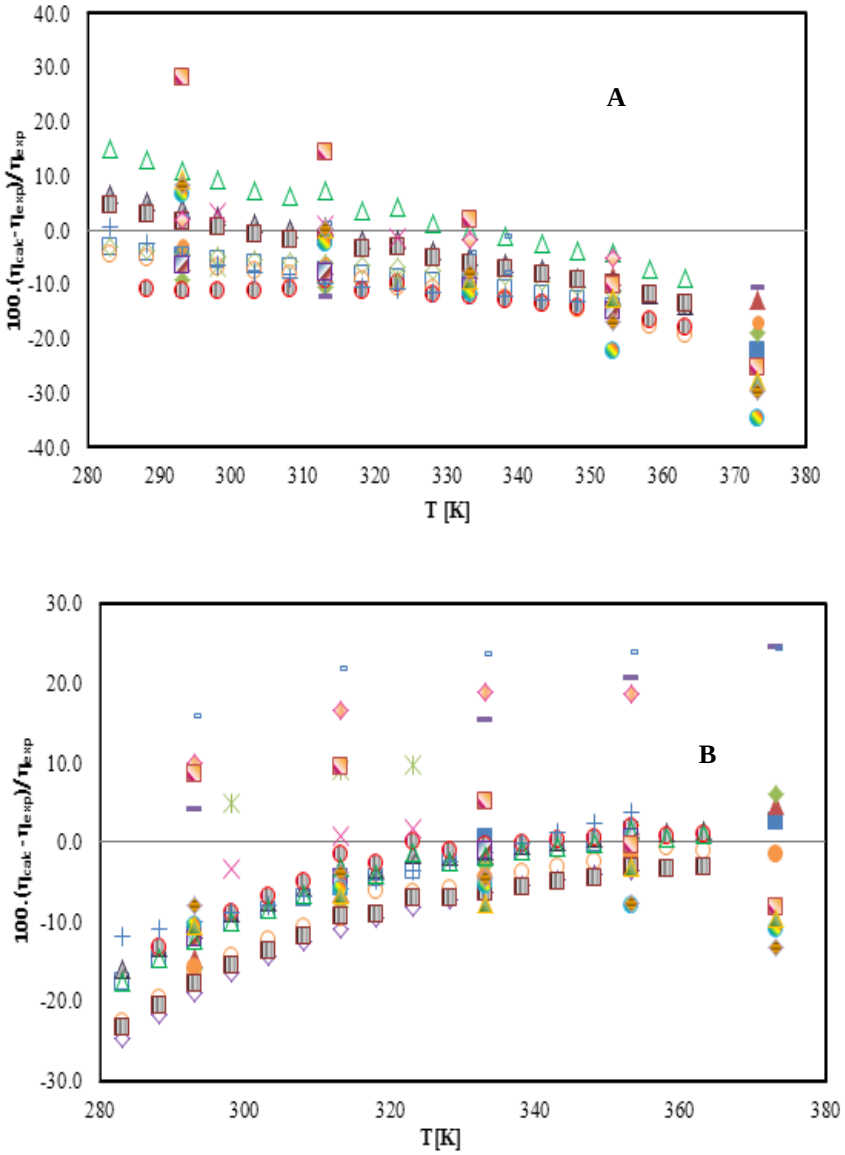

Figure 3.3. 1. Relative deviation between experimental and predicted dynamic viscosity using: (A)Ceriani's Model and Krisnangkura's(B) for 22 types of pure biodiesel, ■ Yuan Soy; ▲ Yuan Palm; ◆ Yuan Canola; – Yuan Coconut; ● Yuan YGME; □ This work Soy A; ◇ This work B1; ○ This work Sunflower; ▲ This work Soy C; ◐ This work Palm; ▥ This work Rapeseed; △ This work GP; × Krisnangkura Palm; ✳ Krisnangkura Coconut; + Blangino Soy; ▫ Feitosa Coconut; ◆ NogueiraBabassu and ▨ Nogueira Cotton seed, ◔ Yuan SMEA, ▧ Yuan SMEB, ▲ Yuan GMSME and ◆ Yuan YGME*.

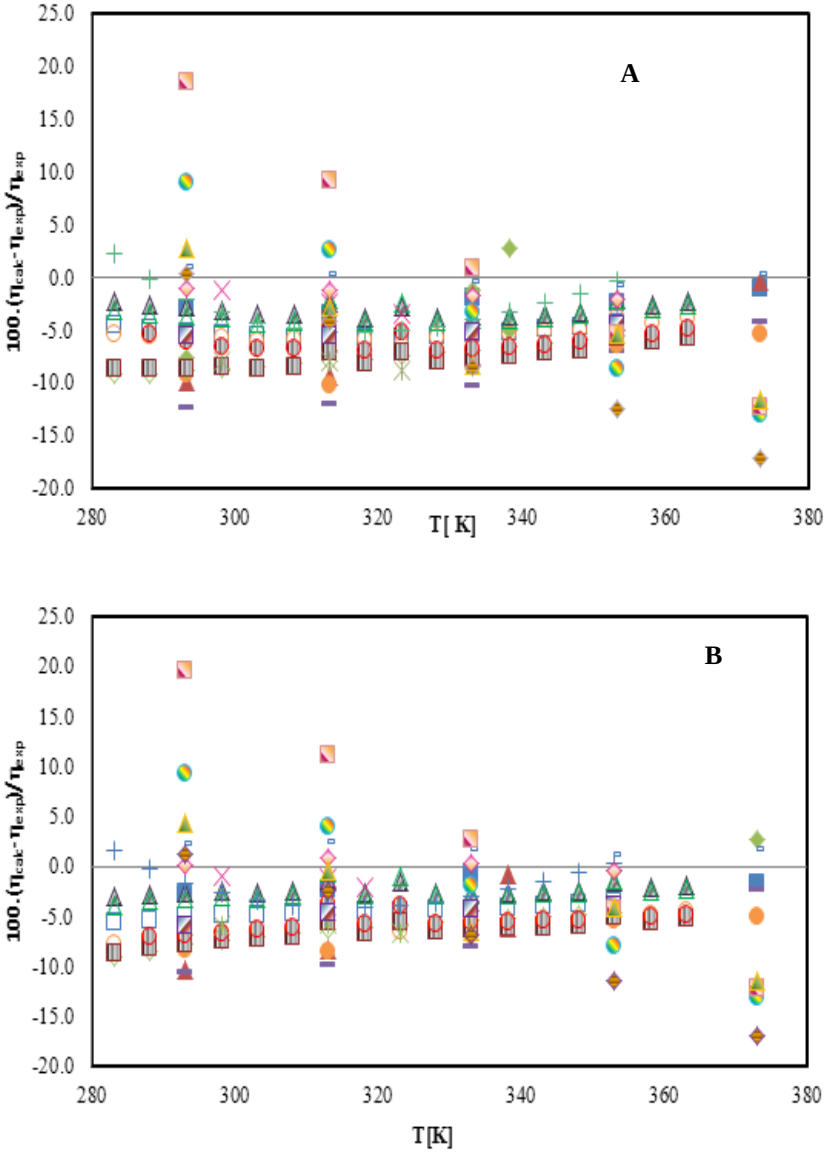

Figure 3.3. 2. Relative deviation between experimental and predicted dynamic viscosity using (A) Yuan's model and (B) Revised Yuan's model for 22 types of pure biodiesel ■ Yuan Soy; ▲ Yuan Palm; ◆ Yuan Canola; – Yuan Coconut; ● Yuan YGME; □ This work Soy A; ◇ This work B1; ○ This work Sunflower; △ This work Soy C; ◍ This work Palm; ▥ This work Rapeseed; △ This work GP; × Krisnangkura Palm; ✳ Krisnangkura Coconut; + Blangino Soy; ▫ Feitosa Coconut; ◈ NogueiraBabassu and ◪ Nogueira Cotton seed, ◔ Yuan SMEA, ◪ Yuan SMEB, ▲ Yuan GMSME and ◆ Yuan YGME*.

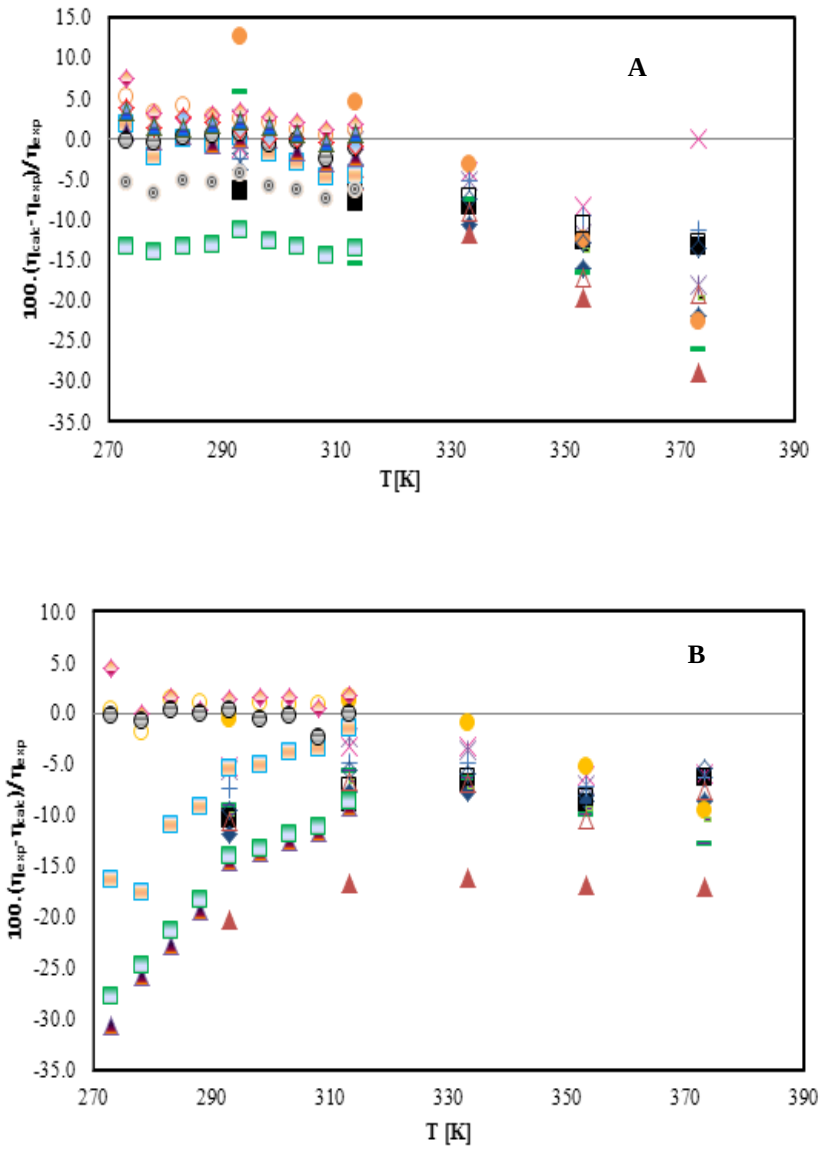

Figure 3.3. 3. Deviation between experimental and predicted dynamic viscosity using (A) Ceriani's model and (B) Krisnangkura's Model for biodiesel blends with diesel fuel, ■ SMEA 25, ◆ SMEA 50, ▲ SMEA 75, × SMEB 25, ✳ SMEB 50, ● SMEB 75, + GMSME 25, - GMSME 50, — GMSME 75, □ YGME 25, ◇ YGME 50, △ YGME 75, ○ B10-B90 Max, ▣ B10-B90 Min, ◈ MO10-MO90 Max, ▲ MO10-MO90 Min, ⛀ ML10-ML90 Max, ▣ ML10-ML90 Min.

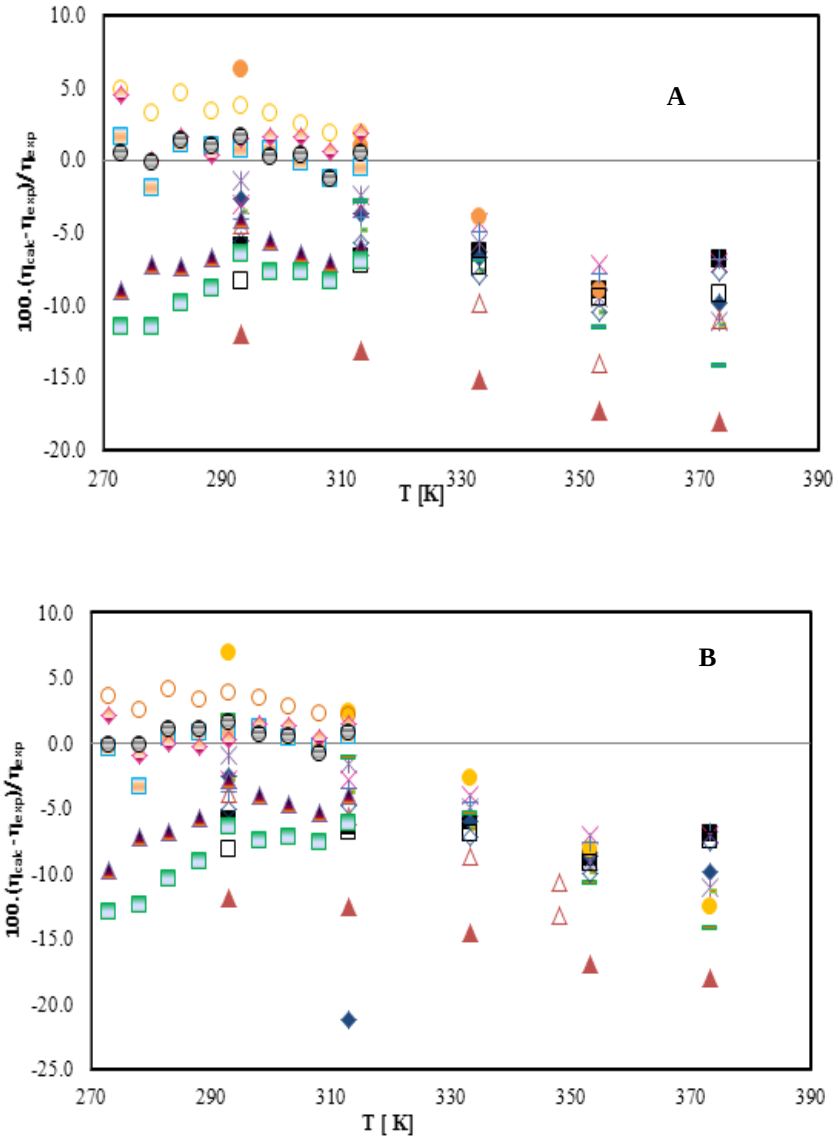

Figure 3.3. 4. Deviation between experimental and predicted dynamic viscosity using (A) Yuan's model and (B) revised Yuan's Model for biodiesel blends with diesel fuel, ■ SMEA 25, ◆ SMEA 50, ▲ SMEA 75, × SMEB 25, ✳ SMEB 50, ● SMEB 75, + GMSME 25, - GMSME 50, ▬ GMSME 75, □ YGME 25, ◇ YGME 50, △ YGME 75, ○ B10-B90 Max, ▣ B10-B90 Min, ◈ MO10-MO90 Max, ▲ MO10-MO90 Min, ⬬ ML10-ML90 Max, ▣ ML10-ML90 Min.

3.3.2. Viscosity of ethylic biodiesels

The two sets of ethylic biodiesels already described in **Section 3.2** are here used again to test the ability of the revised Yuan's model for predicting the viscosity of ethylic biodiesels.

3.3.2.1. Experimental section

The eight samples of ethylic biodiesels described in **section 3.2** are here used again to study the viscosity**.** The measurement of viscosity was done in the temperature range of 288.15 to 368.15 K and at atmospheric pressure using an automated SVM 3000 Anton Paar rotational Stabinger Viscometer following the same procedure described in **Section 3.2.**

3.3.2.2. Results and discussion

Similarly to the methylic biodiesels, the viscosity parameters of FAEE were used to describe the viscosity of ethylic biodiesels. The VTF parameters for the revised Yuan's model are presented in **Table 3.3.7**. Because there were no parameters for several FAEE, to predict the viscosity of biodiesel containing these compounds, it was necessary to resort to a pseudo-component approach, where the biodiesel composition was modified by adding $C_{16:1}$ to $C_{16:0}$ and $C_{20:1}$, $C_{22:0}$, $C_{22:1}$ and C_{24} to $C_{20:0}$.

Table 3.3 7. VTF parameters for the revised Yuan's model

FAME	*A*	*B*	T_0
C8:0	-3.58	926.963	63.493
C10:0	-3.420	883.295	85.943
C12:0	-3.150	818.076	105.827
C14:0	-2.970	793.873	117.701
C16:0	-3.000	854.539	117.650
C18:0	-3.040	920.174	115.962
C18:1	-2.650	759.323	127.320
C18:2	-2.540	715.050	124.130
C18:3	-2.670	795.170	101.670
C20:0	-2.9000	906.9500	122.3300

The experimental viscosities of the eight biodiesels here studied are presented in **Table 3.3.8** where, with the exception of EEWCO, the viscosity of other biodiesels decreases with the level of unsaturation as expected.

Table 3.3 8. Experimental viscosity of biodiesel

	η, mPa.s							
T, K	S	Sf	S+B	P	EEWCO	EEJC	EEBA	EEAI
288.15	7.381	7.412	7.255	7.770	11.88	8.398	7.844	8.813
293.15	6.335	6.356	6.236	6.619	9.902	7.123	6.695	7.459
298.15	5.603	5.616	5.518	5.821	8.558	6.245	5.894	6.534
303.15	4.947	4.954	4.873	5.108	7.377	5.460	5.178	5.708
308.15	4.401	4.404	4.337	4.520	6.415	4.813	4.583	5.030
313.15	3.916	3.917	3.860	4.002	5.587	4.245	4.061	4.435
318.15	3.553	3.552	3.504	3.615	4.971	3.821	3.670	3.992
323.15	3.221	3.218	3.178	3.263	4.423	3.437	3.316	3.591
328.15	2.935	2.931	2.896	2.961	3.961	3.109	3.011	3.249
333.15	2.673	2.670	2.639	2.689	3.554	2.818	2.735	2.942
338.15	2.469	2.464	2.438	2.475	3.229	2.585	2.518	2.700
343.15	2.278	2.273	2.253	2.277	2.936	2.370	2.317	2.475
348.15	2.109	2.103	2.084	2.103	2.681	2.181	2.140	2.279
353.15	1.948	1.942	1.925	1.937	2.451	2.003	1.973	2.096
358.15	1.823	1.817	1.802	1.809	2.260	1.862	1.841	1.950
363.15	1.700	1.694	1.682	1.684	2.082	1.726	1.715	1.811
368.15					1.922	1.604	1.601	1.686

The experimental data here measured were used to evaluate the revised Yuan's model. This model described acceptably the viscosity of biodiesels, presenting an OARD of only 7.5 %. Except the EEWCO and EEAI samples, the results were satisfactory for other samples as shown in **Table 3.3.9.** The high deviation of EEWCO may due to the low conversion of oil to biodiesel or to the degradation of the sample. The adequacy of this model can be also seen in **Figures 3.3.5** and **3.3.6** where the deviations are large at low temperatures but tend to lower and be stable at high temperatures.

Table 3.3 9. ARDs for viscosity of ethylic biodiesels

Biodiesel	Revised Yuan
EEWCO	23
EEJC	8.1
EEBA	4.7
EEAI	12
S	4.9
Sf	3.3
S+B	3.5
P	0.5
OARD, %	**7.5**

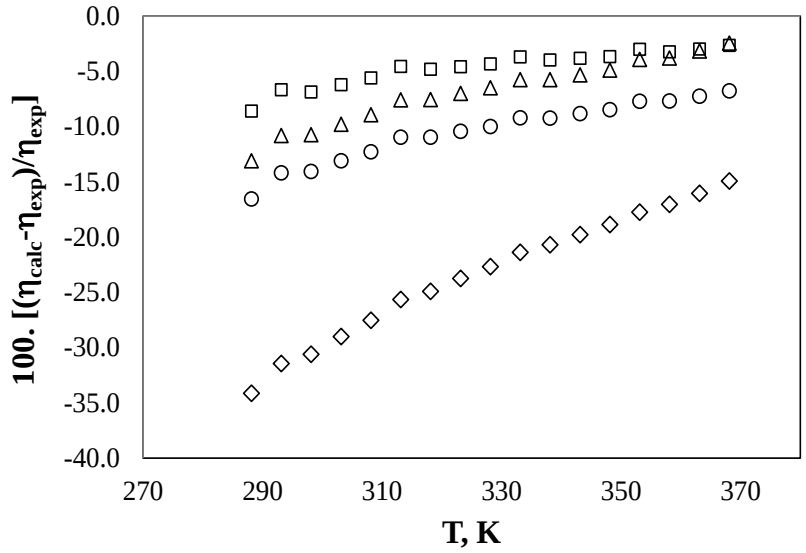

Figure 3.3. 5. Relative deviations between experimental and predicted with the revised Yuan's model for ethylic biodiesel: ◇ EEWCO, □ EEBA, △ EEJC and ○ EEAI. Lines are the results of the model

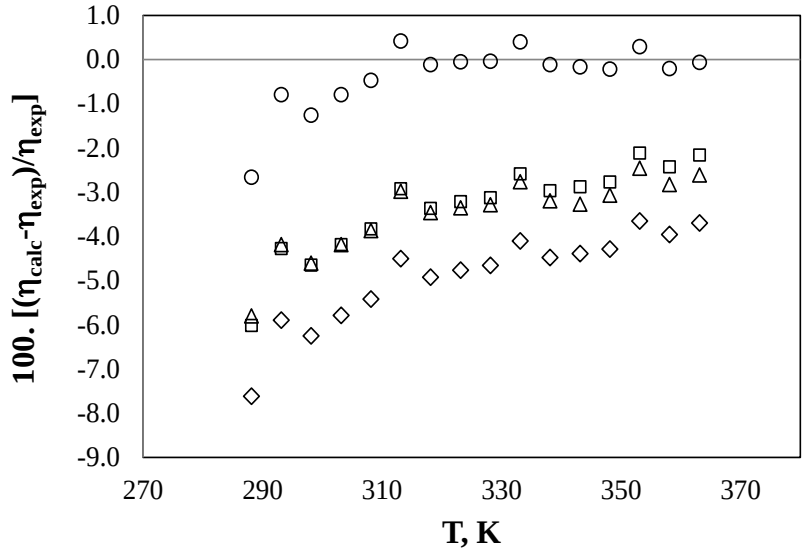

Figure 3.3. 6. Relative deviations between experimental and predicted with the revised Yuan's model for ethylic biodiesel: ◇ S, □ Sf, △ S+B and ○ P. Lines are the results of the model

3.3.3. Conclusions

Viscosity data for seven well-characterized methylic biodiesel samples in terms of their FAME composition were measured and reported. Along with a database compiled from the literature, they were used to evaluate four models able to predict biodiesel viscosities based on information of their FAME compositions. It is shown that, although all of the models studied are able to predict the viscosities of both pure biodiesels and blends of biodiesel with petrodiesel with less than 10% deviation in general, the models of Krisnangkura et al.[148] and Ceriani et al.[150] present deviations that are temperature-dependent and that, at the extremes of the temperature range studied, can have deviations as high as 25%. The deviations presented by the Yuan-type models are more robust over temperature and also lower than those obtained with the two previous models. In particular, the revised version of Yuan's model proposed here on the basis of new and more accurate data for the FAME produces predictions with uncertainties that are close to the experimental uncertainties of the experimental data and can thus be an interesting tool to the design of biofuels or biofuel blends with viscosities that comply with legal specifications.

The Revised Yuan's model was used also to predict the viscosity of eight ethylic biodiesels and the results were acceptable with and overall average relative deviations (OARD) of 7. 5%. Moreover the deviations tend to be stable at high temperatures.

3.4. Measurement and Prediction of biodiesel volatility

This work is also already published as a paper in the journal of Energy & Fuels [160]. This section is again an adapted version of the published paper. Just to underline that the samples used in this section were those produced by Dr. Maria Jorge. The experimental measurement and also the modeling of vapor pressure of biodiesels were done by me.

3.4.1. Introduction

Vapor pressures (and boiling points) express the volatility, safety, and stability of a fuel. Higher value of this property favors the evaporative emissions while lower value leads to delayed ignition, poor atomization, and problematic combustion. Biodiesel fuels have lower vapor pressure and, thus, might cause these problems. To be used in diesel engines, this property must be adjusted by changing the composition of biodiesel to meet the standard values. For this purpose, because the experimental measurement is impractical, the use of predictive models is recommended. Many works in the literature have dealt with the measurement and estimation of vapor pressures for several methyl esters and biodiesels [161-167], but almost none of them described with detail their dependency upon the composition of fatty acid alkyl esters.

This work aims at reporting the experimental data of vapor pressures for 3 pure methyl esters and 10 biodiesel fuels and evaluating the predictive ability of Yuan's, Ceriani's, and CPA EoS models for their description.

3.4.2. Experimental Section: samples and measurement procedure

The three methyl esters here studied were methyl laurate (with 97% of purity from Fluka), methyl myristate (with 98 % of purity from SAFC) and methyl palmitate (with 97% from SAFC). The ten biodiesel fuels addressed in **Section 3.2** are here studied again.

The measurement of vapor pressures was done using an ebulliometer previously used by us to study glycerol containing systems [28]. The ebulliometer was composed of a boiling still with a port for liquid sampling/injection and a condenser. A thermostatic bath was used to control the temperature. The pressure was kept constant trough a vacuum line with a calibrated Baratron Heated Capacitance Manometer 728AMKS, with an accuracy of 0.50%. Circa 20 mL of the sample were used for the measurement. This sample was always mixed with a magnetic stirrer and heated to its boiling point. The temperature was measured using a calibrated Pt100 temperature sensor with an uncertainty of 0.05 K. The measurement of boiling points was carried from 0.026 to 0.250 bar with an uncertainty of ± 0.25 C.

3.4.3. Models of vapor pressure

The vapor pressures or boiling points of the biodiesel fuels here studied were predicted by using three different approaches: Yuan´s, Ceriani's and CPA's model.

3.4.3.1. Yuan's model

Yuan et al. [162] fitted the Antoine equation (Eq. (3.4.1)) to the experimental data of vapor pressures for several pure fatty acid methyl esters (FAME) that compose the biodiesel fuels reported in the works of Rose et al. [161] and Scott et al. [163].

$$\log\left(P^{v}{}_{i}\right) = A - \frac{B}{C+T} \tag{3.4.1}$$

Where $P^{v}{}_{i}$ is the vapor pressure of FAME in Pa, T is the boiling temperature in K and A, B and C are the fitting parameters. To predict the vapor pressures of biodiesel fuels these are considered to behave as an ideal solution and the vapor pressure of the mixture is given as

$$P^{v}{}_{BD} = \sum_{i}\left(x_i P^{v} i\right) \tag{3.4.2}$$

Where $P^{v}{}_{BD}$ is the vapor pressure of biodiesel fuels in Pa and x_i is the molar composition of FAME. Since there were no fitting parameters for C16:1, the contribution of this compound was added to C16:0. The nomenclature for esters here adopted is based on the fatty acid chain length where Cx:y ester represents the methyl ester of fatty acid with x carbons and y unsaturations.

3.4.3.2. Ceriani's model

Ceriani and co-workers have proposed a number of group-contribution models for estimating the thermophysical properties of fatty compounds. and among these one for the vapor pressures [165]. The modeling of viscosity with this model is already described in **Section 3.3**.The model for predicting vapor pressures is shown in Eq. (3.4.3) and (3.4.4)

$$\begin{aligned}\ln P^{v} i = \sum_{k} N_k\left(A_{1k} + \frac{B_{1k}}{T^{1.5}} - C_{1k}\ln T - D_{1k}T\right) + \\ \left[M_i \sum_{k} N_k\left(A_{2k} + \frac{B_{2k}}{T^{1.5}} - C_{2k}\ln T - D_{2k}T\right)\right] + Q\end{aligned} \tag{3.4.3}$$

With

$$Q = \left(f_0 + N_c f_1\right)\left(\alpha + \frac{\beta}{T^{1.5}} - \gamma \ln(T) - \delta T\right) + \left(s_0 + N_{cs} s_1\right) \tag{3.4.4}$$

Where N_k is the number of groups k in the molecule i; M is the component molecular weight that multiplies the "perturbation term"; A_{1k}, B_{1k}, C_{1k}, D_{1k}, A_{2k}, B_{2k}, C_{2k}, and $D_{2k}$are parameters obtained from the regression of the experimental data; k represents the groups of component i; Q is a correction term. f_0, f_1, s_0 and s_1 are optimized constants; α, β, γ and δ are optimized parameters obtained by regression of databank as whole; N_c is the total number of carbon atoms in the molecule and N_{cs} is the number of carbons of the alcohol side chain. The parameter values can be found at Ceriani et al.[165].

3.4.3.3. CPA EoS

Recently the Cubic-Plus-Association Equation of State (CPA EoS) has been extended for application in biodiesel production and purification. It was applied to describe the liquid-liquid, the vapor-liquid and the solid-liquid equilibria of binary and multicomponent systems containing fatty acids, fatty acid esters, water, short alcohols and glycerol[168]. Lately, it successfully described densities at high pressures[141] and surface tensions[136] for the same biodiesels studied in this work.

This equation of state has been extensively described on the above stated publications and therefore it will be shortly addressed here. It consists on the combination of a cubic contribution, in this work the Soave-Redlich-Kwong (SRK), with the Wertheim term in order to explicitly take into account interactions between like molecules (self-association) and different molecules (cross-association)[169-171].

Since biodiesels are composed of fatty acid esters, which are known not to self-associate, the association term disappears. In terms of the compressibility factor the CPA EoS appears as:

$$Z = \frac{1}{1-b\rho} - \frac{a\rho}{RT(1+b\rho)} \tag{3.4.5}$$

where we have the energy parameter, a, the co–volume parameter, b, the molar density, ρ, and the simplified hard–sphere radial distribution function, g.

The energy parameter, *a*, is described has having a Soave-type reduced temperature dependency:

$$a(T) = a_0 \left[1 + c_1\left(1 - \sqrt{T_r}\right)\right]^2 \tag{3.4.6}$$

The classical van der Waals one–fluid mixing rules are used for computing the energy and co–volume parameters when the CPA EoS is extended for mixtures.

$$a = \sum_i \sum_j x_i x_j a_{ij} \qquad a_{ij} = \sqrt{a_i a_j}\left(1 - k_{ij}\right) \qquad b = \sum_i x_i b_i \tag{3.4.7}$$

The three pure component parameters in the cubic term (a_0, c_1 and b) are regressed simultaneously from vapor pressure and liquid density pure component data in order to overcome some of the SRK handicaps in what concerns liquid phase density description.

3.4.3.4. Evaluation of models

The predictive ability of the models aforementioned was evaluated by simply calculating the average relative deviations (ARDs) using Eqs 3.1.1 and 3.1.2 or the average temperature deviation (ΔTm) between the experimental and the predicted normal boiling points (Eq. (3.4.8)).

$$\Delta Tm\,(K) = \frac{\sum_n \left|\left(T_{\exp} - T_{calc}\right)\right|}{N_p} \tag{3.4.8}$$

3.4.4. Results and Discussion

The experimental vapor pressures for three pure methyl esters and ten biodiesel fuels measured at different temperatures are presented in **Tables 3.4.1** to **3.4.3**. The upper temperature limit of the measurements, circa 550 K, is imposed by the degradation of the biodiesel at higher temperatures under the measurement conditions.

Table 3.4. 1. Experimental boiling point for methyl esters

C12:0		C14:0		C16:0	
Tb, K	P^v, kPa	Tb, K	P^v, kPa	Tb, K	P^v, kPa
441.40	5.07	449.14	2.63	492.30	5.27
451.90	8.11	467.17	5.27	504.05	7.90
460.55	10.64	478.96	8.00	512.85	10.64
467.15	13.17	487.43	10.64	520.15	13.37
472.45	15.71	494.51	13.37	534.45	20.37
480.70	20.37	499.64	15.71	549.05	30.40
488.05	25.43	508.05	20.27	560.10	40.63
494.15	30.40	515.70	25.33	569.70	50.76
504.60	40.63	522.17	30.40	577.60	60.90
512.84	50.76	532.89	40.63	584.55	71.03
519.85	60.90	541.49	50.76	590.50	81.06
525.50	70.93	548.77	60.90	595.90	91.19
531.15	81.16	555.11	71.03	600.90	101.43
		560.70	81.06		
		565.85	91.29		
		570.46	101.33		

Table 3.4. 2. Experimental boiling point for biodiesel fuels

Sf		soy A		S		R		P	
Tb, K	P^v, kPa	Tb, K	P^v, kPa	Tb, K	P^v, kPa	Tb, K	P^v, kPa	Tb, K	P^v, kPa
490.98	2.74	497.15	3.85	491.10	2.74	493.51	2.74	490.65	3.85
500.56	3.85	505.55	5.17	499.74	3.85	502.65	3.85	499.79	5.17
505.51	4.56	512.30	6.59	505.80	4.56	507.73	4.56	506.05	6.48
510.44	5.37	518.90	8.11	509.20	5.27	511.19	5.27	512.65	8.21
515.29	6.28	523.15	9.22	515.47	6.28	516.50	6.28	516.73	9.32
520.49	7.40	527.15	10.64	520.40	7.60	522.29	7.60	520.20	10.44
525.48	8.61	534.60	13.27	523.95	8.61	525.94	8.61	527.01	13.37
528.12	9.32	539.37	15.40	524.15	9.32	528.31	9.32	531.33	15.30
532.63	10.64			531.00	10.64	531.90	10.54	537.65	18.34
538.16	12.46			533.35	11.65	535.01	11.65		
545.83	15.40					537.65	12.46		
556.42	20.37					540.40	13.17		
561.21	23.00					543.32	15.20		
565.25	25.43					552.15	18.34		
569.89	28.47								
572.76	30.50								
575.36	32.42								
579.21	35.46								
582.92	38.60								
585.08	40.53								
590.39	45.60								
595.24	50.66								

Table 3.4. 3. Experimental boiling point for biodiesel fuel mixtures

SP		GP		SRP		RP		SR	
Tb, K	P^v, kPa	Tb, K	P^v, kPa	Tb, K	P^v, kPa	Tb, K	P^v, kPa	Tb, K	P^v, kPa
486.15	2.74	490.95	2.84	488.40	2.74	487.15	2.74	492.40	2.74
496.15	3.85	499.45	3.85	497.98	3.85	495.75	3.85	501.60	3.85
500.90	4.56	503.85	4.56	502.80	4.56	498.45	4.56	506.59	4.56
505.65	5.27	507.90	5.27	506.24	5.27	502.93	5.27	510.90	5.27
510.40	6.28	513.15	6.28	512.04	6.28	508.35	6.38	516.15	6.28
516.15	7.60	518.65	7.60	517.54	7.60	515.90	7.60	521.65	7.60
520.65	8.61	523.15	8.71	521.80	8.71	519.65	8.61	525.30	8.61
522.65	9.32	524.90	9.32	523.90	9.32	521.90	9.32	527.80	9.32
527.15	10.64	529.40	10.64	528.19	10.64	525.95	10.64	531.65	10.64
530.15	11.65	531.90	11.65	535.01	11.65	529.36	11.65	534.60	11.65
532.27	12.46	534.40	12.46	537.65	12.46	531.51	12.46		
534.15	13.27	536.65	13.37	534.89	13.17	533.83	13.37		
538.50	15.20			538.74	15.20	536.17	14.19		
544.90	18.34			545.40	18.24	538.37	15.30		
548.55	20.37					543.45	18.24		
552.30	22.70								
556.25	25.33								
560.33	28.37								
563.15	30.40								
568.15	35.46								
571.25	40.53								

The experimental data of vapor pressure for the three pure methyl esters here measured were compared to those previously reported in the literature [161, 166] and they were found to be in acceptable agreement with an average deviation of 1.7 % for C12:0, 3.5 % for C14:0 and 1.6 % for C16:0 as shown in **Figure 3.4.1**. As expected, the vapor pressures are lower (boiling points higher) for the long chain fatty acid esters and thus for biodiesels with larger amounts of these esters in their composition. For example, the palm biodiesel presented a higher vapor pressure than rapeseed biodiesel as the first has a higher percentage of C16:0 and the second is richer in C18:1.

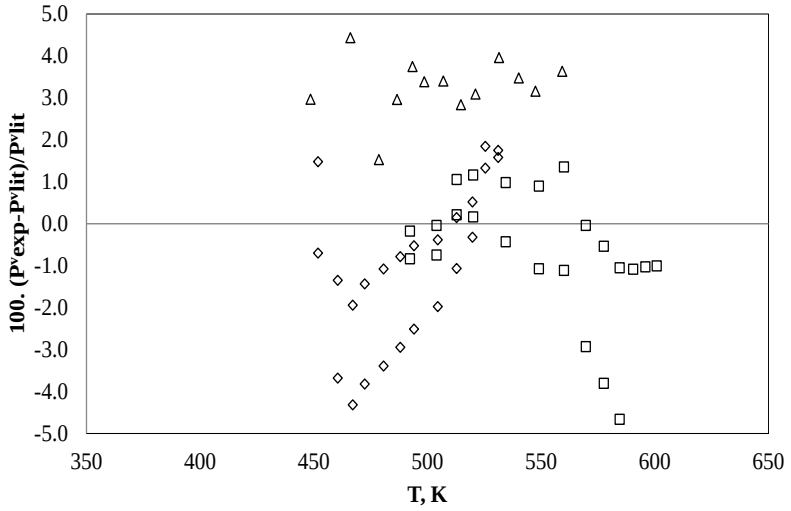

Figure 3.4 1. Relative deviations between the experimental and literature data of vapor pressure for three methyl esters. Methyl Laurate (C12:0), Methyl Myristate (C14:0) and Methyl palmitate (C16:0). [161, 166]

For further completeness, Antoine equation parameters for the three fatty acid esters considered were regressed and presented in **Table 3.4.4**.

Table 3.4. 4. Antoine Equation (Log10 = A – B (T + C), with P in mmHg and T in °C) Constants for FAME

	A	*B*	*C*
C12:0	9.122	3677.486	322.394
C14:0	7.429	2036.858	152.707
C16:0	7.164	2037.26	147.818

The CPA pure-compound parameters for the FAME that compose the biodiesels studied were previously estimated[141] using recently published density experimental data,

in the temperature range of 283.15–373.15 K, and used to successfully describe high-pressure densities[141] and surface tensions[136] of the selected biodiesels. However, when extrapolated for the temperature range of interest for this work, 450–600 K, poor predictions were obtained for the biodiesel vapor pressures. Consequently, a new set of CPA pure-compound parameters for the FAME composing the biodiesels studied is proposed here for applications at high temperatures. The recent density data by Pratas et al. [141] and vapor pressures by Yuan et al.[162] were used in a simultaneous regression for parameter estimation. Critical properties to be applied in eq. 3.4.6 were generated by the Wilson and Jasperson [172] group-contribution model for the saturated FAME and by Ambrose [173] for the unsaturated FAME. These group-contribution models were shown previously to be the best models to calculate critical properties for the correspondent family of compounds [174]. Parameter values are presented in **Table 3.4.5**, as well as critical temperature values and deviations in vapor pressures and liquid densities.

Table 3.4. 5. CPA parameters for pure FAME

FAME	a ($J.m^3.mol^{-2}$)	$c1$	$b \times 10^4$ ($m^3.mol^{-1}$)	P error, %	ρerror, %
C10:0	15.6091	2.53578	9.12143	3.05	10.16
C12:0	19.5572	2.38142	10.1706	1.47	4.34
C14:0	22.4382	2.37557	10.7970	1.58	1.99
C16:0	25.2426	2.35711	11.2031	1.05	0.93
C16:1	25.2426	2.35711	11.2031	1.05	0.93
C18:0	29.2890	2.23414	11.5228	0.65	0.45
C18:1	29.0970	2.17406	11.3055	1.52	0.41
C18:2	26.9235	2.29569	11.1373	4.87	0.42
C18:3	25.0167	2.44113	10.9424	5.60	0.44
C20:0	32.2317	2.14492	11.7254	2.01	0.73
C20:1	31.5768	2.13976	11.5255	2.23	0.66
C22:0	36.1734	2.03297	11.8412	2.48	1.01
C22:1	36.9556	1.97865	11.7285	2.65	1.00
C24:0	40.0294	1.94411	11.9713	2.85	1.27

Higher density errors for C10:0 and C12:0 were obtained, which can be related to the extrapolation for high temperatures of the density–temperature relations proposed in reference [141], which seem to provide poorer density descriptions at high temperatures for these smaller compounds. However, an excellent vapor pressure description, of relevance for this work, is assured, as seen in **Table 3.4.6**. Subsequently, the good vapor pressure description of biodiesels rich in C10:0 or C12:0 is guaranteed.

Because there were no data of the vapor pressure for methyl palmitoleate (C16:1), the parameters of the CPA EoS used for this compound were the same as those of methyl palmitate (C16:0). In terms of ARDs on the vapor pressures, Yuan's and CPA EoS models were shown to be better than Ceriani's model by presenting an OARD of only 3.4 and 0.80%, respectively, compared to 9.9 % of the latter, as shown in **Table 3.4.6**. Even for the pure FAME, Ceriani's model shows large deviations in the range of pressures studied.

Table 3.4. 6. ARDs in vapor pressure for biodiesels and methyl esters obtained with Yuan's, Cerani's and CPA EoS models

Biodiesel	ARD, %		
	Yuan	Ceriani	CPA EoS
Soy A	6.0	13	0.43
S	2.9	4.9	0.41
R	2.5	9.3	0.69
P	5.1	15	0.51
Sf	0.0	7.6	2.2
GP	5.1	11	0.43
SR	2.8	4.1	0.38
SP	2.8	13	1.6
PR	3.7	13	0.61
SRP	3.3	7.6	0.68
OARD, %	**3.4**	**9.9**	**0.80**

Similar results are observed for the boiling points when estimating the average temperature deviations (ΔT_m) or its overall value ($O\Delta T_m$). Yuan's and CPA EoS models describe the experimental data of the boiling points in the range of pressures studied with only 1.12 and 1.25 K of overall average temperature deviation ($O\Delta T_m$), respectively, compared to 4.01 K of Ceriani's model, as shown in **Table 3.4.7**. The predicted boiling points of biodiesel fuels were plotted against the experimental data in **Figure 3.4.2**, where Yuan's and CPA EoS models show a very good agreement with the experimental data, while Ceriani's model presents larger deviations at high temperatures in the range of pressures studied, overpredicting boiling points.

Table 3.4. 7. Temperature difference obtained with Yuan's, Ceriani's and CPA EoS models for the selected biodiesels in the pressure range studied.

Biodiesel	ΔTm, K		
	Yuan	Ceriani	CPA EoS
Soy A	2.02	4.84	1.87
S	0.93	1.73	0.70
R	0.70	3.61	0.66
P	1.72	6.35	2.08
Sf	0.30	3.51	1.52
GP	1.72	4.00	1.49
SR	0.82	1.46	0.85
SP	1.06	6.36	1.05
PR	1.21	5.24	1.27
SRP	0.74	3.00	1.04
OΔTm, K	**1.12**	**4.01**	**1.25**

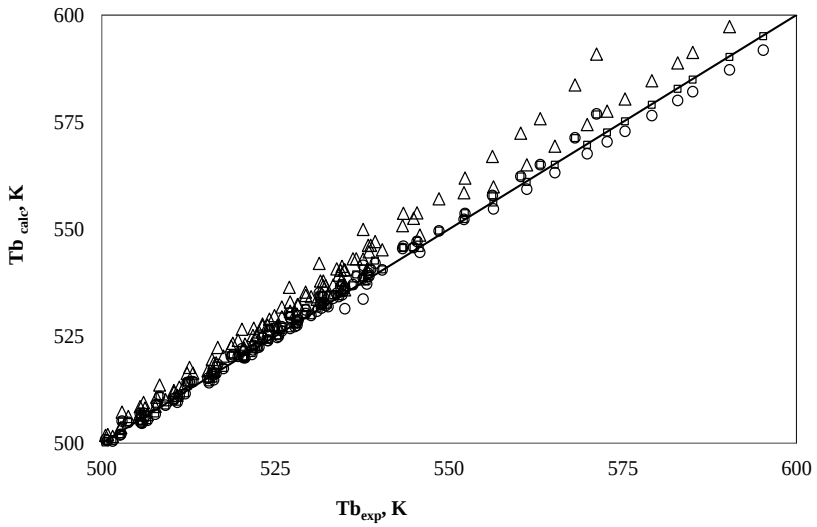

Figure 3.4 2. Linear relationship between predicted and measured normal boiling point for ten biodiesel fuels. —— Ideal, □ Yuan, △ Ceriani and ○ CPA EoS models.

3.4.5. Conclusions

The normal boiling points of ten biodiesel fuels, three methyl esters and one binary mixture of methyl esters were measured and predicted by three different approaches: Yuan's, Ceriani´s and the CPA EoS models. It is shown that Yuan's and CPA EoS models provide a good description of the experimental data with only 1.12 and 1.25 K of overall average temperature difference (OΔTm) in boiling temperatures and 3.41 and 0.80 % in vapor pressures. In addition, a new set of CPA EoS pure compound parameters for fatty acid methyl esters for applications at high temperatures are proposed.

3.5. Measurement and prediction of biodiesel surface tensions

This work is also published as an article in the journal of Energy & Fuels [136]. So this section is an adapted version of the published paper. Note that the biodiesel samples used here were the same used in earlier sections. The experimental measurement and the modeling of surface tension were done by me. The modeling with the CPA EoS was done by Dr. Mariana Belo.

3.5.1. Introduction

Surface tension influences fuel atomization, i.e., the first stage of combustion [37]. A correct atomization permits proper mixing and complete combustion in an injection engine, reducing emissions and increasing the engine efficiency[175]. Higher surface tensions make the drop formation difficult, leading to an inefficient fuel atomization[175]. Furthermore, just like most biodiesel properties, surface tension increases with long fatty acid hydrocarbon chains and a level of unsaturated bonds [176], i.e., more unsaturated biodiesel fuels will present a higher surface tension. Thus, being able to predict this physical property for biodiesels for which composition on fatty acid esters is known makes it possible to optimize biodiesel production and blending processes, with the final aim of improving the fuel performance in the engine, particularly during atomization.

There is, however, a lack of information concerning surface tensions of biodiesels or fatty acid esters from which biodiesels are composed, and when available, the data are limited to a single temperature [176, 177]. To overcome that lack of data, this work provides experimental surface tension data for ten different biodiesel fuels. The experimental data were acquired at temperatures from 303.15 to 353.15 K. The data were used to test two surface tension predictive models: the parachor-based MacLeod-Sugden equation and the density gradient theory based on the CPA EoS.

3.5.2. Experimental Section

Ten biodiesel fuels reported in **Section 3.2** were here used again to study the surface tensions. The detailed compositions of these biodiesels are already reported in **Table 3.2.1** [129].

The measurement of the surface tension of the biodiesel samples was carried out using a Nima Dynamic Surface Tensiometer, model DST9005, previously used for studies of hydrocarbon mixtures [178-180]and ionic liquids[181-183]. This is a sophisticated computer controlled instrument that measures and records the forces that biodiesel exerts to withstand the external force provoked by the immersion of the Pt/Ir Du Noüy ring in the liquid. A Haake F6 bath circulator, equipped with a Pt100 probe, was connected to the tensiometer to guarantee that measurements occurred within an uncertainty of ± 0.01 K. The ring was always cleaned before each measurement in a butane flame. The

measurement was carried from 303.15 to 353.15 K for all biodiesel fuels. For each sample at least five sets of three immersion/detachment cycles were measured, providing a minimum of at least 15 surface tension values, allowing the determination of an average surface tension value for each temperature. To correct the meniscus formed by the Noüyring, the liquid densities of the biodiesels reported in a previous work [129] were introduced before measuring the surface tension.

3.5.3. Prediction of biodiesel surface tensions

The surface tensions of the biodiesel fuels studied here were predicted using two different predictive approaches: the parachor-based MacLeod-Sugden equation with the parachors proposed by Allen et al.[177] and Knotts et al.[184] and the density gradient theory (GT) based on the CPA EoS [185-187] as shown in **Table 3.5.1.**

Table 3.5. 1. Parachors of pure fatty acid methyl esters (FAME)

FAME	Allen's parachors [177]	Knotts' parachors[184]
C10:0	489	495
C12:0	567	574
C14:0	645	657
C16:0	723	737
C16:1	712	726
C18:0	801	817
C18:1	879	806
C18:2	779	795
C18:3	768	782
C20:0	879	897
C20:1	868	886
C22:0	957	978
C22:1	946	967
C24:0	1035	1058

The first model requires prior knowledge of densities and molar masses of biodiesel fuels according to Eq. 3.5.1

$$\gamma = \left(\frac{P_{ch} \cdot \rho}{Mw} \right)^4 \qquad (3.5.1)$$

Where γ, the surface tension, is in $N.m^{-1}$,$\rho$is density in $g.cm^{-3}$, P_{ch} is the parachor in $((mN.m^{-1})^{1/4})/cm^3.mol^{-1}$ and Mw is the molar mass in $g.mol^{-1}$. The densities of the biodiesel fuels were already reported in a previous work [129]. The parachors for the biodiesels were

calculated from the parachors of pure fatty acid methyl esters (FAME) presented in Table by using the mixing rules of eq. 3.5.2.

$$P_{ch}BDF = \sum_i \left(x_i P_{ch} i\right) \tag{3.5.2}$$

Where $P_{ch}BDF$ is the parachor of the biodiesel, x_i and $P_{ch}i$ are the molar fraction and the parachor of pure FAME respectively. A similar mixing rule also was used to estimate the molar mass of biodiesel fuels.

The gradient theory is based on the phase equilibria of the fluid phases separated by an interface [188, 189].

$$\gamma = \int_{n^{vap}}^{n^{liq}} \sqrt{2\, c\, \Delta\Omega(n) \sum_i \sum_j c_{ij} \frac{\partial n_i}{\partial n_N} \frac{\partial n_j}{\partial n_N}}\; dn_N \tag{3.5.3}$$

$$\Delta\Omega(n) = f_0(n) - \sum_i n_i \mu_i + p \tag{3.5.4}$$

where p is the equilibrium pressure, γ is the surface tension, $f_o\,(n)$ is the Helmholtz energy density of the homogeneous fluid, μ_I are the pure-component chemical potentials, n^{liq} and n^{vap} are the liquid and vapor phase molar densities and c is the so-called influence parameter.

The theoretical definition of the pure-component influence parameter, c, can hardly be implemented, as an alternative, after the vapor-liquid equilibrium is determined. This parameter is frequently correlated from surface tension data:

$$c = \frac{1}{2}\left[\frac{\gamma_{\exp}}{\int_{n^{vap}}^{n^{liq}} \sqrt{f_0(n) - n\mu + p}\quad dn}\right]^2 \tag{3.5.5}$$

To use the gradient theory, it is necessary to determine the equilibrium densities of the coexisting phases, the chemical potentials and the Helmholtz energy using an adequate model. For these purposes, the Cubic-Plus-Association equation of state (CPA EoS) will be used in this work.

The CPA EoS was chosen since it presents several advantages over conventional cubic equations and other association models. The CPA EoS allows an accurate description of saturated liquid densities without any need for a volume correction, in contrast to what

succeeds with traditional cubic EoS, and is also mathematically simpler than other association equations of state such as SAFT. Considering biodiesel industry related systems, of interest for this work, it was previously shown that the CPA EoS is the most adequate model to describe the phase equilibria of different systems appearing during the biodiesel production, purification and use, that are characterized by containing polar compounds with strong associative interactions, taking into account its accuracy, range of applicability, simplicity, and predictive character [28, 185, 190-193].

In the current work, the CPA EoS model combines a cubic contribution from the Soave-Redlich-Kwong (SRK) EoS with an association contribution, originally proposed by Wertheim [169-171]. Using a generalized cubic term (for the SRK approach with δ_1 and δ_2 equal to 0), the cubic and association contributions to the Helmholtz energy (A) are given by Eqs 3.5.6 and 3.5.7[194]

$$A^{cubic} = \frac{an}{b(\delta_2 - \delta_1)} \ln\left(\frac{1+b\rho\delta_1}{1+b\rho\delta_2}\right) - nRT\ln(1-b\rho) \tag{3.5.6}$$

$$A^{assoc.} = RT\sum_i n_i \sum_{A_i}\left[\ln(XA_i) - \frac{XA_i}{2} + \frac{1}{2}\right] \tag{3.5.7}$$

Where i is a component index, b is the co-volume parameter, a the energy parameter, ρ is the molar density, $n_i$is the number of moles of molecules of component i, n is the total number of moles and XA_i is the mole fraction of component i not bonded at site A.

The pure component energy parameter of CPA has a Soave-type reduced temperature dependency:

$$a(T) = a_0\left[1 + c_1\left(1 - \sqrt{T_r}\right)\right]^2 \tag{3.5.8}$$

Esters are non-self-associating compounds, and therefore, there are only three pure compound parameters, the parameters of the physical part (a_0, c_1, and b), to be regressed simultaneously from vapor pressure and liquid density data. The CPA pure compound parameters for several ester families were already estimated in previous works [141, 190].

3.5.4. Results and Discussion

The experimental surface tensions for the ten biodiesel fuels here studied and the corresponding standard deviations are reported in **Table 3.5.2**. As expected, this property decreases with increasing temperature and generally also with the level of unsaturation of the FAME constituting the biodiesel, i.e., at the same temperature, the rapeseed and the sunflower biodiesel fuels present the higher surface tensions and the soy type biodiesel the lower surface tension.

Table 3.5. 2. Experimental surface tensions for biodiesel fuels, in $mN \cdot m^{-1}$

T / K	Soy B	σ	R	σ	P	σ	SR	σ	RP	σ
303.15	31.71	0.23	32.18	0.08	31.89	0.03	31.64	0.06		
313.15	30.56	0.05	31.17	0.45	30.55	0.00	30.52	0.03	30.74	0.03
323.15	29.45	0.21	30.14	0.01	29.86	0.01	29.46	0.01	29.70	0.01
333.15	28.16	0.04	28.60	0.04	28.62	0.03	27.90	0.22	28.50	0.00
343.15	27.40	0.02	27.39	0.29	27.84	0.01	27.14	0.76	27.71	0.39
353.15	26.68	0.03			26.62	0.07	26.22	0.20	26.89	0.04

T / K	SP	σ	SRP	σ	Sf	σ	GP	σ	Soy A	σ
303.15	31.27	0.04	31.53	0.01			31.57	0.01	30.89	0.55
313.15	30.47	0.03	30.49	0.03	31.15	0.09	30.55	0.23	29.74	0.38
323.15	29.70	0.02	29.40	0.08	29.39	0.16	29.54	0.27	28.66	0.06
333.15	28.76	0.06	28.56	0.05	28.29	0.02	28.50	0.22	27.98	0.05
343.15	27.68	0.03	27.29	0.01	27.47	0.17	27.59	0.09	26.97	0.13
353.15	26.68	0.04	26.07	0.02	26.04	0.19	26.57	0.02	25.97	0.10

$^{\sigma}$) Standard deviation

Given the scarcity of surface tension data for biodiesel fuels, it was only possible to compare the surface tension data for the soybean and palm biodiesel fuels with those measured by Allen et al. [177] at 313.15 K. It is shown that our data are circa 6 % higher than Allen's data for this temperature. Although the comparison of only one point is not very conclusive, this error is acceptable given the differences in composition between the biodiesel fuels.

Using the parachors suggested by Allen et al. [177], the predictions of surface tensions by the MacLeod-Sugden equation overestimate the experimental data within a 10 % deviation (OARD of 7.7%) as shown in **Figures 3.5.1** and **3.5.2**. This approach provides better predictions of surface tension when the parachors suggested by Knotts et al. [184] are used as seen in **Figures 3.5.3** and **3.5.4**. An OARD of 1.3% is obtained with this model that is not much higher than the experimental uncertainty of the data. A very good

description of the temperature dependency of the experimental data is achieved using this approach, as the RDs obtained for the two version of this model, shown in **Figures 3.5.2** and **3.5.4**, are almost temperature-independent. The average relative deviations (ARD) for the ten biodiesels studied are presented in **Table 3.5.3.** The reported results show the good predictive capacity of parachors through the MacLeod-Sugden equation to compute surface tensions of biodiesel fuels, in particular when the Knotts et al. [184] parachors are used

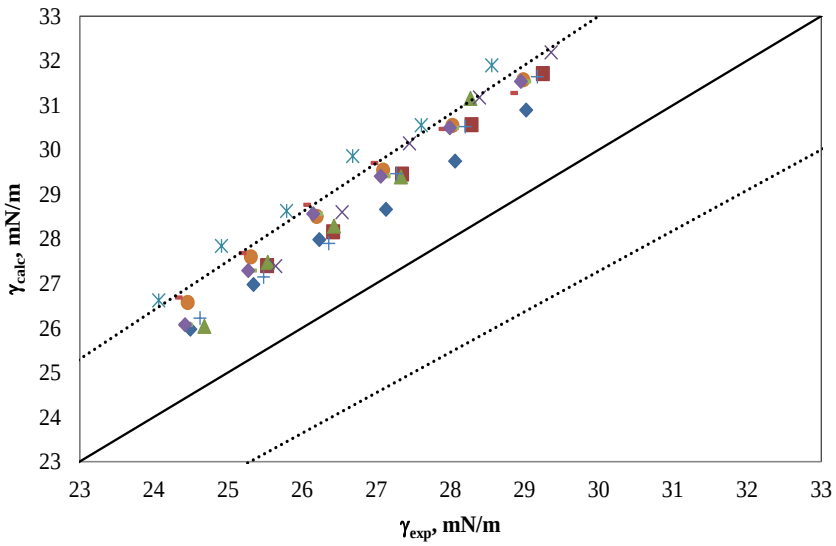

Figure 3.5 1. Linear relationship between predicted surface tensions using the MacLeod-Sugden equation with the parachors of Allen et al. [177]and experimental surface tensions equation for ten types of pure biodiesel fuels: : ◆Soy A,■ Soy B, ▲ Sf, × R, ✳ P, ● GP, + SR, – RP, - SP, ◆ SRP and ⋯⋯ ± 10% of relative deviation.

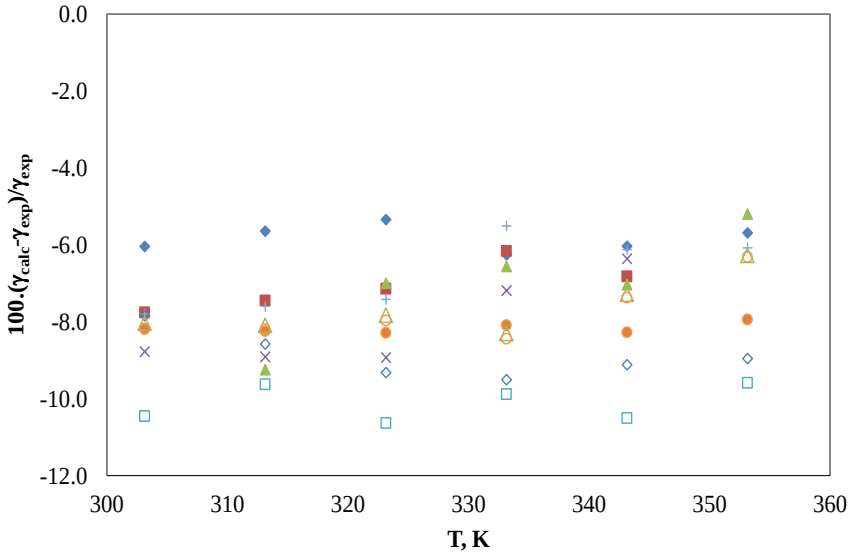

Figure 3.5 2. Relative deviations of the predicted surface tensions obtained with the MacLeod-Sugden equation using the parachors of Allen et al. [177] as a function of temperature for ten biodiesel fuels: ◆Soy A, ■Soy B, ▲Sf, ×R, ✳P, ●GP, + SR, – RP, - SP, ◆SRP

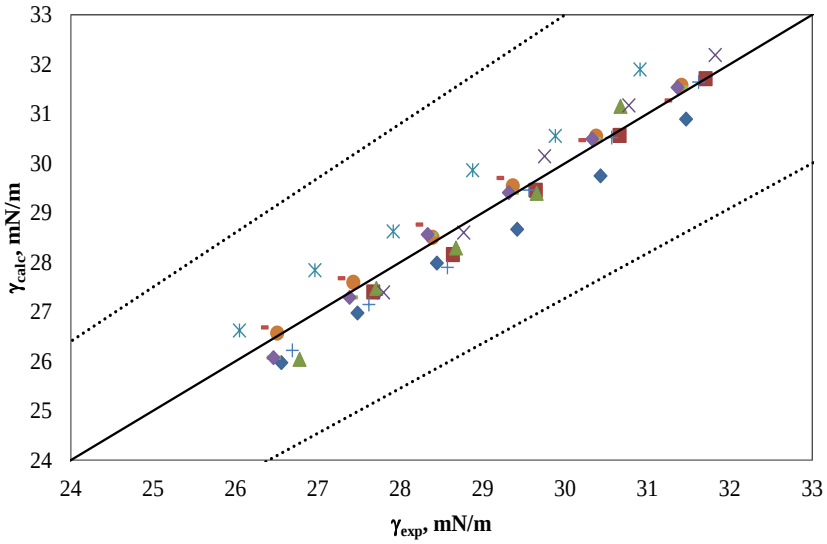

Figure 3.5 3. Linear relationship between predicted surface tensions using the MacLeod-Sugden equation with the parachors of Knotts et al [184] and experimental surface tensions for ten types of pure biodiesel fuels: ◆Soy A, ■Soy B, ▲Sf, ×R, ✳P, ●GP, + SR, – RP, - SP, ◆SRP and ••••••• ± 10% of relative deviation.

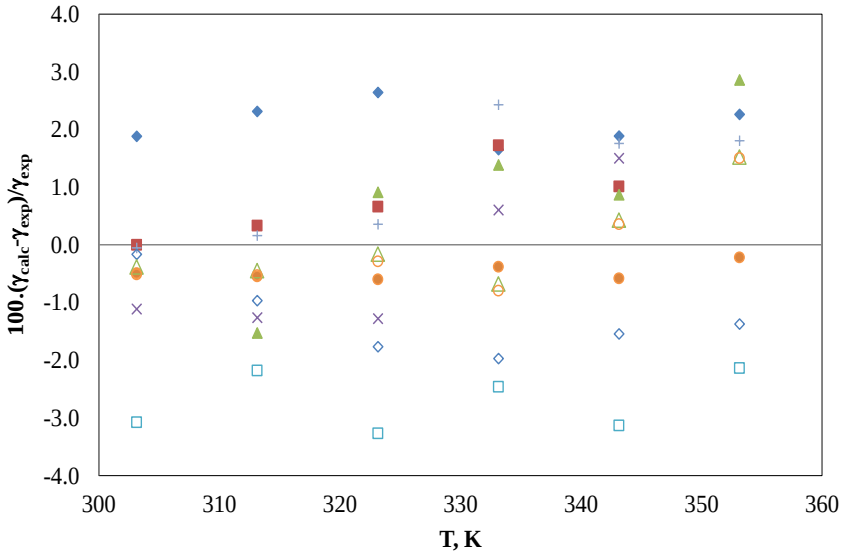

Figure 3.5 4. Relative deviations of the predicted surface tensions obtained with the MacLeod-Sugden equation using the parachors of Knotts et al [184]as a function of temperature for ten biodiesel fuels: ◆Soy A, ■Soy B, ▲Sf, × R, ✳ P, ●GP, + SR, – RP, - SP, ◆ SRP.

Table 3.5. 3. ARD for biodiesel surface tensions obtained with the MacLeod-Sugden equation and with the density gradient theory coupled with the CPA EoS model

	ARD, %		
Biodiesel	Allen's parachors	Knotts'parachors	GT+CPA EoS
Soy B	7.1	0.67	11
R	8.0	1.1	9.4
P	10	2.7	5.1
SR	6.6	1.3	12
PR	7.6	0.60	7.8
SP	8.9	1.3	8.2
SRP	7.7	0.66	9.6
Sf	7.0	1.5	12
GP	8.2	0.47	10
Soy A	5.8	2.1	12
OARD, %	**7.7**	**1.3**	**9.7**

The gradient theory coupled with the CPA EoS was previously used for the description of the surface tensions of a series of esters, with 37 ester compounds evaluated, including formates, acetates, methyl, ethyl, propyl, butyl, and unsaturated methyl esters [186]. As discussed above, the influence parameter definition is too complex to be easily implemented, and alternatively, influence parameters are adjusted from surface tension data and plotted (far from the critical point) using the energy and co-volume parameters of the physical part of the CPA EoS (as $c/ab^{2/3}$) as a function of (1-T_r) [189, 195, 196]. It was

showed in a previous work [186] that, for esters, the influence parameter dependency with the temperature is linear up to a T_r of about 0.70, and consequently, a linear approach for the influence parameter temperature dependence was considered, resulting in only two parameters to be correlated.

$$\frac{c}{ab^{2/3}} = D + E \times (1 - T_r)^2 \tag{3.5.9}$$

Furthermore, plotting the parameters of the linear equation against the acentric factor it was seen that these parameters don't vary significantly, and average values were estimated for *D* and *E*, aiming at using this approach in a predictive way, to estimate surface tensions for biodiesels. For this work $D \times 10^6 = 0.6177$ and $E \times 10^6 = -0.4425$ [186].

Using these assumptions, the density gradient theory coupled with the CPA Eos was used to predict the ten measured biodiesels surface tension data. The surface tensions are in general underpredicted and within a 10% deviation from the reported experimental data, as shown in **Figure 3.5.5**. The RDs are almost temperature-independent, as reported in **Figure 3.5.6**, showing that the temperature dependency of the experimental data is correctly described. The average relative deviations (ARD) for the ten biodiesels studied are presented in **Table 3.5.3**, and an overall value (OARD) of 9.7 % was achieved.

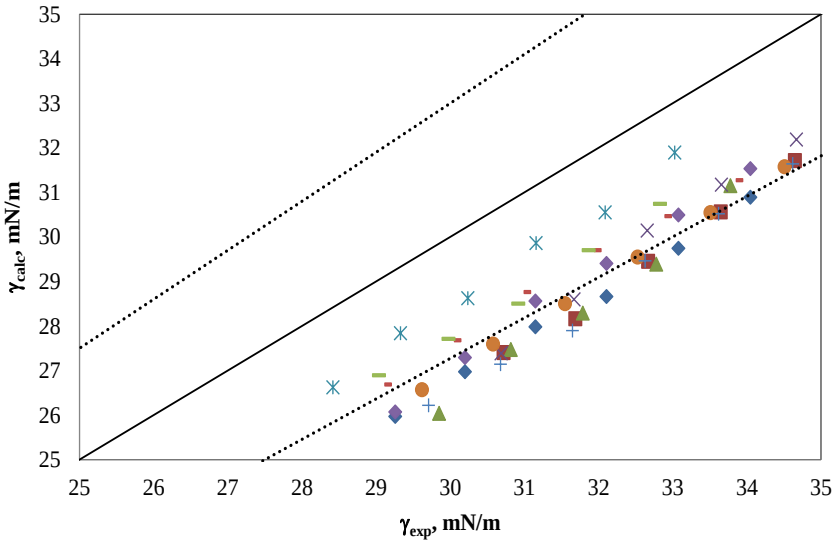

Figure 3.5 5. Linear relationship between experimental and predicted surface tensions using the density gradient theory coupled with the CPA EoS for ten types of pure biodiesel fuels: ◆ Soy A, ■ Soy B, ▲ Sf, × R, ✳ P, ● GP, + SR, – RP, - SP, ◆ SRP and ····· ± 10% of relative deviation

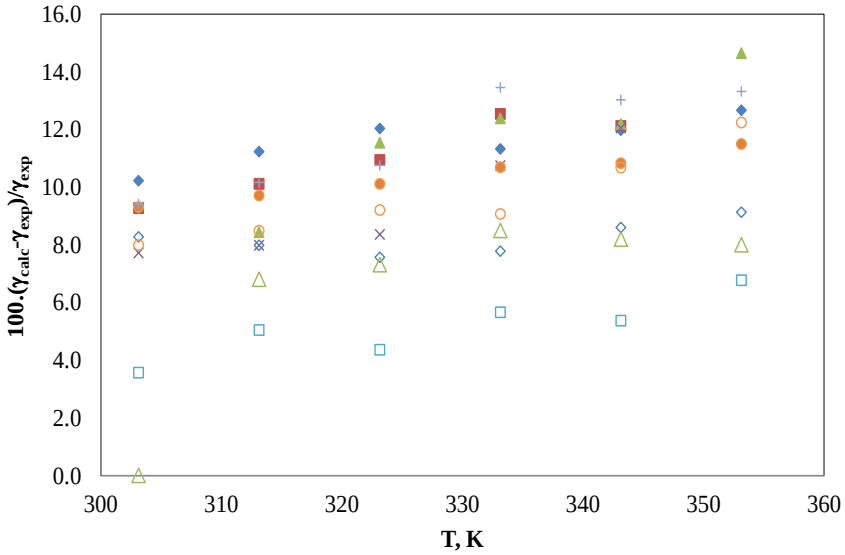

Figure 3.5 6. Relative deviations between predicted surface tensions using the density gradient theory coupled with the CPA EoS and experimental surface tensions as a function of temperature for ten biodiesel fuels: ◆Soy A, ■Soy B, ▲Sf, ×R, ✳P, ●GP, +SR, –RP, -SP, ◆SRP

These results are remarkable because the modeling of biodiesels with the gradient theory is considerably more difficult (and predictive) than for pure esters, because density profiles have to be calculated at each discrete point of the dividing interface limited by the upper and lower phase densities [188]. From the presented results, it is possible to conclude that the coupling of the gradient theory with the CPA EoS provides a more complex yet appealing approach to predict surface tensions of biodiesels, allowing for a simultaneous description of the surface tensions and phase equilibria, using constant parameters for the linear temperature dependence of the ester influence parameters. Additionally, it does not require the *a priori* knowledge of the liquid-phase densities, as occurs with the parachor models.

The surface thermodynamics properties namely surface entropy that corresponds to the slope of the curve of the measured surface tension data as a function of temperature, and surface enthalpy were also determined by using the eqs. (3.5.10) and (3.5.11).

$$S^{\gamma} = -\left(\frac{\partial \gamma}{\partial T}\right) \tag{3.5.10}$$

$$H^{\gamma} = \gamma - T\left(\frac{\partial \gamma}{\partial T}\right) \tag{3.5.11}$$

In equation above S^{γ} is the surface entropy in $J.m^{-2}.K^{-1}$, γ is the surface tension in mN/m, H^{γ} is the surface enthalpy in $J.m^{-2}$, and T is the absolute temperature in K.

The values of the two surface properties and the corresponding expanded uncertainty are presented in **Table 3.5.4**, where it is possible to see that all the biodiesel fuels present similar surface enthalpies but their surface entropies are dependent on the unsaturation degree of the biodiesel. Moreover the surface enthalpy for the biodiesel fuels is temperature independent within the temperature range studied.

Table 3.5. 4. Surface thermodynamics functions for the biodiesel fuels studied

Biodiesel	$(S^{\gamma} \pm S_d).10^5 J.m^{-2}.K^{-1}$	$(H^{\gamma} \pm S_d).\ 10^2 J.m^{-2}$
Soy B	10.72 ± 0.53	6.26 ± 0.17
R	12.15 ± 0.57	6.92 ± 0.18
P	10.21 ± 0.39	6.27 ± 0.13
SR	11.09 ± 0.50	6.52 ± 0.16
RP	9.69 ± 0.48	6.10 ± 0.16
SP	9.22 ± 0.10	5.93 ± 0.53
SRP	10.78 ± 0.30	6.43 ± 0.10
Sf	12.14 ± 0.87	6.89 ± 0.29
GP	9.98 ± 0.08	6.18 ± 0.03
Soy A	9.60 ± 0.30	5.99 ± 0.10

S_d) Expanded uncertainty with an approximately 95 % level of confidence.

3.5.5. Conclusions

Surface tensions of ten biodiesel fuels were measured at temperatures from 303.15 to 353.15 K and at atmospheric pressure.

Two different modeling approaches were used to predict the experimental data: the MacLeod-Sugden equation with two different parachor sets and the density gradient theory coupled with the CPA EoS. The first method presented an OARD of 7.7 % when using the Allen's parachors and of 1.3 % with Knotts' parachors, showing that a simple and empirical method, based on parachors, can be applied to predict, from the composition, the temperature dependence of the biodiesel surface tensions.

Using constant parameters for the linear temperature dependence of the influence parameter for all the fatty acid esters constituting the different biodiesels, the gradient theory in combination with the CPA EoS was shown to predict biodiesels surface tensions with an OARD of 9.7 %, while also providing information concerning the phase equilibria of the biodiesel systems.

These results clearly show that, provided that the biodiesel FAME composition is known, the predictive methods here investigated here can be used to predict surface tensions of biodiesel fuels in a wide range of temperatures.

3.6. Measurement and Prediction of Speed of Sound

As there was no equipment for measuring speeds of sound at the University of Aveiro, the samples here studied were analysed by our collaborators in other universities. The atmospheric speeds of sound of methyl esters and methylic biodiesels were measured in Brasil by Prof. Dr. Márcio L.L. Paredes and his group at the UERJ. The atmospheric speeds of sound of ethyl esters and ethylic biodiesels were measured at the University of Lisboa by Dr. Ângela Santos and her group. The methylic biodiesels were produced by Dr. Maria Jorge while the ethylic biodiesels were produced by Prof. Dr. Meirelles and his group at the University of Campinas in Brasil. This section is an adapted version of the three articles published in the journals of Energy & Fuels and Fuel [197-199].

3.6.1. Introduction

Isentropic bulk modulus and speed of sound are the two properties with important impacts on the injection process of a fuel. While the first measures the compressibility of the fuel under pressure, i.e., it affects the amount of pressure rise that will occur from the fuel pump pulse, the second affects the time required for the pressure rise to proceed through the fuel line and reach the injector. In comparison to petroleum fuel, biodiesel has higher values of both properties. A higher isentropic bulk modulus and higher speed of sound would cause an earlier injection of fuel and also an earlier combustion, which raises peak in-cylinder temperature, thereby increasing thermal NO_x formation [200] namely for injectors activated with pressure [177, 201, 202]. Thus the bulk modulus and speed of sound values are relevant for system modeling and experimental injection rate determination [203]. They are important for the study of the injection rate, injection timing, injection duration, injection pressure, start of combustion, in-cylinder gas pressure and temperature and heat release rate that influence the final NO_x emissions [204].

In case of speed of sound, just like any other thermophysical properties, its magnitude is influenced by the structure of the fatty acid alkyl esters that compose biodiesel fuels such as chain length, branching and level of unsaturation [205]. Thus the knowledge of the relationship between the biodiesel properties and the percentage of fatty esters in biodiesels is of great importance.

Unfortunately there are not so many data available in the literature for fatty acid methyl esters (FAME) [144, 197, 202, 206-210], being the experimental speeds of sound of fatty acid ethyl esters (FAEE) even more scant [211], although some studies were already done for the shorter methyl and ethyl esters [212]. The oldest experimental data of the speed of sound include those reported by Gouw et al. [207] at 20 and 40 °C for methyl esters and by Tat et al.[209] for biodiesel fuels at pressures from atmospheric to 35 MPa. Later, these authors also proposed correlations to estimate the speeds of sound of alkyl monoesters at higher temperatures and pressures[202]. Ott et al.[210] provided the speeds of sound for five methyl esters as a function of the temperature at 83 kPa. Recently, some experimental data were reported by Huber et al.[213] for two commercial biodiesels and by Kumar et al.[214] for *Jatropha curcas* biodiesel at atmospheric pressure. Daridon et al.[211] provided experimental data for several pure fatty acid esters at atmospheric pressure and temperatures from 283.15 to 373.15 K and published [215] high-pressure

speeds of sound for methyl caprate and ethyl caprate. This work provides new experimental data of speed of sound for several fatty esters and biodiesel fuels measured at different temperature and pressure and then using them to evaluate the predictive ability of several methods.

3.6.2. Experimental Details: samples and measurement procedures

3.6.2.1. Speed of Sound of FAME and methylic biodiesels

The eight methyl esters here studied were methyl laurate (with 97% of purity from Fluka), methyl myristate (with 98% of purity from SAFC) and Methyl Oleate (with 99% from Aldrich), methyl caprylate, (with 99% purity from Sigma-Aldrich); methyl caprate, (with 99% purity from Fluka); methyl palmitate, (with 99% purity from Sigma-Aldrich); methyl stearate, (with 99% purity from Fluka) and methyl linoleate, (with 99% purity from Sigma-Aldrich). The ten methylic biodiesel fuels reported by Pratas et al.[129] and addressed in **Section 3.2** are here used again to study the speed of sound.

The density and speed of sound were obtained using an automatic digital densimeter (Anton Paar DSA 5000). DSA 5000 simultaneously determines two physically independent properties within one sample. The instrument is equipped with a density cell and a sound velocity cell combining the known oscillating U-tube method with a highly accurate measurement of the speed of sound.[216] The density and speed of sound meter was calibrated against ultrapure water and air at atmospheric pressure. The calibration was accepted if the measurements were estimated to be within $\pm 2 \times 10^{-3}$ kg m^{-3} and ± 0.02 m s^{-1} of the reference values, respectively. The measurements were obtained in duplicates, and the standard experimental uncertainty was obtained by dividing the modulus of the repeatability differences by the square of two. The value obtained was 0.23 m/s for 142 repetition points [216]. The estimated standard uncertainties in density and speed of sound measurements are 2×10^{-2} kg m^{-3} and 0.1 m s^{-1}, respectively. The standard uncertainty in the temperature is 0.01 K.

3.6.2.2. Speed of Sound of FAEE and ethylic biodiesels

The nine ethyl esters here studied were ethyl butyrate (98% quoted purity from Fluka), ethyl caprylate (>99% quoted purity from Aldrich), ethyl caprate (99% quoted purity from Fluka), ethyl laurate (99% quoted purity from Sigma), ethyl myristate (99% quoted purity from Aldrich), ethyl palmitate (>99% quoted purity from Sigma), ethyl stearate (>99.0% quoted purity from Fluka), ethyl oleate (>98% quoted purity from Aldrich), ethyl linoleate (>99% quoted purity from Sigma). These compounds were used as received without any further purification. The four biodiesel fuels here used (S, Sf, S+B and P) are already described in **Section 3.2**.

Experimental measurements of density and speed of sound were made concurrently using an Anton Paar vibrating tube densimeter and ultrasound speed meter, model DSA 5000M, with an automatic temperature control within ±0.01 K. All measurements were made at ambient pressure. According to the procedure already described elsewhere [217], calibration of the speed of sound cell was made with degassed Millipore ultra-quality water. Measurement and comparison with literature values of speed of sound of toluene and cyclohexane at 25 °C leads us to assume an accuracy of 0.5 m s^{-1}, as claimed by the manufacturer. In the case of density, besides the usual method recommended by the manufacturer of using dry air and degassed ultra-pure water at 293.15 K as reference fluids, a new calibration procedure thoroughly described elsewhere [218] was performed. The calibrants used were ultra-pure water and dodecane with certified density values issued by H§D Fitzgerald, with expanded uncertainties of 0.01 kg m^{-3} (coverage factor $k = 2$, providing a 95% level of confidence). The use of this pair of calibrating fluids allowed a close bracketing of the densities measured, the importance of which has recently been emphasized by Fortin et al.[219] As the temperature range of certified density values for dodecane does not cover values higher than 323.15 K, an extrapolation of those values had to be made. However, a careful analysis of results based on comparison between direct density values (taken from direct readings of the densimeter) and final values obtained from the calibration procedure allowed a reassurance about the validity of that extrapolation.

Every day before starting the measurements, the usual routine procedure of performing a water and air check was invariably adopted. Before injection all samples

were pre-heated, and degassed, at the maximum experimental temperature. Then, for the same single sample injection a complete series of measurements was made, decreasing the temperature from 343.15 K to 293.15 K in decrements of 5 K. At each temperature three to seven data readings were taken and some measurements were repeated with a new injection, allowing asserting an estimate for the repeatability and standard uncertainty for density values lower than 0.0006% and 0.005%, respectively, and for speed of sound of 0.01% and 0.02%, respectively. After each set of measurements the instrument was flushed several times with *n*-heptane at 333 K and with acetone at 313 K, sequentially, and then dried at 343 K during at least 1 h, with a stream of forced room air. To assess the effectiveness of these cleaning actions, new air and water checks were done and whenever deviations higher than 0.002% for density and 0.013% for sound speed were found, a new cycle of cleaning steps was executed.

3.6.3. Models for speed of sound

The description of speed of sound for fatty esters (FAME and FAEE) and biodiesel fuels was done by using the Auerbach's relation, linear mixing rule and the Wada's group contribution method as individually described bellow.

3.6.3.1. Auerbach's model

The Auerbach's model [220, 221] is represented by Eq. (3.6.1), where u is the speed of sound in $m.s^{-1}$, γ is the surface tension in $N.m^{-1}$and ρ is the density in $kg.m^{-3}$. Since this equation requires the prior knowledge of densities and surface tensions, this work uses the data reported in our previous works [129, 136].

$$u = \left(\frac{\gamma}{6.33 \times 10^{-10}.\rho} \right)^{\frac{2}{3}} \tag{3.6.1}$$

This work also considered a modified version of Auerbach's model, in order to achieve a better description of the experimental speed of sound data for biodiesel fuels, by relaxing the value of the constant*c1*of Eq. (3.6.2).

$$u = \left(\frac{\gamma}{6.33 \times 10^{-10} . \rho} \right)^{\left(\frac{2}{3} . c1 \right)} \quad (3.6.2)$$

3.6.3.2. Ideal Mixture Mixing Rules

As biodiesel fuels are a mixture of FAME (or FAEE) of similar molecular weight, their speeds of sound can be estimated using a mixing rule assuming an ideal mixture behavior. This approach, described by Eq. (3.6.3), will be here used to describe the speed of sound of biodiesels, where u_{BD} is the speed of sound of biodiesel in m/s, x_i is the molar composition and u_i is the speed of sound of individual fatty esters in m/s.

$$u_{BD} = \sum_i x_i u_i \quad (3.6.3)$$

To calculate the speed of sound of methylic and ethylic biodiesels some approaches have to be done especially when there are no data for some esters. So for methylic biodiesels, due to lack of experimental data of speed of sound for some minoritary FAME compounds, such as C10:0, C16:1, C20:0, C20:1, C22:0, C22:1 and C24:0, the pseudo-component concept was adopted by adding C10:0 to C12:0, C16:1 toC16:0 and C20:0, C22:0 and C24:0 to C18:0 and C20:1 and C22:1to C18:3. In this work the experimental speed of sound for the methyl esters used, with their respective purities, was that reported by Tat et al. [202] except for C14:0 measured in this work. This methyl ester has 98 % of purity.

The same procedure is valid for the ethylic biodiesels, i.e., since there are no experimental data of speed of sound for some of the less common FAEE, to use the mixing rules, a pseudo-component approach is used by adding C16:1 to C16:0 and C20:1, C22:0 and C24:0 to C20:0.The nomenclature for esters here adopted is based on the fatty acid chain length.

3.6.3.3. Wada's Group Contribution Method

The Wada's Group Contribution Method was previously proposed by Daridon et al.[211] to predict the speed of sound of alkyl esters. This model simply relates speed of

sound (u in m s^{-1}) with density (ρ in kg m^{-3}), molecular mass (Mw in g mol^{-1}) and molecular compressibility (κ_m) according to the following equation:

$$u = \rho^3 \left(\frac{\kappa_m}{Mw} \right)^{7/2} \tag{3.6.4}$$

The molecular compressibility (κ_m) is also known as Wada's constant and its value can easily be decomposed in groups [211] allowing for the establishment of a group contribution model as presented in the following equation:

$$K_m(T) = \sum_{j=1}^{n_G} N_j \, K_{m,j}(1 - \chi(T - T_0)) \tag{3.6.5}$$

Where $K_{m,j}$ connotes the Wada's constant of the group j which occurs N_j times in the given molecule and χ is a constant parameter used to take into account the influence of temperature.

To carry out the predictions of speed of sound using the Wada's model, the ester molecule must be split into five main groups: -CH_3- and -CH_2- to account the linear and saturated alkyl chain, -CH=CH- to describe the contribution of the unsaturation of the alkyl chain and -CH_3COO- and -CH_2COO- to take into account the ester contribution from methyl and ethyl esters, respectively. Then the corresponding Wada's constants reported in Daridon et al. [211], are used to estimate the speed of sound for each ethyl ester in the range of temperatures investigated.

For biodiesels, the application of Wada's model can be carried using two different approaches. The first approach (Wada 1) follows exactly the method described above, i.e., splits the biodiesel molecules into the main groups aforementioned, whose Wada's constants are already known, then predicts their speeds of sound using either the experimental or predicted densities of biodiesels using a linear mixing rule of the densities of the pure fatty acid esters as the two approaches present only ca. 0.1% of difference. The second approach (Wada 2) consists of using a linear mixing rule to predict the speed of sound of biodiesels from that of their pure constituents (fatty esters) according to Eq. (3.6.1), but with the speed of sound of pure esters (u_i) predicted with the Wada's model.

For this approach the estimation of the densities for pure FAEE were the same as those used in Wada 1.

3.6.4. Results and discussion

3.6.4.1. Speed of sound of FAME and methylic biodiesels

The experimental data of speed of sound for eight pure methyl esters and ten biodiesels here studied are reported in **Tables 3.6.1** to **3.6.2**. The experimental data of speed of sound for the methyl esters here measured were compared to those reported in the literature [202, 207, 210, 211]. The results show a good agreement between the experimental and literature data, presenting only deviations within ± 1 % of literature data as seen in **Figures 3.6.1 and 3.6.2**, except for methyl palmitate reported by Tat et al.[202] with a sample of questionable purity. At the same conditions, the speed of sound for methyl linoleate is thus higher than that of methyl palmitate and methyl stearate, as seen in **Table 3.6.1.** These results in biodiesels with a high level of saturated short-chain compounds, such as those based on palm [197] or coconut oil, present lower speeds of sound than those containing high levels of unsaturated compounds, such as biodiesel based on sunflower oil [197].

For biodiesel fuels, very small differences in the speed of sound are observed between the various biodiesels studied. Both the magnitude of the speed of sound and its temperature dependency vary less than 1% between the fluids, unlike what was previously observed for other properties [130, 136, 216]. In spite of the similarities it can be observed, nevertheless, that the increase in concentration of the saturation level of the compounds decreases the speed of sound. The palm biodiesel and the mixtures containing palm present the lower speeds of sound, while the sunflower has the largest speed of sound measured in this work.

Table 3.6. 1. Experimental speed of sounds, in $m \cdot s^{-1}$, for FAME measured at atmospheric pressure (NM= not measured)

T/K	C8:0	C10:0	C12:0	C14:0	C16:0	C18:0	C18:1	C18:2
288.15	1312.31	1344.23	1369.55	NM	NM	NM	1427.25	NM
293.15	1293.2	1325.5	1350.85	NM	NM	NM	1409.44	NM
298.15	1274.01	1306.68	1332.26	1353.19	NM	NM	1391.68	1400.39
303.15	1254.99	1287.99	1313.78	1334.98	NM	NM	1374.06	1382.74
308.15	1236.03	1269.46	1295.44	1316.91	1337.04	NM	1356.62	1365.15
313.15	1217.25	1251.04	1277.24	1298.96	1319.38	1333.43	1339.31	1347.72
318.15	1198.54	1232.81	1259.25	1281.21	1301.76	1315.93	1322.15	1330.49
323.15	1179.99	1214.66	1241.39	1263.57	1284.34	1298.56	1305.06	1313.35
328.15	1161.53	1196.69	1223.68	1246.11	1267	1281.36	1288.19	1296.33
333.15	1143.22	1178.8	1206.08	1228.73	1249.72	1264.32	1271.39	1279.42
338.15	1124.98	1161.06	1188.39	1211.48	1232.72	1247.41	1254.72	1262.69
343.15	1106.88	1143.35	1171.08	1194.32	1215.83	1230.65	1238.21	1245.98

Table 3.6. 2. Experimental Speed of Sound, in $m \cdot s^{-1}$, for Methylic Biodiesel

T / K	S	R	P	SR	RP	SP	SRP	Sf	GP	SoyA
288.15	1430.23	1430.79	1420.04	1430.66	1424.52	1424.92	1426.90	1432.34	1428.88	1428.53
293.15	1412.39	1412.26	1401.86	1412.77	1406.55	1406.86	1408.97	1414.56	1410.97	1410.73
298.15	1394.54	1394.11	1383.88	1394.95	1388.65	1388.94	1391.11	1396.53	1393.10	1392.90
303.15	1376.86	1376.22	1366.08	1377.27	1370.89	1371.17	1373.36	1378.54	1375.39	1375.17
308.15	1359.20	1358.40	1348.38	1359.76	1353.34	1353.61	1355.80	1360.74	1357.86	1357.63
313.15	1341.80	1340.88	1331.14	1342.37	1335.91	1336.17	1338.37	1343.04	1340.47	1340.16
318.15	1324.55	1323.55	1313.88	1325.16	1318.60	1318.86	1321.11	1325.80	1323.21	1322.90
323.15	1307.37	1306.31	1296.69	1308.07	1301.48	1301.73	1303.97	1308.63	1306.07	1305.75
328.15	1290.35	1289.26	1279.72	1291.15	1284.49	1284.74	1287.00	1291.53	1289.12	1288.79
333.15	1273.43	1272.30	1262.94	1274.31	1267.62	1267.86	1270.13	1274.60	1272.26	1271.91
338.15	1256.69	1255.59	1246.18	1257.61	1250.85	1251.09	1253.40	1257.76	1255.52	1255.17
343.15	1240.02	1239.05	1229.66	1241.09	1234.28	1234.51	1236.84	1241.05	1238.99	1238.53

Table 3.6. 3. Experimental density, in $kg.m^{-3}$, for FAME measured at atmospheric pressure

T, K	C8:0	C10:0	C16:0	C18:0	C18:2
288.15	881.3	876.5			
293.15	877.0	872.4			887.6
298.15	873.0	868.3			883.9
303.15	868.2	864.2			880.3
308.15	863.9	860.1	854.3		876.7
313.15	859.5	856.0	850.6	849.8	873.0
318.15	855.1	851.8	846.9	846.2	869.4
323.15	850.7	847.7	843.2	842.6	865.7
328.15	846.3	843.6	839.5	838.9	862.1
333.15	841.7	839.4	835.8	835.3	858.4
338.15	837.4	835.3	832.1	831.7	854.8
343.15	833.0	831.1	828.4	828.1	851.1

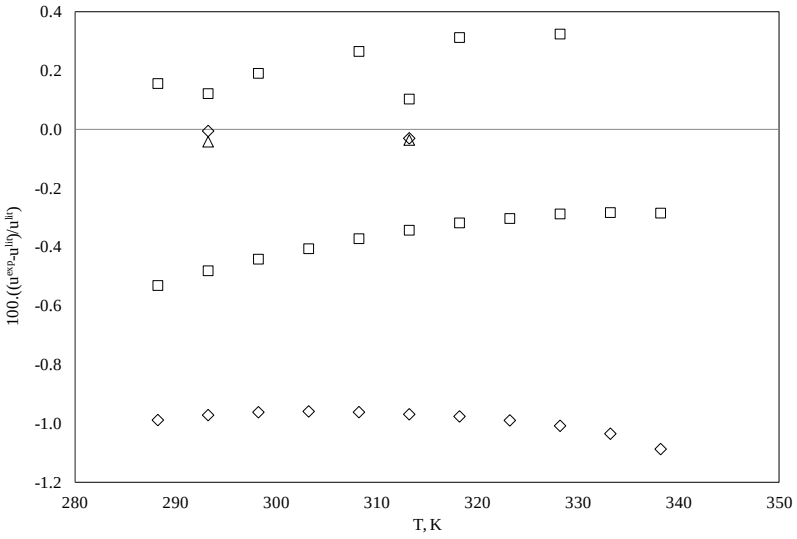

Figure 3.6 1. Relative deviations of the speed of sound of three methyl esters here studied ◇ Methyl Laurate, △ Methyl Myristate and □ Methyl Oleate [202, 207, 210]

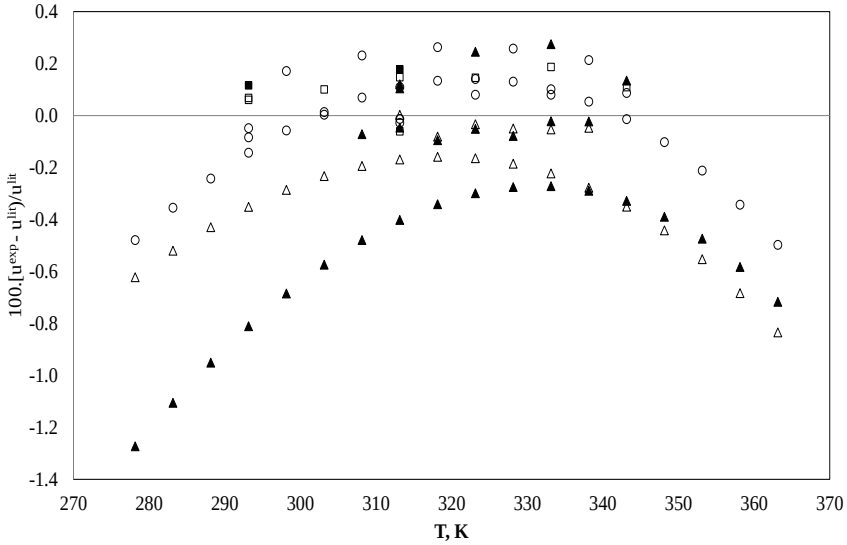

Figure 3.6 2. RDs between experimental and literature data of the speed of sound for esters : (■) methyl caprylate, [207] (□) methyl caprate, [207, 211] (▲) methyl palmitate, [202, 207, 210, 211] (△) methyl stearate, [202, 207, 210, 211] and (°) methyl linoleate. [202, 207, 210, 211]

The experimental speeds of sound of biodiesels were firstly predicted with the Auerbach's equation and the Ideal Mixture Mixing Rules. The results reported in **Table 3.6.4**, however, show that the original Auerbach's equation fails to provide a good description of the experimental data. Aiming at enhancing the description of the data the value of the model parameter was modified. To develop the modified Auerbach's relation, four methyl esters (methyl palmitate, methyl oleate, methyl stearate and methyl linoleate) reported by Ott et al. [210]and three biodiesels (S, SR and SRP) were used as training set to adjust the value of *c1,* while the other methyl esters and biodiesels here measured were used as validation set. A value for *c1 of 0.987* was obtained that provided an OARD of 1.3 % for the training set and of 1.4 % for the validation set in the temperature range 283-373 K. The behavior of the modified Auerbach's model for both set of compounds can be seen separately in **Figures 3.6.3 and 3.6.4** where the deviation between the predicted and experimental data is within ± 4.0%. A deficient temperature dependency of the model is highlighted in these figures.

Table 3.6. 4. ARD of speed of sound for biodiesel fuels using the models here studied.

Biodiesel	ARD, %		
	Auerbach original	Modified Auerbach	Ideal Mixture
BD-A**[213]**	8.1	1.9	0.18
BD-B**[213]**	8.4	1.8	0.23
BD-JC**[214]**	7.5	2.1	0.11
Methyl Soy ester**[202]**	7.8	1.9	0.090
Methyl Canola**[202]**	8.2	1.7	0.2
Methyl Tallow**[202]**	8.0	2.0	0.76
Methyl Lard**[202]**	8.5	1.6	0.24
Methyl oxidized soy**[202]**	11	1.9	1.1
Methyl hydrogenated soy**[202]**	7.9	1.9	0.39
NIST SRM 2772 B100**[121]**	7.9	2.0	0.34
NIST SRM 2773 B100**[121]**	8.2	1.8	0.53
S	9.3	1.5	0.34
Soy A	8.0	1.2	0.29
R	11	1.5	0.33
P	12	1.5	0.46
Sf	9.8	1.4	0.33
SP	10	1.2	0.36
SR	9.0	1.5	0.25
PR	11	1.5	0.46
SRP	9.9	1.5	0.38
GP	9.8	1.2	0.37
OARD, %	**9.1**	**1.7**	**0.37**

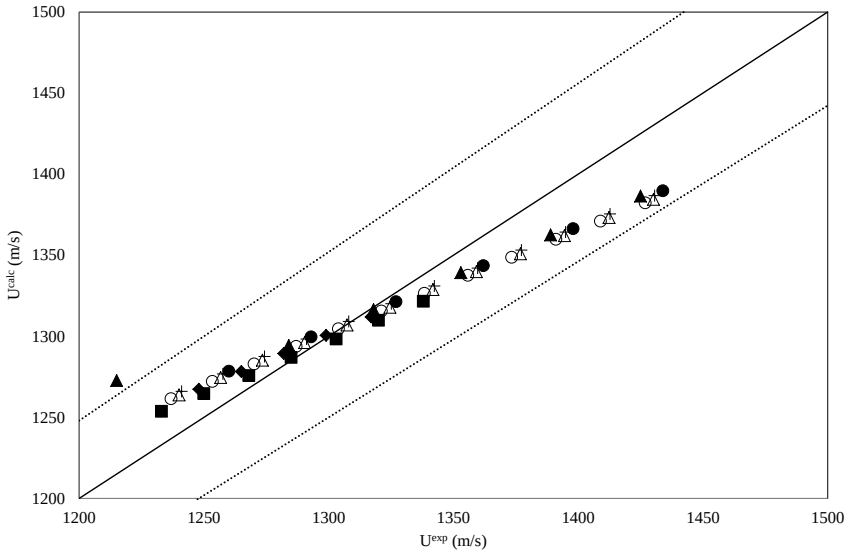

Figure 3.6 3. Predicted vs. experimental speed of sound of the training set for modified Auerbach's model. ■ Methyl palmitate, ◆ Methyl stearate, ▲ Methyl oleate, ● Methyl linoleate, △ S, + SR, ○ SRP and ····· ±4%

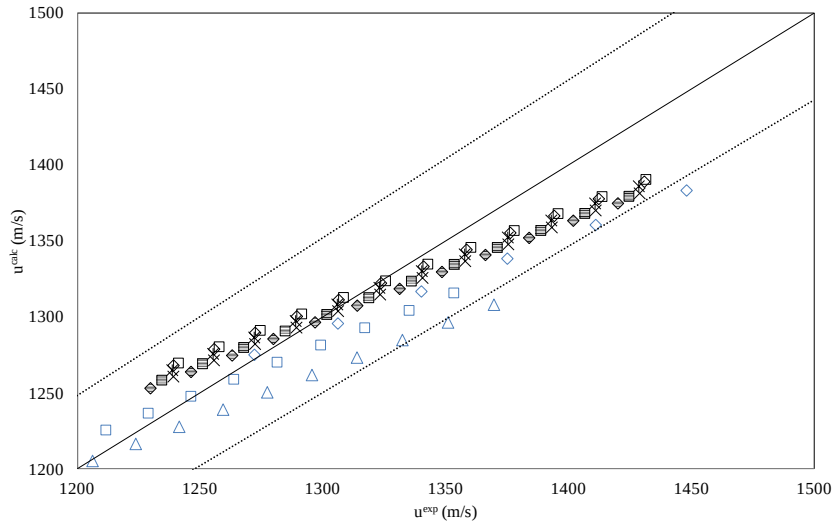

Figure 3.6 4. Predicted vs. experimental speed of sound of the validation set for the modified Auerbach's model. △ Methyl Laurate, □ Methyl Myristate, ◇ Methyl oleate, ✳ soy A, ◇ R, ◆ P, □ Sf, × GP, ▭ SP and ····· ±4%

The ARD for the ten biodiesels here studied and eleven other biodiesels previously reported in the literature are presented in **Table 3.6.4** for the various models investigated. Here it can be seen that the ideal mixture mixing rules is seen to be the more appropriate model for describing the speeds of sound for biodiesel fuels, presenting only an OARD of 0.37 % for 21

biodiesel fuels here studied and the individual value of ARD was almost of the same magnitude for all biodiesels in comparison with 9.1 and 1.6 % of the original Auerbach's equation and the modified Auerbach's model respectively. The behavior of predictions of speed of sound for biodiesel fuels are shown in **Figure 3.6.5.** It is possible to observe again that the ideal mixture mixing rules is the most appropriate model for describing the experimental data, allowing a good prediction of their temperature dependency.

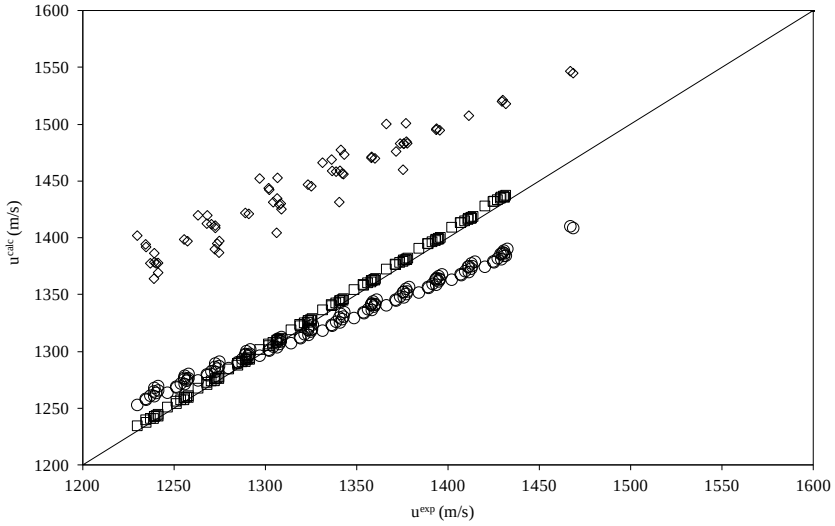

Figure 3.6 5. Predictive ability of the three models evaluated in describing the experimental data of speed of sound for the biodiesel fuels here studied: ◇ Auerbach original, ○ Modified Auerbach and □ Ideal mixture mixing rules

To estimate the speed of sounds for methylic biodiesel fuels at high pressures, this work used the experimental data of speed of sound reported by Tat et al.[202] to develop a correlation. The experimental data displays very similar pressures dependencies for the speeds of sound observed for the pure FAME's and for the biodiesel fuels, that are linear in the range of pressures (0-35 MPa) studied by Tat et al.[202] For the same pressure range, a linear behavior is also observed for the experimental data reported by Pairy et al.[203]. It should thus be possible to describe the pressure dependency of the speed of sound up to 40 MPa by

$$u = u_0 + aP \tag{3.6.6}$$

Where u is the speed of sound in m/s, u_0 is the speed of sound at atmospheric pressure, a is the pressure gradient and P is the pressure in MPa. To develop a high pressure correlation for the

speed of sound of biodiesel fuels the six FAME, C12:0, C16:0, C18:0, C18:1, C18:2 and C18:3 reported by Tat et al.[202], were used as the training set while the other six biodiesels as the validation set. After fitting the Eq. (3.6.6) to the experimental data of the training set, the numerical value of the pressure gradient was obtained (a=4.53 m s^{-1} MPa^{-1}). This correlation of speed of sound provided an OARD of 0.37 % for the training set and 0.56 % for the validation set as detailed in **Table 3.6.5**. The validity of these correlations is limited to the pressures below 40 MPa and should not be extrapolated to higher pressures. As shown by Pairy et al. [203] for higher pressures the pressure dependency of the speed of sound is no longer linear. Unfortunately at present the data available precludes the development of a correlation for higher pressures.

Table 3.6. 5. ARDs of speed of sound for methyl esters and biodiesel fuels at high pressure [202, 203]

Compound	ARD, %	
	Training set	Validation set
C12:0	0.46	
C16:0	0.38	
C18:0	0.35	
C18:1	0.34	
C18:2	0.34	
C18:3	0.35	
Methyl Soy Ester		0.35
Methyl Canola		0.34
Methyl Tallow		0.37
Methyl Lard		0.33
Methyl Oxidized Soy		0.35
Methyl Hydrogenated soy		0.24
Rapeseed Methyl Ester		0.82
OARD, %	**0.37**	**0.56**

The experimental speeds of sound for some methyl esters presented in **Table 3.6.1** were also used to assess the Wada's group contribution model. The adequacy of this model for predicting the speeds of sound of the fatty acid esters here studied is reported in **Figure 3.6.6**. The results show that the speed of sound of the methyl esters is well-described by this model, with temperature-dependent deviations that change only slightly, within ±0.3%, in the range of

temperatures studied. Individual deviations for each ester are reported in **Table 3.6.6**, with maximum values for C8:0 and C18:2 that are lower than 0.2% and an OARD of just 0.12%.

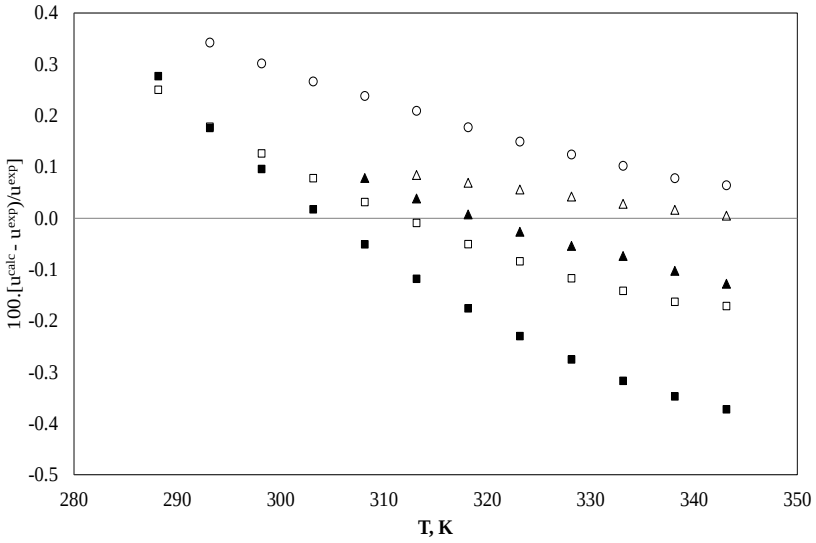

Figure 3.6 6. RDs between experimental and predicted data of the speed of sound for methyl esters using Wada's model: (■) methyl caprylate, (□) methyl caprate, (▲) methyl palmitate, (△) methyl stearate, and (°) methyl linoleate

Table 3.6. 6. ARDs of the Speed of Sound for FAME Using Wada's Model

FAME	ARD, %
C8:0	0.20
C10:0	0.10
C16:0	0.064
C18:0	0.043
C18:2	0.19
OARD, %	**0.12**

The molar additivity rule is here used again to predict the speed of sound of the biodiesel fuels using Wada's group contribution model. The ARDs for the individual fuels are presented in **Table 3.6.7**, where it is shown that the model can describe 19 fuels at atmospheric pressure with an OARD of 0.29 %.

Table 3.6. 7. ARD of Wada's group contribution model for the speed of sound for biodiesel fuels.

Biodiesel	ARD, %	
	Atmospheric pressure	High pressure
BD-A [213]	0.11	
BD-B[213]	0.10	
BD-JC[214]	0.13	
Methyl Soy ester[202]	0.11	0.58
Methyl Canola[202]	0.18	0.74
Methyl Tallow[202]	0.37	1.1
Methyl Lard[202]	0.68	0.99
Methyl oxidized soy[202]	0.59	1.7
Methyl hydrogenated soy[202]	1.4	1.0
S (Soybean) [129]	0.52	
Soy A (Soybean) [129]	0.26	
R (Rapeseed) [129]	0.15	
P (Palm) [129]	0.11	
Sf (Sunflower) [129]	0.13	
SP (Soybean + Sunflower) [129]	0.21	
SR(Soybean+ Rapeseed) [129]	0.13	
PR (Palm + Rapeseed) [129]	0.15	
SRP (Soybean+Rapeseed+Palm) [129]	0.11	
GP (Soybean + Rapeseed) [129]	0.11	
OARD, %	**0.29**	**1.0**

The deviations between the predicted and experimental data are shown in Figure 3.5, where it is shown that the model provides a good description of the experimental data. Unlike the pure esters, for the biodiesels studied here, the deviations seem to be stable within the range of temperatures studied and present deviations within ±0.5%. The largest deviations, with a maximum of 1.5%, are only observed for an oxidized soy biodiesel, as shown in **Figure 3.6.7**. In comparison to the models described in our previous work, [197] the accuracy of Wada's model seems to be better than that of Auerbach's relation and closer to the ideal mixture mixing rules.

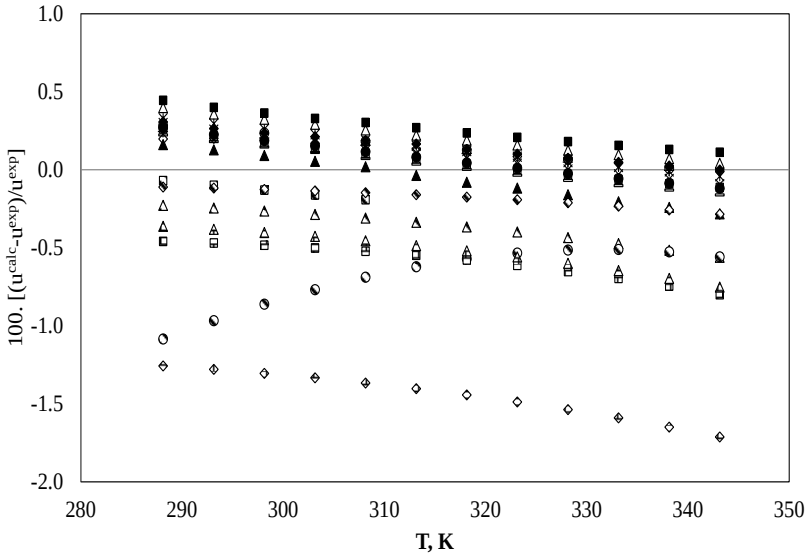

Figure 3.6 7. Relative deviations between experimental and predicted data of speed of sound for biodiesel fuels using the Wada's model. □ Soy A[129], ■ S[129], ◆Sf[129], ◇ R [129], ▲ P [129], △ GP [129], × SR [129], ✳ SP [129], ━ RP [129], ● SRP [129], ○ BD-A [213], + BD-B [213], ◘ BD-JC [214], ◆ Methyl Soy ester[202], ◭ Methyl canola [202], ◔ Tallow [202], ▣ Lard [202], ◈ Oxidized soy [202] and ◬ Hydrogenated soy [202]

An extension of Wada's model was also developed to predict the speed of sound of biodiesel fuels at high pressures. For this purpose, a linear pressure dependency, described by eq 3.6.7, was fitted to the high-pressure speed of sound of methyl caprate recently reported by Ndiaye et al.[215].

$$u_{BD}(P) = u_{BD}(P_0) + aP \tag{3.6.7}$$

In this equation, u_{BD} (P_0) (m/s) is the speed of sound of biodiesel at atmospheric pressure, estimated by Wada's group contribution model, a is the fitting parameter, and P (MPa) is the pressure. The best fitting was obtained for a value of a of 4.19 m $s^{-1}Mpa^{-1}$. The model proposed here was tested against the speed of sound for six biodiesel fuels reported by Tat et al.[209] for pressures up to 35 Mpa with an OARD of 1.0 %. These results are comparable to those obtained with Eq 3.6.6. Deviations for the individual fuels are presented at **Table 3.6.7**, while the predictive profile is presented in **Figures 3.6.8** and **3.6.9** for methyl soy ester and methyl hydrogenated soy, respectively. As shown in the figures, the pressure

dependency of the speed of sound is correctly described and is approximately linear in the pressure range considered. The data by Ndiaye et al.[215] suggest that the pressure dependency of the speed of sound for higher pressures may no longer be linear, and thus, eqs. 3.6.6 and 3.6.7 should not be used to extrapolate the speed of sound to higher pressures.

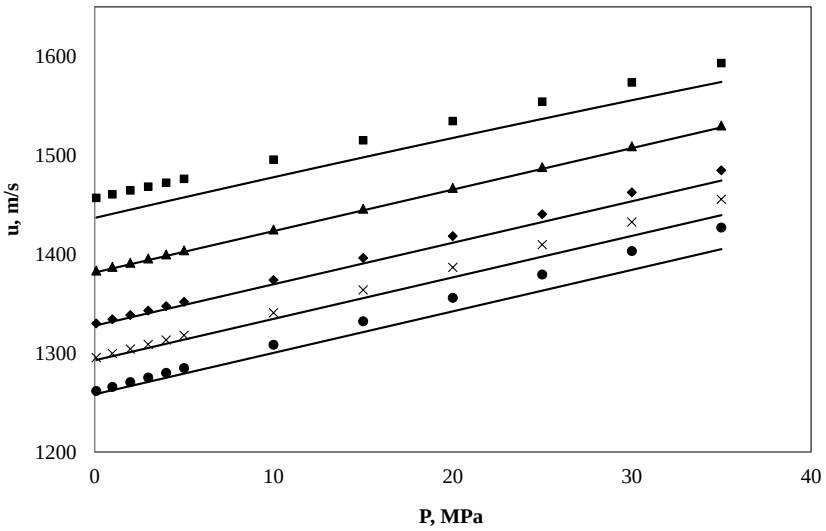

Figure 3.6 8. Comparison of experimental data to predicted data of the speed of sound for methyl soy ester [202] at high pressures and different temperatures: (■) 283.15 K, (▲) 303.15 K, (◆) 318.15 K, (×) 328.15 K, and (●) 338.15 K. The full line is the predicted data

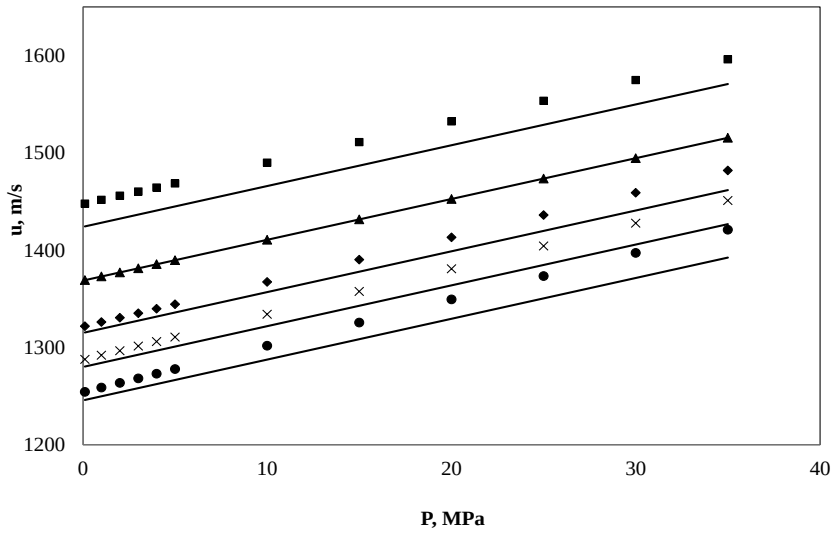

Figure 3.6 9. Comparison of experimental data to predicted data of the speed of sound for methyl hydrogenated hydrogenated soy ester [202] at high pressures and different temperatures: (■) 283.15 K, (▲) 303.15 K, (◆) 318.15 K, (×) 328.15 K, and (●) 338.15 K. The full line is the predicted data

3.6.4.2. Speed of sound of FAEE and ethylic biodiesels

The FAEE compositions of the studied biodiesels are reported in **Table 3.6.8.** The experimental densities and speeds of sound for nine fatty acid ethyl esters and four ethylic biodiesels, measured at atmospheric pressure and temperatures from 293.15 to 343.15 K, are presented in **Tables 3.6.9** to **3.6.11**.

Table 3.6. 8. Composition of the biodiesels studied, in mass percentage

FAEE	Biodiesel			
	S	Sf	S+B	P
C8:0	-	-	-	0.03
C10:0	-	-	-	0.03
C12:0	-	-	0.03	0.42
C14:0	0.07	0.09	0.30	0.72
C16:0	10.92	5.66	11.81	38.67
C16:1	0.08	0.09	0.16	0.15
C18:0	2.93	3.11	3.23	4.49
C18:1	27.45	35.32	27.53	44.51
C18:2	52.65	54.46	49.90	10.29
C18:3	4.96	0.28	5.87	0.26
C20:0	0.29	0.20	0.31	0.25
C20:1	0.18	0.13	0.20	0.10
C22:0	0.37	0.49	0.44	0.04
C22:1	-	0.04	0.08	0.03
C24:0	0.099	0.14	0.15	0.02

Table 3.6. 9. Experimental density and Speed of Sound of Ethylic biodiesels

	ρ / kg.m^{-3}				u / m s^{-1}			
T / K	S	Sf	S+B	P	S	Sf	S+B	P
293.15	876.64	875.65	875.44	866.65	1402.10	1402.40	1400.00	1390.27
298.15	872.99	872.01	871.79	862.97	1384.09	1384.20	1381.98	1372.07
303.15	869.36	868.37	868.13	859.31	1366.24	1365.85	1364.13	1354.08
308.15	865.72	864.74	864.49	855.65	1348.59	1347.97	1346.48	1336.28
313.15	862.09	861.11	860.84	851.99	1331.13	1330.55	1328.93	1318.66
318.15	858.46	857.49	857.20	848.34	1313.83	1313.36	1311.61	1301.24
323.15	854.83	853.85	853.55	844.68	1296.70	1296.12	1294.38	1283.98
328.15	851.20	850.23	849.92	841.04	1279.74	1279.22	1277.38	1266.90
333.15	847.56	846.61	846.28	837.39	1262.96	1262.49	1260.55	1249.99
338.15	843.94	843.00	842.65	833.74	1246.38	1245.97	1243.93	1233.24
343.15	840.32	839.38	839.02	830.09	1230.04	1229.69	1227.55	1216.68

Table 3.6. 10. Experimental Speed of Sound of FAEE in $m.s^{-1}$

T / K	C6:0	C8:0	C10:0	C12:0	C14:0	C16:0	C18:0	C18:1	C18:2
293.15	1195.13	1280.73	1313.21	1339.55	1361.05			1396.59	1405.24
298.15	1173.94	1261.39	1294.31	1320.91	1342.60			1378.54	1387.18
303.15	1152.95	1242.35	1275.62	1302.49	1324.34	1342.65		1360.67	1369.28
308.15	1132.16	1223.50	1257.14	1284.26	1306.23	1324.67		1342.98	1351.56
313.15	1111.52	1204.60	1238.82	1266.16	1288.32	1306.90		1325.49	1334.05
318.15	1091.01	1186.02	1220.66	1248.26	1270.61	1289.33	1304.71	1308.17	1316.70
323.15	1070.67	1167.59	1202.67	1230.54	1253.08	1271.96	1287.43	1291.03	1299.47
328.15	1050.49	1149.35	1184.87	1213.00	1235.76	1254.78	1270.34	1274.04	1282.49
333.15	1030.43	1131.23	1167.20	1195.61	1218.51	1237.76	1253.46	1257.24	1265.67
338.15	1010.55	1113.31	1149.72	1178.43	1201.52	1220.91	1236.80	1240.64	1249.03
343.15	990.85	1095.65	1132.43	1161.44	1184.74	1204.31	1220.46	1224.26	1232.62

Table 3.6. 11. Experimental density of FAEE in $kg.m^{-3}$

T / K	C6:0	C8:0	C10:0	C12:0	C14:0	C16:0	C18:0	C18:1	C18:2
293.15	878.96	866.48	863.97	862.15	860.95			868.87	880.49
298.15	873.68	862.16	859.90	858.25	857.18			865.24	876.83
303.15	868.38	857.84	855.83	854.35	853.39	852.48		861.62	873.17
308.15	863.07	853.52	851.76	850.45	849.62	848.79		858.00	869.53
313.15	857.73	849.17	847.69	846.56	845.84	845.10		854.39	865.88
318.15	852.38	844.84	843.61	842.65	842.06	841.42	841.02	850.77	862.23
323.15	847.00	840.49	839.53	838.74	838.28	837.74	837.42	847.16	858.59
328.15	841.60	836.14	835.45	834.84	834.51	834.07	833.82	843.56	854.95
333.15	836.17	831.78	831.36	830.94	830.73	830.40	830.23	839.95	851.31
338.15	830.71	827.41	827.26	827.03	826.95	826.73	826.65	836.35	847.67
343.15	825.23	823.04	823.16	823.12	823.18	823.06	823.06	832.75	844.04

For pure ethyl esters, the magnitude of densities is in very good agreement with that reported by Pratas et al. [152] Their speeds of sound decrease with the temperature and increase with the ester chain length as seen in **Figures 3.6.10** and **3.6.11**. Moreover, for the same chain length, the presence of unsaturated bonds in the ester molecule increases the magnitude of speed of sound as expected since this property also depends directly on the density. Due to the lack of experimental data for ethyl esters, our experimental data were only compared to those reported by Daridon et al. [211] and Ndiaye et al. [215, 222]. The data showed to be in very good agreement, presenting a deviation below ±0.20 % as shown in **Figure 3.6.12**.

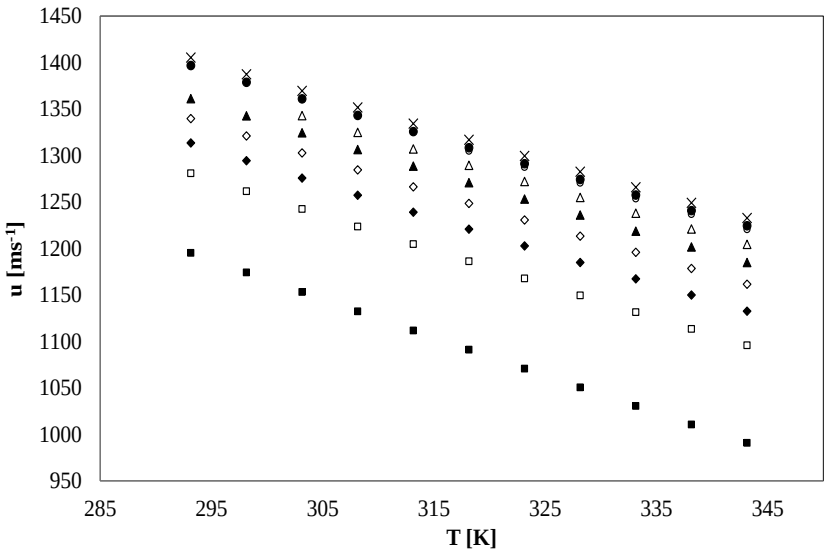

Figure 3.6 10. The dependency of speed of sound of FAEE on temperature. ■Butyrate, □ Caprylate, ◆ Caprate, ◇Laurate, ▲ Myristate, △ Palmitate, ○ Stearate, ● Oleate and × Linoleate

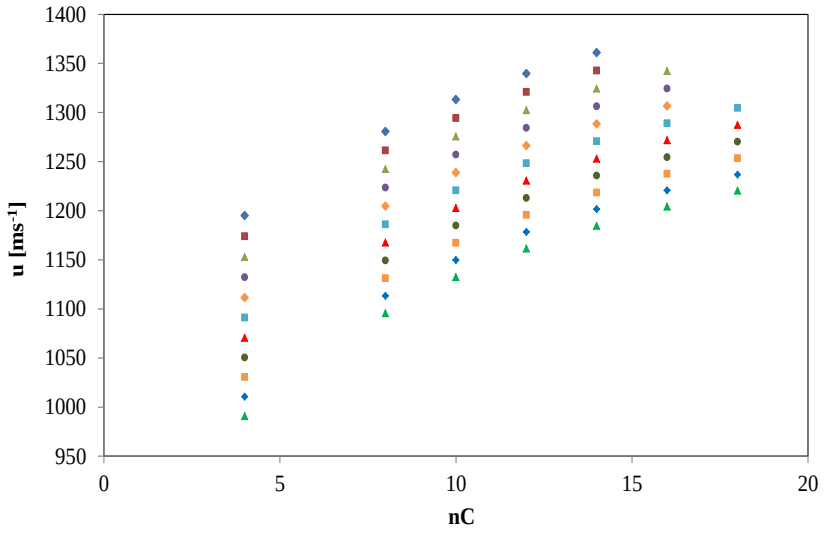

Figure 3.6 11. The dependency of speed of sound of FAEE on carbon chain length at different temperatures in Kelvin.. ◆293.15, ■ 298.15, ▲ 303.15, ● 308.15, ◆ 313.15, ■ 318.15, ▲ 323.15, ● 328.15, ■ 333.15, ◆ 338.15, ▲ 343.15

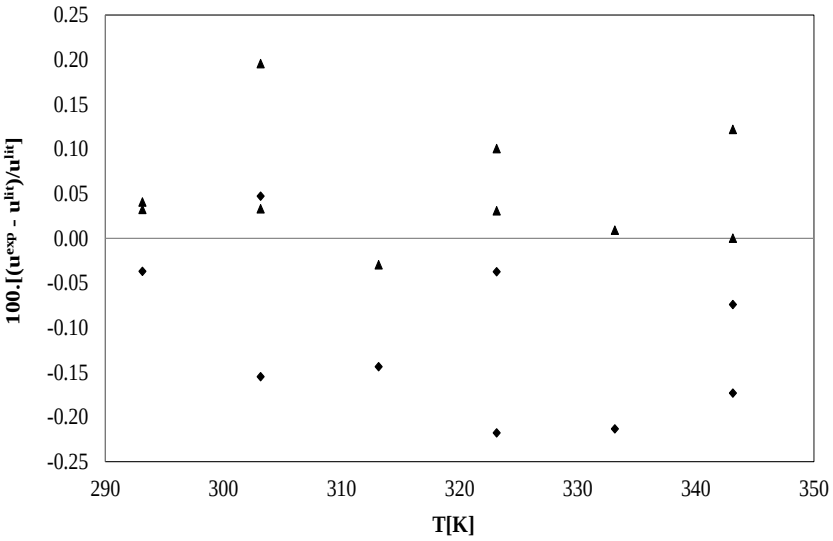

Figure 3.6 12. RDs for ethyl esters available in the literature ◆ Caprate [211, 222] and▲ Myristate [211, 215]

For the ethylic biodiesels, the difference of densities between the fluids is mainly expressed by the difference of FAEE compositions. Moreover, since the FAME present a higher value for density than the corresponding FAEE with the same number of carbon atoms in acid moiety, as already shown in Pratas et al. [152] the magnitude of the densities for

ethylic biodiesels is expected to be lower than that of the corresponding methylic biodiesels. Regarding the speed of sound, as previously observed for methylic biodiesels [206], a difference in the speed of sound of only ca. 1.0% is observed between the four types of biodiesels studied. The same observation is valid for its temperature dependency.

The experimental data here reported was used to test the predictive ability of the Wada's model previously proposed [211]. The results reported in **Table 3.6.12** suggest that the Wada's model provide a very good description of the experimental speeds of sound for both the ethyl esters and the ethylic biodiesels respectively. For the nine ethyl esters studied the model tends to slightly overpredict the experimental speed of sound. Moreover, the deviations are very stable in the range of temperatures studied, except for the short-chain esters like ethyl butyrate where the model presents larger deviations as seen in **Figure 3.6.13**. This limitation might be related with the inadequacy of the Wada's constants here used for description of speed of sound of the short-chain esters. Further work to overcome this problem is being undertaken but it does not impact on the systems of interest for the biodiesel industry. By excluding the ethyl butyrate of the remaining ethyl esters due to the larger deviations, the Wada's model presents only an OARD of 0.14%. For the biodiesels, the Wada 1 approach presents an OARD of 0.59 % (**Table 3.6.12**). Using the Wada 2 approach the OARD obtained was of only 0.45 %. The predictions presented in **Figure 3.6.14** show that the deviations are temperature independent. Therefore, the Wada's model applied directly or through the mixing rules can be extended to other biodiesel fuels provided that the composition of fatty esters is well known.

Table 3.6. 12. ARD of speed of sound estimated by Wada's model for FAEE and ethylic biodiesels

FAEE	ARD, %	Biodiesel	Wada 1	Wada 2
C8:0	0.12	S	0.81	0.31
C10:0	0.11	Sf	0.65	0.26
C12:0	0.089	S+B	0.60	0.46
C14:0	0.094	P	0.30	0.75
C16:0	0.043			
C18:0	0.053			
C18:1	0.15			
C18:2	0.44			
OARD, %	**0.14**		**0.59**	**0.45**

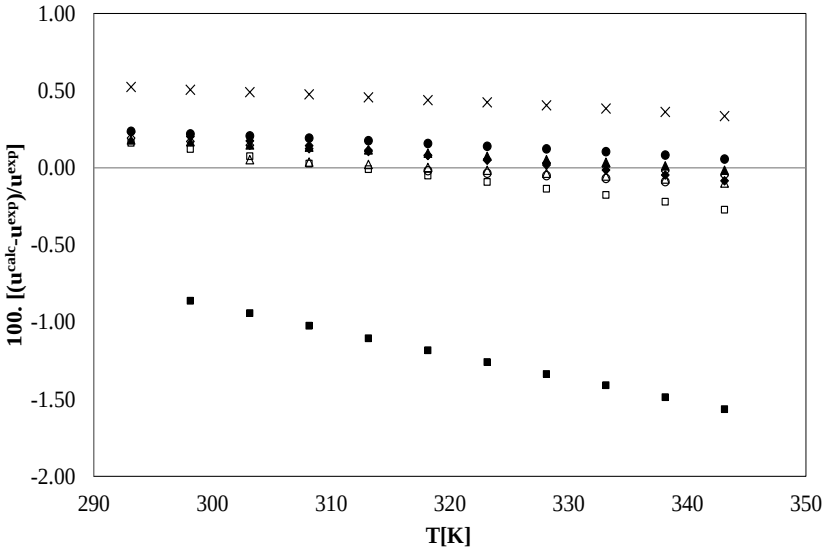

Figure 3.6 13. RDs between experimental and predicted speed of sound of FAEE using Wada's group contribution method. ■Butyrate, □ Caprylate, ◆ Caprate, ◇ Laurate, ▲ Myristate, △ Palmitate, ○ Stearate, ● Oleate and × Linoleate

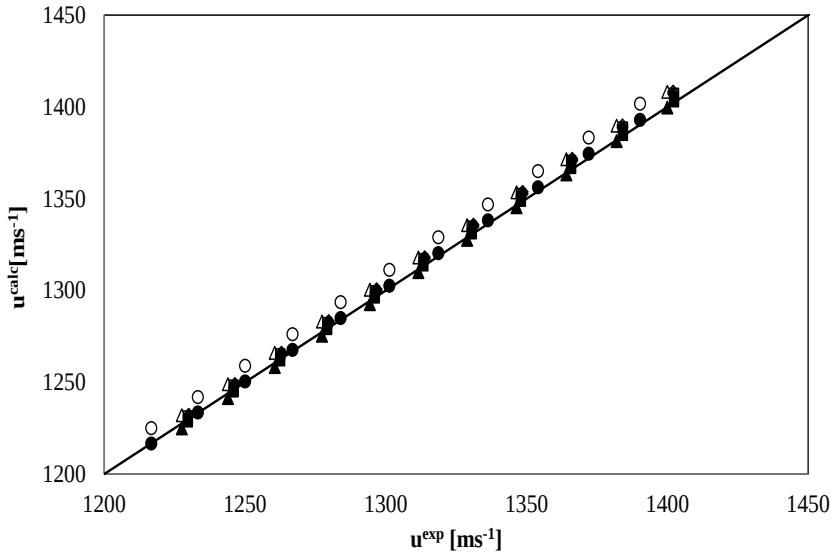

Figure 3.6 14. Experimental and predicted speed of sound of biodiesel fuels using Wada1 (close symbols) and Wada 2 (open symbols) ◆ S, ■ Sf, ▲ S+B and ● P

Finally since the fuel injection systems operate at high injection pressures, the prediction of high pressure speeds of sound would be of importance. But, unlike for methylic biodiesels, there are yet no data for FAEE to extend the atmospheric pressure model here proposed to high pressures as previously done for methylic biodiesels [197, 206]. The measurement of high pressure speed of sound for fatty acid ethyl esters and ethylic biodiesels is being carried in our laboratories and will be object of future works.

3.6.5. Conclusions

The experimental speeds of sound for eight pure methyl esters and ten methylic biodiesel fuels were measured at temperatures from 288 to 343 K and at atmospheric pressure. These data were then used, along with other literature data, to evaluate the capacity of two versions of Auerbach's relation, ideal mixture mixing rules and Wada's model to predict the speed of sound of biodiesel fuels from the knowledge of their composition. For all biodiesel studied, the overall average relative deviation (OARD)value obtained for these models were 1.64, 0.37 and 0.29 % respectively for the modified Auerbach model, ideal mixture mixing rules and Wada's model respectively.

Correlations for estimating the speed of sounds for biodiesels at high pressures were also developed with validity up to 40 MPa. The first correlation based on the literature data provides an OARD of 0.56 % for seven biodiesels tested. The second correlation that uses the Wada's model was applied presents a global deviation of 1.0%.

The experimental speeds of sound for nine FAEE and four ethylic biodiesels, measured at atmospheric pressure and temperature from 293.15 to 343.15 K, were also here reported and were used to assess the predictive ability of the Wada's model. It is shown that this method describes very well the experimental data of speed of sound for pure esters and biodiesel fuels, presenting only OARDs of 0.25% and 0.45%, respectively.

This means that when the measurement of speed of sound is impractical for any biodiesel, these models can be a useful tool for predicting the speed of sound in a wide range of temperatures and pressures provided that the composition of fatty esters is known.

3.7. High pressure density and Speed of Sound of two biodiesel fuels: measurement and prediction

In previous section (**section 3.6**) the study of high-pressure speed of sound was done only up to 45 MPa due to lack of experimental data at pressures above this value. Up to this limit the trend was linear but above this limit this trend was no longer valid anymore as shown by the data of Ndiaye et al.[215]. Thereat Habrioux et al. [223] provided experimental data of speed of sound and density for biodiesel fuels at pressures up to 200 and 100 MPa respectively for two biodiesel fuels (Soybean and Rapeseed) presented here in **Supporting information B.** This data is already submitted as article to the Journal of Energy & Fuels. My contribution to this paper was to develop correlations capable of describing the speed of sound and density of biodiesel fuels at pressures above 40 MPa.

3.7.1. Experimental measurement

The measurements of speed of sound at high pressure was based on a pulse echo technique working at 3 $MH_Z$with a path length fixed to L_0=30mm. This length constitutes an acceptable compromise between shorter distances that reduce measuring accuracy and longer that increase the damping of the wave. The frequency of 3MHz is low enough to avoid dispersion phenomena and is also a good compromise between lower frequencies (that give clear signal but with a lower precision) and higher frequencies (that give more damping of wave into the fluid but with a better precision). The apparatus is essentially made up of an acoustic sensor composed of two piezoelectric disks (12 mm in diameter) facing each other at both ends of a stainless steel cylindrical support. One of them generates the ultrasonic wave that travels into the fluid sample while the other is used to receive different echoes. The entire acoustic sensor is located within a stainless-steel high-pressure vessel closed at one end by a plug in which three electric connections were machined. These electric connections allow connecting both piezoelectric elements to a high voltage Ultrasonic Pulser – Receiver device (high-voltage pulse generator (Panametrics Model 5055PR). The speed of sound is determined from the measurement of the time between two successive echoes by using the base time of an oscilloscope (TEKTRONIX TDS 1022B). The path length needed for calculating speed of sound was determined at different temperatures and pressures by measuring the time of flight of the wave into a liquid of known speed of sound. Water and heptane were used for this calibration. This calibration leads to an uncertainty in the speed of sound of about 0.06%. However, the ultimate error in speed of sound measurement depends in addition on the thermal stability as well as on the uncertainty in the measurement of both temperature and pressure. In order to ensure a satisfactory thermal stability, the full cell is immersed in a thermostated bath (HUBER CC410) filled with silicone oil and the temperature is directly measured into the fluid by a platinum probe (Pt100, 1.2 mm diameter) housed in a metal finger. With this configuration, temperature uncertainty leads to an additional error of 0.04 % in speed of sound. According to the pressure range investigated, two identical manometers (HOTTING BALDWIN MESSTECHNIK MVD 2510) were used to measure the pressure. One is calibrated in the full pressure scale (with an uncertainty of 0.2 MPa) whereas the other

is only calibrated up to 100 MPa in order to achieve a better accuracy in this range (0.02 MPa). These pressure sensor involve an error in speed of sound less than 0.1 % up to 100 MPa and 0.2 % between (100 and 200) MPa. Consequently the overall experimental uncertainty in the reported speed of sound values is estimated to be 0.2% between (0.1 and 100) MPa and 0.3% between (100 and 210 MPa).

Density of biodiesels was measured by a densimeter ANTON-PAAR mPDS 2000V3 connected to a high pressure volumetric pump working up to 100MPa. The principle of this apparatus is to measure the period of oscillation of a U-shape tube and to deduce the density which is related to the square of the period by a linear law. Vacuum and a liquid of reference were to determine the parameters of this linear function. Water and hexane were considered as reference. The temperature of the densimeter is controlled by an external circulating fluid using thermostatic bath (HUBER MINISTAT 125) and is measured with a Pt100 with an uncertainty of ±0.1 K in the temperature range investigated. The pressure is transmitted to the cell by the liquid itself using a volumetric pump and measured with a HBM pressure gauge (with an uncertainty of 0.2 MPa) fixed on the circuit linking the pump to the U-tube cell. Taking into account the uncertainty of the temperature, the pressure, the density of the reference fluid as well as the error in the measurements of the period of oscillation for the vacuum and for both the reference and the studied liquid, the overall experimental uncertainty in the reported density values is estimated to be ±0.5 $kg \cdot m^{-3}$ (0.06%).

3.7.2. Results and discussion

The experimental data of speed of sound here measured was used to assess an extension of the Wada's modelto high pressures. This extension is described by Eq. (3.7.1)

$$u(T,P) = u_0 + a(P - P_0)T - b(P - P_0)^2 T^2 \qquad (3.7.1)$$

where u_0 (m/s)is the atmospheric speed of sound predicted with the Wada's model at the referent pressure P_0, T (K) is the absolute temperature and P (MPa) is the absolute pressure. The parameters *a* and *b* are the fitting parameters whose values were estimated by fitting the Eq.(3.7.1) to the experimental high pressure speeds of sound of methyl caprate reported by

Ndiaye et al.[222]The values obtained for *a* and *b* were 1.47×10^{-2} $m.MPa^{-1}K^{-1}s^{-1}$ and 7.02×10^{-8} $m.MPa^{-2}K^{-2}s^{-1}$ respectively. Using this model the experimental data of speed of sound at high-pressure were predicted with an AADs of 0.54 % for biodiesel S and 0.52 % for biodiesel R and an overall value (OAAD) of 0.53% as shown in **Table 3.7.1.**

Table 3.7. 1. ARDs for speed of sound at temperatures from 293.15 to 393.15 K and pressures from atmospheric to 200 MPa

	ARD , %						
Biodiesel	293.15	313.15	333.15	353.15	373.15	393.15	Average
S	0.52	0.55	0.44	0.50	0.56	0.64	0.54
R	0.39	0.39	0.48	0.57	0.62	0.69	0.52
OARD, %							**0.53**

The adequacy of the proposed approach for the description of the speeds of sound is also highlighted in the **Figures 3.7.1** and **3.7.2** where it is shown that the model provides a very good description of the experimental speeds of sound of the biodiesels studied up to 200 MPa, confirming thus the suitability of the extended Wada's model to provide reliable predictions of the speed of sound for any biodiesel fuel at high pressures.

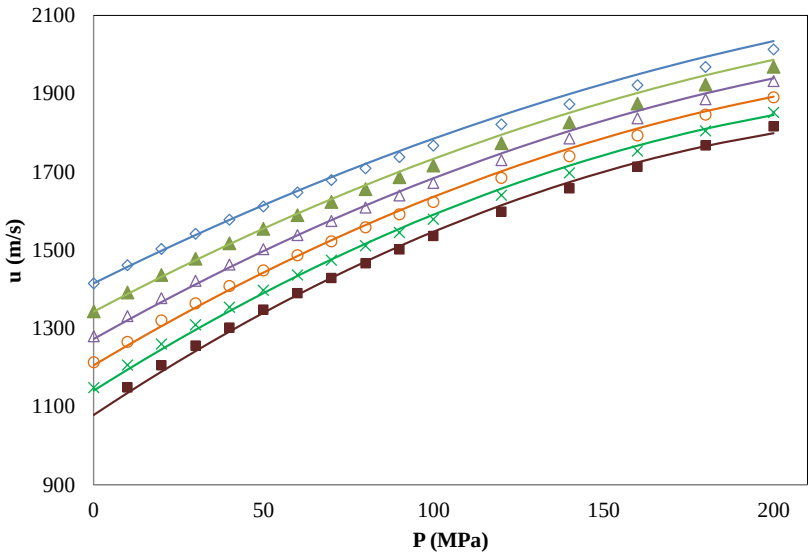

Figure 3.7 1. Experimental and predicted high pressure speed of sound for **biodiesel S** using an extension of Wada's model at different temperatures ◇ 293.15 K, ▲ 313.15 K, △ 333.15K, ○ 353.15 K, × 373.15 K and ■ 390.15 K.

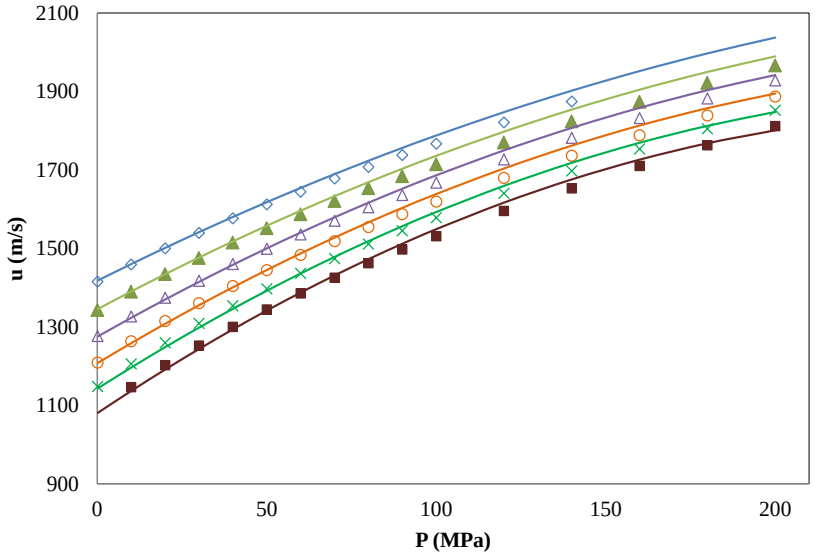

Figure 3.7 2. Experimental and predicted high pressure speed of sound for **biodiesel R** using an extension of Wada's model at different temperatures ◇ 293.15 K, ▲ 313.15 K, △ 333.15K, ○ 353.15 K, × 373.15 K and ■ 390.15 K.

Similarly to the speed of sound, the high-pressure densities for the two biodiesels here studied were also predicted using a quadratic approach described by the Eq. (3.7.2)

$$\rho(T,P) = \rho_0 - c(P - P_0)T + d(P - P_0)^2 / T \qquad (3.7.2)$$

With ρ_0 (kg. m^{-3}) being the atmospheric density, T (K) the absolute temperature and P (MPa) the absolute pressure. The fitting parameters *c* and *d* were estimated from the experimental data of methyl myristate and ethyl myristate reported by Ndiaye et al.[222] whose values were 8.15×10^{-4} kg.m^{-3} MPa^{-1}K^{-1} and 2.22×10^{-1} kg.m^{-3}.MPa^{-2} K^{-2} for *c* and *d* respectively. Eq.(3.7.2) predicts very well the high-pressure densities for the two biodiesels studied, presenting only an OARD of 0.14 % as shown in **Table 3.7.2.**

Table 3.7. 2. ARDs for densities at temperatures from 293.15 to 393.15 K and pressures from atmospheric to 100 MPa

	ARD, %	
T/K	S	R
293.15	0.11	0.10
303.15	0.09	0.12
313.15	0.14	0.15
323.15	0.10	0.08
333.15	0.06	0.06
343.15	0.07	0.06
353.15	0.08	0.07
363.15	0.08	0.09
373.15	0.14	0.16
383.15	0.24	0.25
393.15	0.38	0.41
OARD, %	**0.14**	**0.14**

Furthermore the suitability of this approach to predict the densities at high pressures is also underlined in the **Figures 3.7.3** and **3.7.4** where it is shown that a very good description of the high pressure densities is achieved.

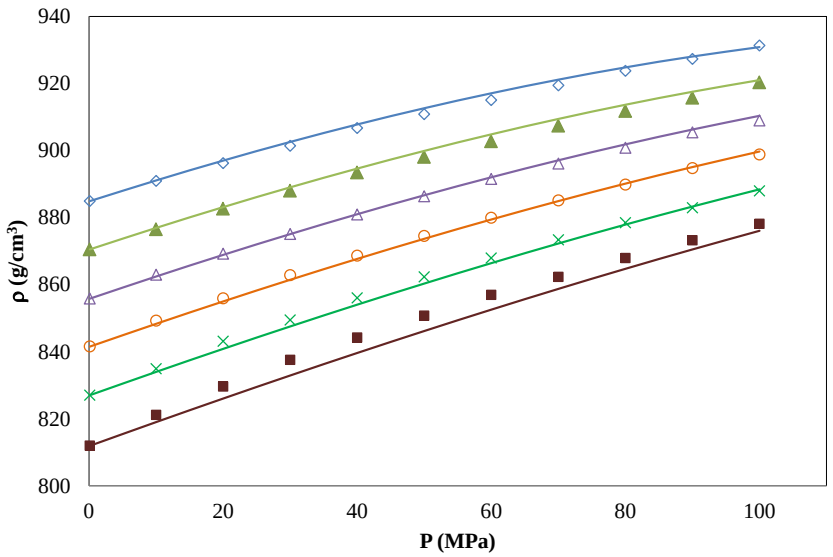

Figure 3.7 3. Experimental and predicted high pressure densities for biodiesel S using an extension of Wada's model at different temperatures ◇ 293.15 K, ▲ 313.15 K, △ 333.15K, ○ 353.15 K, × 373.15 K and ■ 390.15 K.

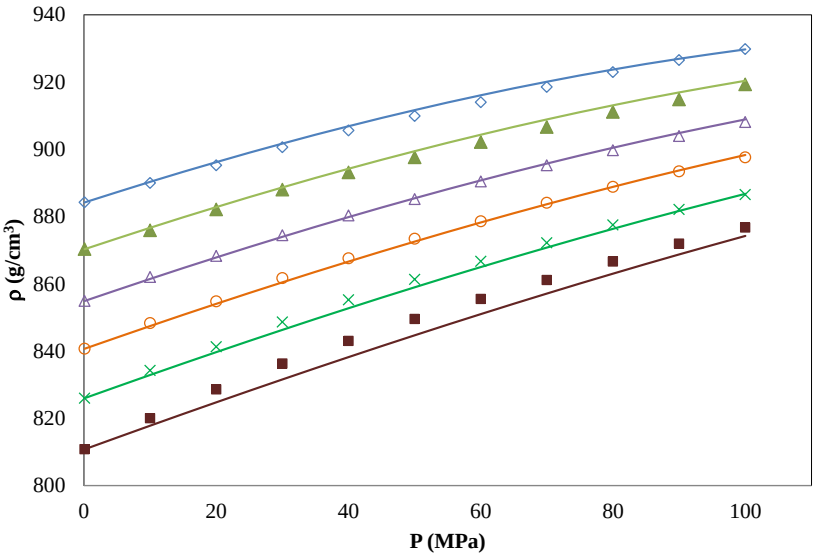

Figure 3.7 4. Experimental and predicted high pressure densities for biodiesel R using an extension of Wada's model at different temperatures ◇ 293.15 K, ▲ 313.15 K, △ 333.15K, ○ 353.15 K, × 373.15 K and ■ 390.15 K.

3.7.3. Conclusions

High-pressure speeds of sound and densities of two biodiesels (soybean and rapeseed) were here measured and predicted using quadratic extrapolations of the atmospheric pressure data. These approaches described very well the experimental data, presenting only overall average relative deviations (OARD) of 0.53 % for speed of sound and 0.14 % for density.

3.8. High pressure viscosity of biodiesel fuels: measurement and prediction

This part of work reports new experimental data of high-pressure viscosities for three biodiesel fuels (soybean, rapeseed and their binary mixture) measured at temperatures from 283.15 K to 393.15 K and pressures from atmospheric up to 140 MPa and proposes a correlation capable of describing the experimental data. The FAME compositions of biodiesels are already presented in **Section 3.2**. The measurements of viscosity were done by Prof. Dr. José Juan Segovia Puras at the University of Valladolid, Spain.

3.8.1. Introduction

The modern injection system called “common rail injection systems” uses high pressures (up to 200 MPa) to pump the fuel and avoid the leakage.[224, 225] At this point, the prior knowledge of high-pressure viscosities of biodiesel becomes crucial for previewing the engine performance and the quality of emissions. Most data available in the literature reports the temperature dependency of viscosity for biodiesel fuels at atmospheric pressure. Only few works have focused on measuring and predicting the high-pressure viscosities of biodiesel fuels and their blends with petrodiesel.[224-228] Thereat, this work aims to report new experimental data of high- pressure viscosity for three methylic biodiesels (soybean, rapeseed and their binary mixture) measured at temperatures from 283.15 to 393.15 K and pressures from atmospheric to 140 MPa, and to propose a correlation capable of predicting them and their mixtures with petrodiesel.

3.8.2. Experimental section

The three biodiesel samples here studied: Soybean (S), Rapeseed (R) and their binary mixture (SR) are already described in Section 3.2.

The experimental measurements of high-pressure viscosities were done using a vibrating-wire instrument developed in the TERMOCAL laboratory (**Figure 3.8.1**). This instrument is capable of operating at temperatures between 273.15 and 423.15K and at pressures up to 140 MPa. Calibration was performed by means of measurements in vacuum, air, and toluene. The estimated uncertainty of the results is 1 % in viscosity.

The vibrating wire viscometer has been designed to operate in the viscosity range 0.3–30mPa·s. The vibrating wire and magnetic assembly were housed in a commercially-available pressure vessel HIP rated for operation at 140 MPa, this vessel was immersed in a bath Hart Scientific 6020. The temperature of the fluid was measured using two platinum resistance thermometer (PRT) and a ASL F100 thermometer. This thermometer was calibrated with an uncertainty of ±0.02 K. The pressure was measured in the external pipework by means of a Druck DPI 104 transducer, with a full scale reading of 140 MPa and an uncertainty of ±0.02% kPa/kPa. The pressure was generated by a HiP pump, model 68-5.75-15.

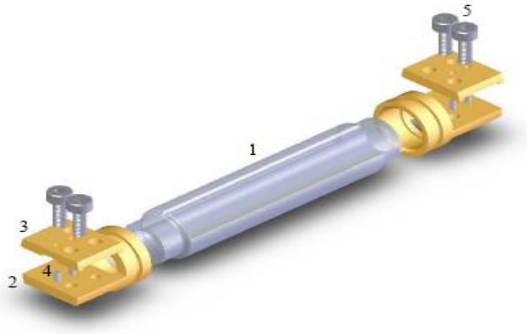

Figure 3.8. 1. vibrating wire vibrating wire sensor for 150 µm wire diameter: (1) flow tube, (2) end support, (3) clamp, (4) pin, (5) cap-head screws.

3.8.3. Results and discussion

The experimental viscosities of the three biodiesels here studied are presented in **Table 3.8.1** where it is seen, as expected, that the magnitude of viscosity is higher for saturated biodiesel at the same temperature and pressure (i.e., biodiesel R is more viscous than biodiesel S) and increases with the pressure due to the increasing molecular interactions (i.e., the molecules become more compacted with the pressure rise).

Table 3.8. 1. Experimental high-pressure dynamic viscosity in mPa.s of biodiesels S, R & SR

P (MPa)\T (K)	293.15	313.15	333.15	353.15	373.15	393.15
	Biodiesel S					
0.1	6.33	3.99	2.80	2.13	1.64	1.35
1	6.33	4.01	2.82	2.14	1.65	1.37
5	6.67	4.18	2.94	2.22	1.71	1.45
10	7.11	4.47	3.11	2.32	1.86	1.52
20	8.11	4.94	3.39	2.55	2.03	1.68
30	8.94	5.53	3.81	2.84	2.23	1.83
40	10.0	6.10	4.17	3.12	2.44	1.98
50	11.6	6.70	4.57	3.39	2.67	2.16
60	12.8	7.41	4.98	3.73	2.90	2.32
70	14.6	8.11	5.44	4.05	3.12	2.51
80	16.2	9.00	5.99	4.38	3.31	2.68
100	21.5	10.9	7.02	4.98	3.81	3.03

120	29.9	13.4	8.42	5.68	4.27	3.39
140		16.1	9.95	6.58	4.86	3.76
			Biodiesel R			
0.1	6.93	4.22	2.86	2.11	1.68	1.33
1	6.97	4.27	2.92	2.16	1.68	1.36
5	7.37	4.46	3.02	2.27	1.77	1.41
10	7.75	4.77	3.22	2.37	1.85	1.50
20	9.00	5.32	3.62	2.64	2.07	1.63
30	10.3	5.98	3.93	2.91	2.25	1.80
40	11.6	6.64	4.41	3.21	2.48	1.98
50	12.9	7.33	4.87	3.52	2.73	2.15
60	14.8	8.03	5.33	3.79	2.93	2.34
70	17.3	9.02	5.79	4.19	3.15	2.50
80	19.6	9.99	6.34	4.52	3.37	2.69
100	26.8	11.9	7.53	5.24	3.90	3.07
120		14.8	8.96	5.99	4.49	3.44
140			10.5	6.96	5.06	3.85
			Biodiesel SR			
0.1	6.76	4.20	2.98	2.28	1.78	1.49
1	6.86	4.24	3.03	2.29	1.80	1.51
5	7.24	4.39	3.15	2.40	1.92	1.57
10	7.61	4.65	3.28	2.48	1.99	1.66
20	8.55	5.25	3.65	2.74	2.18	1.83
30	9.88	5.80	4.06	3.01	2.37	1.96
40	10.9	6.45	4.46	3.29	2.60	2.14
50	12.0	7.04	4.82	3.61	2.80	2.32
60	13.4	7.85	5.22	3.87	3.06	2.50
70	15.4	8.75	5.85	4.28	3.28	2.70
80	17.3	9.49	6.32	4.63	3.51	2.85
100		11.3	7.34	5.39	3.96	3.20
120		13.8	8.63	6.10	4.49	3.58
140		17.0	10.2	7.03	5.13	3.93

To model the experimental viscosities presented above we followed an approach similar to that previously proposed by us for the densities and speed of sound [223]. For that purpose two set of compounds were used to develop a correlation described by Equation (3.8.1)

$$\ln \eta = \ln \eta_0 + a \frac{(P-P_0)}{T^b} \qquad (3.8.1)$$

with η being the dynamic viscosity in mPa.s, P the absolute pressure in MPa, T is the absolute temperature in K and a and b the fitting parameters. The experimental data reported by Duncan et al.[224] were used as the training set to adjust the values of the fitting parameters a and b. The validation set was the three biodiesel here studied (S, R and SR).

The values of 1.2 and 0.84 were obtained respectively for parameters a and b with which the Eq. (3.8.1) predicts very well the experimental data, presenting only an OARD of 3.0 % for the training set and of 3.9 % for the validation set in the temperature range of 283–393 K and pressure range of 0.1–140 MPa as seen in **Table 3.8.2**.

Table 3.8. 2. ARDs of viscosity for biodiesels at high pressure

Reference	Biodiesel	ARD, %	
		Training set	Validation set
Duncan et al.[225]	Soybean1	3.0	
Duncan et al.[224]	Soybean2	3.6	
	Canola	3.1	
	Canola used	2.9	
	Vistive	2.7	
	Coconut	2.5	
This work	S		3.7
	R		4.7
	SR		3.1
	OARD, %	**3.0**	**3.9**

The behavior of the correlation here developed for both set of compounds can be seen separately in **Figures 3.8.1 and 3.8.2** for the training and validation sets. The adequacy of this correlation to describe the pressure dependency of dynamic viscosity of biodiesels at different temperatures for the validation set is shown in the **Figures 3.8.3-3.8.5** where the three biodiesels studied presented higher deviations only high at the lowest temperature of 283.15 K, while for all other temperatures the deviations are low. This approach can be easily extended to predict the high pressure viscosities of any biodiesel provided that the atmospheric

pressure values are known either experimentally or can be estimated as we proposed in a previous work [146].

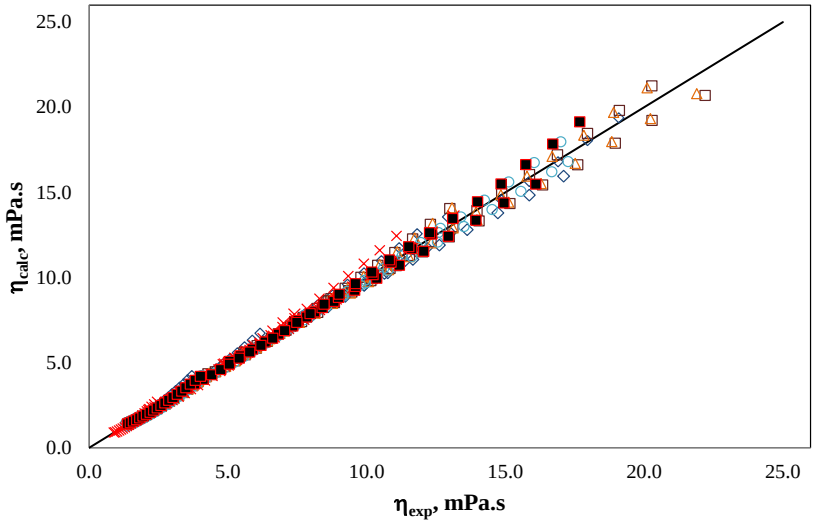

Figure 3.8. 2. Experimental and predicted viscosity of the training set for equation 1. ◇ Soybean1[225], □ Canola [224], △ Canola used [224], ○ Vistive [224], × Coconut [224] and ■ Soybean2 [224].

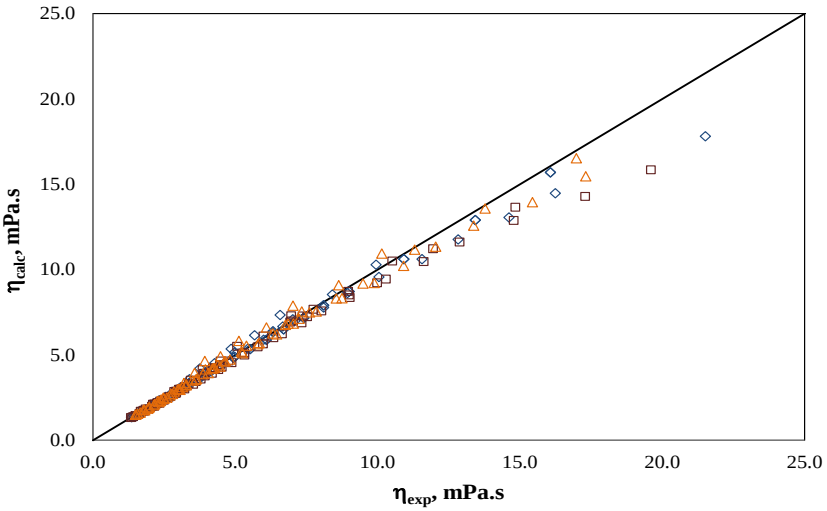

Figure 3.8. 3. Experimental and predicted viscosity of the validation set for equation 1 ◇ S, □ R and △ SR.

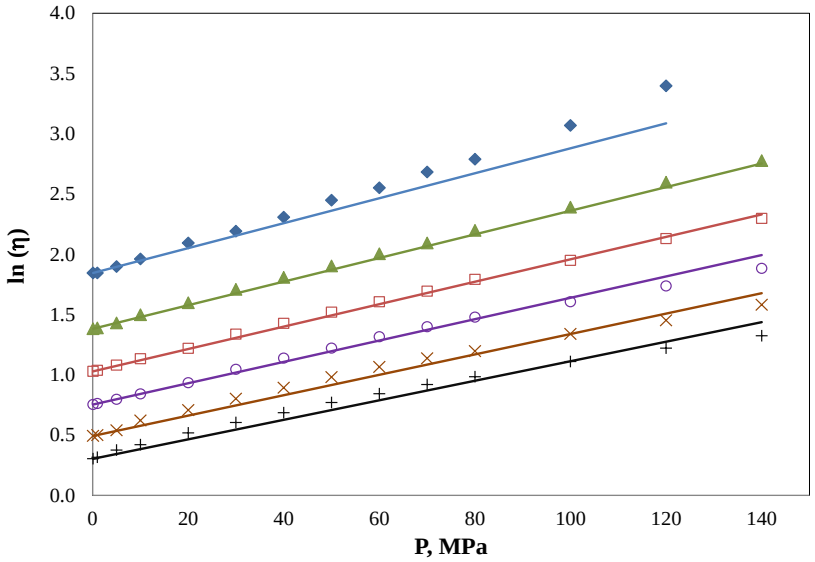

Figure 3.8. 4. High-pressure viscosities of biodiesel S at different temperatures. ◆ 283.15 K, ▲ 313.15 K, □ 333.15 K, ○ 353.15 K, × 373.15 K and + 393.15 K. Lines are the results predicted with the correlation.

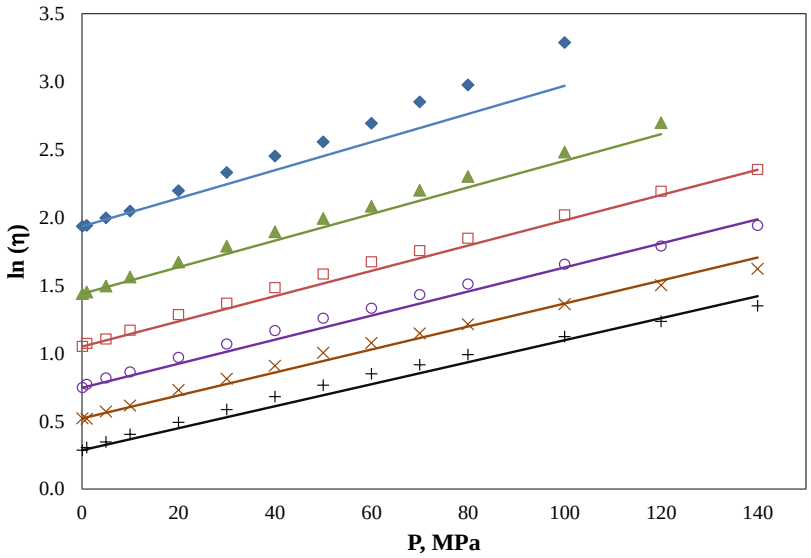

Figure 3.8. 5. High-pressure viscosities of biodiesel R at different temperatures. ◆ 283.15 K, ▲ 313.15 K, □ 333.15 K, ○ 353.15 K, × 373.15 K and + 393.15 K. Lines are the results predicted with the correlation.

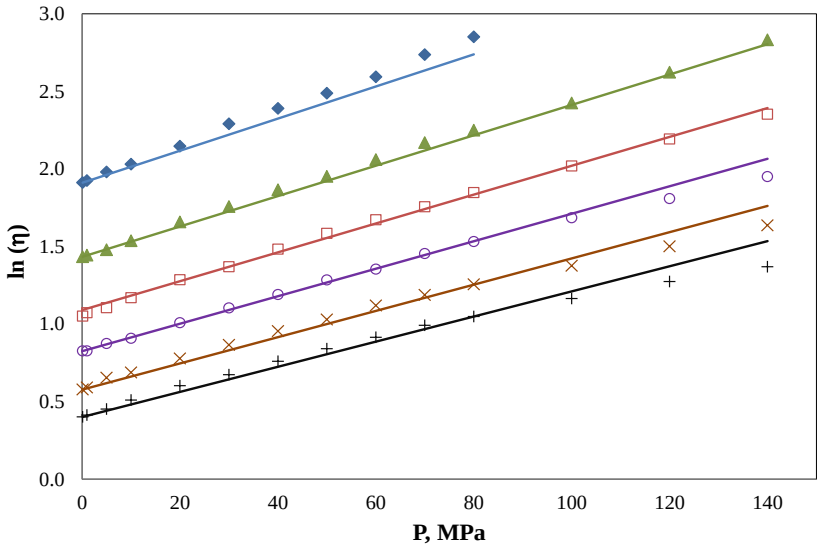

Figure 3.8. 6. High-pressure viscosities for biodiesel R at different temperatures ◆ 283.15 K, ▲ 313.15 K, □ 333.15 K, ○ 353.15 K, × 373.15 K and + 393.15 K. Lines are the results predicted with the correlation.

The correlation here developed was also extended to describe mixtures of biodiesels with diesel. To do this, however, a separate parameter fitting of Eq. (1) was done for diesel using the experimental data reported by Duncan et al.[225] The values of 134.5 and 1.6 were obtained for *a* and *b,* respectively. The viscosities of the mixtures were predicted using the Grundberg-Nissan mixing rules expressed by the Eq. (3.8.2)

$$ln(\eta_{blend}) = x_{diesel} ln(\eta_{diesel}) + x_{biodiesel} ln(\eta_{biodiesel}) \qquad (3.8.2)$$

where x_{diesel} and $x_{biodiesel}$ are the mole fractions of diesel and biodiesel in the blended fuel, respectively, and η_{diesel} and $\eta_{biodiesel}$ are the dynamic viscosities of pure diesel and biodiesel at a particular temperature and pressure, respectively. Using the equations (3.8.1) and (3.8.2) together, the prediction of high-pressure viscosities of the blends was excellent, presenting only an OARD of 3.3 % as shown in **Table 3.8.3**. The adequacy of this model can be seen also in the **Figures 3.8.6-3.8.8** for three representative blends (B5, B40 and B80).

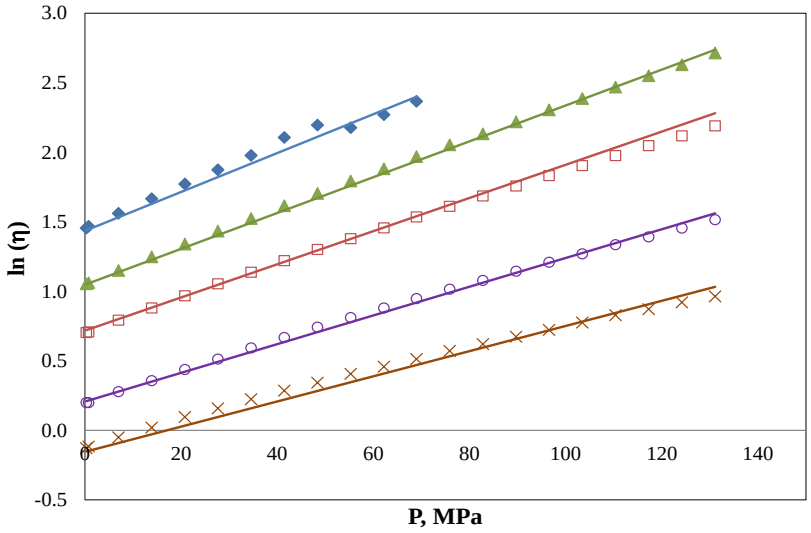

Figure 3.8. 7. High-pressure viscosities for B5 at different temperatures. ◆ 283.15 K, ▲ 298.15 K, □ 313.15 K, ○ 343.15 K and × 373.15 K. Lines are the results predicted with the Grundberg-Nissan mixing rules using the molar fraction apporach.

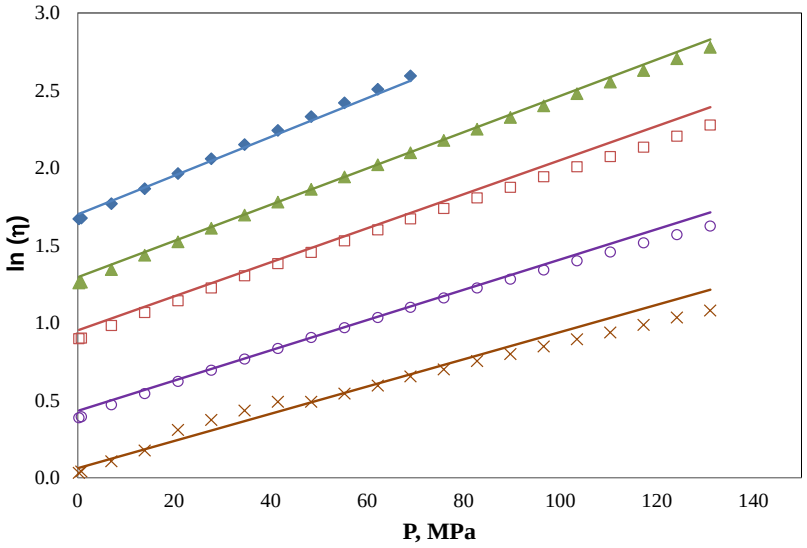

Figure 3.8. 8. High-pressure viscosities for B40 at different temperatures. ◆ 283.15 K, ▲ 298.15 K, □ 313.15 K, ○ 343.15 K and × 373.15 K. Lines are the results predicted with the Grundberg-Nissan mixing rules using the molar fraction approach.

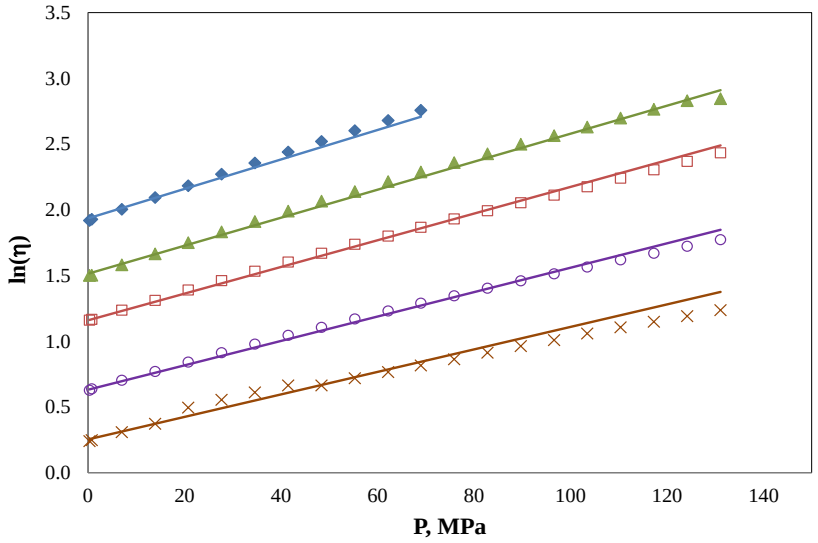

Figure 3.8. 9. High-pressure viscosities for B80 at different temperatures. ◆ 283.15 K, ▲ 298.15 K, □ 313.15 K, ○ 343.15 K and × 373.15 K. Lines are the results predicted with the the Grundberg-Nissan mixing rules using the molar fraction approach.

In practice, however, the informations about the blends of biodiesels with diesel fuel are normally given in volume fractions and sometimes there are no data on molecular weight and also density of diesel fuel (at different temperatures) to convert the volume fraction into the molar fraction to be used in the Eq. (3.8.1). So, this work tried to use directly the volume fraction in the Grundberg Nissan equation, instead of molar fraction, according to the Eq. (3.8.3) to predict the experimental high-pressure viscosities of the blends, where v_{diesel} and $v_{biodiesel}$ are the volume fractions of diesel and biodiesel in the blended fuel, respectively

$$ln(\eta_{blend}) = v_{diesel} ln(\eta_{diesel}) + v_{biodiesel} ln(\eta_{biodiesel}) \qquad (3.8.3)$$

Fortunately the results of prediction using this approach are equal to that using the molar fraction, suggesting that one can use it to calculate the viscosities of the blends The ARDS of this approach are presented in **Table 3.8.3** and its adequacy can also be seen in **Figure 3.8.9** for B80.

Table 3.8. 3. ARDs of viscosity for diesel + biodiesel at high pressure

		ARD, %	
Reference	Blend	Volume fraction approach	Molar fraction Approach
Duncan et al.[225]	B5	3.2	2.9
	B10	3.6	2.8
	B20	2.6	2.8
	B40	3.0	3.6
	B60	3.6	3.5
	B80	3.5	2.8
	OARD, %	**3.3**	**3.1**

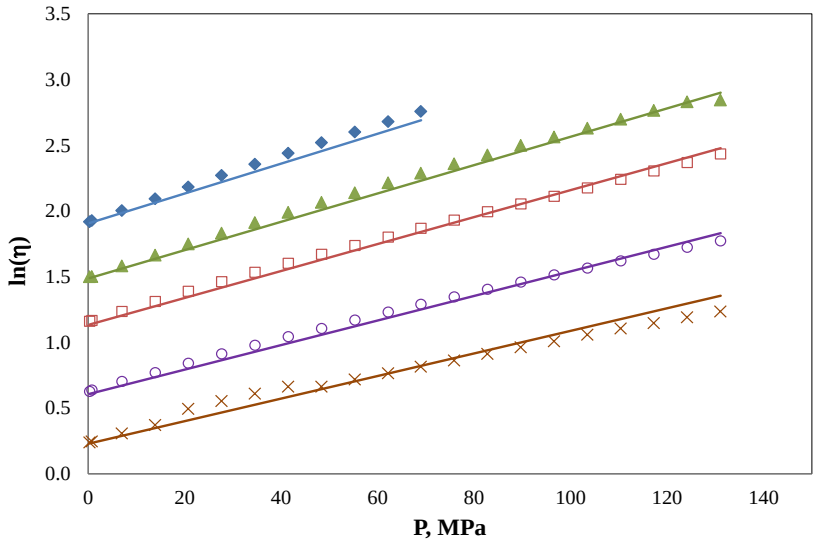

Figure 3.8. 10. High-pressure viscosities for B80 at different temperatures ◆ 283.15 K, ▲ 298.15 K, □ 313.15 K, ○ 343.15 K and × 373.15 K. Lines are the results predicted with the the Grundberg-Nissan mixing rules using the volume fraction approach.

3.8.4. Conclusions

New experimental data of high-pressure viscosity for three methylic biodiesels, measured at temperature from 283.15 to 393.15 K and pressures from atmospheric to 140 MPa were here reported and a correlation to predict the viscosities at high pressure for the biodiesels is proposed based on literature data. It is shown that this correlation provides good predictions for the viscosities of the studied biodiesels and, coupled with the Grundberg-Nissan mixing rules, describes very well the experimental data of viscosity for biodiesel fuels blends with diesel, presenting OARDs of 3.9 and 3.3%, respectively. This good description of the data suggests that this correlation can be extended to the prediction of the viscosity of other biodiesel fuels provided that experimental viscosity at atmospheric pressure is known.

3.9. High-Pressure density of vegetable oils

This work is already submitted to the Journal of Chemical Engineering Data. Because there was no equipment at our laboratory for measuring the high-pressure densities of the vegetable oils, the experimental measurement of density was done in Spain at the University of Vigo by Prof. Manuel Piñeiro and his group. The whole modeling part was done by myself.

3.9.1. Introduction

For any fluid and process, density is important as it gives enough information about the amount of material being processed and correlates with many other transport and acoustic properties such as viscosity, surface tension, volatility, and speed of sound, among others that are not only necessary for an efficient design, control and optimization of operation conditions but also for a reliable development of models. Density data is also important for the high pressure processing of vegetable oils as already stated in Sections 3.1 and 3.2 of this thesis. Nevertheless, there is little information concerning the measurement of high-pressure density of vegetable oils, and much less the models to predict their behavior. Some experimental data are only available at atmospheric pressure.

This work aims to provide the experimental densities of seven different vegetable oils at temperatures from 283.15 to 363.15 K and pressures from 0.1 to 45 MPa, correlating them using the modified Tait-Tammann equation and using them to evaluate the predictive ability of the three versions of GCVOL group contribution method, the Halvorsen's model and the Zong's Fragment-Based Approach model. The development of a high pressure extension of these models will also be here proposed.

3.9.2. Experimental details

3.9.2.1. Samples and density measurement

Oils of soybean (S), rapeseed (R), sunflower (Sf), castor (C), palm (P), *Aleurites moluccana (Am)* and *Jatropha curcas (Jc)* were here used. The first five oils were obtained from Portuguese companies (S from Bunge Ibérica Portugal SA, Sf, P and R from Sovena and C from José M. Vaz Pereira SA) while the last two non-edible oils were obtained by solid-liquid extraction of the corresponding seeds in a Soxlet with n-hexane. The composition of fatty acids in these oils was measured by conversion of the oil into fatty esters. The fatty acid profiles of the biodiesel S, P, Sf and R are already presented in the **section 3.2** and those of the two non-edible oils (*Am* and *Jc*) and the castor oil (C) are presented here in **Table 3.9.1**. The

conversion of these oils into biodiesels was done using the methodology of Ghadge et al.[229] whose details are described in **Chapter 5**. The experimental procedure of density measurement is already described in **Section 3.2.**

Table 3.9. 1. The fatty esters profile of the oils studied (wt. %)

FAME	Biodiesel		
	C	*Jc*	*Am*
C10:0	0.00	0.00	0.03
C12:0	0.34	0.04	0.10
C14:0	0.00	0.11	0.10
C16:0	2.68	17.57	8.55
C16:1	0.00	0.00	0.00
C18:0	0.65	3.88	2.47
C18:1	3.29	36.67	24.04
C18:2	8.31	41.65	43.79
C18:3	0.82	0.09	20.91
C20:0	0.00	0.00	0.00
C20:1	0.00	0.00	0.00
C22:0	0.00	0.00	0.00
C22:1	0.00	0.00	0.00
C24:0	0.00	0.00	0.00
C18:1 OH	83.91	0.00	0.00

3.9.3. Density models

The modified Tait-Tammann equation [230], the GCVOL group contribution method, the Halvorsen‘s model [231, 232] and the Zong’sFragment-Based Approach model [233] were here used here to describe the temperature and pressure dependency of densities of vegetable oils. The first two approaches were previously applied elsewhere with success to the description of the experimental densities of fatty esters [152, 153] and biodiesels [129].

3.9.3.1. Modified Tait-Tammann correlation

This correlation relates density (ρ/g.cm^{-3}) with temperature (T/K) and pressure (P/MPa) in a polynomial form, involving several fitting parameters according to the Eqs. (3.9.1) to (3.9.3) that are adjusted to the experimental data.

$$\rho = \frac{\rho\,(T, P = 0.1MPa)}{\left[1 - C\,\frac{(B+P)}{(B+0.1)}\right]} \tag{3.9.1}$$

where

$$\rho(T, P = 0.1MPa) = a_1 + a_2 T + a_3 T^2 \tag{3.9.2}$$

and

$$B = b_1 + b_2 T + b_3 T^2 \tag{3.9.3}$$

3.9.3.2. Halvorsen's model

This model is detailed in Halvorsen et al. [231] Shortly it combines the fatty acid critical properties and the respective composition to predict the density of oils using the eq. (3.9.4),

$$\rho_{oil} = \frac{\left(\sum_i x_i MW_i\right)}{R\left(\sum_i \frac{x_i T_{Ci}}{P_{Ci}}\right)\left(\sum_i x_i Z_{RA}\right)\left[1 + (1 - T_r)^{2/7}\right]} + F_C \tag{3.9.4}$$

where ρ_{oil} (g.cm^{-3}) is the density of the vegetable oil, R (cm^3.bar.mol^{-1}.K^{-1}) is the universal gas constant, $Tr$is the reduced temperature, Fc is a correction factor characteristic of the oil, x_i is the mole fraction, MW$_i$ (g.mol^{-1}) is the fatty acid molecular weight, Pc_i (bar) is the critical pressure, ZRAi is the Rackett parameter and Tc_i (K) is the critical temperature.

The *Tr and Fc* can be estimated using the eqs. (3.9.5) to (3.9.8).

$$T_R = \frac{T}{T_{c,mix}} \tag{3.9.5}$$

$$T_{c,mix} = \sum_i x_i T_{ci} \tag{3.9.6}$$

$$F_C = 0.0236 + k\left| 875 - MW_{oil} \right| \tag{3.9.7}$$

$$Mw_{oil} = 3\sum Mw_{esters} + 38.0488 \tag{3.9.8}$$

In Eq. (3.9.7), the value of the constant k is equal to 0.000082 when the molecular weight of the oil is greater than 875 g.mol^{-1} and 0.000098 when the molecular weight is less than 875 g/mol.

3.9.3.3. Zong's model

Zong et al.[233] developed a fragment- based approach to estimate the thermophysical properties of triglyceride mixtures. In case of density, this can be calculated using the Eq. (3.9.9), where ρ_{oil} is the oil density and ρ_i the density of triglyceride i (in g.cm^{-3}) and $w_i$the mass fraction of triglyceride i.

$$\frac{1}{\rho_{oil}} = \sum_i w_i \frac{1}{\rho_i} \tag{3.9.9}$$

This approach requires the knowledge of representative triglyceride molecules. Then, the density of each triglyceride molecule is simply estimated from its molar volume using the Eq. (3.8.10), where $V_A^l$is the liquid molar volume contribution of fragment A (in cm^3.mol^{-1}) and $N_{frag,A}$is the number of fragment A in the oil.

$$V^l = \sum_A N_{frag,A} V_A^l(T) \tag{3.8.10}$$

The temperature dependency of liquid molar volume, V_A^l, is given by Eq. (3.9.11), where $B_{1,A}$ and $B_{2,A}$ are the temperature dependency parameters of fragment A and T is the temperature (K). The values parameters $B_{1,A}$ and $B_{2,A}$ are reported by Zong et al.[233]

$$V_A^l = \frac{1 + B_{2,A} T}{B_{1,A}} \tag{3.9.11}$$

3.9.3.4. GCVOL group contribution method

This method fractionates the molecule into various functional groups and then uses the molar volume of each group to estimate the density of the molecule according to the Eq. (3.8.12) where x is the molar fraction, Mw (g.mol^{-1}) is the molecular weight and V (mol.cm^{-3}) is the molar volume.

$$\rho = \frac{\sum_i x_i Mw_i}{\sum x_i V_i} \tag{3.9.12}$$

The oil molecular weight is calculated from the measured average composition of fatty acids using Eq. (3.9.8) while the molar volume is estimated using the Eq. (3.9.13).

$$V = \sum_i n_i \Delta v_i \tag{3.9.13}$$

In Eq. (3.9.13) n_i is the number of groups i, and the temperature dependency of the molar group, Δvi (cm^3 mol^{-1}), is given by the polynomial function described in Eq. (3.9.14) where T can vary between the melting point and the normal boiling point when the model is used to predict densities of solvents.

$$\Delta v_i = A_i + B_i T + C_i T^2 \tag{3.9.14}$$

According to the parameters *Ai, Bi,* and *Ci* used the GCVOL method can be divided in three different versions: The original version uses the parameters reported by Elbro et al.[142] This version presents 36 different group parameters for a variety of chemical classes, such as alkanes, aromatic, alkenes, alcohols, ketones, aldehydes, esters, ethers, chlorides, and siloxanes. The extended version uses the parameters reported by Ihmels et al.[143]and the revised version uses the parameters proposed by Pratas et al.[129].

3.9.4. Results and discussions

The experimental densities for seven vegetable oils measured at temperatures from 283.15 to 363.15 K and pressures from atmospheric to 45 MPa are reported in **Table 3.9.2.**The density differs between the oils according to the nature of fatty acids that compose the oil, following the same trends previously observed for biodiesels [129]. The unsaturated oils have densities higher than those of saturated oils. However the effect of unsaturation level seems to outweigh the effect of carbon chain length and thus, for the same level of unsaturation, the density of the short-chain oils is not necessarily higher than that of the longer ones. At similar conditions, the density of sunflower oil, highly unsaturated, is higher than that of palm oil, with low unsaturated content, even though this has short chain length than that the other.

Table 3.9. 2. Experimental density data for the vegetable oils

	ρ (± 0.1 kg m^{-3}) at P (± 2.10^{-3}, MPa)													
T (± 0.05 K)	0.10	1.00	2.00	3.00	4.00	5.00	10.00	15.00	20.00	25.00	30.00	35.000	40.00	45.00
							C							
283.15	967.4	967.9	968.3	968.8	969.3	969.7	972.1	974.3	976.5	978.6	980.7	982.8	984.8	986.8
293.15	960.5	960.9	961.5	961.9	962.4	962.9	965.3	967.6	969.9	972.2	974.3	976.5	978.6	980.6
303.15	953.6	954.1	954.6	955.1	955.6	956.1	958.7	961.0	963.4	965.7	968.0	970.2	972.4	974.5
323.15	939.7	940.2	940.7	941.4	941.9	942.4	945.1	947.8	950.4	953. 0	955.3	957.7	960.0	962.3
343.15	925.7	926.3	926.9	927.5	928.1	928.7	931.6	934.5	937.3	939.9	942.6	945.1	947.6	950.1
363.15	911.8	912.3	913.0	913.7	914.4	915.1	918.3	920.7	924.4	927.4	930.0	932.8	935.4	938.1
							S							
283.15	927.9	928.3	928.9	929.3	929.9	930.4	932.9	935.3	937.7	940.1	942.2	944.5	946.6	948.8
293.15	920.7	921.2	921.8	922.3	922.9	923.4	925.9	928.4	930.9	933.4	935.7	938.0	940.3	942.4
303.15	913.8	914.4	914.9	915.4	916.0	916.6	919.3	921.8	924.5	927.0	929.4	931.7	934.0	936.3
323.15	900.1	900.7	901.2	901.9	902.5	903.1	906.0	908.8	911.6	914.3	916.9	919.4	921.9	924.4
343.15	886.5	887.2	887.8	888.5	889.1	889.8	893.0	896.1	899.1	901.9	904.7	907.4	910.0	912.6
363.15	873.3	873.9	874.6	875.3	876.0	876.8	880.2	883.5	886.7	889.8	892.8	895.6	898.3	901.1
							R							
283.15	925.9	926.4	926.9	927.4	927.9	928.4	930.9	933.4	935.7	938.0	940.3	942.5	944.6	946.8
293.15	918.9	919.4	919.9	920.5	921.0	921.6	924.2	926.8	929.2	931.6	933.9	936.2	938.4	940.6
303.15	912.0	912.5	913.1	913.7	914.2	914.8	917.5	920.1	922.6	925.1	927.6	930.0	932.3	934.6
323.15	898.3	898.9	899.5	900.2	900.8	901.3	904.3	907.2	909.9	912.6	915.2	917.8	920.2	922.6
343.15	884.9	885.5	886.2	886.8	887.5	888.1	891.3	894.5	897.4	900.3	903.1	905.7	908.3	910.9
363.15	871.6	872.3	873.0	873.8	874.4	875.1	878.5	881.7	884.9	888.0	891.0	893.7	896.5	899.2
							Sf							
283.15	928.2	928.6	929.2	929.6	930.2	930.7	933.2	935.7	938.1	940.4	942.6	944.9	947.0	949.1
293.15	921.3	921.8	922.3	922.9	923.4	923.9	926.6	929.0	931.5	934.0	936.3	938.6	940.8	943.0
303.15	914.5	915.0	915.6	916.1	916.7	917.3	920.0	922.5	925.1	927.5	930.0	932.4	934.8	937.0
323.15	900.8	901.3	902.0	902.6	903.2	903.8	906.7	909.6	912.4	915.1	917.6	920.2	922.7	925.0
343.15	887.3	887.9	888.6	889.2	889.9	890.6	893.8	896.9	899.8	902.6	905.5	908.1	910.8	913.4
363.15	874.0	874.6	875.3	876.0	876.8	877.5	880.9	884.2	887.4	890.5	893.5	896.4	899.2	902.0

	ρ (± 0.1 kg m^{-3}) at P (± 2.10^{-3}, MPa)													
T (± 0.05 K)	0.10	1.00	2.00	3.00	4.00	5.00	10.00	15.00	20.00	25.00	30.00	35.000	40.00	45.00
							P							
293.15	914.9	915.4	915.9	916.5	917.0	917.5	920.1	922.7	925.1	927.6	930.0			
303.15	907.9	908.4	909.0	909.5	910.1	910.6	913.3	915.9	918.5	921.0	923.5	925.9	928.2	930.5
313.15	900.3	900.8	901.4	902.0	902.6	903.2	906.0	908.8	911.5	914.1	916.6	919.0	921.4	923.9
323.15	893.4	893.9	894.6	895.2	895.8	896.4	899.4	902.2	905.0	907.7	910.3	912.9	915.4	917.8
343.15	879.7	880.4	881.0	881.7	882.3	883.0	886.2	889.3	892.3	895.2	898.0	900.7	903.3	906.0
363.15	866.4	866.9	867.7	868.4	869.2	869.9	873.4	876.6	879.9	883.0	886.1	889.0	891.8	894.6
							Am							
283.15	927.5	928.0	928.5	929.0	929.5	930.0	932.6	935.0	937.5	939.8	942.0	944.3	946.4	948.5
293.15	920.4	920.9	921.5	922.0	922.5	923.1	925.7	928.3	930.7	933.2	935.5	937.8	940.1	942.3
303.15	913.4	913.9	914.5	915.0	915.6	916.2	918.8	921.5	924.0	926.5	929.0	931.4	933.8	936.0
323.15	899.6	900.1	900.7	901.4	901.9	902.5	905.5	908.3	911.1	913.9	916.5	919.0	921.5	924.0
343.15	886.0	886.6	887.3	887.9	888.6	889.2	892.5	895.5	898.6	901.4	904.3	907.0	909.6	912.2
363.15	872.5	873.1	873.8	874.6	875.3	876.0	879.4	882.7	886.0	889.1	892.2	895.2	898.0	900.7
							Jc							
283.15	915.9	916.4	916.9	917.4	918.0	918.5	921.0	923.6	925.9	928.3	930.7	933.0	935.1	937.2
293.15	908.8	909.4	909.9	910.5	911.0	911.6	914.2	916.8	919.3	921.8	924.2	926.5	928.8	931.0
303.15	901.9	902.5	903.1	903.6	904.1	904.7	907.6	910.2	912.8	915.3	917.8	920.3	922.7	924.9
323.15	888.1	888.7	889.4	890.0	890.6	891.2	894.2	897.1	899.9	902.7	905.4	908.0	910.5	912.9
343.15	874.5	875.1	875.8	876.5	877.1	877.8	881.1	884.2	887.3	890.2	893.1	895.8	898.5	901.2
363.15	860.9	861.6	862.3	863.1	863.8	864.6	868.1	871.5	874.8	878.0	881.1	884.1	886.9	889.8

The correlation of the densities with the modified Tait-Tammann equation was carried by fitting the equation parameters to the experimental data. The values of the parameters are reported in **Table 3.9.3**.

Table 3.9. 3. Coefficients of the Tait-Tammann correlation

Oil	a_1	a_2	a_3	b_1	b_2	b_3	c
	(kg m^{-3})	(kg m^{-3}K^{-1})	(×10^{7} kg m^{-3} K^{-2})		(MPa)	(×10^{-4}MPa K)	
C	1158.3	-0.65699	-0.60509	559.07	-1.8349	17.0266	0.08654
S	1153.4	-0.88605	3.15489	515.56	-1.8490	19.2847	0.08227
R	1144.1	-0.84312	2.55582	544.20	-2.0660	23.0248	0.08104
Sf	1134.1	-0.76542	1.35090	453.02	-1.4354	12.7604	0.08382
Am	1149.3	-0.85776	2.62644	484.07	-1.5960	14.9382	0.08568
Jc	1127.3	-0.79324	1.64399	464.03	-1.5057	13.6891	0.08576
P	1181.1	-1.08028	5.88217	476.10	-1.5472	14.1997	0.08627

A description of the data with an OARD of only 0.0045 % (**Table 3.9.4**) was obtained. The adequacy of this correlation to describe the data is illustrated in **Figure 3.9.1** for *Aleurites moluccana* oil and by the RDs between the experimental and the correlated densities shown in **Figures 3.9.2 and 3.9.3**. The correlated results are very coherent with the experimental data and the deviations are shown to be pressure and temperature-independent with a maximum deviation of ± 0.020%.

Table 3.9. 4. ARDs from the modified Tait-Tammann correlation, the GCVOL method, the Halvorsen's model and the Zong's model

	ARD, %					
Oil	Modified Tait-Tammann	Original GCVOL	Extended GCVOL	Revised GCVOL	Halvorsen	Zong
C	0.0042	6.2	2.9	0.74	0.55	
S	0.0039	7.0	1.9	1.6	0.088	1.3
R	0.0027	6.8	2.0	1.5	0.19	1
Sf	0.0030	5.1	4.0	0.36	0.090	0.23
Am	0.0040	6.6	2.5	1.1	0.29	1.6
Jc	0.0031	5.8	3.2	0.51	0.99	2.1
P	0.011	7.0	1.8	1.8	0.16	0.46
OARD, %	**0.0045**	**6.3**	**2.6**	**1.1**	**0.34**	**1.1**

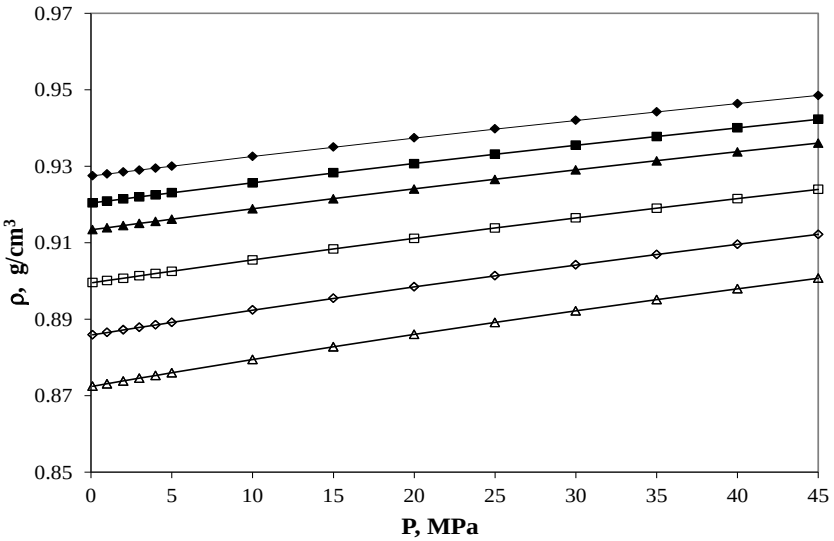

Figure 3.9. 1. Density isotherm for Aleurites moluccana oil. Experimental data Experimental data (◆ 283.15 K, ■ 293.15 K, ▲ 303.15K, □ 323.15 K, ◇ 343.15K and △ 363.15 K) and modified Tait-Tammann results (solid lines).

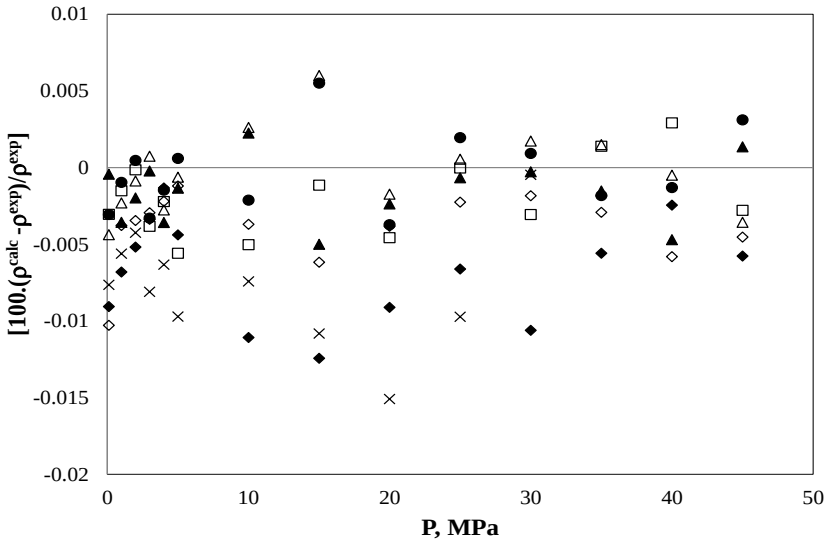

Figure 3.9. 2. RDs between experimental and predicted densities as a function of the pressure at 293.15 K using a modified Tait-Tammann correlation for seven vegetable oils. □ C, ◆ S, △ R, ● *Am*, ◇ *Jc*, ▲ Sf and × P

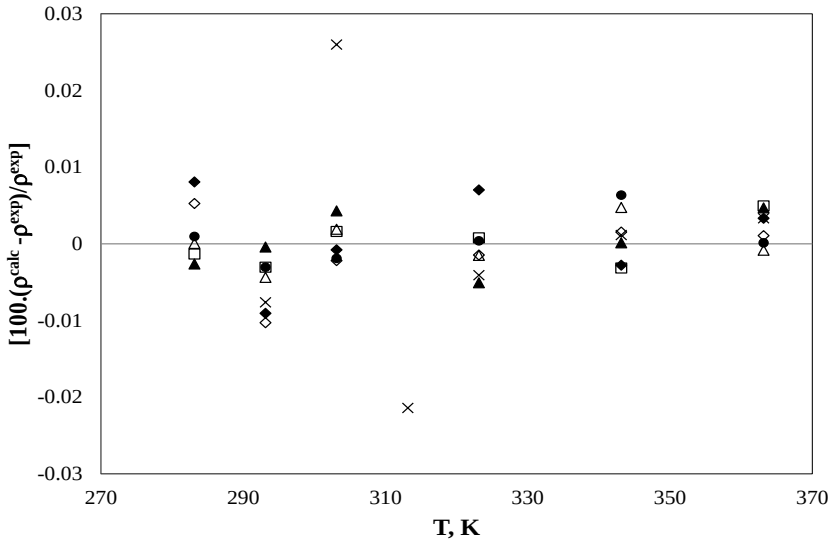

Figure 3.9. 3. RDs between experimental and predicted densities as a function of the temperature at atmospheric pressure using a modified Tait-Tammann correlation for seven vegetable oils. □ C, ◆ S, △ R, ● *Am*, ◇ *Jc*, ▲ Sf and × P

The Halvorsen's model requires the prior knowledge of the critical properties of fatty acids to estimate the densities of vegetable oils. So these properties were obtained directly from Halvorsen et al. [231] for the majority of fatty acids except for the ricinoleic acid whose

critical properties were calculated apart using the Joback's method [234]. Using these properties, along with the fatty acid composition, the description of densities for seven vegetable oils was excellent with an OARD of only 0.34% (**Table 3.8.4**). Nevertheless, the relative deviations are slightly temperature-dependent with a maximum of 1.4 %, especially for the castor oil, as shown in **Figure 3.8.4**.

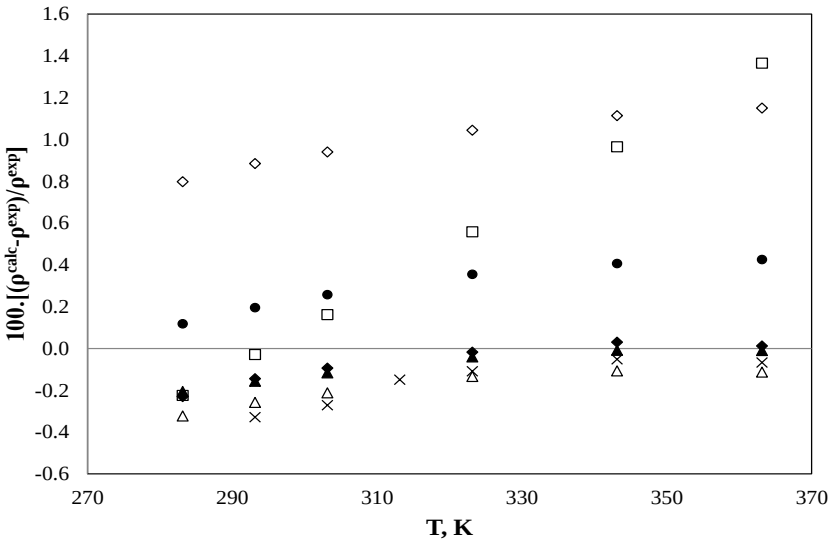

Figure 3.9. 4. RDs between experimental and predicted densities as a function of the temperature at atmospheric pressure using Halverson's model for seven vegetable oils. □ C, ◆ S, △ R, ● *Am*, ◇ *Jc*, ▲ Sf and × P

The Zong's model estimates the density of vegetable oils from that of the triglyceride molecules. Thus, the first step of prediction was the building up of the triglyceride molecules to represent the fatty acid fragments present in oils. For example, Zong et al.[233] used 8 of 33 representative triglyceride molecules to describe successfully the experimental densities of three Brazilian oils (buriti oil, brazil nut oil and grape seed oil) with an average relative deviation of less than 0.80 %. Since on this work the composition of the oil in triglycerides was unknown, and only the fatty acid profile was available, to use this method we defined pseudocompounds to describe the oil composition. The pseudocomponents were triglycerides, formed by three identical fatty acids, with compositions defined to match the fatty acid profile of the oils as reported in **Table 3.8.5**.

Table 3.9. 5. Composition of Triglycerides for Zong's model

		Mass fraction						
Fatty acid	Triglyceride	S	R	P	Sf	C	*Am*	*Jc*
C14:0	MMM	0.0008	0.0007	0.0075	0.0012	0.0291	0.0010	0.0011
C16:0	PPP	0.1094	0.0540	0.4470	0.0908	0.0327	0.0856	0.1758
C18:0	SSS	0.0401	0.0167	0.0428	0.0606	0.0079	0.0248	0.0388
C18:1	OOO	0.2336	0.6418	0.4066	0.8439	0.0402	0.2408	0.3668
C18:2	LiLiLi	0.5447	0.2150	0.0950	0.0016	0.0100	0.4385	0.4166
C18:3	LnLnLn	0.0714	0.0718	0.0010	0.0019	0.0100	0.2094	0.0009
C18:1OH	RRR	0.0000	0.0000	0.0000	0.0000	0.8701	0.0000	0.0000

The temperature-dependency parameters of the fragments, $B_{1,A}$ and $B_{2,A}$,were reported by Zong et al.[233] Based on these parameters, the Zong's model provided a good description of the density of the six vegetable oils here studied, with an OARD of 1.2% (**Table 3.9.4**). The density of castor oil was not predicted with this method because there were no values of parameters $B_{1,A}$ and $B_{2,A}$ for the ricinoleic acid. This model produced deviations that are almost stable over the range of temperatures studied, with a maximum of 2.5 % as shown in **Figure 3.9.5.**

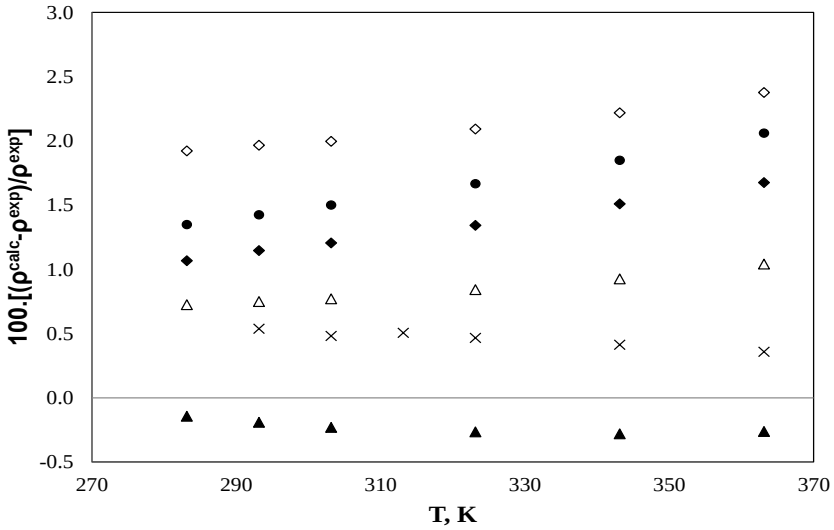

Figure 3.9. 5. RDs between experimental and predicted densities as a function of the temperature at atmospheric pressure using the Zong's model for six vegetable oils. ◆ S, △ R, ● *Am*, ◇ *Jc*, ▲ Sf and × P

The density prediction with GCVOL group contribution method began with the division of the molecule of vegetable oil into several functional groups: CH_3 and CH_2 to describe the contribution of the linear and saturated alkyl chain, CH=CH to consider the unsaturation of the alkyl chain, and finally CHCOO and CH_2COO to take into account the ester contributions and CHOH to consider the alcohol contribution. This method was then applied in three different versions according to the values of parameters *Ai, Bi*, and *Ci* for the groups described above. As stated above, the original version used the parameters reported by Elbro et al.[142]. The extended version used the parameters reported by Ihmels et al.[143] and the revised version used the new parameters proposed by Pratas et al. [129] to describe the unsaturation group.

Between the three versions of the GCVOL method studied, the revised version was the most adequate form to describe the temperature dependency of density for oils with an OARD of only 1.1 % followed by the extended version with an OARD of 2.6 %. The original version presented a very high deviation (OARD of 6.3 %). For all cases the deviations are somewhat temperature-dependent with a maximum of 2.5 % for the revised version. The performance of the revised GCVOL method is presented in **Figure 3.9.6.**

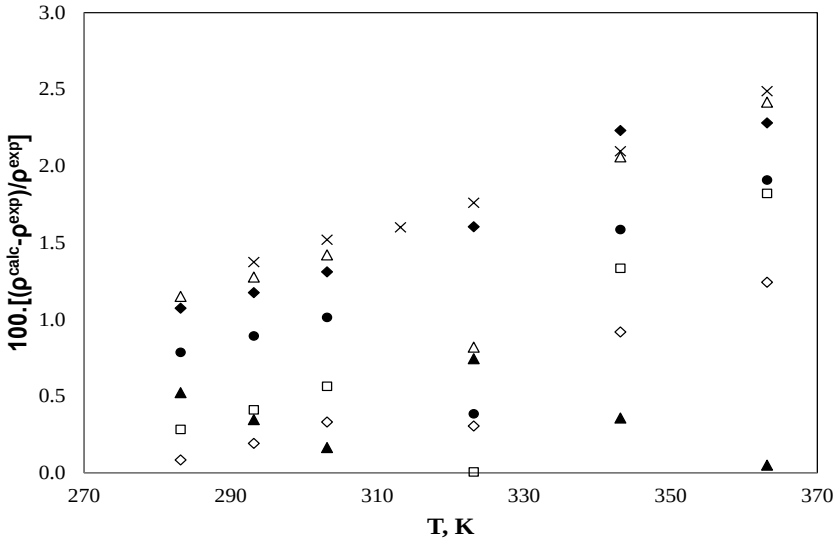

Figure 3.9. 6. RDs between experimental and predicted densities as a function of the temperature at atmospheric pressure using revised version of GCVOL group contribution method for seven vegetable oils. □ C, ◆ S, △ R, ● *Am*, ◇ *Jc*, ▲ Sf and × P

An extension of the models here studied to high pressure is also proposed to describe the pressure-dependency of density for vegetable oils according to the Eq. (3.8.15), where ρ is the density in g/cm^3, *Mw* is the molecular weight in g/mol, *V(T)* is the molar volume at atmospheric pressure in cm^3.mol^{-1}, *P* is the absolute pressure in MPa, and *c* is a fitting parameter.

$$\rho(T,P) = \frac{Mw}{V(T)(1+cP)} \tag{3.9.15}$$

To estimate the *c* parameter, the experimental data of three vegetable oils (P, S and *Jc*) were used for the fitting purpose. The *c* values obtained were-4.29×10^{-4}MPa^{-1}for the Halvorsen method, -2.80×10^{-4} MPa^{-1}for the Zong's model and -5.99×10^{-4} MPa^{-1}for the revised GCVOL method. The other two versions of GCVOL method were not used to predict high-pressure densities of vegetable oils as they describe poorly the temperature-dependency.

The description of the experimental high-pressure densities for all vegetable oils was very good for the three methods studied, presenting OARDs of 0.75, 1.04 and 0.41 % for the models of Halvorsen, Zong and revised GCVOL respectively, as shown in **Table 3.9.6**.Moreover, the RDs for all methods are slightly pressure-dependent with maximum deviations of less than 2.0 % as seen in **Figures 3.9.7-3.9.9**. These models are thus adequate to describe the temperature and pressure dependency of the density for vegetable oils, provided that the fatty acid profile is known.

Table 3.9. 6. ARDs from the revised GCVOL method, the Halvorsen's model and the Zong's model at high pressures

	ARD,%		
Oil	Revised GCVOL	Halvorsen	Zong
C	0.14	0.41	
S	0.11	0.37	0.81
R	0.12	1.8	0.49
Sf	0.11	0.49	0.68
Am	0.12	0.22	1.1
Jc	1.2	0.7	1.5
P	1.0	1.3	1.7
OARD, %	**0.41**	**0.75**	**1.0**

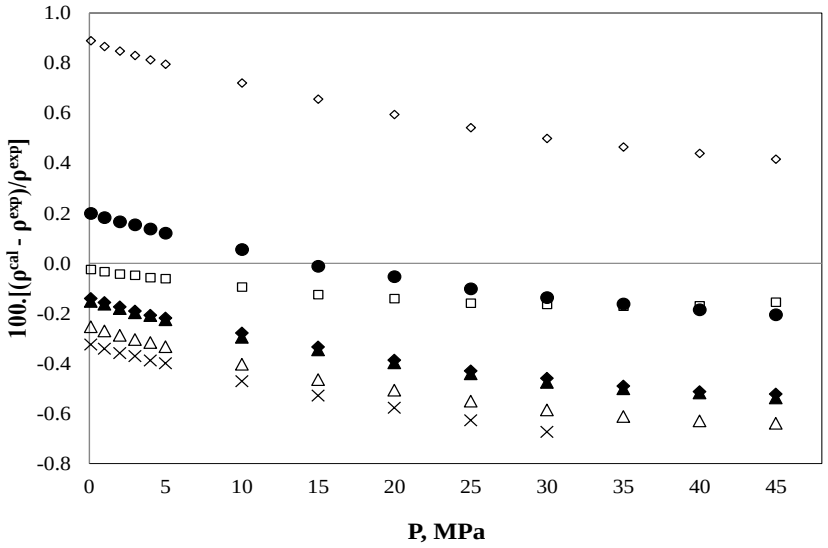

Figure 3.9. 7. RDs between experimental and predicted densities as a function of the pressure at 293.15 K using an extension of the Halvorsen's model for seven vegetable oils. □ C, ◆ S, △ R, ● *Am*, ◇ *Jc*, ▲ Sf and × P

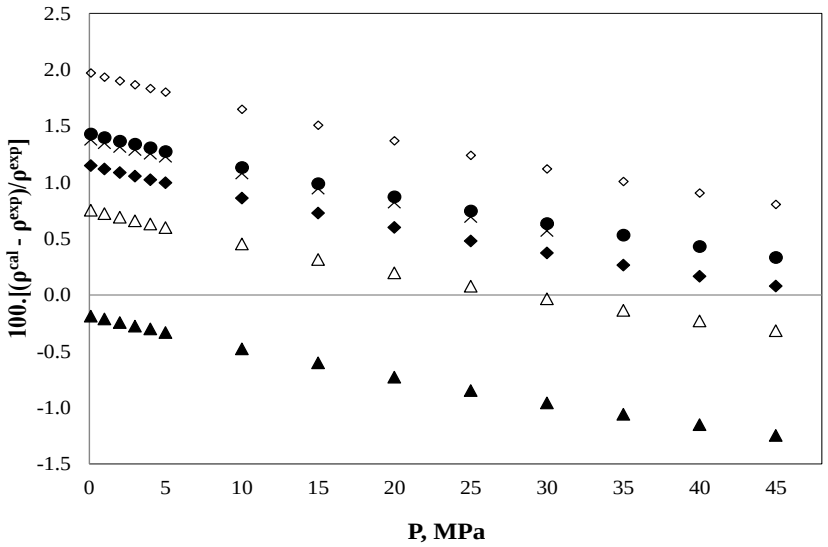

Figure 3.9. 8. RDs between experimental and predicted densities as a function of the pressure at 293.15 K using an extension of the Zong's model for six vegetable oils. ◆ S, △ R, ● *Am*, ◇ *Jc*, ▲ Sf and × P

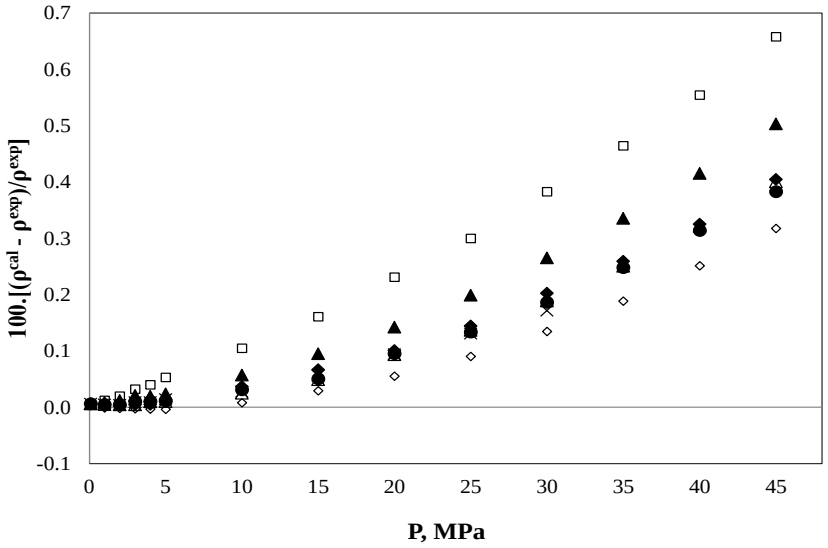

Figure 3.9. 9. RDs between experimental and predicted densities as a function of the pressure at 293.15 K using an extension of the Revised GCVOL model for seven vegetable oils. □ C, ◆ S, △ R, ● *Am*, ◇ *Jc*, ▲ Sf and × P

3.9.5. Conclusions

The experimental data of high pressure densities for seven vegetable oils were here reported for temperatures ranging from 283.15 to 363.15 K and pressures from atmospheric to 45 MPa. These data were correlated with the Tait-Tammann equation and used to assess the adequacy of GCVOL group contribution method, Halvorsen's model and Zong's model for prediction of vegetable oils density. The Halvorsen's model and Zong's model described very well the temperature dependency of oil density with overall average relative deviations (OARDs) of 0.34 and 1.1%, respectively. Between the three versions of the GCVOL method studied, the revised version was the most adequate for prediction of the densities of oils, presenting an OARD of 1.2 %. An extension of the models here studied to high pressure was also proposed. The models provided very good predictions of density with OARDs of 0.75, 1.04 and 0.41 % for the models of Halvorsen, Zong and revised GCVOL, respectively and the deviations were just slightly pressure-dependent with a maximum deviation of less than 2.0 %.

CHAPTER4

Modeling the Thermodynamic Properties of Fatty Esters and Biodiesels with the Soft-SAFT EoS

This chapter concerns the use of Soft-SAFT EoS to compute the thermodynamic properties of fatty esters (FAME and FAEE) and biodiesels. As these molecules are non-self-associating fluids, their properties were defined by only three molecular parameters: m_i (chain length), σ_{ii} (segment diameter) and ε_{ii}/k_B (dispersive energy between segments). The results for several properties of fatty esters and biodiesels like density, surface tension, speed of sound and viscosity are here presented both at atmospheric and at high pressure.

The completeness of this chapter was achieved with the direct cooperation of Dr. Mariana Belo from our group and Dr. Felix Llovel from Matgas, in Barcelona. The biodiesels here studied were the ten described earlier in Chapter 3. Other calculations were done by me.

4.1. Introduction

So far many works have been dedicated to predict the thermophysical properties of biodiesels, as well as of fatty esters that compose them, to assess their quality as fuel. Accurate thermodynamic properties are needed over a wide range of temperature and pressure to optimize biodiesel production, processing and application. Unfortunately most of the available data do not cover wide ranges of temperature and pressure. So **Chapter 3** exposes the experimental and predicted data for several properties of feed oils, biodiesels and fatty esters with an emphasis on high-pressures.

The molecular based equations of state (EoS) are also an alternative tool to compute these properties. CPA EoS, for example has been used to predict thermodynamic properties of some pure esters and biodiesels as density [141] and surface tensions and vapor pressure as already described in Sections 3.2 and 3.4 respectively. This chapter aims at applying a variant of SAFT (Statistical Associating Fluid Theory), soft-SAFT, for describing the thermodynamic properties of fatty esters. This variant of SAFT has been used with success in many works to model the thermodynamic properties, phase behavior and critical behavior of alkanes [235], alkanols [236], perfluoroalkanes [237, 238], ionic liquids (ILs) [239] and of several poly(ethylene glycol) mixtures[240]. The solubility behavior of several gases such as CO_2, H_2, and Xe in ILs [241], water [242-244], alkanes [235, 245] and perfluoroalkanes [246, 247] was also successfully described with this equation. There is still no work, however, addressing the description of fatty esters thermodynamic properties using soft-SAFT EoS. Consequently, this chapter will present new sets of molecular parameters capable of computing density, surface tension, speed of sound and viscosity of fatty esters in a wide range of temperatures and pressures.

4.2. The soft-SAFT EoS

According to the type of the reference fluid adopted, there are several variant of the SAFT EoS, all of them based on the Wertheim's first-order thermodynamic perturbation theory. The original version developed by Chapman et al.[248] uses the hard-sphere fluid as reference fluid; the SAFT-VR developed by Gil-Villegas et al.[249] uses the square-well fluid with a variable range; the PC-SAFT proposed by Gross et al [250] uses the hard-chain fluid and the soft-SAFT, developed by Blas and Vega [251, 252] and applied in this work uses the Lennard- Jones fluid as reference.

The soft-SAFT is an accurate version of SAFT written, as all other versions, in terms of a sum of contributions to the total Helmholtz free energy of the system: [253, 254]

$$a^{res} = a - a^{id} = a^{ref} + a^{chain} + a^{assoc} + a^{polar} \tag{4.1}$$

Where a^{res} and a^{id} are the residual Helmholtz free energy and the ideal contribution respectively. Subsequently, *ref*, *chain*, *assoc* and *polar* represent the reference term, the chain formation, the association and the polar interactions.

For the reference term, soft-SAFT uses Lennard-Jones (LJ) spherical fluid which takes into account the repulsive and the attractive interactions of the monomers that constitute the chain. This term includes two molecular parameters representing the monomer: the segment diameter, σ_{ii}, and the dispersive energy between segments, ε_{ii}/k_B [255]. In our approach, the reference term is computed using the equation of Johnson et al.[256].

The chain and association terms derive directly from the following Wertheim's theory [257, 258],

$$a^{chain} = \rho\ k_B T \sum_i x_i (1 - m_i) \ln g_{LJ} \tag{4.2}$$

$$a^{assoc} = \rho\ k_B T \sum_i x_i \sum_\alpha \left(\ln\ X_i^\alpha - \frac{X_i^\alpha}{2} \right) + \frac{M_i}{2} \tag{4.3}$$

Being ρ the molecular density, T the temperature, m the chain length, x_i the molar fraction of component i, k_B the Boltzman constant and $g_{L,J}$ the radial distribution function at density

$\rho = m\rho_{monomer}$ of a LJ spheres, with m_i being the chain length parameter. The description of $g_{L,J}$ it given by the fitted computer simulation data, as a function of density and temperature, proposed by Johnson et al.[256] X_i^{α} is the fraction of pure component *i* not bonded at site α and M_i the number of association sites of type α in component *i*. X_i^{α} is given by:

$$X_i^{\alpha} = \frac{1}{1 + N_{avog}\rho \sum_j x_j \sum_{\beta} X_j^{\beta} \Delta_{\alpha\beta,ij}} \tag{4.4}$$

The specific site-site function, $\Delta_{\alpha\beta,ij}$, is described as:

$$\Delta_{\alpha\beta,ij} = K_{\alpha\beta,ij} f_{\alpha\beta,ij} g_{ij}^{LJ} \tag{4.5}$$

Being $K_{\alpha\beta,ij}$ the site-site bonding-volume of association and the Mayer f-function:

$$f_{\alpha\beta,ij} = \left[\exp\left(\frac{\varepsilon_{\alpha\beta,ij}^{HB}}{k_B T} \right) - 1 \right] \tag{4.6}$$

The Mayer function includes the site-site association energy parameter $\varepsilon_{\alpha\beta}^{HB} / k_B$.

Within the soft-SAFT framework, non-self-associating molecules are defined by three molecular parameters: the chain length, m_i, the segment diameter, σ_{ii}, and the dispersive energy between segments, ε_{ii}/k_B. For associating molecules two more parameters are included to model the associating interactions: the site-site association energy, $\varepsilon_{\alpha\beta,ij}^{HB}/k_B$, and the site-site bonding-volume of association, $K_{\alpha\beta,ij}$.

The Density Gradient Theory (DGT) was coupled to the soft-SAFT equation to compute interfacial properties. DGT was first proposed by van der Waals[259] and then rediscovered by Cahn et al.[260] The expression for the Helmholtz energy of the system is given by:

$$A = \int \left[a_0(\rho) + \sum_i \sum_j \frac{1}{2} c_{ij} \nabla\rho_i \nabla\rho_j \right] d^3 r \tag{4.7}$$

where $a_0(\rho)$ is the Helmholtz free energy density of the homogeneous fluid at the local density ρ and ρ_i is the molar density of component *i*. c_{ij} is the influence parameter that is assumed to be temperature independent. Its value is normally regressed from interfacial tension experimental data.

Assuming a planar interface and neglecting the c_{ij} density dependence it is possible to derive an expression relating interfacial tensions and the square of the density gradient:[261]

$$\gamma = \sum_i \sum_j \int_{-\infty}^{\infty} c_{ij} \frac{d\rho_i}{dz} \frac{d\rho_j}{dz} dz = 2 \int_{-\infty}^{\infty} \left[a_0(\rho) - \sum_i \rho_i \mu_{0i} - p_0 \right] dz \tag{4.8}$$

Where μ_{0i} and p_0 are the equilibrium chemical potential and pressure, respectively, and *z* is the direction perpendicular to the interface. Further details about the implementation of the DGT approach into soft-SAFT can be found in previous works [262, 263].

The derivative properties of a thermodynamic potential function can be written in several ways. They can be considered as derivatives of the Helmholtz energy and the pressure, which are direct calculations from the soft-SAFT equation. Hence, the expressions for the main derivative properties calculated in this work are:

$$C_V = -T \left(\frac{\partial^2 A}{\partial T^2} \right)_\upsilon \tag{4.9}$$

$$k_T = \rho \left(\frac{\partial P}{\partial \rho} \right)_T \tag{4.10}$$

$$\mu = T \left(\frac{\partial P}{\partial T} \right)_\upsilon - \left(\frac{\partial P}{\partial \rho} \right)_T \tag{4.11}$$

$$\alpha = k_T \left(\frac{\partial P}{\partial T} \right)_\upsilon \tag{4.12}$$

$$C_P = C_V + \frac{T\alpha^2}{k_T \rho} \tag{4.13}$$

$$u = \sqrt{\frac{C_P}{C_v}\left(\frac{\partial P}{\partial \rho}\right)_T} \tag{4.14}$$

Where C_V ($Jmol^{-1}K^{-1}$) is the isochoric heat capacity, k_T (MPa^{-1}) isothermal compressibility coefficient, α (K^{-1}) is the thermal expansion coefficient, *Cp* is the isobaric heat capacity ($Jmol^{-1}K^{-1}$) and *u* (ms^{-1}) is the speed of sound.

The calculation of viscosity with the soft-SAFT EoS is normally done by coupling it with the Friction Theory (FT) or the free-volume theory (FVT). Both theories divide the dynamic viscosity into two parts according to the Eq. (4.15) but use differently the dense-state correction term.

$$\eta = \eta_0 + \Delta\eta \tag{4.15}$$

In the equation above η_0 is the viscosity of dilute gas given by Chung et al.[264], and $\Delta\eta$ is the dense-state correction term. In case of using FVT, this term is connected to the molecular structure through a representation of the free-volume fraction (f_v) based on an empirical relation proposed by Doolittle[265],

$$\Delta\eta = A\exp\left(\frac{B}{f_v}\right) \tag{4.16}$$

Allal et al.[266] relate the free-volume fraction with the intermolecular energy controlling the potential field in which the molecular diffusion takes place. The final expression of this contribution is

$$\Delta\eta = \rho\ L\ E\ \sqrt{\frac{10^3 M}{3RT}}\exp\left(B\left(\frac{E}{RT}\right)^{3/2}\right)[\mu P] \tag{4.17}$$

R is the universal constant in J/(mol K), *M* is the molecular weight in g/mol and *P* is pressure in MPa. The molar density ρ (in mol/cm^3) is the only property derived from the EOS. Equation 4.17 is an approximation of the intermolecular energy. Its first term is considered to be the energy barrier a molecule has to overcome to diffuse, and the second term is considered to be

the energy needed to form a vacant passage for the diffusion. *E* is interpreted as the flow energy barrier only.

At last the application of FVT requires three additional parameters related to the viscosity of the pure fluid. *L* is the length parameter [Å], absorbing the average quadratic length, which is related to the structure of the molecules and the characteristic relaxation time, α is the proportionality between the energy barrier and the density in J m^3/(mol kg) and *B* is a positive number characteristic of the free-volume overlap. Using a *transferable* approach, the α parameter is taken from the equivalent *n*-alkane, while the remaining two parameters *B* and L_v are fitted to viscosity data of the pure fluid at several isobars [267].

4.3. Results and discussion

Several thermodynamic properties of fatty esters (FAME and FAEE) namely density, surface tension, speed of sound and viscosity were here computed with the soft-SAFT EoS at wide ranges of temperature and pressure using only three molecular parameters: the chain length, m_i, the segment diameter, σ_{ii}, and the dispersive energy between segments, ε_{ii}/k_B and some other fitting parameters like influence parameter *(c)* for surface tension and parameters α, β and L for viscosity. The results for each property are described below.

4.3.1. Regression of molecular parameters

As already stated earlier, and similarly to alkanes, the fatty esters molecules are non-self-associating fluids and so, within the Soft-SAFT EoS framework, their properties can be effectively defined by the three molecular parameters aforementioned. Before doing a separate optimization of these parameters for FAME, however, as this work is an extension of our previous works [24,46] and given that soft-SAFT EoS has the ability to provide *transferable* parameters from a certain family of compounds to those of other families, we started the description of FAME thermodynamic properties using the molecular parameters correlated directly from the trend lines of alkanes [252, 267, 268] . The results, however, were far from

acceptable, i.e., the slopes of the predicted and the experimental densities did not match each other when depicting them in the same representation as illustrated in **Figure 4.1** for methyl caprate, methyl palmitate and methyl stearate.

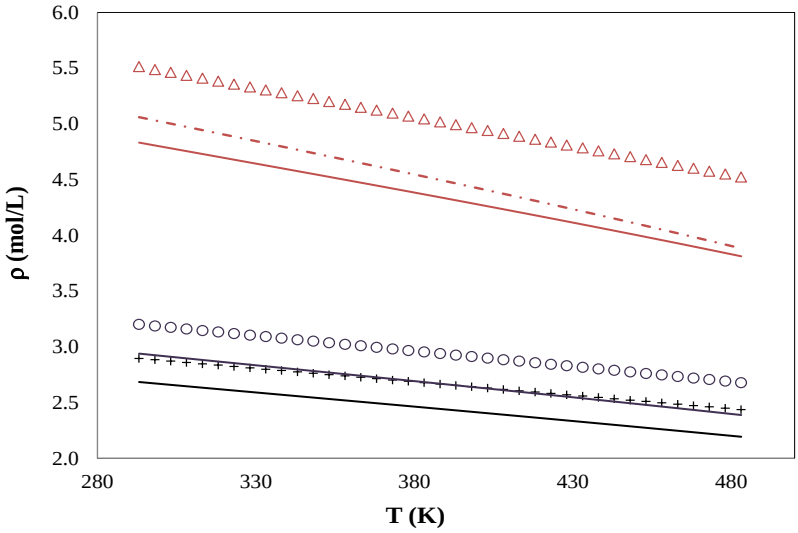

Figure 4 1. Density vs. temperature for FAME at atmospheric pressure. Symbols represent experimental data △ Methyl caprate, ○ Methyl palmitate and + Methyl stearate. Lines are the soft-SAFT results using the molecular parameters correlated from alkanes.

This deviation may be due to the fact that the convergence criteria of this EoS is highly sensitive to the initial conditions, on the one hand, and the fluids (alkanes and esters) are quite different due to the presence of the ester group, on the other hand. Thereat, new sets of molecular parameters were regressed for FAME, at a strict reduced-temperature (Tr) range, using the experimental data of vapor pressure and liquid density reported respectively by Yuan *et al.*[162] and Pratas *et al.*[152, 153]. The results are presented in **Table 4.1.**With these parameters soft-SAFT is able to compute FAME densities with an OARD of only 0.047 %.

Table 4. 1. Molecular parameters and soft-SAFT ARD for FAME densities

FAME	Mw, g/mol	m	σ□ (Å□)	ε/kB (K)	ARD_P^v %	ARD_ ρ^L %
C8:0	158.2	4.043	3.986	293.900	5.5	0.12
C10:0	186.3	4.274	4.164	309.700	2.4	0.033
C12:0	214.3	4.568	4.291	320.831	6.1	0.012
C14:0	242.4	4.940	4.374	328.605	6.4	0.036
C16:0	270.5	5.221	4.472	339.425	7.7	0.038
C18:0	298.5	5.562	4.542	348.794	7.6	0.015
C18:1	296.5	5.551	4.508	342.101	6.3	0.039
C18:2	294.5	5.260	4.556	343.349	7.2	0.028
C18:3	292.5	5.227	4.533	346.466	4.9	0.017
C20:0	326.6	5.860	4.600	346.704	3.9	0.085
C20:1	311.5	5.631	4.576	353.606	5.2	0.013
C22:0	354.6	6.100	4.673	351.695	8.2	0.015
C22:1	352.6	6.080	4.653	352.095	3.3	0.15
C24:0	382.7	6.400	4.727	356.651	6.9	0.064
OARD, %					**5.8**	**0.047**

Moreover, the slopes of the experimental and predicted density now properly match the range of temperatures studied as shown in **Figure 4.2**. Vapor pressures were also acceptably described with the equation of state as shown in **Figure 4.3** with an OARD of 5.8 %

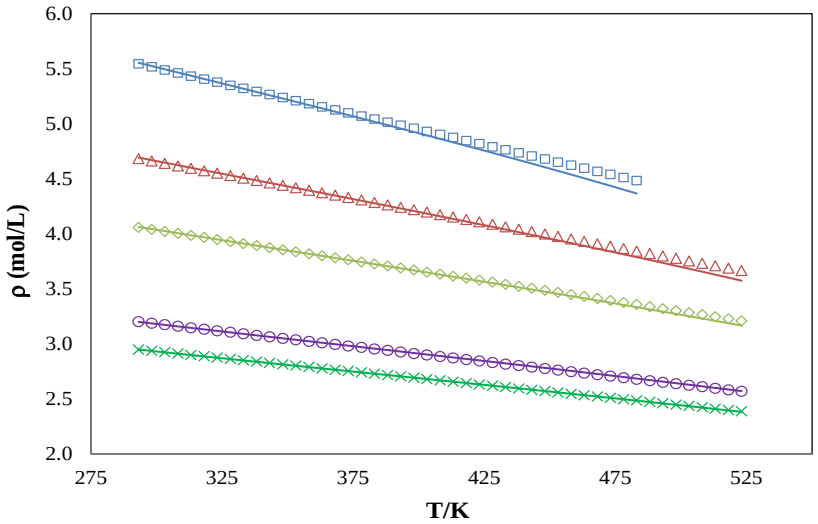

Figure 4 2. Density vs. temperature for FAME at atmospheric pressure. . □ Methyl Caprylate, △ Methyl caprate, ◇ Methyl Laurate, ○ Methyl palmitate and × Methyl oleate.Lines (soft-SAFT results).

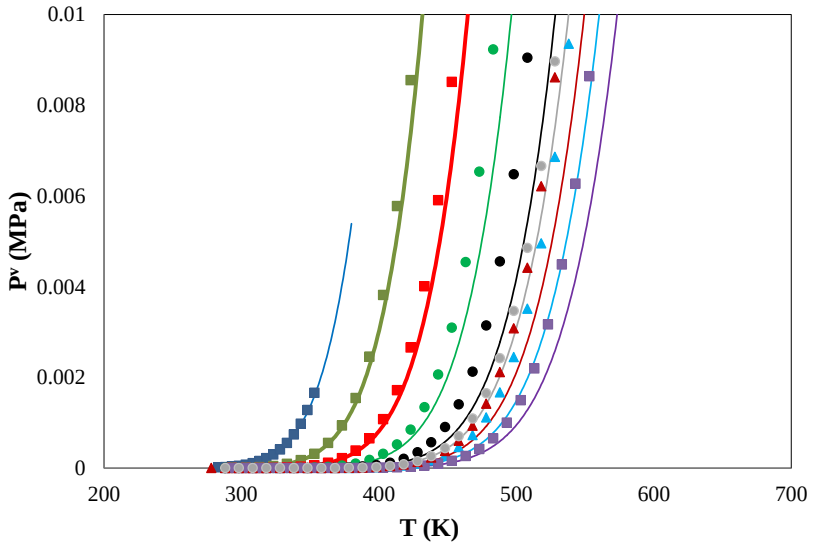

Figure 4 3. Vapor pressure vs. temperature for some FAME. Symbols represent experimental data ■ C8:0, ■ C10:0, ■ C12:0, ● C14:0, ● C16:0, ▲ C18:0, ▲ C18:1, ● C18:2 and ■ C20:1

After knowing the molecular parameters for FAME, those for FAEE were easily calculated using the following equations that relate linearly each parameter with the molecular weight of a fatty ester:

$$m = 0.0107 M_W + 2.31 \quad (4.18)$$

$$m\sigma^3 = 1.8525 M_W - 38.279 \quad (4.19)$$

$$m\varepsilon/k_B = 4.908 M_W + 419.84 \quad (4.20)$$

These trends are similar to those reported by Pàmies et al.[235] for alkanes or at least ensure similar trends of all compounds in function of molecular weight, i.e., when depicting the molecular parameters of FAME and alkanes in the same representation, as a function of the molecular weight, there are similar trends easily seen, either as individual m, σ, ε/k_B, or as $m^*\sigma^3$ and $m^*\varepsilon/k_B$ (**Figures 4.4** to **4.8**). The parameter m presents a sharper gradient for the alkanes than for the esters due to the reasons already mentioned above.

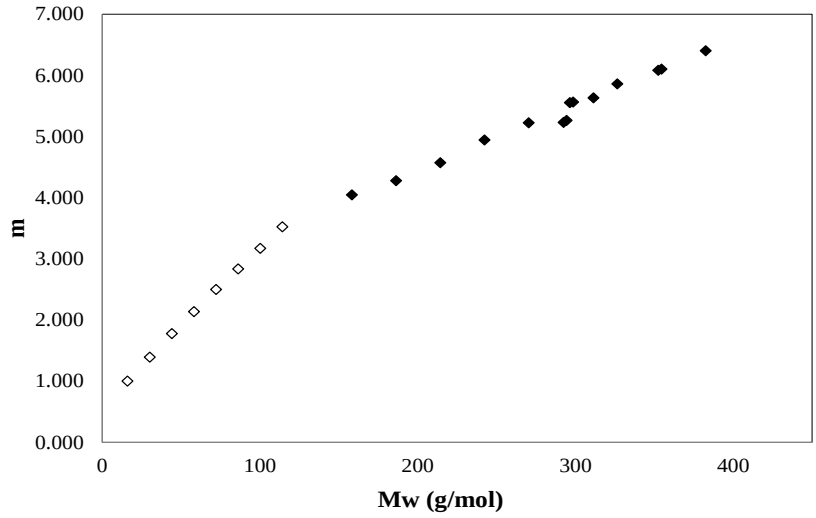

Figure 4 4. Parameter m vs. molecular weight for ◇ Alkanes and ◆ FAME.

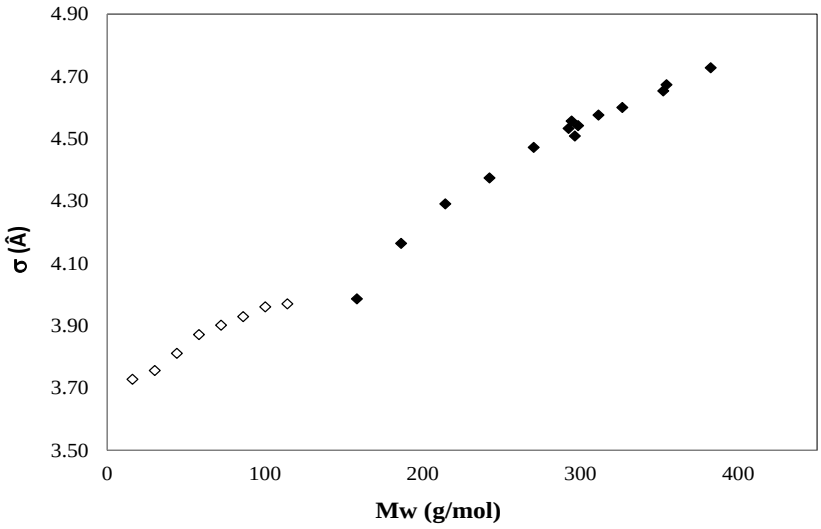

Figure 4 5. Parameter σ vs. molecular weight for ◇ Alkanes and ◆ FAME

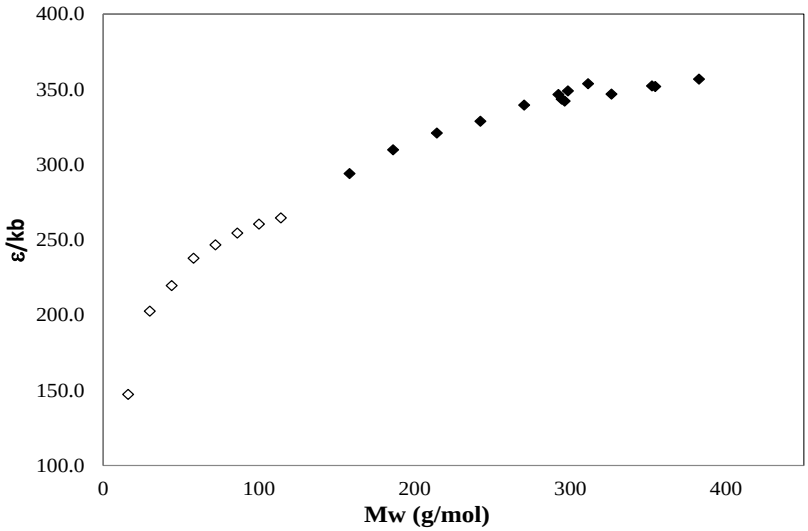

Figure 4 6. Parameter ε/k_B vs. molecular weight for ◇ Alkanes and ◆ FAME.

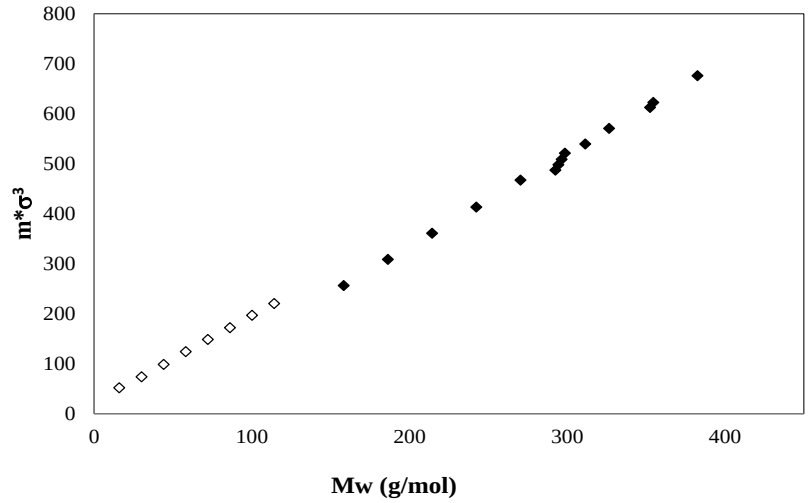

Figure 4 7. Parameter $m^*\sigma^3$ vs. molecular weight for ◇ Alkanes and ◆ FAME.

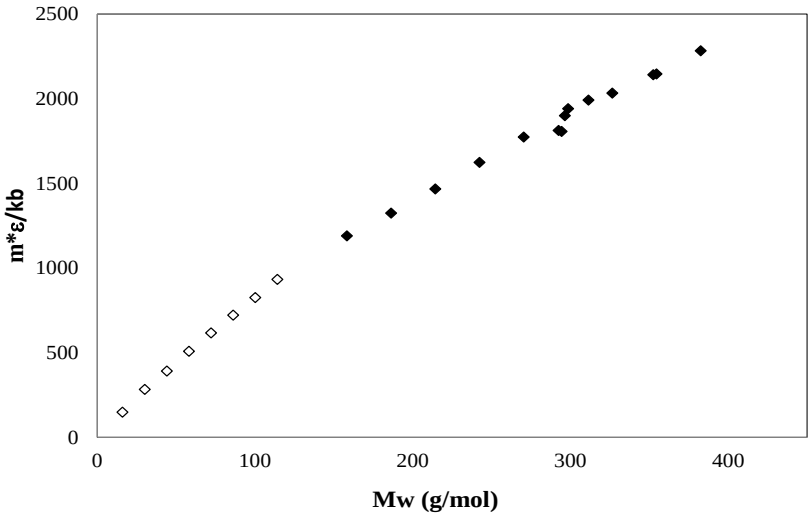

Figure 4 8. Parameter $m^*\varepsilon/k_B$ vs. molecular weight for ◇ Alkanes and ◆ FAME.

Howsoever, using the molecular parameters correlated from the trend-lines of FAME, the densities of the FAEE were very well predicted by Soft SAFT with an OARD of 1.4 % (**Table 4.2)**. Moreover the coexistence of the experimental and predicted data is also very acceptable as seen in **Figure 4.9.**

Table 4. 2. Molecular parameters and soft-SAFT ARD for FAEE densities

FAEE	Mw, g/mol	m	σ□Å□	ε/kB (K)	ARD_ρL %
C8:0	172.3	4.153	4.074	304.659	1.5
C10:0	200.3	4.453	4.212	315.042	1.4
C12:0	228.4	4.754	4.326	324.113	1.2
C14:0	256.4	5.054	4.421	332.106	1.3
C16:0	284.5	5.354	4.503	339.203	0.9
C18:0	312.5	5.654	4.573	345.547	1.4
C18:1	310.5	5.633	4.568	345.114	0.4
C18:2	308.5	5.611	4.563	344.677	1.4
C18:3	306.5	5.589	4.559	344.237	3.6
C20:0	340.6	5.954	4.634	351.251	1.4
C20:1	338.6	5.933	4.630	350.860	No data
C22:0	368.6	6.255	4.689	356.407	
C22:1	366.6	6.233	4.685	356.053	
C24:0	396.7	6.555	4.737	361.092	
OARD, %					**1.4**

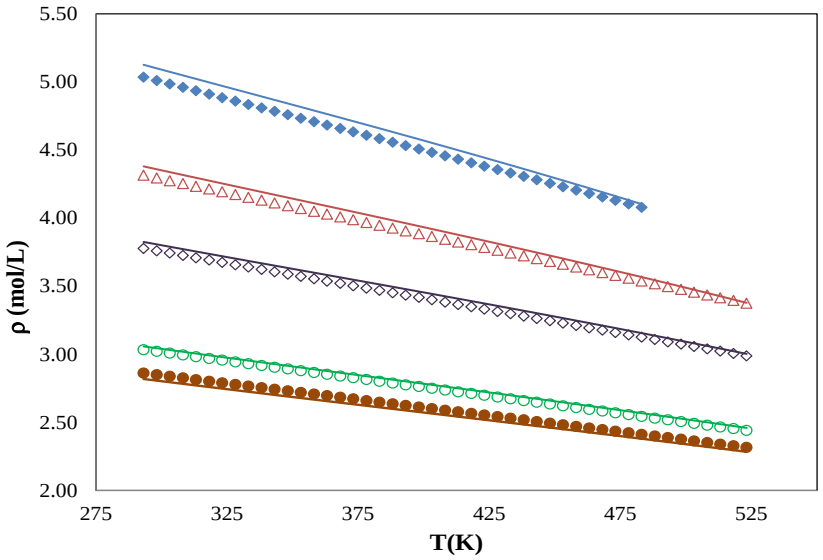

Figure 4 9. Density vs. temperature for FAEE at atmospheric pressure. Symbols represent experimental data ◆ Ethyl Caprylate, △ Ethyl caprate, ◇ Ethyl Laurate, ○ Ethyl palmitate and ● Ethyl linoleate. Lines are the soft-SAFT results.

4.3.2. Thermodynamic properties of fatty esters

4.3.2.1. High pressure densities

The high-pressure densities for fatty acid esters were very well predicted with the soft-SAFT EoS, using the molecular parameters regressed from density data at atmospheric pressure presenting an OARD of only 1.1% (0.49 % for FAME and 1.8 % for FAEE) as shown in **Table 4.3**. The adequacy of this model is also shown in **Figures 4.10** to **4.14** for methyl caprate, methyl linoleate and ethyl laurate. It can be seen that the experimental density temperature and pressure dependencies are correctly described, matching the predicted data slope with the experimental one, contrarily to what happened with other EoS [141].

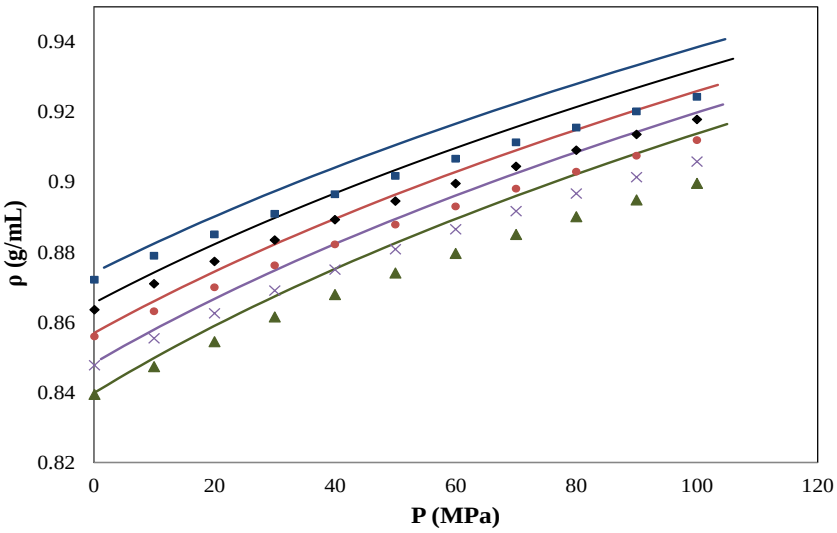

Figure 4 10. High-pressure density for methyl caprate at different temperatures. . Symbols represent experimental data ■ 293.15 K, ◆ 303.15K, ● 313.15K, × 323.15 and ▲ 333.15K. Lines are the soft-SAFT results.

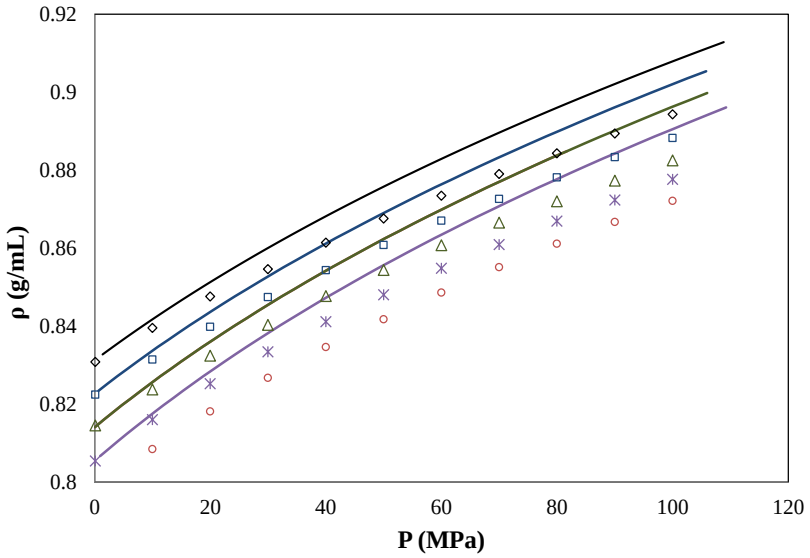

Figure 4 11. High-pressure density for methyl caprate at different temperatures. Symbols represent experimental data □ 343.15 K, ◇ 353.15K, ○ 363.15K, ✳ 373.15 and △ 383.15K. Lines are the soft-SAFT results.

Table 4. 3. ARDs for High pressure density for FAME and FAEE

ARD, %													
FAME\T, K	283.15	293.15	303.15	313.15	323.15	333.15	343.15	353.15	363.15	373.15	383.15	393.15	
C10:0 [222]		0.81	0.66	1.0	0.85	1.3	1.1	0.50	0.87	0.63	0.96	0.80	0.86
C12:0 [141]	0.53	0.46	0.57	0.43	0.34	0.49							0.47
C14:0 [141]		0.38	0.31	0.38	0.33	0.30							0.34
C18:1 [141]		0.41	0.35	0.29	0.43	0.32							0.36
FAME\T, K	270	290	310	330	350	370	390	410	430	450	470		
C18:1 [269]	0.22	0.17	0.20	0.27	0.21	0.26	0.12	0.23	0.35	0.40	0.51		0.27
C18:2 [269]	0.26	0.30	0.20	0.28	0.34	0.21	0.27	0.33	0.37	0.46	0.99		0.36
FAEE\T, K	283.15	293.15	303.15	313.15	323.15	333.15	343.15	353.15	363.15	373.15	383.15	393.15	
C12:0 [141]		1.6	1.6	1.4	1.9	1.8	1.7	2.2	1.7	2.1	2.0	2.5	1.8
OARD, %													**1.1**

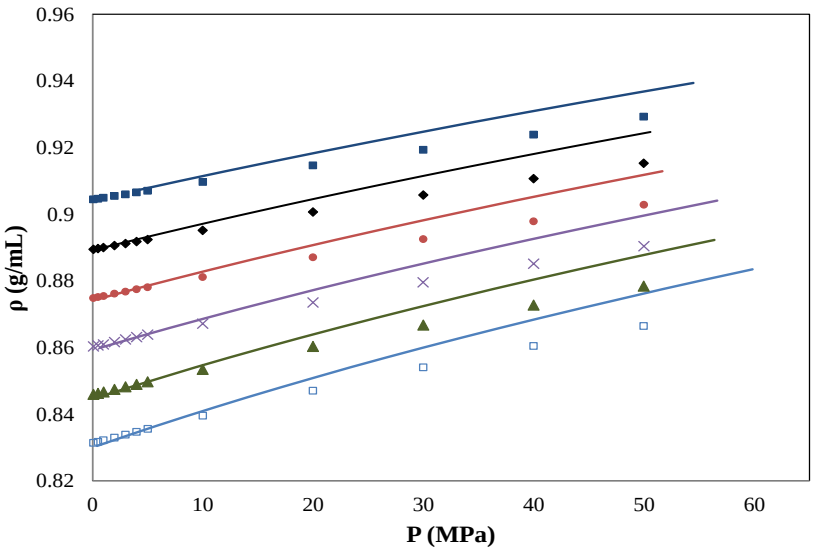

Figure 4 12. High-pressure density for methyl linoleate at different temperatures. Symbols represent experimental data ■ 270 K, ◆ 293K, ● 310 K, × 330K, ▲ 350K and □ 370 K. Lines are the soft-SAFT results.

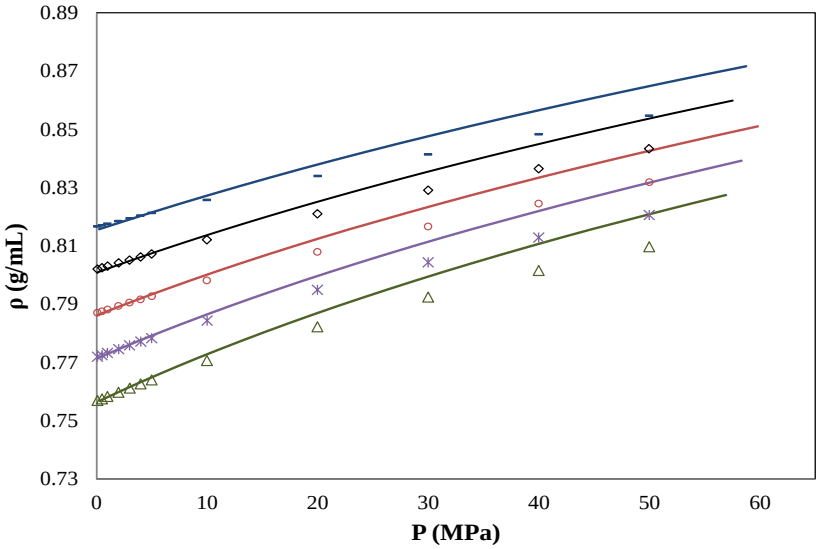

Figure 4 13. High-pressure density for methyl linoleate at different temperatures. Symbols represent experimental data – 390 K, ◇ 410K, ○ 430K, ✳ 450K and △ 470K. Lines are the soft-SAFT results.

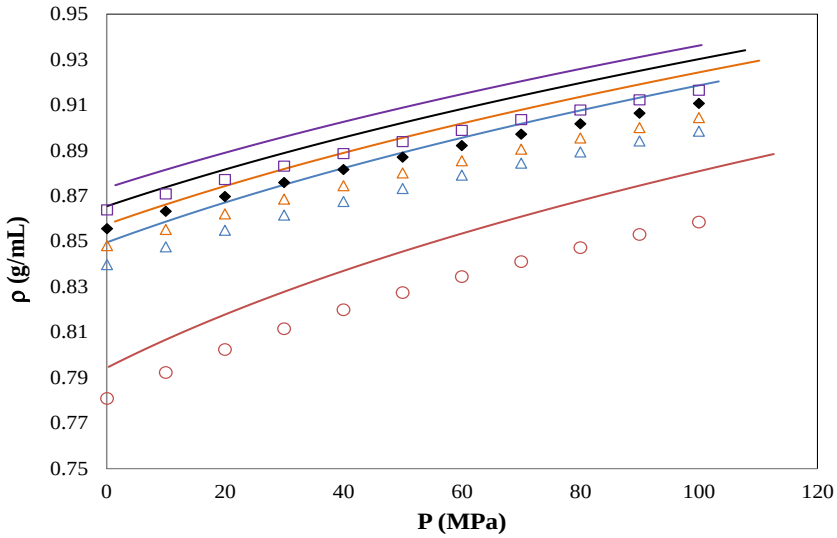

Figure 4 14. High-pressure density for ethyl laurate at different temperatures. Symbols represent experimental data □ 293.15 K, ◆ 313.15 K, △ 313.15K, △ 323.15K and ○ 393.15 K. Lines are the soft-SAFT results.

4.3.2.2. Surface tensions

Unlike density, the calculation of surface tension with the soft SAFT EoS needs, beyond the molecular parameters, an extra fitting parameter called the influence parameter (c). This was optimized for each FAME using surface tensions data predicted with the Parachor's model reported by the Knotts et al.[184] at temperatures from 293.15 to 423.15 K. The optimized values are presented in **Table 4.4** and depicted in **Figure 4.15**. The trend line obtained is:

$$c = 6\times10^{-5} Mw^2 + 0.1806 \qquad (4.21)$$

Table 4. 4. Influence parameters and ARD of surface tension for FAME at temperature from 293.15 to 423.15 K

FAME	Mw (g/mol)	c (J.m^5/mol^2) ×10^{18}	ARD, %
C8:0	158.2	0.889	0.57
C10:0	186.3	1.27	1.4
C12:0	214.4	1.85	1.9
C14:0	242.4	2.42	2.2
C16:0	270.5	3.03	2.7
C18:0	298.5	3.70	3.0
C18:1	296.5	3.81	2.6
C18:2	294.5	4.02	2.4
C18:3	292.5	4.00	2.2
C20:0	326.6	4.67	2.9
C20:1	311.5	4.18	3.0
C22:0	354.6	5.78	2.8
C22:1	352.6	5.68	2.9
C24:0	382.7	6.83	2.9
OARD, %			**2.4**

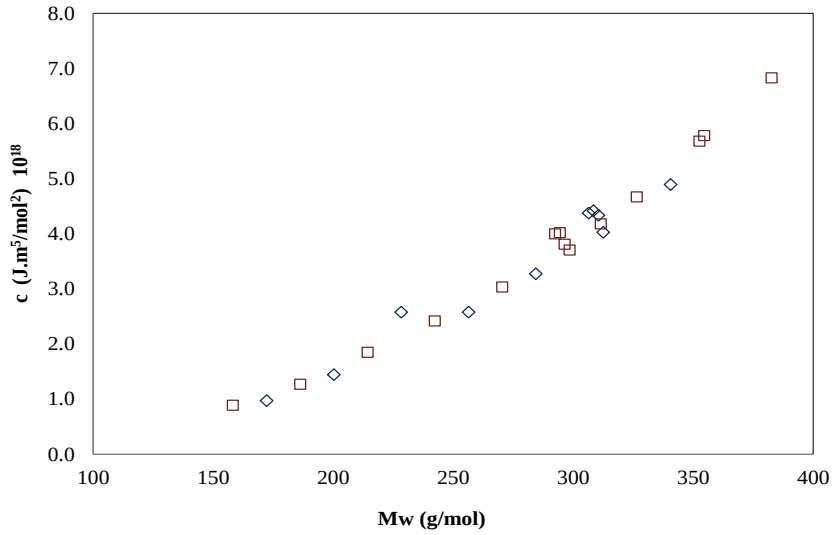

Figure 4 15. Influence parameters as a function of molecular mass for □ FAME and ◇ FAEE

Unlike what happened with the molecular parameters, the influence parameters follow a second order polynomial trend with the molecular weight. With these parameters, the Soft-SAFT EoS computed very well the surface tensions of FAME, presenting only an OARD of 0.52 %. The adequacy of this model can also be seen in **Figures 4.16 and 4.17** for several FAME.

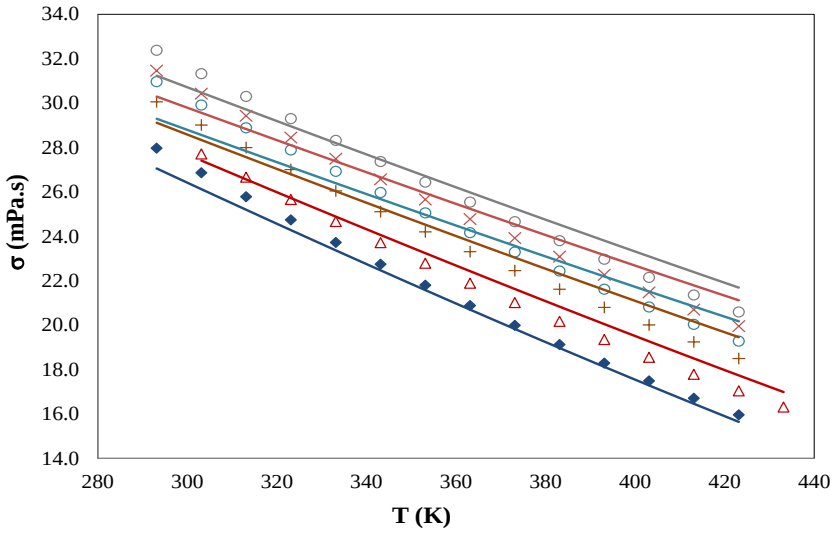

Figure 4 16. Surface tension for FAME at different temperatures. Symbols represent experimental data. ◆Methyl caprylate, △ Methyl caprate, + Methyl myristate, ○ Methyl palmitate, × Methyl oleate and ○ methyl linoleate. Lines are the soft-SAFT results

For FAEE, before calculating their own influence parameters, these were first calculated from the FAME trend (with Eq. 4.21), but with these values the prediction of surface tension of FAEE was somehow poor as seen in **Figure 4.17** for ethyl myristate, ethyl stearate and ethyl oleate. The OARD was 6.1 % as seen in **Table 4.5**. So, new regression of the influence parameters was done for FAEE using again the experimental data reported by Knotts et al.[184]. With the new influence parameters, the prediction of the surface tensions of FAEE by soft-SAFT was excellent with an OARD of only 0.53 % as shown in **Table 4.6**.The adequacy of this model to describe the FAEE surface tensions is seen in **Figure 4.18**.

Table 4. 5. Influence parameters deduced directly from the trend lines proposed for FAME and correspondent ARD for FAEE surface tensions at temperature from 293.15 to 423.15 K

FAEE	Mw, g/mol	c (J.m^5/mol^2)×10^{18}	ARD, %
C8:0	172.3	1.15	8.7
C10:0	200.3	1.65	6.8
C12:0	228.4	2.24	7.0
C14:0	256.4	2.92	7.1
C16:0	284.5	3.70	7.0
C18:0	312.5	4.57	7.3
C18:1	310.5	4.51	3.7
C18:2	308.5	4.44	3.1
C18:3	306.5	4.38	3.0
C20:0	340.6	5.54	7.6
OARD, %			**6.1**

Table 4. 6. Adjusted influence parameters and ARDs of surface tension for FAEE at temperature from 293.15 to 423.15 K

FAEE	Mw, g/mol	c (J.m^5/mol^2)×10^{18}	ARD, %
C8:0	172.3	0.97	1.6
C10:0	200.3	1.44	2.0
C12:0	228.4	2.58	2.3
C14:0	256.4	2.58	2.5
C16:0	284.5	3.27	2.7
C18:0	312.5	4.03	2.9
C18:1	310.5	4.33	2.7
C18:2	308.5	4.42	2.7
C18:3	306.5	4.37	3.4
C20:0	340.6	4.89	3.0
OARD, %			**2.6**

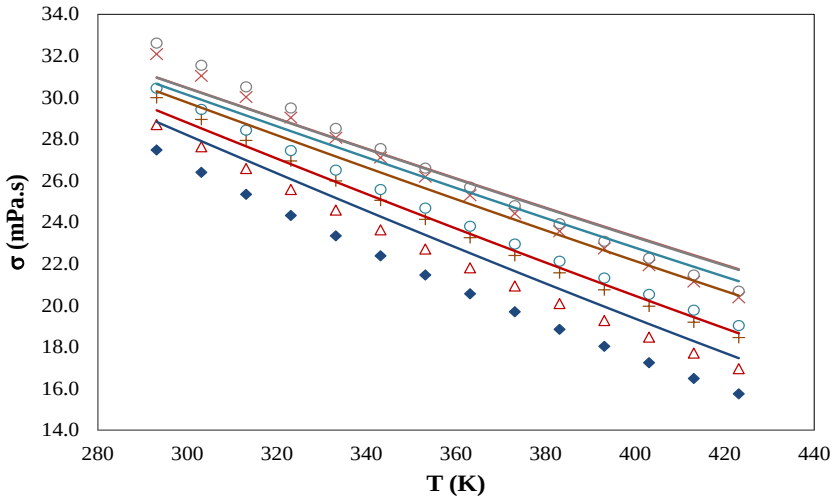

Figure 4 17. Surface tension for FAEE at different temperatures. Symbols represent experimental data. ◆Methyl caprylate, △ Methyl caprate, + Methyl myristate, ○ Methyl palmitate, × Methyl oleate and ○ methyl linoleate. Lines are the soft-SAFT results.

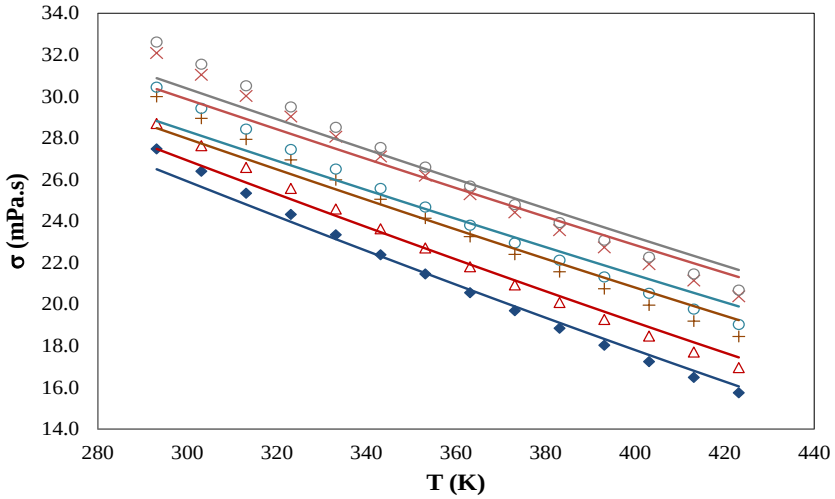

Figure 4 18. Surface tension for FAEE at different temperatures. Symbols represent experimental data. ◆Methyl caprylate, △ Methyl caprate, + Methyl myristate, ○ Methyl palmitate, × Methyl oleate and ○ methyl linoleate. Lines are the soft-SAFT results.

4.3.2.3. Speed of sound

Unlike the surface tension, no extra fitting parameter is required in the algorithm of soft SAFT beyond the molecular parameters for the estimation of speeds of sound. Consequently the speeds of sound of fatty esters were calculated in soft-SAFT using the Eq. 4.14

The soft SAFT provides all the variables involved in the equations above except the *Cp* whose values reported in the output of soft-SAFT were only residual while the prediction of speed of sound needs the contribution of the ideal *Cp*. The ideal *Cp* was calculated using the Joback's group contribution method [234]. The results are illustrated in **Figures 4.19** and **4.20** for several FAME and FAEE, respectively. The high-pressure speeds of sound were also predicted by soft-SAFT for some esters. The results are shown in **Figures 4.21** to **4.23e**, for methyl caprate, methyl oleate and ethyl laurate. The lag between the experimental and predicted data is high but its magnitude is almost equal for the majority of esters. This deviation could be solved within the algorithm of soft-SAFT through a fitting parameter.

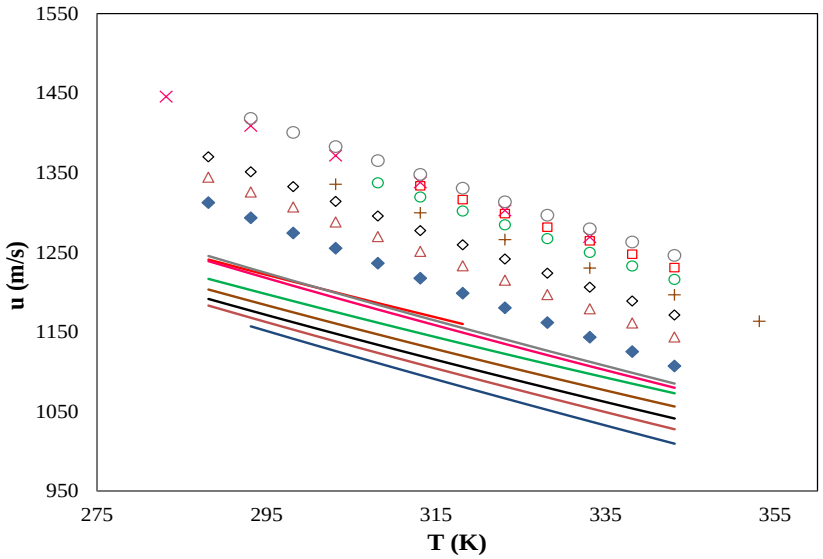

Figure 4 19. Atmospheric speeds of sound for FAME at different temperatures. Symbols represent experimental data. ◆Methyl caprylate, △ Methyl caprate, ◇ Methyl laurate, + Methyl myristate, ○ Methyl palmitate, □ Methyl stearate, × Methyl oleate and ○ methyl linoleate. Lines are the soft-SAFT results.

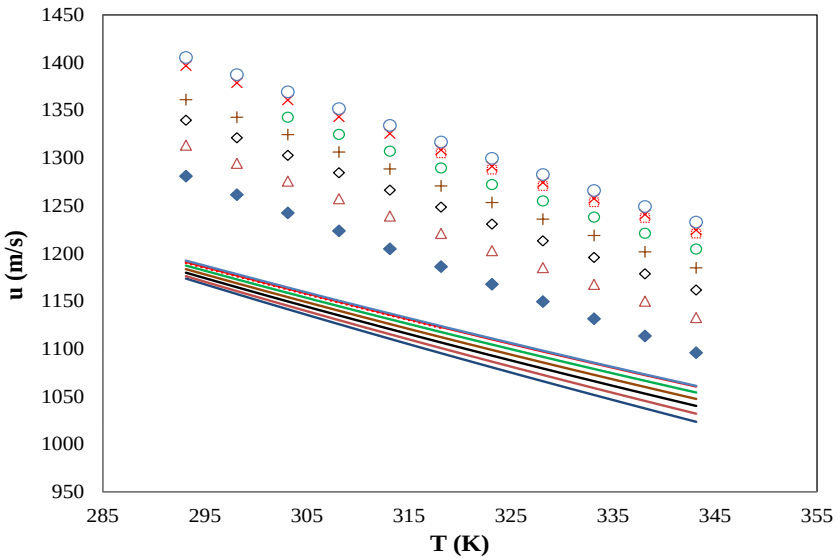

Figure 4 20. Atmospheric speeds of sound for FAEE at different temperatures. Symbols represent experimental data. ◆Methyl caprylate, △ Methyl caprate, ◇ Methyl laurate, + Methyl myristate, ○ Methyl palmitate, □ Methyl stearate, × Methyl oleate and ○ methyl linoleate. Lines are the soft-SAFT results.

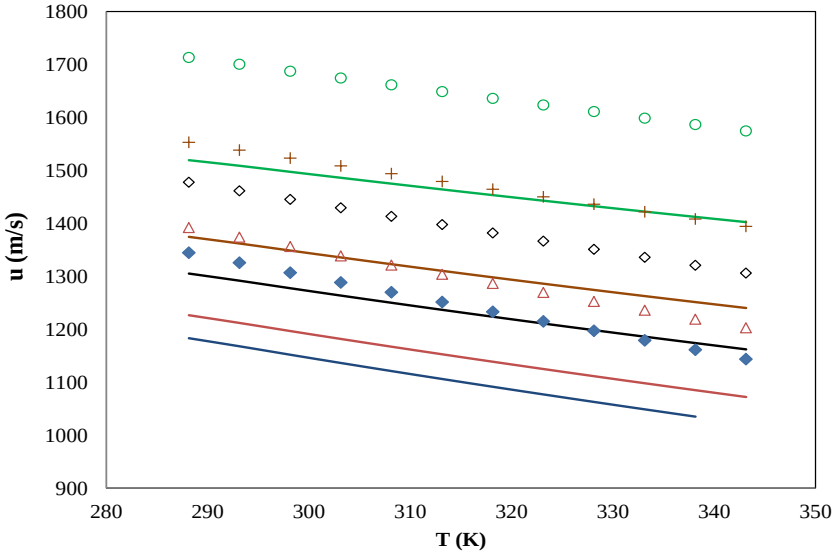

Figure 4 21. High-pressure speeds of sound for methyl caprate at different temperatures. Symbols represent experimental data. ◆ 0.1 MPa, △ 10 MPa, ◇ 30 MPa, + 50MPa and ○ 100 MPa. Lines are the soft-SAFT results.

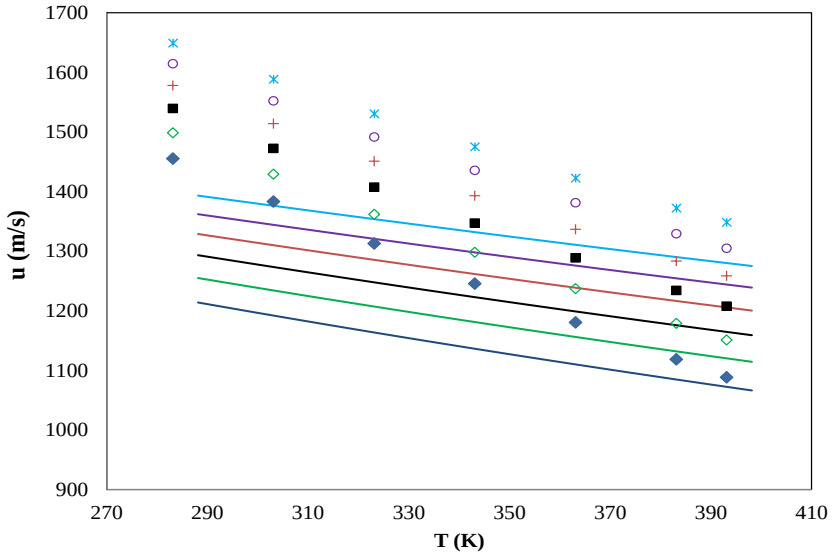

Figure 4 22. High-pressure speeds of sound for methyl oleate at different temperatures. Symbols represent experimental data ◆ 0.1 MPa, ◇ 10 MPa, ■ 20 MPa, + 30 MPa, ○ 40 MPa and ✳ 50 MPa. Lines are the soft-SAFT results.

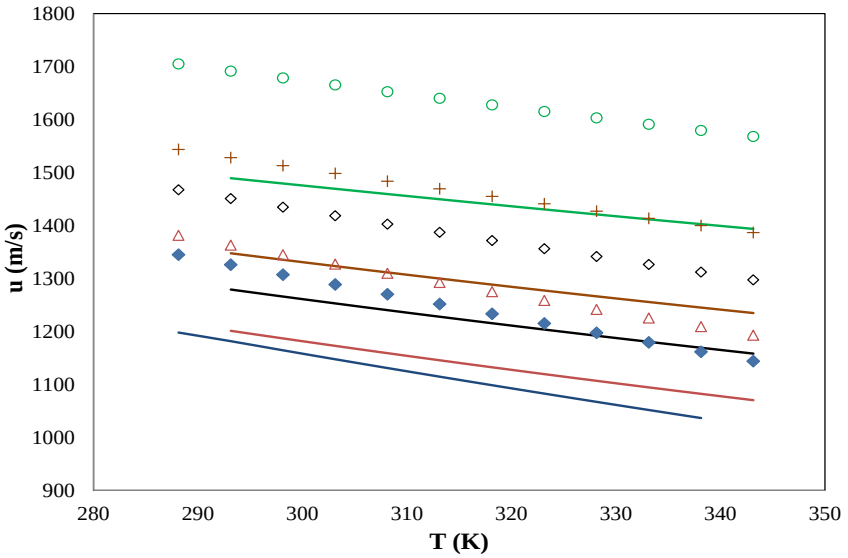

Figure 4 23. High-pressure speeds of sound for ethyl laurate at different temperatures. Symbols represent experimental data. ◆ 0.1 MPa, △ 10 MPa, ◇ 30 MPa, + 50MPa and ○ 100 MPa. Lines are the soft-SAFT results.

4.3.2.4. Viscosity

Just like surface tensions, the description of viscosities of fatty esters with soft-SAFT also needs, beyond the molecular parameters aforementioned, the prior knowledge of other three parameters α, β and L. Before optimizing them, they were directly deduced

from the trend lines of the parameters already proposed for the alkanes by Llovel et al.[267].The predictions, however, were very poor as seen in **Table 4.7**

Table 4. 7. ARDs for viscosity obtained from parameters deduced directly from the trend lines proposed for alkanes.

FAME	Mw, g/mol	α(J m^3/mol kg)	β	L (Å)	ARD, %
C8:0	172.3	148.7	0.005873	0.8231	81
C10:0	200.3	172.7	0.005331	0.8062	72
C12:0	228.4	196.6	0.004883	0.7894	81
C14:0	256.4	220.5	0.004529	0.7726	55

Therefore, the viscosity parameters were separately optimized using the experimental viscosities reported by Pratas *et al*.[152, 153] in the range of temperatures between 288.15 and 378.15 K. Other constants necessary for calculating viscosities such as critical volume, critical temperature and acentric factor were estimated using the Joback's group contribution method [234]. The optimized parameters α, β □and□ L along with the errors for FAME viscosities soft-SAFT description are shown in **Table 4.8**.

Table 4. 8. Soft-SAFT viscosity parameters and ARDs for FAME viscosities at T from 288.15 to 378.15 K

FAME	Mw, g/mol	α(J m^3/mol kg)	β	L (Å)	ARD, %
C8:0	158.2	123.9	0.006210	0.8200	0.48
C10:0	186.3	145.9	0.005648	0.7900	2.1
C12:0	214.4	180.7	0.004759	0.7700	7.0
C14:0	242.4	201.6	0.004521	0.7600	4.9
C16:0	270.5	216.2	0.004500	0.7500	4.9
C18:0	298.5	248.1	0.004100	0.7200	7.9
C18:1	296.5	231.3	0.004111	0.7100	2.8
C18:2	294.5	230.0	0.003745	0.7061	1.3
C18:3	292.5	229.9	0.003510	0.6900	0.70
C20:0	326.6	274.6	0.003653	0.7000	5.1
C20:1	311.5	270.8	0.003447	0.6800	4.0
C22:0	354.6	309.2	0.003232	0.6800	6.2
C22:1	352.6	270.8	0.003447	0.6600	4.0
C24:0	382.7	340.4	0.002961	0.6600	5.5
OARD, %					**3.7**

These parameters provide a good description of the viscosities for FAME but, unlike the molecular parameters, the outcoming parameters for FAEE obtained from linear correlations did not work to predict FAEE viscosities (**Table 4.9**).

Table 4. 9. Soft-SAFT viscosity parameters deduced directly from the trend lines proposed for FAME viscosity parameters and correspondent ARD for FAEE viscosities at T from 288.15 to 378.15 K.

FAEE	Mw (g/mol)	α(J m^3/mol kg)	β	L (Å)	ARD, %
C10:0	200.32	160.469	0.006097	0.7835	51.4
C12:0	228.38	186.972	0.005816	0.7638	88.2
C14:0	256.43	213.474	0.005536	0.7442	109.4

Although the trend lines of these parameters are similar for all the three families of compounds studied (**Figures 4.24-4.26**), the use of any common correlation of each parameter can not predict very well the experimental data of viscosities, confirming thus the high sensibility of the model to the parameters values in terms of the convergence criteria.

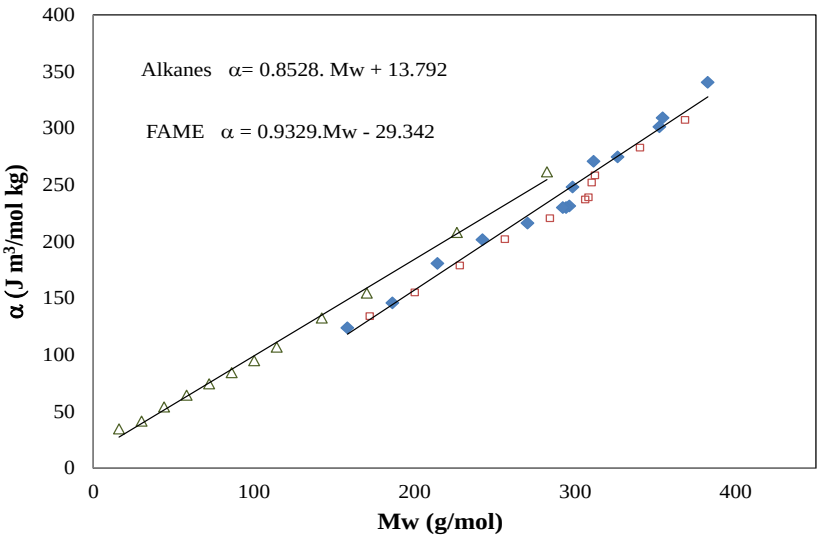

Figure 4 24. Viscosity parameter α vs. molecular mass for ◆ FAME, ▫ FAEE and △ Alkanes[267]

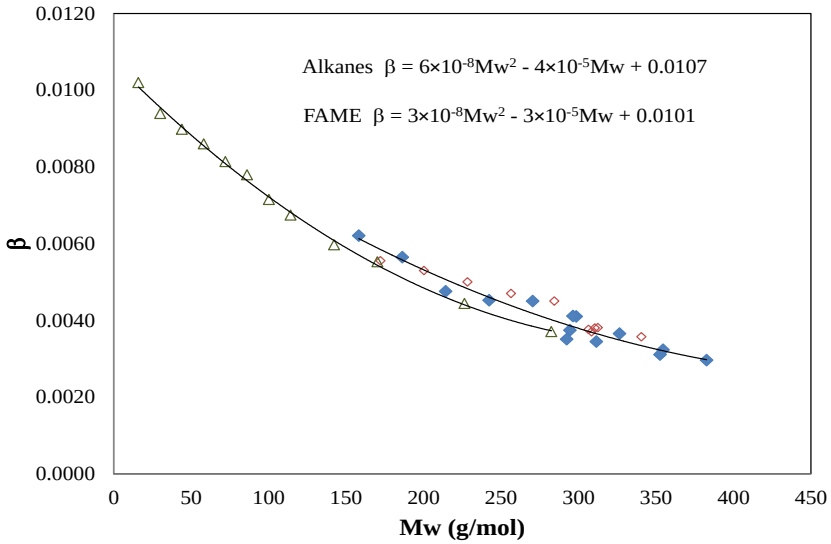

Figure 4 25. Viscosity parameter β vs. molecular mass for ◆ FAME and ▫ FAEE △ Alkanes[267]

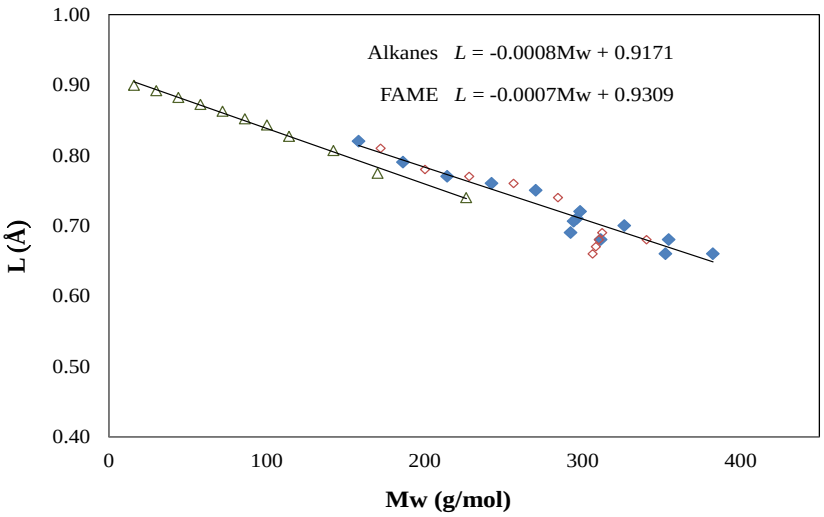

Figure 4 26. Viscosity parameter L vs. molecular mass for ◆ FAME and ▫ FAEE △ Alkanes [267]

Therefore, a separate fitting of α, β and L was done for FAEE using the experimental data reported by Pratas et.al.[152, 153] The results are shown in **Table 4.10** where the FAEE viscosities were predicted with an OARD of only 1.4 % and the adequacy of the model is seen in **Figures 4.27** and **4.30**).

Table 4. 10. Soft-SAFT viscosity parameters (regressed from experimental data) and soft-SAFT ARD for FAEE viscosities at T from 288.15 to 378.15 K

FAEE	Mw (g/mol)	α (J m^3/mol kg)	β	L (Å)	ARD, %
C8:0	172.27	136.273	0.00568	0.7300	1.2
C10:0	200.32	160.680	0.00513	0.7045	0.85
C12:0	228.38	178.800	0.00500	0.6600	1.7
C14:0	256.43	203.700	0.00470	0.6300	1.5
C16:0	284.48	220.500	0.00459	0.6200	1.6
C18:0	312.54	232.200	0.00381	0.5700	1.5
C20:0	340.59	253.100	0.003572	0.5436	1.7
OARD, %					**1.4**

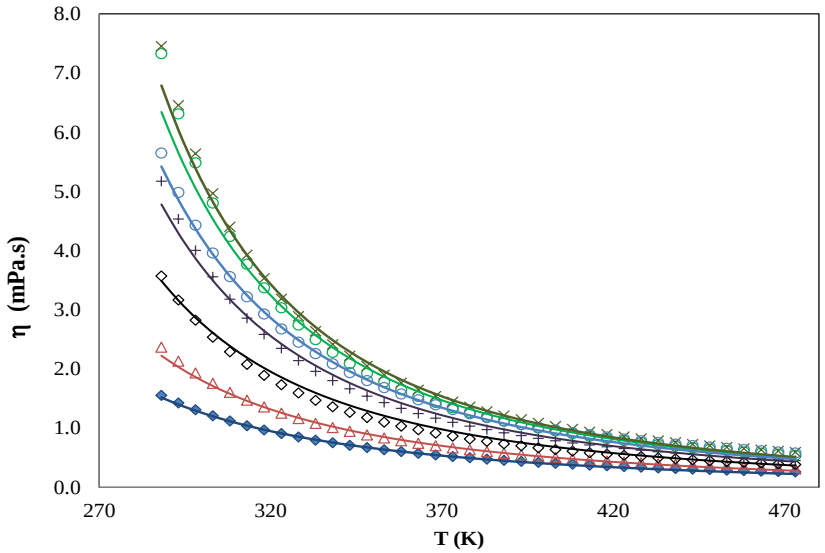

Figure 4 27. Viscosity of FAME at different temperatures. Symbols represent experimental data. ◆Methyl caprylate, △ Methyl caprate, ◇ Methyl laurate, + Methyl laurate, ○ Methyl palmitate, × Methyl Oleate and ○ Methyl linoleate. Lines are the soft-SAFT results.

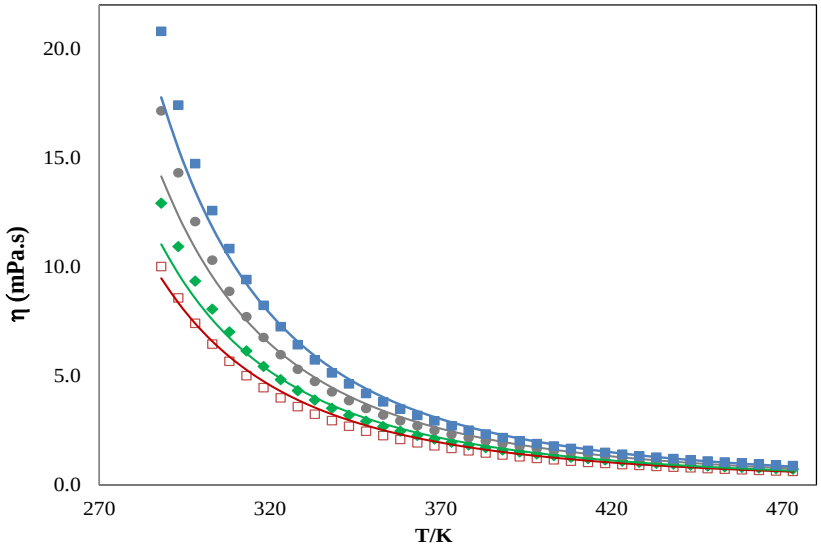

Figure 4 28. Viscosity of FAME at different temperatures. Symbols represent experimental data. □Methyl Stearate, ◆ Methyl arachidate, ● Methyl behenate and ■ Methyl lignocerate. Lines are the soft-SAFT results.

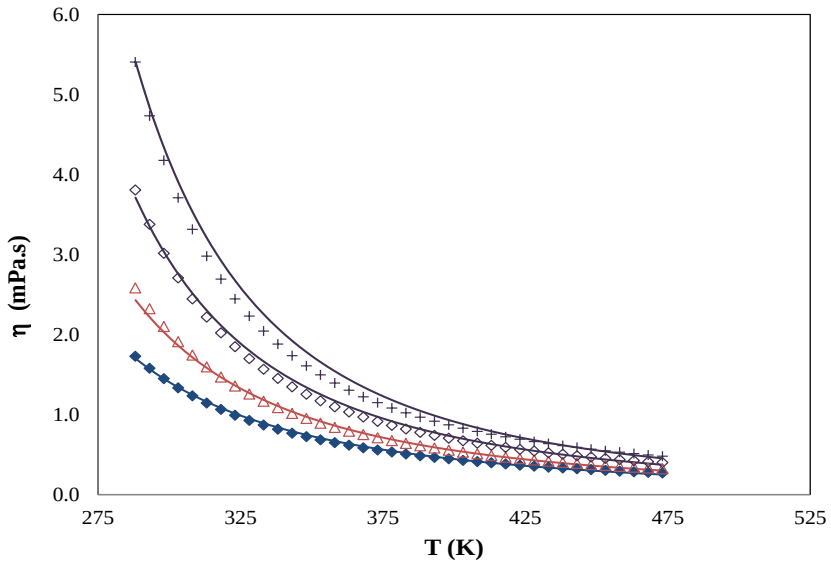

Figure 4 29. Viscosity of FAEE at different temperatures. Symbols represent experimental data. ◆ethyl caprylate, △ethyl caprate, ◇ ethyl laurate, + ethyl laurate. Lines are the soft-SAFT results.

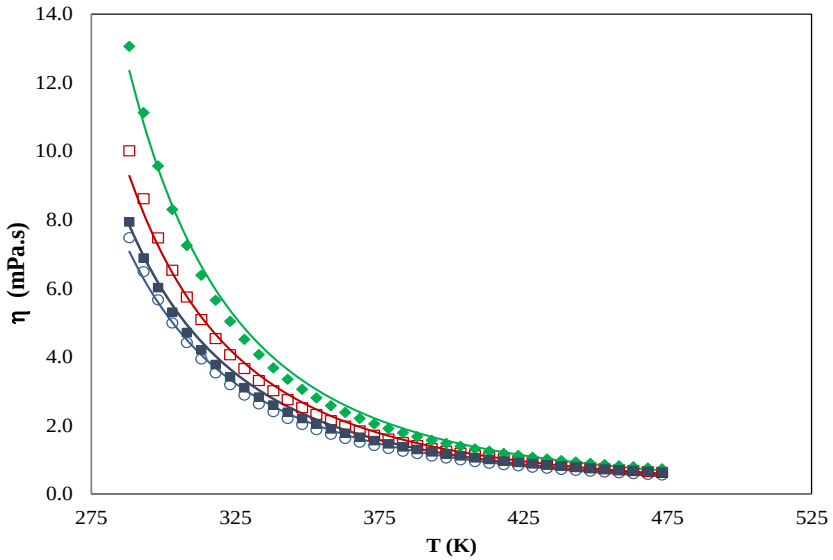

Figure 4 30. Viscosity of FAEE at different temperatures. Symbols represent experimental data. ○Ethyl palmitate □ Ethyl Stearate, ■ Ethyl Oleate and ◆ Ethyl arachidate. Lines are the soft-SAFT results.

4.3.3. Thermodynamic properties of Biodiesels

4.3.3.1. High-pressure density of biodiesel fuels

Using the pure esters molecular parameters optimized using density data at atmospheric pressure, it was possible to predict the high pressure density of biodiesels (mixtures of esters with the compositions presented on **Table 3.2.2 in Section 3.2**) and their mixtures. The prediction was very good in the range of pressures studied as seen in **Figures 4.31 to 4.37**.

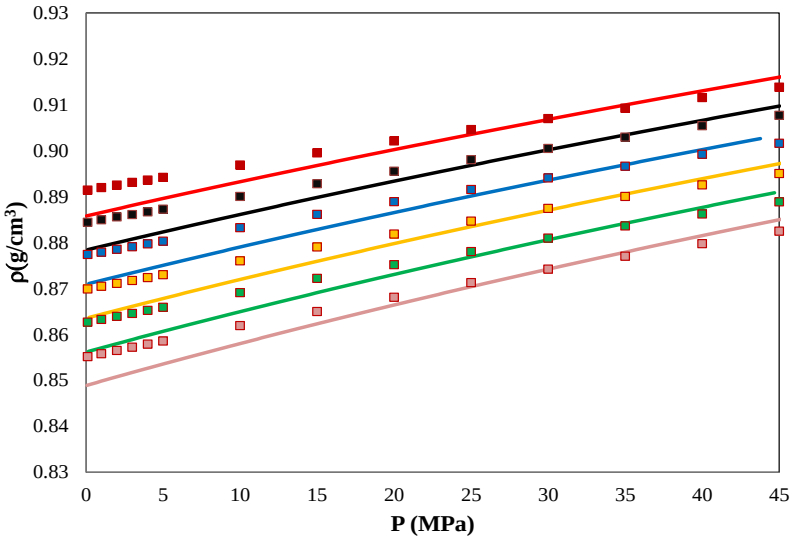

Figure 4 31. HP density of biodiesel R at different T. Symbols are experimental data. ■ 283.15K, ■293.15K, ■ 303.15 K, ■ 313.15 K, ■ 323.15 K and ■ 333.15 K. Lines are soft-SAFT results.

The results for Biodiesel S were compared to those predicted with CPA EoS in previous work [141]. Soft SAFT produced better prediction of high pressure densities than CPA EoS as seen in particularly in **Figures 4.32 a and 4.33.**

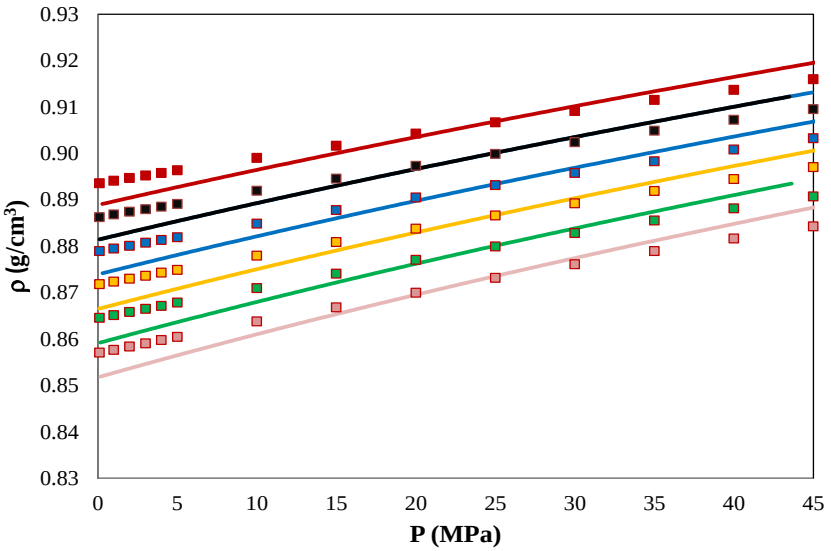

Figure 4 32. HP density of biodiesel S at different temperatures. Symbols represent experimental data. ■ 283.15K, ■293.15K, ■ 303.15 K, ■ 313.15 K, ■ 323.15 K and ■ 333.15 K. Lines are the soft-SAFT results.

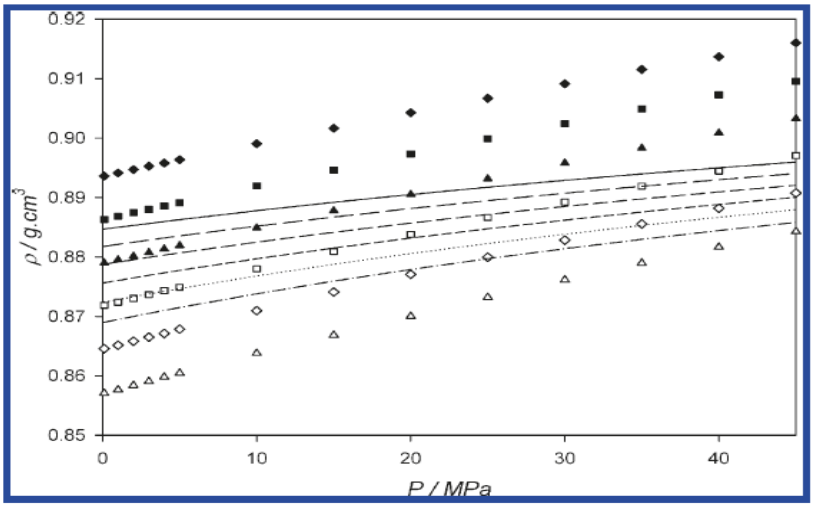

Figure 5. Density isotherms for soybean biodiesel. Experimental data (◆, 283.15 K; ■, 293.15 K; ▲, 303.15 K; □, 313.15 K; ◇, 323.15 K; △, 333.15 K) and CPA EoS results (solid line, 283.15 K; long dash line, 293.15 K; medium dash line, 303.15 K; short dash line, 313.15 K; dotted line, 323.15 K; dash−dot line, 333.15 K).

Figure 4 33. Previous results of density for Biodiesel S predicted with the CPA EoS [141].

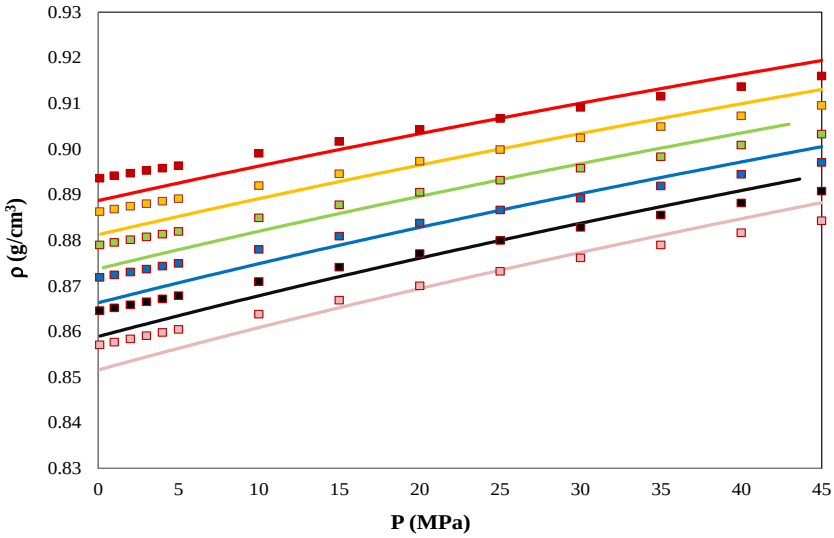

Figure 4 34. HP density of biodiesel Sf at different temperatures. Symbols represent experimental data. ■ 283.15K, ■293.15K, ■ 303.15 K, ■ 313.15 K, ■ 323.15 K and ■ 333.15 K. Lines are the soft-SAFT results.

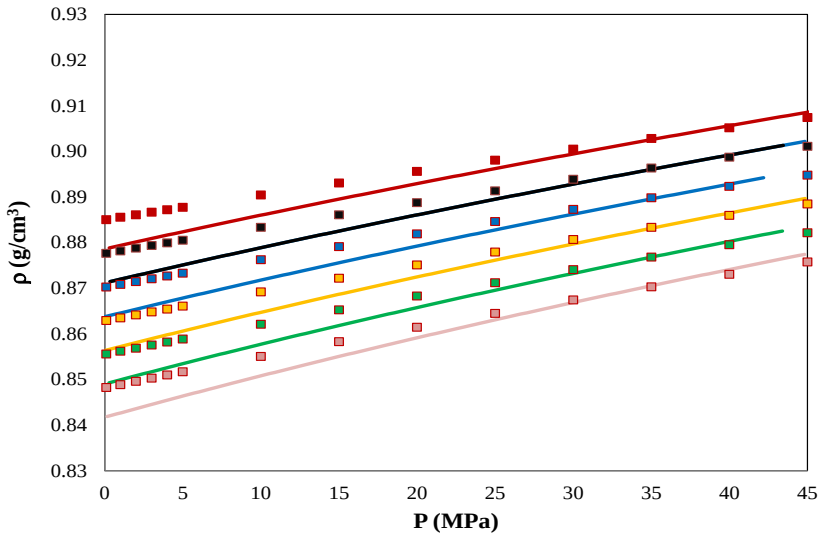

Figure 4 35. HP density of biodiesel P at different temperatures. Symbols represent experimental data. ■ 283.15K, ■293.15K, ■ 303.15 K, ■ 313.15 K, ■ 323.15 K and ■ 333.15 K. Lines are the soft-SAFT results.

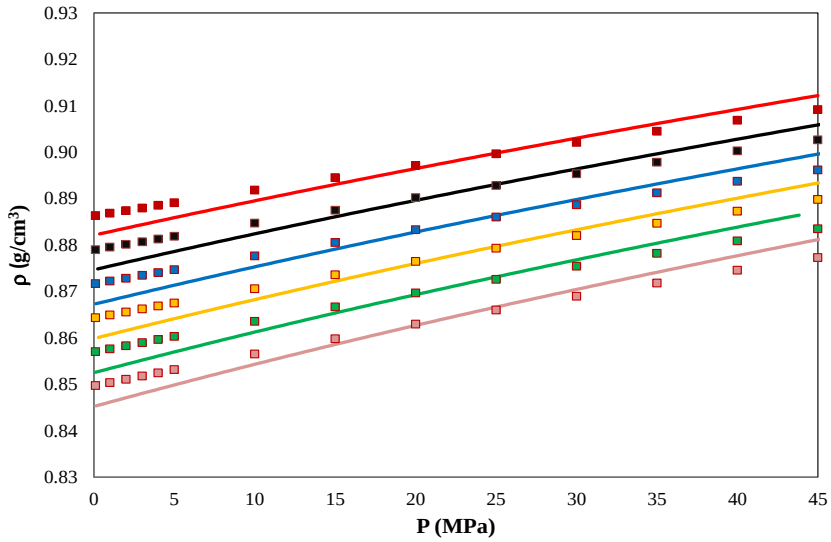

Figure 4 36. HP density of biodiesel RP at different temperatures. Symbols represent experimental data. ■ 283.15K, ■293.15K, ■ 303.15 K, ■ 313.15 K, ■ 323.15 K and ■ 333.15 K. Lines are the soft-SAFT results.

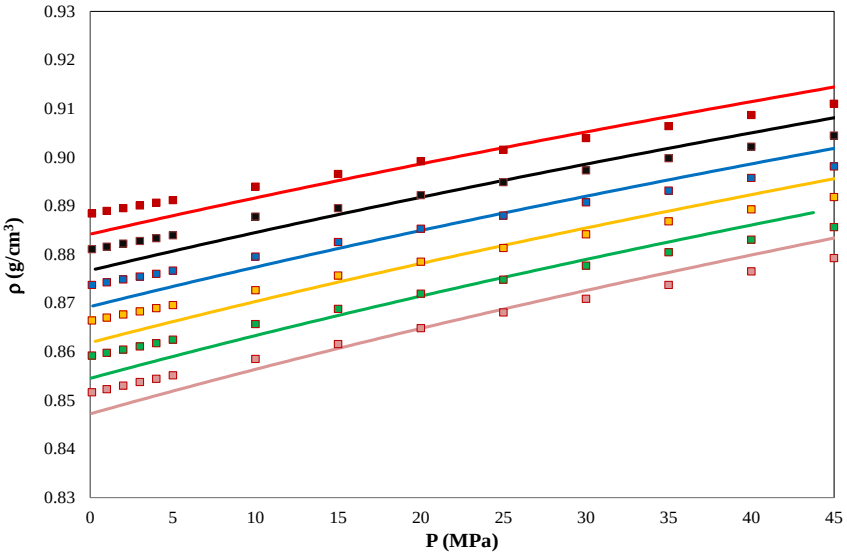

Figure 4 37. HP density of biodiesel SRP at different temperatures. Symbols represent experimental data. ■ 283.15K, ■293.15K, ■ 303.15 K, ■ 313.15 K, ■ 323.15 K and ■ 333.15 K. Lines are the soft-SAFT results

The results presented above for biodiesels are only valid for pressure up to 45 MPa. At this limit the soft-line seemed to be linear, but above this value the trendline of density is no longer linear as seen in **Figures 4.38** and **4.39** for two biodiesels (R and S). Even the prediction still has some degradative effect at pressure higher than 45 MPa, the curvatures of experimental and predicted data matched each other.

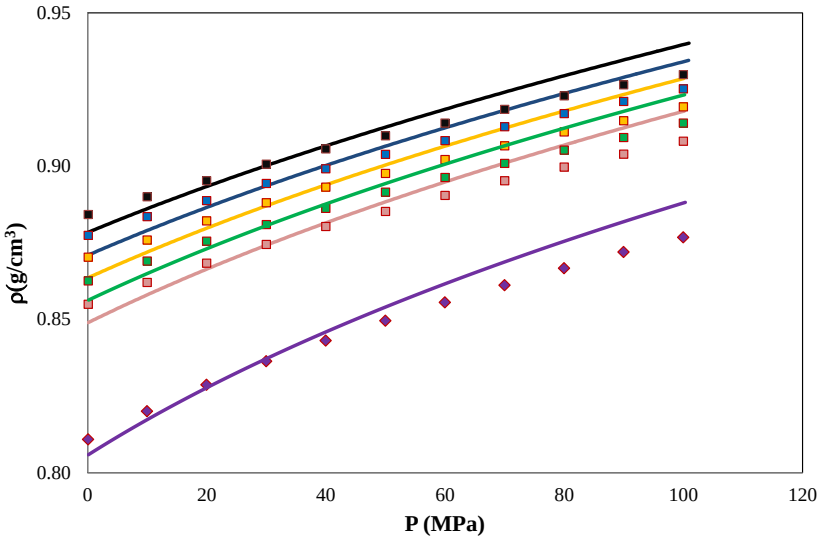

Figure 4 38. HP density of biodiesel SRP at different temperatures. Symbols represent experimental data. ■ 293.15K, ■ 303.15 K, ■ 313.15 K, ■ 323.15 K , ■ 333.15 K and ◆ 393.15 K. Lines are the soft-SAFT results

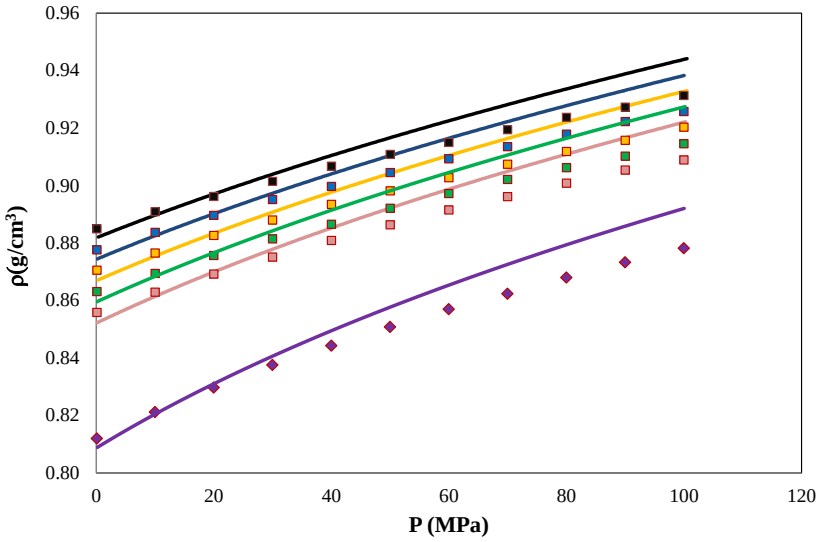

Figure 4 39. HP density of biodiesel SRP at different temperatures. Symbols represent experimental data. ■ 293.15K, ■ 303.15 K, ■ 313.15 K, ■ 323.15 K , ■ 333.15 K and ◆ 393.15 K. Lines are the soft-SAFT results

4.3.3.2. Viscosity of biodiesel fuels

Using the pure esters molecular parameters together with the viscosity parameters mentioned above, it was possible to predict the viscosity of biodiesels and their mixtures at pressures from atmospheric to 140 MPa (compositions of biodiesels presented on **Table 3.2.2 in Section 3.2**). The prediction was very good in the range of temperatures and pressures studied as seen in **Figures 4.40 to 4.44.** Even the deviations are large at low temperature and at high pressure (as occurred with the pure FAME), the trendlines of the experimental and predicted data coincided.

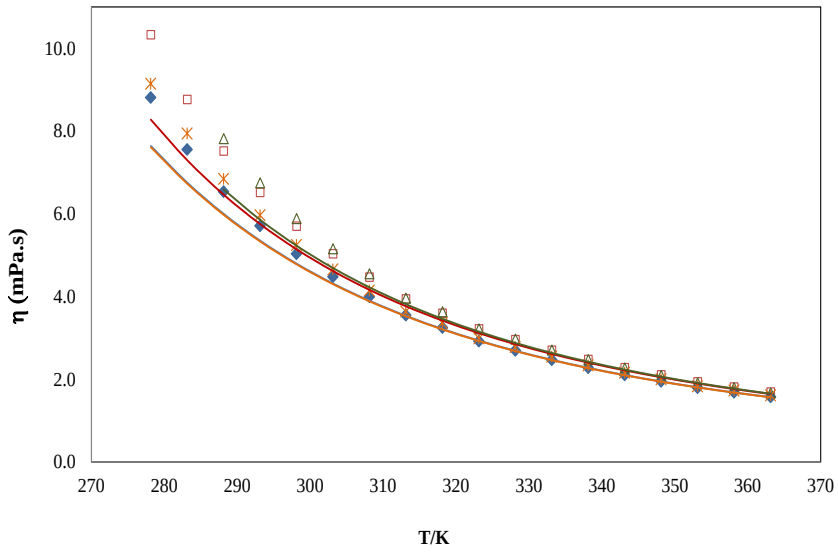

Figure 4 40. Atmospheric viscosity of biodiesels at different temperatures. Symbols represent experimental data. □ R, ◆ S, △ P and ✳ Sf.Lines are the soft-SAFT results.

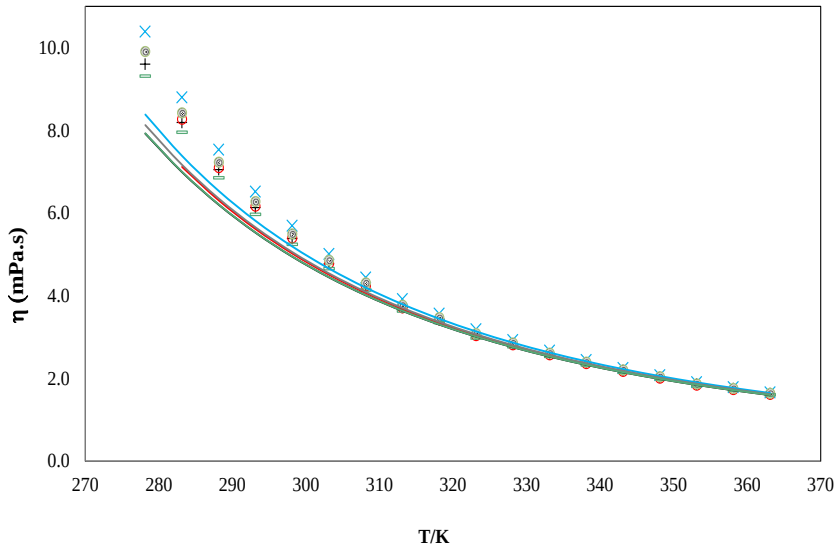

Figure 4 41. Atmospheric viscosity of biodiesels at different temperatures. Symbols represent experimental data.+SR, ○ SP, × R P, ◎ SRP and ▬ GP . Lines are the soft-SAFT results.

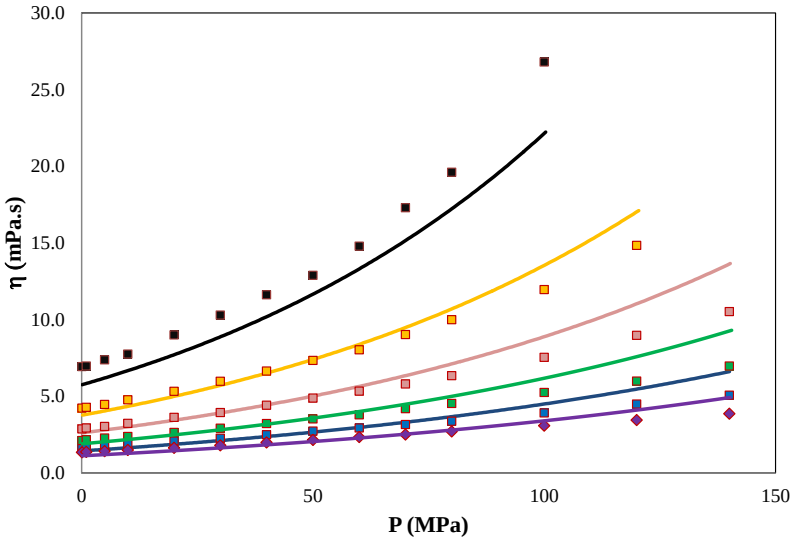

Figure 4 42. Atmospheric viscosity of biodiesel R at different temperatures. Symbols represent experimental data. ■ 293.15 K, ■ 313.15 K, ■ 333.15 K, ■ 353.15 K, ■ 373.15 K and ◆ 393.15 K. Lines are the soft-SAFT results.

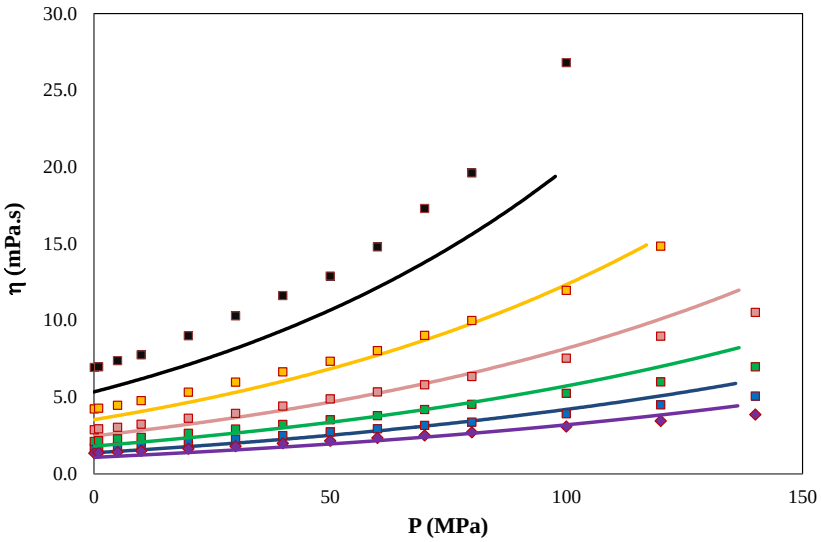

Figure 4 43. High pressure viscosity of biodiesel S at different temperatures. Symbols represent experimental data. ■ 293.15 K, ■ 313.15 K, ■ 333.15 K, ■ 353.15 K, ■ 373.15 K and ◆ 393.15 K. Lines are the soft-SAFT results.

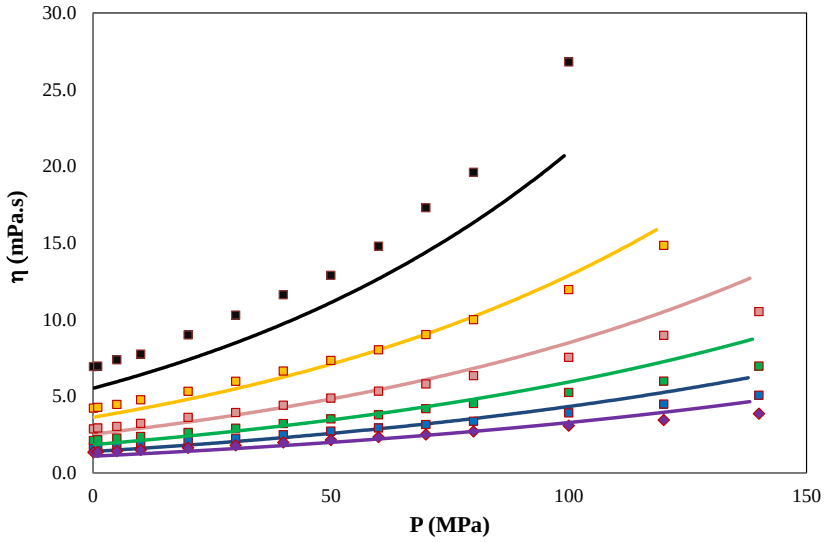

Figure 4 44. High pressure viscosity of biodiesel SR at different temperatures. Symbols represent experimental data ■ 293.15 K, ■ 313.15 K, ■ 333.15 K, ■ 353.15 K, ■ 373.15 K and ◆ 393.15 K.. Lines are the soft-SAFT results.

4.1. Conclusions

The ability of soft-SAFT to describe and predict several thermodynamic properties of fatty acid esters and biodiesels was here tested. It is here shown that this model was capable of computing several properties of fatty esters and biodiesels using only three molecular parameters: m_i (chain length), σ_{ii} (segment diameter)and ε_{ii}/k_B (dispersive energy between segments) as these compounds are non-self-associating fluids. Using these parameters and some other fitting parameters like influence parameter for surface tension and α, β and □L for viscosities, the overall average relative deviations (OARD) for FAME were 0.49 % for the high-pressure density prediction, 2.4 % for surface tensions description and 3.7 % for viscosity calculations. The OARD for FAEE were 1.8 % for high-pressure density, 2.6 % for surface tensions and 1.4 % for viscosity description. The better description of high-pressure densities for pure methyl esters also reflected in a better description of high pressure density of biodiesels.

The unique challenge linked to the prediction process was about the transferability of the parameters. First, the molecular parameters correlated from alkane's trend lines were not able to describe the densities of fatty esters. Second, even with the transferable molecular parameters for FAME, the influence parameter and viscosity parameters were

for FAEE correlated from the FAME trend lines were not able to compute the surface tension and viscosity of fatty acid ethyl esters. This situation happens due to the parameter values in terms of the convergence criteria. Howsoever, using all the parameters here studied the predictions of high-pressure density and also viscosity of biodiesel fuels were done with success.

CHAPTER 5

Production of biodiesel from resources endogenous of Timor Leste

This chapter reports the production and the study of fuel properties of biodiesels from several non-edible oils preferentially those with high level of free fatty acids endogenous of Timor Leste. Production of methylic biodiesel directly from the oils of *Jatropha curcas*, *Aleurites moluccana* and coffee waste was performed by me at our Laboratory with the yield of methyl esters obtained being superior to 93% and their fuel properties meet the international biodiesel standards.

This section aims to, first, demonstrate these oils as a model for the utilization of bioresources in Timorese arid lands for cost-effective biodiesel production and, second, to asses the ability of the models described in Chapter 3 to predict the density, viscosity and surface tensions of these biodiesels. The models used were revised GCVOL method for density, revised Yuan's model for viscosity and Mac-Sugden model with Knotts' parachors for surface tension.

5.1. Introduction

As already highlighted in the introductory chapter of this thesis, the current social and economic circumstances of Timor Leste ask for the development of biodiesel in the country. A biodiesel refinery would be an adequate solution for the problems related to lack of electricity and jobs and mainly to poverty and deprivation. Biodiesel development is highly recommended because, first, the exploration of the Timorese undersea fossil resources (oil and gas) has not been favorable for the population's life (the corresponding revenues have been plumping the Petroleum Fund but with no positive impacts on the incomes and the living conditions of the population). Second, a majority of population is subsistence farmers and so their productions will have appropriate destinations with the existence of a biodiesel refinery. Third, in a country with poor technology and know-how to manage the environmental problems linked to the use of petroleum fuels, biodiesel is more benefic than petroleum based-fuels due to several benefits already mentioned in **Chapter1**.

To avoid direct confrontation between food supply and biodiesel production, the Timorese lands offer many feedstocks for biodiesel production. Among other existing plants, the oleaginous plants like *Aleurites moluccana (Am)* and *Jatropha curcas (Jc)* are powerful sources for biodiesel production because they exist in abundance and are not used by Timorese people as food, even if the *Am* oil is edible, their seeds can provide circa 30-60 % of oil [270], their cultivations do not require arable lands and the harvesting of seeds is done almost twice per year.

For decades Timorese people used the *Am (*candle nut*)* tree for preparing traditional coffins and the seeds and oil as medicinal and fuel for light. The oil has been used for treating burns, therapeutic massages and preventing stretch marks during pregnancy. During the Indonesian occupation, the seeds were sent to Indonesia for food purposes. Nowadays, the Acelda Company is processing them for cosmetic purposes. Howsoever, crude candlenut oil generally contains about 15% free fatty acids [270]. In terms of the fatty acid profiles, the Timorese Am oil has a high percentage of oleic acid (18:1), linoleic acid (C18:2) and palmitic acid (C16:0) [271].

Regarding *Jatropha*, there is plenty of information about it in the literature. It is a non-edible plant capable of growing in very poor soils or idle lands and its seeds contain circa 30% to 40% of oil. Unlike the *Aleurites*, *Jatropha* has not been used much by Timorese people. Howsoever, the oil contains about 14% free fatty acid and in terms of fatty acid profiles it is rich of linoleic (C18:2) and stearic (C18:0) acids[272].

Timor Leste also has abundant coffee plantations especially in the occidental part of the country. It has been crucial to the country's overall economy and has served as the primary source of income for about 25 % of the country's population [65]. However, some works already addressed the use of coffee waste oil or defective beans oil for biodiesel production [273, 274]. The main constituents of coffee oil are C16:0 and C18:2 [274]. This fact will value the Timorese coffee in the international market.

The specific objective of this work was to synthesize biodiesels from the oils of *Jatropha*, *Aleurites moluccana* and coffee waste and to evaluate, on one hand, if their fuel properties were comparable with those established in the standards and, on the other hand, could be acceptably estimated using the predictive models previously proposed in **Chapter 3**.

5.2. Production of biodiesel from oils of *Aleurites moluccana, Jatropha curcas* and coffee waste

5.2.1. Experimental section

5.2.1.1. Materials

Oils of *Am* and *Jc* were obtained by solid-liquid extraction of the corresponding seeds in a Soxlet unit with 250 mL of n-hexane. The seeds were obtained directly from Timor Leste. CW oil was obtained by the same process from the wastes collected at the University of Aveiro. Absolute methanol (CH_3OH) (99.9 % quoted purity from Lab-Scan Analytical Science), sodium methoxide (CH_3ONa) (95 % quoted purity from Aldrich) sulfuric acid (H_2SO_4) (95 % quoted purity from Sigma-Aldrich) and phosphoric acid (H_3PO_4) (85 % quoted

purity from Panreac) were available at our Laboratory. The two potential feedstocks for biodiesel production are shown in **Figure 3.1**.

Figure 5 1. The two potential feedstock sources for biodiesel production: Am (left image) and Jc (right image)

5.2.1.2. Determination of free fatty acids (FFA) level

Before performing the synthesis of biodiesel, the level of free fatty acids (FFA) of the oils was first determined by acid-base titration in order to formulate an adequate reaction for biodiesel production. So 0.4 g of oil was dissolved in 50 mL of ethanol and titrated in duplicate with sodium hydroxide (NaOH). The FFA level was then calculated using the equation 5.1 or 5.2

$$\%FFA = \frac{(V \times N \times Mw_{C18:1})}{W \times 1000} \times 100\% \quad (5.1)$$

$$\%FFA = \frac{(V \times N \times Mw_{C18:2})}{W \times 1000} \times 100\% \quad (5.2)$$

Where V is the sodium hydroxide solution consumed in the titration (mL), N the normality of the potassium hydroxide solution, W the weight of oil sample (g) and Mw the molecular weight (g/mol). The FFA level was expressed as oleic acid or linoleic acid because these fatty acids are dominant in the oils studied. The FFA levels, expressed as oleic acid, were 7.0 % for *Am* oil and 4.0 % for coffee waste oil. The FFA value of the *Am* oil is not as high as that reported by Harry et al.[270], but is far above the threshold of the alkali-catalysed transesterification reaction, meaning that the synthesis of biodiesel must involve at least one step of esterification reaction.

5.2.1.3. Synthesis of biodiesel

The production of biodiesel from these oils followed the methodology of Ghadge et al.[229] as this methodology starts with at least two steps of esterification reactions in order to reduce the FFA level of the oil to a permissible value for the transesterification reaction. So the whole process occurred in three steps: two esterifications reactions and one transesterification reaction. The experiments were carried out in a 250 mL three necked round flask equipped with mechanical stirrer, a reflux condenser and a thermometer. The flask was initially filled with oil and heated to the desired reaction temperature. Then the catalyst dissolved in methanol was added to the flask to start the reaction.

The esterification reactions occurred at 60º C using of 1 % in volume fraction of H_2SO_4 and 45 % (v/v) of methanol. Each esterification step took place during circa 2 hr. After that, the reaction was stopped and the upper-phase containing the remaining methanol, glycerol and catalyst was removed from the mixture in a separating funnel. The lower phase was used as feedstock for further step of esterification reaction.

The transesterification reaction also occurred at 60º C using 1 % (w/v) of sodium methoxide as catalyst and 35 % (v/v) of methanol during 24 hr under methanol reflux. The reaction time chosen was adopted for convenience and to guarantee a complete reaction conversion. After this period, the reaction was quenched by adding 1 % (v/v) of phosphoric acid with 85 % of purity. The final mixture was then separated in two phases in a separating funnel. The upper phase (biodiesel) was then purified by washing with hot distillated water until a neutral pH was achieved and then dried in the oven during more than 2 hr.

Four different biodiesels were produced from oils of: *Am*, *Jc*, *Am* +*Jc* and *Am*+CW. The biodiesel production from pure CW oil was not performed due to the confusing visualization (black color) in the phase separation.

5.2.1.4. Determination of FAME composition

The FAME composition in biodiesel samples was analysed by gas chromatography following the same procedures described in **Chapter 3.** The yield of the FAME obtained after

the reaction was estimated using the equation 5.3 where w_i is the mass fraction and m_{FAME} is the mass of FAME *i* and m_{BD} is the mass of biodiesel.

$$Yield\ (\%) = \frac{\sum_i w_i . mFAME_i}{mBD} \times 100\% \qquad (5.3)$$

5.2.1.5. Measurement of density, viscosity and surface tension

Only three physical properties were here used to evaluate the ability of the models described in **Chapter 3** for description of density, viscosity and surface tension. Density and viscosity were measured in the temperature range of 288.15 to 368.15 K and at atmospheric pressure using an automated SVM 3000 Anton Paar rotational Stabinger Viscometer following the same procedure described in **Sections 3.1 and 3.2.** The surface tensions were measured at temperature from 293.15 to 343.15 for two pure biodiesels (*Am* and *Jc*) using a Nima Dynamic Surface Tensiometer, model DST9005, with a procedure described in **Section 3.4**.

5.2.2. Predictive models

The models chosen here to predict the density, viscosity and surface tension were the revised GCVOL method, the revised Yuan's model and the Knotts Parachors's model respectively. Only these models were chosen to use here because they provided very good predictions of the experimental data of these properties for several biodiesels as highlighted in **Chapter 3**.

5.2.3. Results and discussion

The detailed FAME composition of biodiesels is shown in **Table 5.1** and the corresponding chromatograms are presented in **Supporting information C**.

Table 5. 1. FAME composition of methylic biodiesels in mass fraction [a]

FAME	*Am*	*Jc*	*Jc*+*Am*	*Am*+CW
C10:0	0.03	0.00	0.059	0.0
C12:0	0.10	0.04	0.022	0.0
C14:0	0.10	0.11	0.065	0.058
C16:0	8.55	17.57	11.01	14.0
C16:1	0.00	0.00	0.38	0.03
C18:0	2.47	3.88	3.9	3.9
C18:1	24.04	36.67	30.6	20.4
C18:2	43.79	41.65	39.6	40.7
C18:3	20.91	0.09	14.3	19.8
C20:0	0.00	0.00	0	0.62
C20:1	0.00	0.00	0	0.38
C22:0	0.00	0.00	0	0.09
C22:1	0.00	0.00	0	0.0
C24:0	0.00	0.00	0	0.0

[a)] Biodiesel *Jc* + *Am* contains 25 mL of *Jc* oil and 35 mL of *Am* oil. Biodiesel *Am* + Cw contains 45 mL of *Am* oil and 15 mL of CW oil

The FAME profiles of the oils are very similar to those reported in the literature. The composition of *Jc* oil is similar to that studied by Berchmans et al. [275] and by Tiwari et al.[272]. The composition of *Am* oil is also not so different from other Timorese samples studied by Ako et al.[271] (these authors have studied the fatty acid profiles of different *Am* oils from Timor Leste). All the samples have C18:1 and C18:2 as major constituents. The slight differences in the composition between them may due to the rainfall, latitude or genetics and not due to the differences of processing procedures.

To verify if the biodiesels here produced had acceptable fuel properties, their density and viscosity where compare with the values established for biodiesel standards. **Table 5.2** shows the properties of these biodiesels are within the limits.

Table 5. 2. Fuel properties of biodiesels here produced

Property	Unit	*Am*	*Jc*	*Jc*+*Am*	CW+ *Am*	Biodiesel Standards **[276]**	
						ASTM D 6751-02	DIN EN 14214
ρ @ 15 ºC	kg/m^3	887[k]	883	890	889		860-900
ν @ 40 ºC	mm^2/s	3.9	4.3	3.8	4.2	1.9-6.0	3.5-5.0

[k] measured at 20 ºC

The experimental data of density, viscosity and surface tension of biodiesels are presented in **Tables 5.3 and 5.4**. The data show that the most unsaturated biodiesel presents high values of density and surface tension and low values of viscosity. This result is literally expected because the first two properties increase with the level of unsaturation while the last decreases with this parameter as already shown elsewhere by Pratas et al. [152, 153]. So, at the same temperature, it is seen that *Am* biodiesel, being less saturated, presents density and surface tension higher than those of *Jc* biodiesel while this presents viscosity higher than that. Any disagreement between the values of biodiesel surface tensions may be due to the experimental error.

Table 5. 3. Experimental density and viscosity of biodiesel

	ρ, kg.m^{-3}				η, mPa.s			
T, K	*Am*	*Jc*	*Am*+*Jc*	*Am*+CW	*Am*	*Jc*	*Am*+*Jc*	*Am*+CW
288.15		882.6	889.7	889.0		7.037	7.122	6.698
293.15	886.8	878.9	885.9	885.3	5.389	6.036	6.102	5.772
298.15	883.1	875.2	882.2	881.6	4.788	5.323	5.388	5.116
303.15	879.4	871.5	878.5	877.9	4.253	4.691	4.751	4.532
308.15	875.7	867.8	874.8	874.2	3.806	4.167	4.223	4.045
313.15	872.0	864.2	871.2	870.5	3.407	3.703	3.755	3.611
318.15	868.3	860.5	867.5	866.8	3.107	3.355	3.403	3.286
323.15	864.6	856.9	863.9	863.2	2.830	3.038	3.086	2.988
328.15	861.0	853.3	860.3	859.6	2.590	2.765	2.811	2.730
333.15	857.3	849.6	856.6	855.9	2.368	2.519	2.560	2.493
338.15	853.7	846.0	853.0	852.3	2.197	2.325	2.365	2.310
343.15	850.0	842.4	849.3	848.6	2.035	2.144	2.182	2.137
348.15	846.4	838.8	845.7	845.0	1.890	1.984	2.020	1.984
353.15	842.8	835.2	842.1	841.3	1.749	1.831	1.865	1.836
358.15	839.2	831.6	838.5	837.7	1.644	1.715	1.747	1.725
363.15	835.6	828.0	834.9	834.1	1.539	1.600	1.630	1.614
368.15	832.0	824.4	831.3		1.443	1.496	1.524	

Table 5. 4. Experimental surface tension, in mN/m for Biodiesel

	γ, mN/m[n2]					
T, K	*Am*	±σ	*Jc*	±σ	*Am*+*Jc*	±σ
298.15	31.70	0.071	31.31	0.085	31.38	0.089
303.15	30.85	0.066	30.78	0.13	31.14	0.10
313.15	29.35	0.045	29.26	0.07	30.04	0.16
318.15	29.28	0.069	28.87	0.19	29.23	0.16
323.15	28.60	0.053	28.44	0.02	28.59	0.064
328.15	28.41	0.030	28.14	0.058	28.33	0.12
333.15	27.65	0.055	27.18	0.400	28.09	0.19
343.15	27.33	0.028	26.86	0.078	27.76	0.059

[n2]) The measurement of surface tension was not possible for biodiesel Am+CW

Due to the lack of information about the properties of *Am* biodiesel in the literature, only the experimental data of *Jc* biodiesel were used for comparative purposes. So the density and the viscosity of this biodiesel were compared to those reported by Veny et al.[133], Baroutian et al.[277] and Kumar et al.[278]. Although the FAME composition is different for the *J*c samples analysed, their densities are quite similar. **Figure 5.2** shows the deviations between our data and the literature that where it is seen that the deviations are practically stable in the range of temperatures studied with a maximum of ± 0.4 %. Regarding the viscosity, the comparison was also done and our data seems to be coherent with that reported by Chhetri et al.[228] (OARD of 6 %) but significantly different from those reported by Baroutian et al. [277] (OARD obtained is circa 11 %).

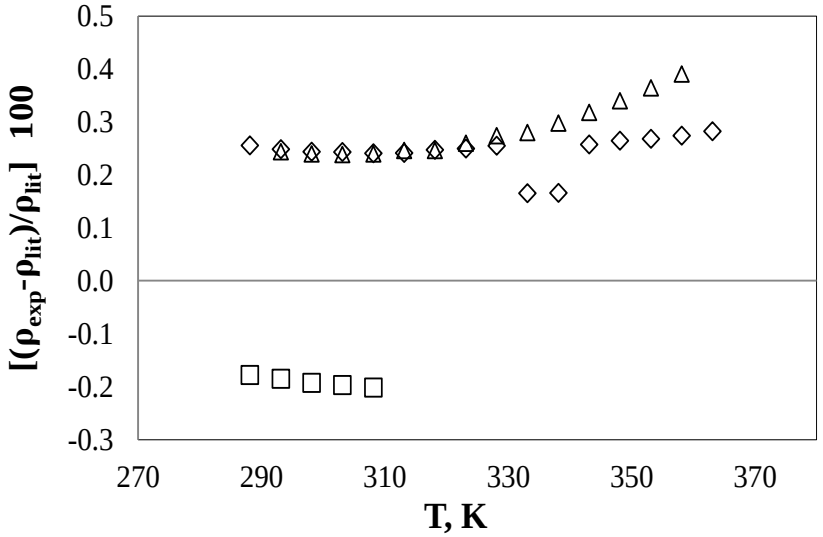

Figure 5 2. Relative deviations between experimental and literature density as function of temperature for Jc biodiesel: ◇ Veny et al.[133] □ Kumar et al.[278] and △ Baroutian et al. [277]

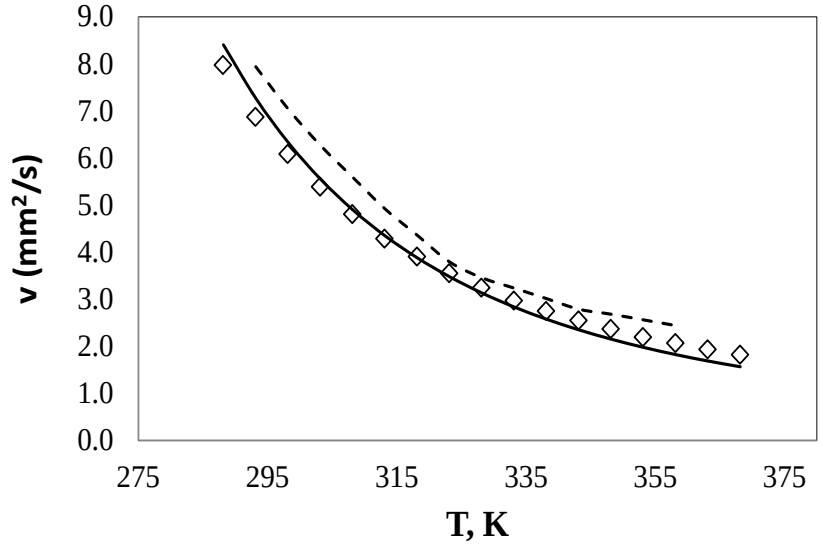

Figure 5 3. Relative deviations between experimental and literature kinematic viscosity as function of temperature for Jc biodiesel: ◇ Our data —— Chhetri et al.[133] and - - - - - Baroutian et al. [277]

To fulfill the objective of this work, the experimental data of density, viscosity and surface tension were used to asses respectively the ability of the revised GCVOL group contribution method, the revised Yuan's model and the Knotts' parachor model. The results show that the models predicted very well the experimental data of these properties, presenting only OARDs of 0.33 % for density, 3.8 % for viscosity and 1.8 % for surface tension as shown

in **Table 5.5**. The adequacy of these models can also be seen in **Figures 5.4 to 5.6** where, regardless of the magnitude of the deviations shown, these seem to be very stable in the range of temperatures studied.

Table 5. 5. ARDs of fuel properties estimated with several models

	ARD, %		
Biodiesel	Revised GCVOL	Revised Yuan	Knott's parachor
Am	0.70	1.1	2.5
Jc	0.15	2.2	1.8
Am+*Jc*	0.32	6.8	1.5
Am+CW	0.14	5.0	-
OARD, %	**0.33**	**3.8**	**1.8**

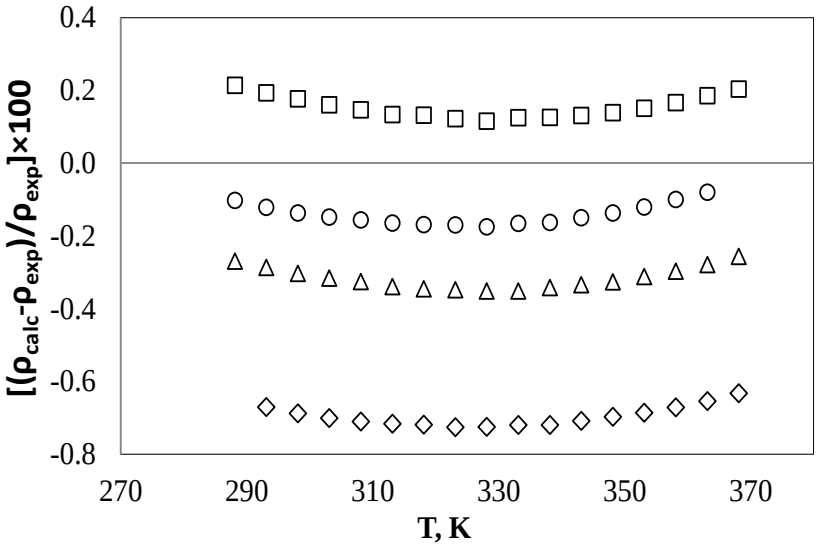

Figure 5 4. Relative deviations between experimental and predicted densities as function of temperature using Revised version of GCVOL model for 4 biodiesels: ◇ Am, □ Jc, △ Am+Jc and ○ Am+CW

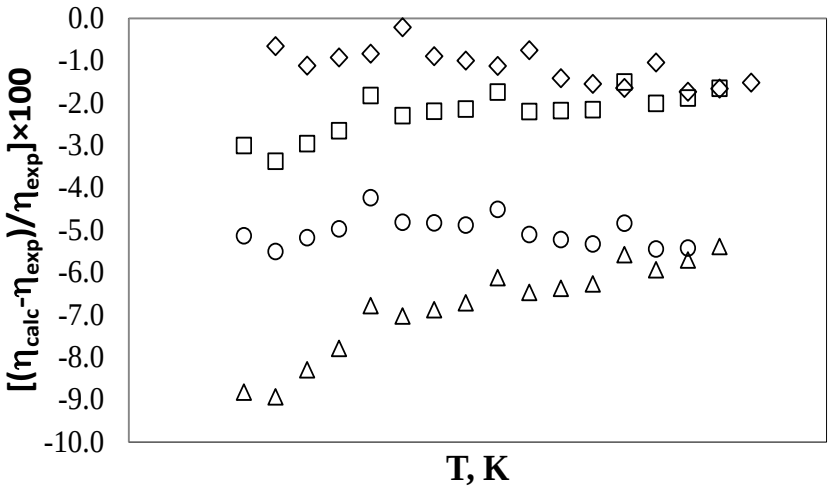

Figure 5 5. Relative deviations between experimental and predicted viscosities as function of temperature using Revised Yuan's model for 4 biodiesels: ◇ *Am*, □ *Jc*, △ *Am*+*Jc* and ○ *Am*+CW

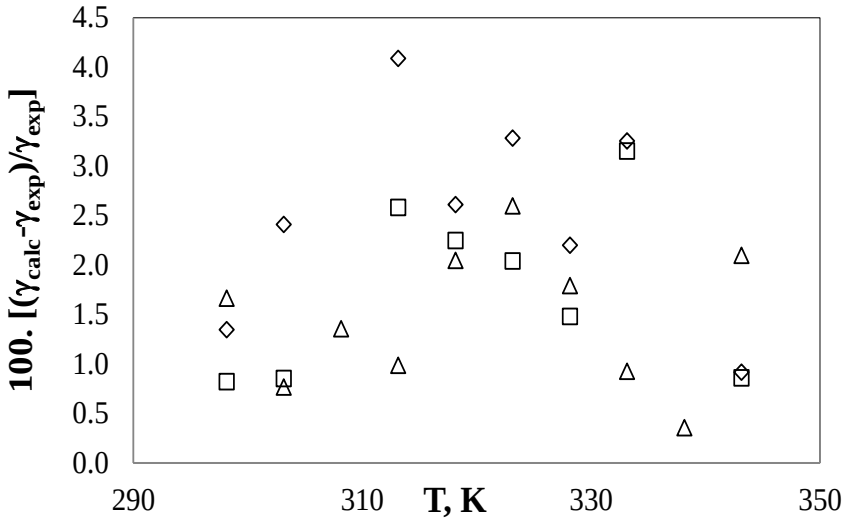

Figure 5 6. Relative deviations between experimental and predicted surface tension as function of temperature using Knotts Parachor's model for 3 biodiesels: ◇ *Am* and □ *Jc* and △ *Am*+*Jc*

To evaluate the accuracy of our data, the literature density for *Jc* biodiesel was also used to asses the revised GCVOL method. The results in **Figure 5.7** show that this model predicted better our data (with an OARD of 0.15 %) than the literature data (OARDs of 0.28 % for Baroutian's data and 0.24 % for Veny's data).

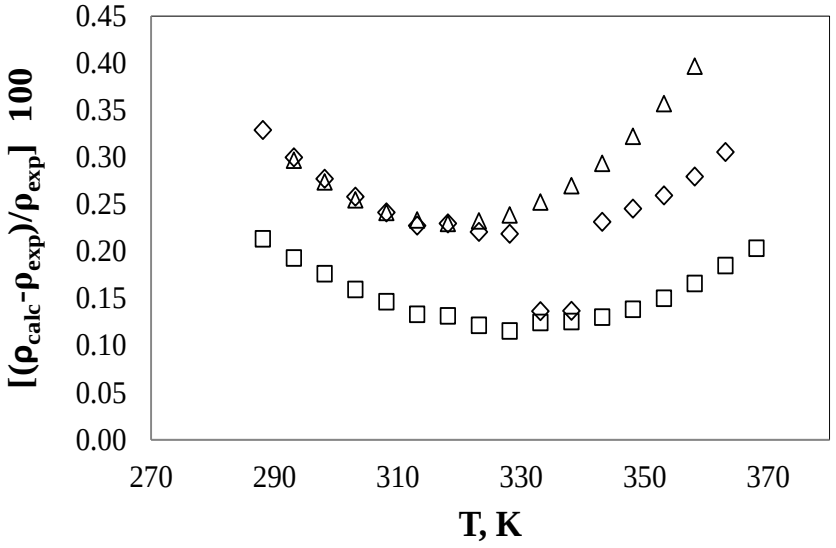

Figure 5 7. Relative deviations between experimental and literature density as function of temperature for Jc biodiesel: ◇ Veny et al.[133] □ our data and △ Baroutian et al[277]

The binary mixture of *Am* biodiesel with *Jc* biodiesel, at the same proportion, was also here studied. The objective of measuring its properties was to evaluate the ability of the Ideal mixture mixing rules and the Grundberg Nissan mixing rules for computing density and viscosity. The experimental and predicted data are presented in **Figure 5.8** where it is seen that the data matched very well each other.

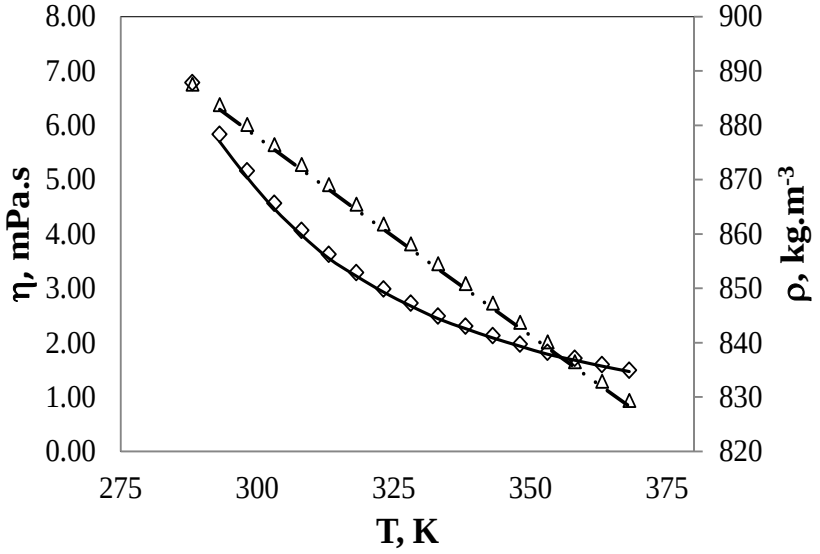

Figure 5 8. Experimental vs. predicted density and viscosity for *Am+Jc* biodiesel: ◇ experimental viscosity, △ experimental density, — · · Ideal mixture and —— Grundberg Nissan

5.3. Conclusions

Four methylic biodiesels were here produced from the oils endogenous of Timor Leste and their density, viscosity and surface tension were measured and predicted with the revised GCVOL group contribution method, the revised Yuan's model and the Knott's parachors model, respectively. The properties of biodiesels produced were within the standards and the predictions with the models were better for density and very acceptable for viscosity and surface tension. The OARDs obtained were 0.33 % for density, 3.8 % for viscosity and 2.1 % for surface tension.

General conclusions

The key objectives of this thesis were achieved, i.e., it was able to produce/process biodiesel from resources endogenous of Timor Leste and to study measurement/modeling of the thermodynamic properties of biodiesels, vegetable oils and alkyl esters.

Considering the enzymatic synthesis of biodiesel, the production of multiphase lipase fermentation of Bacillus sp. ITP-001 was done. It was possible to improve the lipase production using oxygen vectors and good inducers. At the optimum production conditions (200 rpm and 20% oxygen vector), perfluorodecaline increased the lipase activity to circa 4-fold, n-dodecane by about 11 % and silica A by about 29 %. Without oxygen vector, coffee waste oil was the best inducer. But in presence of perfluorodecaline, coconut oil was the better inducer.

In the study of the thermodynamic properties, new experimental data for various properties such as density, viscosity, surface tension, vapor pressure and speed of sound for esters and biodiesel were provided. For vegetable oils only high-pressure densities were measured. Howsoever, various predictive models capable of describing well these experimental data in a wide range of temperatures and pressures were recommended. For density, the revised GCVOL method is the most suitable for both biodiesel and vegetable oils. For the latter, the model of Zong and Halvorsen also reveal to be good. For viscosity, the model of Yuan is recommended as it describes very well the viscosity of biodiesels. For surface tension, the model of Mac-Sugden using the parachors of Knotts and the CPA model are recommended. For vapor pressure, the model of Yuan and CPA are the most suitable. For speed of sound, various models are suitable from ideal mixture mixing rules, modified Auerbach to Wada's model.

The description of density and speed of sound of biodiesels at pressures up to 200 MPa were also studied using a quadratic dependence of these properties on pressure. But at pressure up to 40 MPa, the linear approach using extensions of the models recommended above for these properties is acceptable.

The modeling of thermodynamics with Soft-SAFT EoS was also done with success. This EoS revealed to be adequate for predicting several properties of fatty esters and biodiesels at wide range of temperature and pressures.

The production of biodiesel from *Aleurites moluccana, Jatropha curcas* and coffee grounds was successfully studied. Their basic properties such as density and viscosity were shown to conform with the standards. The experimental data of these biodiesels plus those of ethylic biodiesels produced from non-edible resources were used to test the adequacy of the models recommended above and the results were acceptable. Models of density, viscosity and surface tension were able to describe the experimental data of biodiesels produced. Only the model of viscosity does not describe very well the viscosity of some ethylic biodiesels, but the magnitude of the corresponding deviations is not very different from that obtained with other models not addressed in this work.

Finally, it is concluded that the production of biodiesel in Timor Leste is contextually recommended and technically feasible. The development of this fuel in the country is adequate for solving the problems related to lack of electricity and jobs and namely to poverty and deprivation.

Final Remarks and Future Works

The main reason for having included the chapter 2 (production of lipase by *Bacillus* sp. ITP-001) in this thesis was to use lipase as catalyst in the enzymatic transesterification of biodiesel. Unfortunately, the processing of lipase did not achieve the final stage. The fermentation broths from bioreactor were only posteriorly purified but not dried nor immobilized for further use in transesterification reactions. Consequently the enzymatic synthesis of biodiesel was not performed. So the processing of lipase from the fermentation broths that includes the lyophilization and immobilization on chemical or physical supports can be an interesting future work in this field.

Regarding the modeling of thermodynamic properties, many basic fuel properties of biodiesels were studied especially at atmospheric pressure. The calculations high-pressure viscosity (with empiric correlations) and heat of combustion of biodiesels were not concluded and could not be included in this thesis. These works can also be done in near future. Moreover, given the high adequacy of soft-SAFT equation of state to describe the high-pressure densities and viscosities of biodiesel fuels, it is recommended to continue modeling with this EoS other properties of methylic or ethylic biodiesel fuels like surface tension and vapor pressure both at atmospheric pressure and mainly at high pressure.

Finally, to better analyze the fuel properties of biodiesel fuel, some other properties beyond those already studied here must also be evaluated. The analysis of oxidation stability, quality of emissions and biodegradability can be a future work of great relevance. The biodiesels from the resources endogenous of Timor Leste were here produced and their properties were analysed, but, for the practical applications, the study about them must be extended. In the future one can blend them with diesel fuels to study the outcoming properties as fuel. The production plant of biodiesel can also be simulated with some simulation tools like Aspen.

List of Publications

Pratas, M.J., S.V.D. Freitas, M.B. Oliveira, S.C. Monteiro, A.S. Lima, and J.A.P. Coutinho, Densities and Viscosities of Fatty Acid Methyl and Ethyl Esters. *J.Chem.Eng.Data*. 2010. vol. 55 (9): p. 3983-3990.

Pratas, M.J., S.V.D. Freitas, M.B. Oliveira, S.C. Monteiro, A.S. Lima, and J.A.P. Coutinho, Biodiesel Density: Experimental Measurements and Prediction Models.*Energy & Fuels.* 2011. vol. 25 (5): p. 2333-2340.

Freitas, S.V.D., M.B. Oliveira, A.J. Queimada, M.J. Pratas, A.S. Lima, and J.A.P. Coutinho, Measurement and Prediction of Biodiesel Surface Tensions.*Energy Fuels* 2011. vol. 25 (10): p. 4811-4817.

Freitas, S.V.D., M.J. Pratas, R. Ceriani, A.S. Lima, and J.A.P. Coutinho, Evaluation of Predictive Models for the Viscosity of Biodiesel.*Energy & Fuels*. 2011. vol. 25 (1): p. 352-358.

Pratas, M.J., S. Freitas, M.B. Oliveira, S.C. Monteiro, A.S. Lima, and J.A.P. Coutinho, Densities and Viscosities of Minority Fatty Acid Methyl and Ethyl Esters Present in Biodiesel.*J.Chem.Eng.Data*. 2011. vol. 56 (5): p. 2175-2180.

Freitas, S.V.D., M.B. Oliveira, Á.S. Lima, and J.A.P. Coutinho, Measurement and Prediction of Biodiesel Volatility.*Energy & Fuels*. 2012. vol. 26 (5): p. 3048-3053.

Freitas, S.V.D., M.L.L. Paredes, J.-L.Daridon, Á.S. Lima, and J.A.P. Coutinho, Measurement and Prediction of the Speed of Sound of Biodiesel Fuels. *Fuel* 2013. vol. 103: p. 1018-1022.

Freitas, S.V.D., D.L. Cunha, R.A. Reis, Á.S. Lima, J.L. Daridon, J.A.P. Coutinho, and M.L.L. Paredes, Application of the Wada's Group Contribution method to the prediction of the speed of sound of biodiesel. *Energy & Fuels*. 2013. vol. 27 (3): p. 1365-1370

Freitas, S.V.D., Â. Santos, M.-L.C.J. Moita, L.A. Follegatti-Romero, T.P.V.B. Dias, A.J.A. Meirelles, J.-L.Daridon, Á.S. Lima, and J.A.P. Coutinho, Measurement and prediction of speeds of sound of fatty acid ethyl esters and ethylic biodiesels. *Fuel*. 2013. vol. 108 (0): p. 840-845.

Freitas, S.V.D., Piñeiro, M. M., Lima, A.S. and Coutinho, J.A.P., *High Pressure density of vegetable oils*. 2013. J Chem Eng Data. Submitted.

Habrioux, M., Freitas, S.V.D, Coutinho, J. A.P. Coutinho, Daridon, J.L. High pressure density and speed of sound of two biodiesel fuels.Energy & Fuels. 2013. Submitted.

Freitas S.V.D., Oliveira, M. B., Lima, A.S. Llovell, F., Vega, L.F. and Coutinho, J.A.P., modeling thermodynamic properties of fatty esters with the Soft-SAFT EoS. 2012. In preparation

Bibliography

1. Öner, C. and Ş. Altun, *Biodiesel production from inedible animal tallow and an experimental investigation of its use as alternative fuel in a direct injection diesel engine.* Applied Energy. 2009. vol. 86 (10): p. 2114-2120.
2. Crabbe, E., C. Nolasco-Hipolito, G. Kobayashi, K. Sonomoto, and A. Ishizaki, *Biodiesel production from crude palm oil and evaluation of butanol extraction and fuel properties.* Process Biochem. 2001. vol. 37: p. 65 - 71.
3. International Energy Agency. *CO2 Emissions From Fuel Combustion Highlights* 2012.
4. ExxonMobil. *The Outlook of Energy:A view to 2040*, 2013.
5. Organization of the Petroleum Exporting Countries. *World Oil Outlook 2012*, 2012.
6. Escobar, J.C., E.S. Lora, O.J. Venturini, E.E. Yáñez, E.F. Castillo, and O. Almazan, *Biofuels: Environment, technology and food security.* Renewable and Sustainable Energy Reviews. vol. 13 (6-7): p. 1275-1287.
7. IEO 2010. *International Energy Outlook*, 2010.
8. European Biofuels Technology Platform.*R&D&D Funding*.[Online]. [Accessed. 30 March 2013]. Available:http://www.biofuelstp.eu/funding.html#ner300res
9. U.S. Department of Energy.*Obama Administration to Fund Next Generation Biofuels Research*.[Online]. [Accessed. 28 March 2012]. Available:http://apps1.eere.energy.gov/news/daily.cfm/hp_news_id=345
10. Christou, M., E. Alexopoulou, C. Panoutsou, and A. Monti, *Overview of the markets for energy crops in EU27.* Biofuels, Bioproducts and Biorefining. 2010. vol. 4 (6): p. 605-619.
11. Hart Energy's Global Biofuels Center. *Global Biofuels Outlook 2010-2020*, 2012.
12. IPIECA. *Biofuels, sustainability and the petroleum industry*, 2009.
13. Filho, A., H. Pacini, G.O. Silva, and F.G. Lima, *When is pure ethanol attractive as a fuel option? Quantifying the gasoline vs ethanol dilemma faced by consumers in Brazil.* . Journal of Academy of Business and Economics. 2005. vol. 11 (3).
14. U.S.Energy Information Administration. *Annual Energy Outlook 2012 with Projections to 2035*, 2012.
15. Moser, B., *Biodiesel production, properties, and feedstocks.* In Vitro Cellular & Developmental Biology - Plant. 2009. vol. 45 (3): p. 229-266.
16. Vasudevan, P. and M. Briggs, *Biodiesel production—current state of the art and challenges.* Journal of Industrial Microbiology & Biotechnology. 2008. vol. 35 (5): p. 421-430.
17. Prio Energy.*Produção de Biodiesel*.[Online].Prio. [Accessed. 22 June 2013]. Available:http://www.prioenergy.com/produtos-e-servicos/producao-de-biodiesel/
18. Hoekman, S.K., A. Broch, C. Robbins, E. Ceniceros, and M. Natarajan, *Review of biodiesel composition, properties, and specifications.* Renewable and Sustainable Energy Reviews. 2012. vol. 16 (1): p. 143-169.
19. Knothe, G., J. Van Gerpen, and J. Krahl, eds. *The Biodiesel Handbook*. 2005: United States of America.
20. Sharma, Y.C. and B. Singh, *Development of biodiesel: Current scenario.* Renewable and Sustainable Energy Reviews. 2009. vol. 13 (6–7): p. 1646-1651.

21. Knothe, G., *Biodiesel: Current Trends and Properties.* Topics in Catalysis. 2010. vol. 53 (11): p. 714-720.
22. Fukuda, H., A. Kondo, and H. Noda, *Biodiesel fuel production by transesterification of oils.* J Biosci Bioeng. 2001. vol. 92: p. 405 - 416.
23. Kerschbaum, S. and G. Rinke, *Measurement of the temperature dependent viscosity of biodiesel fuels.* Fuel. 2004. vol. 83 (3): p. 287-291.
24. Marchetti, J.M., V.U. Miguel, and A.F. Errazu, *Possible methods for biodiesel production.* Renewable and Sustainable Energy Reviews. 2007. vol. 11 (6): p. 1300-1311.
25. Parawira, W., *Biotechnological production of biodiesel fuel using biocatalysed transesterification: A review.* Critical Reviews in Biotechnology. 2009. vol. 29 (2): p. 82 - 93.
26. Singh, S.P. and D. Singh, *Biodiesel production through the use of different sources and characterization of oils and their esters as the substitute of diesel: A review.* Renewable and Sustainable Energy Reviews. 2010. vol. 14 (1): p. 200-216.
27. Demirbas, A., *Progress and recent trends in biodiesel fuels.* Energy Conversion and Management. 2009. vol. 50 (1): p. 14-34.
28. Oliveira, M.B., A.R.R. Teles, A.J. Queimada, and J.A.P. Coutinho, *Phase equilibria of glycerol containing systems and their description with the Cubic-Plus-Association (CPA) Equation of State.* Fluid Phase Equilibr. 2009. vol. 280 (1–2): p. 22-29.
29. Anand, K., A. Ranjan, and P.S. Mehta, *Estimating the Viscosity of Vegetable Oil and Biodiesel Fuels.* Energy & Fuels. 2009. vol. 24 (1): p. 664-672.
30. Knothe, G., *Biodiesel Derived from a Model Oil Enriched in Palmitoleic Acid, Macadamia Nut Oil.* Energy & Fuels. 2010. vol. 24 (3): p. 2098-2103.
31. Demirbas, A., *New Biorenewable Fuels from Vegetable Oils.* Energy Sources, Part A: Recovery, Utilization, and Environmental Effects. 2010. vol. 32 (7): p. 628-636.
32. Zhang, Y., M.A. Dubé, D.D. McLean, and M. Kates, *Biodiesel production from waste cooking oil: 1. Process design and technological assessment.* Bioresource Technology. 2003. vol. 89 (1): p. 1-16.
33. Phan, A.N. and T.M. Phan, *Biodiesel production from waste cooking oils.* Fuel. 2008. vol. 87 (17–18): p. 3490-3496.
34. Anand, K., R.P. Sharma, and P.S. Mehta, *A comprehensive approach for estimating thermo-physical properties of biodiesel fuels.* Applied Thermal Engineering. 2011. vol. 31 (2-3): p. 235-242.
35. Alptekin, E. and M. Canakci, *Characterization of the key fuel properties of methyl ester-diesel fuel blends.* Fuel. 2009. vol. 88 (1): p. 75-80.
36. Murugesan, A., C. Umarani, R. Subramanian, and N. Nedunchezhian, *Bio-diesel as an alternative fuel for diesel engines—A review.* Renewable and Sustainable Energy Reviews. 2009. vol. 13 (3): p. 653-662.
37. Joshi, R.M. and M.J. Pegg, *Flow properties of biodiesel fuel blends at low temperatures.* Fuel. 2007. vol. 86 (1–2): p. 143-151.
38. Benjumea, P., J. Agudelo, and A. Agudelo, *Basic properties of palm oil biodiesel-diesel blends.* Fuel. 2008. vol. 87 (10-11): p. 2069-2075.
39. Saka, S. and D. Kusdiana, *Biodiesel fuel from rapeseed oil as prepared in supercritical methanol.* Fuel. 2001. vol. 80 (2): p. 225-231.
40. Leung, D.Y.C., X. Wu, and M.K.H. Leung, *A review on biodiesel production using catalyzed transesterification.* Applied Energy. 2010. vol. 87 (4): p. 1083-1095.

41. Gerpen, J.V., *Biodiesel processing and production.* Fuel Processing Technology. 2005. vol. 86 (10): p. 1097-1107.
42. Balat, M., *Current Alternative Engine Fuels.* Energy Sources. 2005. vol. 27 (6): p. 569-577.
43. Canakci, M. and H. Sanli, *Biodiesel production from various feedstocks and their effects on the fuel properties.* J. Ind. Microbiol.Biotechnol. 2008. vol. 35 (5): p. 431-441.
44. Lotero, E., Y. Liu, D.E. Lopez, K. Suwannakarn, D.A. Bruce, and J.G. Goodwin, *Synthesis of Biodiesel via Acid Catalysis.* Industrial & Engineering Chemistry Research. 2005. vol. 44 (14): p. 5353-5363.
45. Sharma, Y.C. and B. Singh, *Development of biodiesel from karanja, a tree found in rural India.* Fuel. 2008. vol. 87 (8–9): p. 1740-1742.
46. Monyem, A., J.H. Van Gerpen, and M. Canakci, *The effect of timing and oxidation on emissions from biodiesel-fueled engines.* American Society of Agricultural and Biological Engineers. 2001. vol. 44 (1): p. 35-42.
47. Agarwal, D., S. Sinha, and A.K. Agarwal, *Experimental investigation of control of NOx emissions in biodiesel-fueled compression ignition engine.* Renewable Energy. 2006. vol. 31 (14): p. 2356-2369.
48. Pehan, S., M.S. Jerman, M. Kegl, and B. Kegl, *Biodiesel influence on tribology characteristics of a diesel engine.* Fuel. 2009. vol. 88 (6): p. 970-979.
49. Chhetri, A.B. and M.R. Islam, *Towards Producing a Truly Green Biodiesel.* Energy Sources, Part A: Recovery, Utilization, and Environmental Effects. 2008. vol. 30 (8): p. 754 - 764.
50. Röttig, A., L. Wenning, D. Bröker, and A. Steinbüchel, *Fatty acid alkyl esters: perspectives for production of alternative biofuels.* Applied Microbiology and Biotechnology. 2010. vol. 85 (6): p. 1713-1733.
51. Balat, M., *Potential alternatives to edible oils for biodiesel production - A review of current work.* Energy Conversion and Management. 2011. vol. 52 (2): p. 1479-1492.
52. Demirbas, A. and H. Kara, *New Options for Conversion of Vegetable Oils to Alternative Fuels.* Energy Sources, Part A: Recovery, Utilization, and Environmental Effects. 2006. vol. 28 (7): p. 619 - 626.
53. Saraf, S. and B. Thomas, *Influence of Feedstock and Process Chemistry on Biodiesel Quality.* Process Safety and Environmental Protection. 2007. vol. 85 (5): p. 360-364.
54. La'o hamutuk.*Information about the Treaty between Australia and Timor-Leste on Certain Maritime Arrangements in the Timor Sea (CMATS)*.[Online].La'o hamutuk, . [Accessed. 24 March 2013]. Available:http://www.laohamutuk.org/Oil/Boundary/CMATSindex.htm
55. La'o hamutuk.*Timor-Leste Petroleum Fund*.[Online].La'o Hamutuk. [Accessed. 25 March 2013]. Available:http://www.laohamutuk.org/Oil/PetFund/05PFIndex.htm
56. RDTL, *Timor-Leste Strategic development Plan 2011 - 2030*. 2010.
57. The World Bank. *Timor-Leste Key Issues in Rural Energy Policy*, 2010.
58. UNDP. *Human Development Report 2013: The Rise of the South: Human Progress in a Diverse World*, 2013.
59. Pacific Department Asian Development Bank. *Power Sector Development Plan For Timor-Leste*, 2004.

60. Sunil, N., K.S. Varaprasad, N. Sivaraj, T. Suresh Kumar, B. Abraham, and R.B.N. Prasad, *Assessing Jatropha curcas L. germplasm in-situ--A case study.* Biomass and Bioenergy. 2008. vol. 32 (3): p. 198-202.
61. Steinmetz, E.F., *Aleurites Moluccana.* Pharmaceutical Biology. 1965. vol. 5 (4): p. 784 - 787.
62. Koji, T., *Kemiri (Aleurites moluccana) and forest resource management in Eastern Indonesia: an eco-historical perspective.* Asian and African Area Studies. 2002. vol. 2: p. 5–23.
63. Sulistyo, H., S.S. Rahayu, G. Winoto, and I.M. Suardjaja, *Biodiesel Production from High Iodine Number Candlenut Oil.* Proceedings of World Academy of Science: Engineering & Technology. 2008. vol. 36: p. 1316-1319.
64. La'o hamutuk.*Agro-Fuels projects in Timor-Leste.*[Online]. [Accessed. 31 March 2013]. Available:http://www.laohamutuk.org/Agri/08Agrofuels.htm
65. Oxfam.*Overview of the Coffee Sector in Timor Leste*.[Online].Oxfam. [Accessed. 1 April 2013]. Available:http://gov.east-timor.org/MAFF/ta200/TA218.pdf
66. Kondamudi, N., S.K. Mohapatra, and M. Misra, *Spent Coffee Grounds as a Versatile Source of Green Energy.* Journal of Agricultural and Food Chemistry. 2008. vol. 56 (24): p. 11757-11760.
67. Houde, A., A. Kademi, and D. Leblanc, *Lipases and their industrial applications.* Applied Biochemistry and Biotechnology. 2004. vol. 118 (1): p. 155-170.
68. Pandey, A., S. Benjamin, C.R. Soccol, P. Nigam, N. Krieger, and V.T. Soccol, *The realm of microbial lipases in biotechnology.* Biotechnol. Appl. Biochem. 1999. vol. 29 (2): p. 119-131.
69. Rajendran, A. and V. Thangavelu, *Optimization of medium composition for lipase production by Candida rugosa NCIM 3462 using response surface methodology.* Canadian Journal Of Microbiology. 2007. vol. 53 (5): p. 643-655.
70. Shu, Z.-Y., H. Jiang, R.-F. Lin, Y.-M. Jiang, L. Lin, and J.-Z. Huang, *Technical methods to improve yield, activity and stability in the development of microbial lipases.* J. Mol. Catal. B: Enzym. 2010. vol. 62 (1): p. 1-8.
71. Treichel, H., D. de Oliveira, M. Mazutti, M. Di Luccio, and J. Oliveira, *A Review on Microbial Lipases Production.* Food and Bioprocess Technology. vol.
72. Gupta, R., N. Gupta, and P. Rathi, *Bacterial lipases: an overview of production, purification and biochemical properties.* Applied Microbiology and Biotechnology. 2004. vol. 64 (6): p. 763-781.
73. Dalmau, E., J.L. Montesinos, M. Lotti, and C. Casas, *Effect of different carbon sources on lipase production by Candida rugosa.* Enzyme Microb. Technol. . 2000. vol. 26 (9–10): p. 657-663.
74. Lakshmi, B.S., P. Kangueane, B. Abraham, and G. Pennathur, *Effect of vegetable oils in the secretion of lipase from Candida rugosa (DSM 2031).* Lett In App Microbiol. 1999. vol. 29 (1): p. 66-70.
75. Obradors, N., J.L. Montesinos, F. Valero, F.J. Lafuente, and C. Solà, *Effects of different fatty acids in lipase production by Candida rugosa.* Biotechnol. Lett. . 1993. vol. 15 (4): p. 357-360.
76. Carvalho, N., R. de Souza, H. de Castro, G. Zanin, Á. Lima, and C. Soares, *Sequential Production of Amylolytic and Lipolytic Enzymes by Bacterium Strain Isolated from Petroleum Contaminated Soil.* Applied Biochemistry and Biotechnology. 2008. vol. 150 (1): p. 25-32.

77. Feitosa, I.C., J.M.d.P. Barbosa, S.C. Orellana, A.S. Lima, and C.M.F. Soares, *Produção de lipase por meio de microrganismos isolados de solos com histórico de contato com petróleo.* Acta Scientiarum. Technology. 2010. vol. 32 (1): p. 27-31.
78. Nielsen, D.R., A.J. Daugulis, and P.J. Mclellan, *A novel method of simulating oxygen mass transfer in two-phase partitioning bioreactors.* Biotechnology and Bioengineering. 2003. vol. 83 (6): p. 735-742.
79. Elibol, M. and F. Mavituna, *A remedy to oxygen limitation problem in antibiotic production: addition of perfluorocarbon.* Biochemical Engineering Journal. 1999. vol. 3 (1): p. 1-7.
80. Rols, J.L. and G. Goma, *Enhanced oxygen transfer rates in fermentation using soybean oil-in-water dispersions.* Biotechnology Letters. 1991. vol. 13 (1): p. 7-12.
81. Martin, S., P. Soucaille, and J.S. Condoret, *Bubble free gaseous transfer in bioreactors using perfluorocarbons.* Bioprocess and Biosystems Engineering. 1995. vol. 13 (6): p. 293-300.
82. Amaral, P., A. de Almeida, T. Peixoto, M. Rocha-Leão, J. Coutinho, and M. Coelho, *Beneficial effects of enhanced aeration using perfluorodecalin in Yarrowia lipolytica cultures for lipase production.* World Journal of Microbiology and Biotechnology. 2007. vol. 23 (3): p. 339-344.
83. Leonhardt, A., E. Szwajcer, and K. Mosbach, *The potential use of silicon compounds as oxygen carriers for free and immobilized cells containing l-amino acid oxidase.* Applied Microbiology and Biotechnology. 1985. vol. 21 (3): p. 162-166.
84. Olle, B., S. Bucak, T.C. Holmes, L. Bromberg, T.A. Hatton, and D.I.C. Wang, *Enhancement of Oxygen Mass Transfer Using Functionalized Magnetic Nanoparticles.* Industrial & Engineering Chemistry Research. 2006. vol. 45 (12): p. 4355-4363.
85. Wei, D.z. and H. Liu, *Promotion of L-asparaginase production by using n-dodecane.* Biotechnol Techn. 1998. vol. 12 (2): p. 129-131.
86. Jia, S., M. Wang, P. Kahar, Y. Park, and M. Okabe, *Enhancement of yeast fermentation by addition of oxygen vectors in air-lift bioreactor.* Journal of Fermentation and Bioengineering. 1997. vol. 84 (2): p. 176-178.
87. Ju, L.K., J.F. Lee, and W.B. Armiger, *Enhancing oxygen transfer in bioreactors by perfluorocarbon emulsions.* Biotechnology Progress. 1991. vol. 7 (4): p. 323-329.
88. Elibol, M., *Use of perfluorocarbon in the culture of Saccharomyces cerevisiae.* Biotechnology Techniques. 1996. vol. 10 (12): p. 987-990.
89. Elibol, M. and F. Mavituna, *Use of perfluorocarbon for oxygen supply to immobilised Streptomyces coelicolor A3(2).* Proc Biochem. 1996. vol. 31 (5): p. 507-512.
90. Gotoh, T., G. Mochizuki, and K.-i. Kikuchi, *Perfluorocarbon-mediated aeration applied to recombinant protein production by virus-infected insect cells.* Biochemical Engineering Journal. 2001. vol. 7 (1): p. 69-78.
91. Amaral, P.F.F., M.H.M. Rocha-Leão, I.M. Marrucho, J.A.P. Coutinho, and M.A.Z. Coelho, *Improving lipase production using a perfluorocarbon as oxygen carrier.* J. Chem. Technol. Biotechnol. . 2006. vol. 81 (8): p. 1368-1374.
92. Dias, A.M.A., M. Freire, J.A.P. Coutinho, and I.M. Marrucho, *Solubility of oxygen in liquid perfluorocarbons.* Fluid Phase Equilib. 2004. vol. 222–223 (0): p. 325-330.

93. Dias, A.M.A., C.M.B. Gonçalves, J.L. Legido, J.A.P. Coutinho, and I.M. Marrucho, *Solubility of oxygen in substituted perfluorocarbons.* Fluid Phase Equilib. 2005. vol. 238 (1): p. 7-12.
94. Freire, M.G., P.J. Carvalho, L.M.N.B.F. Santos, L.R. Gomes, I.M. Marrucho, and J.A.P. Coutinho, *Solubility of water in fluorocarbons: Experimental and COSMO-RS prediction results.* J Chem Thermodynamics. 2010. vol. 42 (2): p. 213-219.
95. Amaral, P.F., M.G. Freire, M.H. Rocha-Leao, I.M. Marrucho, J.A. Coutinho, and M.A. Coelho, *Optimization of oxygen mass transfer in a multiphase bioreactor with perfluorodecalin as a second liquid phase.* Biotechnol Bioeng. 2008. vol. 99 (3): p. 588-98.
96. Silva, T., A. Mendes, R. Mendes, V. Calado, S. Alves, J. Vasconcelos, and A. Reis, *Effect of n-dodecane on Crypthecodinium cohnii fermentations and DHA production.* Journal of Industrial Microbiology and Biotechnology. 2006. vol. 33 (6): p. 408-416.
97. Karimi, A., F. Golbabaei, M. Neghab, M.R. Mehrnia, K. Mohammad, M.R. Pourmand, and A. Nikpey, *Investigation of Oxygen Transfer in a Two-phase Partition Stirred Tank Bioreactor in the Presence of SiliconeOil.* Chem. Biochem. Eng. Q. 2011. vol. 25 (2): p. 209-219.
98. Kaya, A. and A. Schumpe, *Surfactant adsorption rather than "shuttle effect"?* Chem Eng Sci. 2005. vol. 60 (22): p. 6504-6510.
99. Sidhpuria, K.B., A.L. Daniel-da-Silva, T. Trindade, and J.A.P. Coutinho, *Supported ionic liquid silica nanoparticles (SILnPs) as an efficient and recyclable heterogeneous catalyst for the dehydration of fructose to 5-hydroxymethylfurfural.* Green Chem. 2011. vol. 13 (2): p. 340-349.
100. Rooney, D. and L.R. Weatherley, *The effect of reaction conditions upon lipase catalysed hydrolysis of high oleate sunflower oil in a stirred liquid–liquid reactor.* Process Biochem. 2001. vol. 36: p. 947-953.
101. Bonjoch, N.P. and P.R. Tamayo, *Protein Content Quantification by Bradford: Method Handbook of Plant Ecophysiology Techniques*, M.J. Reigosa Roger, Editor. 2003, Springer Netherlands. p. 283-295.
102. Soccol, C.R., B. Marin, M. Rainbault, and J.M. Lebeault, *Breeding and growth of Rhizopus in raw cassava by solid state fermentation.* Appl Microbiol Biotechnol. 1994. vol. 41 (330-336).
103. Lima, Á.S. and R.M. Alegre, *Evaluation of emulsifier stability of biosurfactant produced by Saccharomyces lipolytica CCT-0913.* Brazilian Archives of Biology and Technology. 2009. vol. 52: p. 285-290.
104. Makhzoum, A., J.S. Knapp, and R.K. Owusu, *Factors affecting growth and extracelluar lipase production by Pseudomonas fluorescens 2D.* Food Microbiol. 1995. vol. 12 (0): p. 277-290.
105. Luedeking, R. and E.L. Piret, *A kinetic study of the lactic acid fermentation. Batch process at controlled pH.* J. Biochem. Microbiol. Technol.Eng. 1959. vol. 1 (4): p. 393-412.
106. Puthli, M.S., V.K. Rathod, and A.B. Pandit, *Optimization of lipase production in a triple impeller bioreactor.* Biochemical Engineering Journal. 2006. vol. 27 (3): p. 287-294.
107. Deive, F.J., M. Angeles Sanromán, and M.A. Longo, *Evaluation of a novel Bacillus strain from a north-western Spain hot spring as a source of extracellular thermostable lipase.* J Chem Technol Biotechnol. 2009. vol. 84 (10): p. 1509-1515.

108. CEN, *European Committee for Standardization. AutomotiVe fuels -Fatty acid methyl esters (FAME) for diesel engines -Requirements and test methods; E.S.E. EN 14214, Brussels, Belgium*. 2003.
109. ASTM, *American Society for Testing and Materials Standard D6751. Standard Specification for Biodiesel Fuel Blend Stock (B100) for Middle Distillate Fuels; ASTM: West Conshohocken, PA*. 2009.
110. Farr, D., *High pressure technology in the food industry*. Trends in Food Sci Technol. 1990. vol. 1 (0): p. 14-16.
111. Hendrickx, M., L. Ludikhuyze, I. Van den Broeck, and C. Weemaes, *Effects of high pressure on enzymes related to food quality.* Trends in Food Sci Technol. 1998. vol. 9 (5): p. 197-203.
112. Messens, W., J. Van Camp, and A. Huyghebaert, *The use of high pressure to modify the functionality of food proteins.* Trends in Food Sci Technol. 1997. vol. 8 (4): p. 107-112.
113. Correia, I., A. Nunes, J.A. Saraiva, A.S. Barros, and I. Delgadillo, *High pressure treatments largely avoid/revert decrease of cooked sorghum protein digestibility when applied before/after cooking.* LWT-Food Sci Technol. 2011. vol. 44 (4): p. 1245-1249.
114. Castro, S.M., J.A. Saraiva, J.A. Lopes-da-Silva, I. Delgadillo, A.V. Loey, C. Smout, and M. Hendrickx, *Effect of thermal blanching and of high pressure treatments on sweet green and red bell pepper fruits (Capsicum annuum L.).* Food Chem. 2008. vol. 107 (4): p. 1436-1449.
115. Rollbusch, C., *Effects of hydraulic nozzle flow rate and high injection pressure on mixture formation, combustion and emissions on a single-cylinder DI light-duty diesel engine.* Int J Engine Res. 2012. vol. 13 (4): p. 323-339.
116. Rajkumar, S., P.S. Mehta, and S. Bakshi, *Phenomenological modeling of combustion and emissions for multiple-injection common rail direct injection engines.* Int J Engine Res. 2012. vol. 13 (4): p. 307-322.
117. Karra, P.K., M.K. Veltman, and S.-C. Kong, *Characteristics of Engine Emissions Using Biodiesel Blends in Low-Temperature Combustion Regimes.* Energ Fuel. 2008. vol. 22 (6): p. 3763-3770.
118. Eller, F.J., S.C. Cermak, and S.L. Taylor, *Supercritical carbon dioxide extraction of cuphea seed oil.* Industrial Crops and Products. 2011. vol. 33 (2): p. 554-557.
119. Sovová, H., A.A. Galushko, R.P. Stateva, K. Rochová, M. Sajfrtová, and M. Bártlová, *Supercritical fluid extraction of minor components of vegetable oils: β-Sitosterol.* J Food Eng. 2010. vol. 101 (2): p. 201-209.
120. Eller, F., J. Moser, J. Kenar, and S. Taylor, *Extraction and Analysis of Tomato Seed Oil.* J Am Oil Chem Soc. 2010. vol. 87 (7): p. 755-762.
121. Laesecke, A., T.J. Fortin, and S. J.D., *Density, Speed of Sound, and Viscosity Measurements of Reference Materials for Biofuels.* Energy Fuels. 2012. vol. 26: p. 1844-1861.
122. Cherng-Yuan, L. and L. Yi-Wei, *Fuel Characteristics of Biodiesel Produced from a High-Acid Oil from Soybean Soapstock by Supercritical-Methanol Transesterification.* Energies (19961073). 2012. vol. 5 (7): p. 2370-2380.
123. Eggers, R., U. Sievers, and W. Stein, *High pressure extraction of oil seed.* J Am Oil Chem Soc. 1985. vol. 62 (8): p. 1222-1230.
124. Bulley, N., M. Fattori, A. Meisen, and L. Moyls, *Supercritical fluid extraction of vegetable oil seeds.* J Am Oil Chem Soc. 1984. vol. 61 (8): p. 1362-1365.

125. Birtigh, A., M. Johannsen, G. Brunner, and N. Nair, *Supercritical-fluid extraction of oil-palm components.* J Supercrit Fluid. 1995. vol. 8 (1): p. 46-50.
126. Catchpole, O.J., J.-C. von Kamp, and J.B. Grey, *Extraction of Squalene from Shark Liver Oil in a Packed Column Using Supercritical Carbon Dioxide.* Ind Eng Chem Res. 1997. vol. 36 (10): p. 4318-4324.
127. Pinnarat, T. and P.E. Savage, *Assessment of Noncatalytic Biodiesel Synthesis Using Supercritical Reaction Conditions.* Ind Eng Chem Res. 2008. vol. 47 (18): p. 6801-6808.
128. Demirbas, A., *Biodiesel from waste cooking oil via base-catalytic and supercritical methanol transesterification.* Energ Convers Manage. 2009. vol. 50 (4): p. 923-927.
129. Pratas, M.J., S.V.D. Freitas, M.B. Oliveira, S.C. Monteiro, A.S. Lima, and J.A.P. Coutinho, *Biodiesel Density: Experimental Measurements and Prediction Models.* Energ Fuel. 2011. vol. 25 (5): p. 2333-2340.
130. Dzida, M. and P. Prusakiewicz, *The effect of temperature and pressure on the physicochemical properties of petroleum diesel oil and biodiesel fuel.* Fuel. 2008. vol. 87 (10–11): p. 1941-1948.
131. Heywood, J.R., *Internal Combustion Engine Fundamentals, McGraw-Hill, New York.* 1988. vol.
132. Baroutian, S., M.K. Aroua, A.A.A. Raman, and N.M.N. Sulaiman, *Density of Palm Oil-Based Methyl Ester.* Journal of Chemical & Engineering Data. 2008. vol. 53 (3): p. 877-880.
133. Veny, H., S. Baroutian, M. Aroua, M. Hasan, A. Raman, and N. Sulaiman, *Density of Jatropha curcas Seed Oil and its Methyl Esters: Measurement and Estimations.* International Journal of Thermophysics. 2009. vol. 30 (2): p. 529-541.
134. Mohan, D., C.U. Pittman, and P.H. Steele, *Pyrolysis of Wood/Biomass for Bio-oil: A Critical Review.* Energy & Fuels. 2006. vol. 20 (3): p. 848-889.
135. Blangino, E., A.F. RiverÃ³s, and S.D. Romano, *Numerical expressions for viscosity, surface tension and density of biodiesel: analysis and experimental validation.* Physics and Chemistry of Liquids: An International Journal. 2008. vol. 46 (5): p. 527 - 547.
136. Freitas, S.V.D., M.B. Oliveira, A.J. Queimada, M.J. Pratas, A.S. Lima, and J.A.P. Coutinho, *Measurement and Prediction of Biodiesel Surface Tensions.* Energ. Fuel 2011. vol. 25 (10): p. 4811-4817.
137. Coupland, J. and D. McClements, *Physical properties of liquid edible oils.* Journal of the American Oil Chemists' Society. 1997. vol. 74 (12): p. 1559-1564.
138. Ndiaye, E.H.I., D. Nasri, and J.L. Daridon, *Speed of Sound, Density, and Derivative Properties of Fatty Acid Methyl and Ethyl Esters under High Pressure: Methyl Caprate and Ethyl Caprate.* Journal of Chemical & Engineering Data. 2012. vol. 57 (10): p. 2667-2676.
139. Piñeiro, M.M., D. Bessières, J.M. Gacio, H. Saint-Guirons, and J.L. Legido, *Determination of high-pressure liquid density for n-perfluorohexane and n-perfluorononane.* Fluid Phase Equilibr. 2004. vol. 220 (1): p. 125-134.
140. Piñeiro, M.M., D. Bessières, J.L. Legido, and H. Saint-Guirons, *PρT Measurements of Nonafluorobutyl Methyl Ether and Nonafluorobutyl Ethyl Ether Between 283.15 and 323.15 K at Pressures Up to 40 MPa.* Int J Thermophys. 2003. vol. 24 (5): p. 1265-1276.
141. Pratas, M.J., M.B. Oliveira, M.J. Pastoriza-Gallego, A.J. Queimada, M.M. Piñeiro, and J.A.P. Coutinho, *High-Pressure Biodiesel Density: Experimental*

Measurements, Correlation, and Cubic-Plus-Association Equation of State (CPA EoS) Modeling. Energ. Fuel 2011. vol. 25 (8): p. 3806-3814.
142. Elbro, H.S., A. Fredenslund, and P. Rasmussen, *Group contribution method for the prediction of liquid densities as a function of temperature for solvents, oligomers, and polymers.* Ind Eng Chem Res. 1991. vol. 30 (12): p. 2576-2582.
143. Ihmels, E.C. and J. Gmehling, *Extension and Revision of the Group Contribution Method GCVOL for the Prediction of Pure Compound Liquid Densities.* Ind Eng Chem Res. 2002. vol. 42 (2): p. 408-412.
144. Tat, M. and J. Van Gerpen, *Effect of temperature and pressure on the speed of sound and isentropic bulk modulus of mixtures of biodiesel and diesel fuel.* Journal of the American Oil Chemists' Society. 2003. vol. 80 (11): p. 1127-1130.
145. Cosseron, A.-F., H. Bennadji, G. Leyssens, L. Coniglio, T.J. Daou, and V. Tschamber, *Evaluation and Treatment of Carbonyl Compounds and Fine Particles Emitted by Combustion of Biodiesels in a Generator.* Energy & Fuels. 2012. vol. 26 (10): p. 6160-6167.
146. Freitas, S.V.D., M.J. Pratas, R. Ceriani, A.S. Lima, and J.A.P. Coutinho, *Evaluation of Predictive Models for the Viscosity of Biodiesel.* Energy & Fuels. 2011. vol. 25 (1): p. 352-358.
147. Shu, Q., B. Yang, J. Yang, and S. Qing, *Predicting the viscosity of biodiesel fuels based on the mixture topological index method.* Fuel. 2007. vol. 86 (12–13): p. 1849-1854.
148. Krisnangkura, K., T. Yimsuwan, and R. Pairintra, *An empirical approach in predicting biodiesel viscosity at various temperatures.* Fuel. 2006. vol. 85 (1): p. 107-113.
149. Refaat, A.A., *Correlation between the chemical structure of biodiesel and its physical properties.* International Journal of Environmental Science and Technology. 2009. vol. 6 (4): p. 677-694.
150. Ceriani, R., C.B. Gonçalves, J. Rabelo, M. Caruso, A.C.C. Cunha, F.W. Cavaleri, E.A.C. Batista, and A.J.A. Meirelles, *Group Contribution Model for Predicting Viscosity of Fatty Compounds.* Journal of Chemical & Engineering Data. 2007. vol. 52 (3): p. 965-972.
151. Yuan, W., A.C. Hansen, and Q. Zhang, *Predicting the temperature dependent viscosity of biodiesel fuels.* Fuel. 2009. vol. 88 (6): p. 1120-1126.
152. Pratas, M.J., S. Freitas, M.B. Oliveira, S.C. Monteiro, A.S. Lima, and J.A.P. Coutinho, *Densities and Viscosities of Fatty Acid Methyl and Ethyl Esters.* J Chem Eng Data. 2010. vol. 55 (9): p. 3983-3990.
153. Pratas, M.J., S. Freitas, M.B. Oliveira, S.C. Monteiro, A.S. Lima, and J.A.P. Coutinho, *Densities and Viscosities of Minority Fatty Acid Methyl and Ethyl Esters Present in Biodiesel.* J Chem Eng Data. 2011. vol. 56 (5): p. 2175-2180.
154. Carvalho, P.J., T. Regueira, L.M.N.B.F. Santos, J. Fernandez, and J.A.P. Coutinho, *Effect of Water on the Viscosities and Densities of 1-Butyl-3-methylimidazolium Dicyanamide and 1-Butyl-3-methylimidazolium Tricyanomethane at Atmospheric Pressure†.* Journal of Chemical & Engineering Data. 2009. vol. 55 (2): p. 645-652.
155. Yuan, W., A. Hansen, Q. Zhang, and Z. Tan, *Temperature-dependent kinematic viscosity of selected biodiesel fuels and blends with diesel fuel.* Journal of the American Oil Chemists' Society. 2005. vol. 82 (3): p. 195-199.

156. Blangino, E., A.F. Riveros, and S.D. Romano, *Numerical expressions for viscosity, surface tension and density of biodiesel: analysis and experimental validation.* Physics and Chemistry of Liquids. 2008. vol. 46 (5): p. 527-547.
157. Knothe, G. and K.R. Steidley, *Kinematic viscosity of biodiesel components (fatty acid alkyl esters) and related compounds at low temperatures.* Fuel. 2007. vol. 86 (16): p. 2560-2567.
158. Feitosa, F.X., M.d.L. Rodrigues, C.B. Veloso, C.l.L. Cavalcante, M.n.C.G. Albuquerque, and H.B. de Santâ Ana, *Viscosities and Densities of Binary Mixtures of Coconut + Colza and Coconut + Soybean Biodiesel at Various Temperatures.* Journal of Chemical & Engineering Data. vol.
159. Nogueira, C.A., F.X. Feitosa, F.A.N. Fernandes, R.l.S. Santiago, and H.B. de Sant'Ana, *Densities and Viscosities of Binary Mixtures of Babassu Biodiesel + Cotton Seed or Soybean Biodiesel at Different Temperatures.* Journal of Chemical & Engineering Data. 2010. vol. 55 (11): p. 5305-5310.
160. Freitas, S.V.D., M.B. Oliveira, Á.S. Lima, and J.A.P. Coutinho, *Measurement and Prediction of Biodiesel Volatility.* Energy & Fuels. 2012. vol. 26 (5): p. 3048-3053.
161. Rose, A. and W.R. Supina, *Vapor Pressure and Vapor-Liquid Equilibrium Data for Methyl Esters of the Common Saturated Normal Fatty Acids.* J. Chem. Eng. Data. 1961. vol. 6 (2): p. 173-179.
162. Yuan, W., A.C. Hansen, and Q. Zhang, *Vapor pressure and normal boiling point predictions for pure methyl esters and biodiesel fuels.* Fuel. 2005. vol. 84 (7–8): p. 943-950.
163. Scott, T.A., D. Macmillan, and E.H. Melvin, *Vapor Pressures and Distillation of Methyl Esters of Some Fatty Acids.* Ind. Eng. Chem. 1952. vol. 44 (1): p. 172-175.
164. Widegren, J.A. and T.J. Bruno, *Vapor pressure measurements on saturated biodiesel fuel esters by the concatenated gas saturation method.* Fuel. 2011. vol. 90 (5): p. 1833-1839.
165. Ceriani, R. and A.J.A. Meirelles, *Predicting vapor–liquid equilibria of fatty systems.* Fluid Phase Equilibr. 2004. vol. 215 (2): p. 227-236.
166. Goodrum, J.W., *Volatility and boiling points of biodiesel from vegetable oils and tallow.* Biomass Bioenerg. 2002. vol. 22 (3): p. 205-211.
167. Guo, Y., F. Yang, Y. Xing, D. Li, W. Fang, and R. Lin, *Study on volatility and flash point of the pseudo binary mixtures of sunflower-based biodiesel+methylcyclohexane.* Fluid Phase Equilibr. 2009. vol. 276 (2): p. 127-132.
168. Oliveira, M.B., V.t. Ribeiro, A.J. Queimada, and J.A.P. Coutinho, *Modeling Phase Equilibria Relevant to Biodiesel Production: A Comparison of gE Models, Cubic EoS, EoS−gE and Association EoS.* Ind. Eng. Chem. Res. . 2011. vol. 50 (4): p. 2348-2358.
169. Kontogeorgis, G.M., M.L. Michelsen, G.K. Folas, S. Derawi, N. von Solms, and E.H. Stenby, *Ten Years with the CPA (Cubic-Plus-Association) Equation of State. Part 1. Pure Compounds and Self-Associating Systems.* Industrial & Engineering Chemistry Research. 2006. vol. 45 (14): p. 4855-4868.
170. Kontogeorgis, G.M., M.L. Michelsen, G.K. Folas, S. Derawi, N. von Solms, and E.H. Stenby, *Ten Years with the CPA (Cubic-Plus-Association) Equation of State. Part 2. Cross-Associating and Multicomponent Systems.* Industrial & Engineering Chemistry Research. 2006. vol. 45 (14): p. 4869-4878.

171. Oliveira, M.B., J.A.P. Coutinho, and A.J. Queimada, *Mutual solubilities of hydrocarbons and water with the CPA EoS.* Fluid Phase Equilibria. 2007. vol. 258 (1): p. 58-66.
172. Wilson, G.M. and L.V. Jasperson, *AIChE Spring Meeting, New Orleans, LA.* 1996. vol.
173. Ambrose, D., *Vapor-Liquid Critical Properties: II. Critical Pressure and Critical Volume.* NPL Rep. Chem. 1980. vol. 107, Teddington, UK.
174. Lopes, J.C.A., L. Boros, M.A. Krähenbühl, A.J.A. Meirelles, J.L. Daridon, J. Pauly, I.M. Marrucho, and J.A.P. Coutinho, *Prediction of Cloud Points of Biodiesel.* Energ. Fuel. 2007. vol. 22 (2): p. 747-752.
175. Ejim, C.E., B.A. Fleck, and A. Amirfazli, *Analytical study for atomization of biodiesels and their blends in a typical injector: Surface tension and viscosity effects.* Fuel. 2007. vol. 86 (10–11): p. 1534-1544.
176. Shu, Q., J. Wang, B. Peng, D. Wang, and G. Wang, *Predicting the surface tension of biodiesel fuels by a mixture topological index method, at 313 K.* Fuel. 2008. vol. 87 (17–18): p. 3586-3590.
177. Allen, C., K. Watts, and R. Ackman, *Predicting the surface tension of biodiesel fuels from their fatty acid composition.* Journal of the American Oil Chemists' Society. 1999. vol. 76 (3): p. 317-323.
178. Rolo, L.I., A.I. Caço, A.J. Queimada, I.M. Marrucho, and J.A.P. Coutinho, *Surface Tension of Heptane, Decane, Hexadecane, Eicosane, and Some of Their Binary Mixtures.* Journal of Chemical & Engineering Data. 2002. vol. 47 (6): p. 1442-1445.
179. Queimada, A.J., F.A.E. Silva, A.I. Caço, I.M. Marrucho, and J.A.P. Coutinho, *Measurement and modeling of surface tensions of asymmetric systems: heptane, eicosane, docosane, tetracosane and their mixtures.* Fluid Phase Equilibria. 2003. vol. 214 (2): p. 211-221.
180. Freire, M.G., P.J. Carvalho, A.J. Queimada, I.M. Marrucho, and J.A.P. Coutinho, *Surface Tension of Liquid Fluorocompounds.* Journal of Chemical & Engineering Data. 2006. vol. 51 (5): p. 1820-1824.
181. Carvalho, P.J., C.M.S.S. Neves, and J.A.P. Coutinho, *Surface Tensions of Bis(trifluoromethylsulfonyl)imide Anion-Based Ionic Liquids.* Journal of Chemical & Engineering Data. 2010. vol. 55 (9): p. 3807-3812.
182. Carvalho, P.J., M.G. Freire, I.M. Marrucho, A.n.J. Queimada, and J.A.P. Coutinho, *Surface Tensions for the 1-Alkyl-3-methylimidazolium Bis(trifluoromethylsulfonyl)imide Ionic Liquids.* Journal of Chemical & Engineering Data. 2008. vol. 53 (6): p. 1346-1350.
183. Freire, M.G., P.J. Carvalho, A.M. Fernandes, I.M. Marrucho, A.J. Queimada, and J.A.P. Coutinho, *Surface tensions of imidazolium based ionic liquids: Anion, cation, temperature and water effect.* Journal of Colloid and Interface Science. 2007. vol. 314 (2): p. 621-630.
184. Knotts, T.A., W.V. Wilding, J.L. Oscarson, and R.L. Rowley, *Use of the DIPPR Database for Development of QSPR Correlations: Surface Tension†.* Journal of Chemical & Engineering Data. 2001. vol. 46 (5): p. 1007-1012.
185. Oliveira, M.B., A.n.J. Queimada, and J.A.P. Coutinho, *Modeling of Biodiesel Multicomponent Systems with the Cubic-Plus-Association (CPA) Equation of State.* Industrial & Engineering Chemistry Research. 2009. vol. 49 (3): p. 1419-1427.

186. Oliveira, M.B., J.A.P. Coutinho, and A.J. Queimada, *Surface tensions of esters from a combination of the gradient theory with the CPA EoS.* Fluid Phase Equilibria. 2011. vol. 303 (1): p. 56-61.
187. Oliveira, M.B., I.M. Marrucho, J.A.P. Coutinho, and A.J. Queimada, *Surface tension of chain molecules through a combination of the gradient theory with the CPA EoS.* Fluid Phase Equilibria. 2008. vol. 267 (1): p. 83-91.
188. Miqueu, C., B. Mendiboure, A. Graciaa, and J. Lachaise, *Modeling of the Surface Tension of Multicomponent Mixtures with the Gradient Theory of Fluid Interfaces.* Industrial & Engineering Chemistry Research. 2005. vol. 44 (9): p. 3321-3329.
189. Queimada, A.J., C. Miqueu, I.M. Marrucho, G.M. Kontogeorgis, and J.A.P. Coutinho, *Modeling vapor–liquid interfaces with the gradient theory in combination with the CPA equation of state.* Fluid Phase Equilibria. 2005. vol. 228–229 (0): p. 479-485.
190. Oliveira, M.B., F.R. Varanda, I.M. Marrucho, A.J. Queimada, and J.A.P. Coutinho, *Prediction of Water Solubility in Biodiesel with the CPA Equation of State.* Industrial & Engineering Chemistry Research. 2008. vol. 47 (12): p. 4278-4285.
191. Oliveira, M.B., S.I. Miguel, A.J. Queimada, and J.A.P. Coutinho, *Phase Equilibria of Ester + Alcohol Systems and Their Description with the Cubic-Plus-Association Equation of State.* Industrial & Engineering Chemistry Research. 2010. vol. 49 (7): p. 3452-3458.
192. Oliveira, M.B., M.J. Pratas, I.M. Marrucho, A.J. Queimada, and J.A.P. Coutinho, *Description of the mutual solubilities of fatty acids and water with the CPA EoS.* AIChE Journal. 2009. vol. 55 (6): p. 1604-1613.
193. Oliveira, M.B., A.J. Queimada, and J.A.P. Coutinho, *Prediction of near and supercritical fatty acid ester + alcohol systems with the CPA EoS.* The Journal of Supercritical Fluids. 2010. vol. 52 (3): p. 241-248.
194. Queimada, A.J., F.L. Mota, S.P. Pinho, and E.A. Macedo, *Solubilities of Biologically Active Phenolic Compounds: Measurements and Modeling.* The Journal of Physical Chemistry B. 2009. vol. 113 (11): p. 3469-3476.
195. Cornelisse, P.M.W., C.J. Peters, and J. de Swaan Arons, *Application of the Peng-Robinson equation of state to calculate interfacial tensions and profiles at vapour-liquid interfaces.* Fluid Phase Equilibria. 1993. vol. 82 (0): p. 119-129.
196. Miqueu, C., B. Mendiboure, A. Graciaa, and J. Lachaise, *Modelling of the surface tension of pure components with the gradient theory of fluid interfaces: a simple and accurate expression for the influence parameters.* Fluid Phase Equilibria. 2003. vol. 207 (1–2): p. 225-246.
197. Freitas, S.V.D., M.L.L. Paredes, J.-L. Daridon, Á.S. Lima, and J.A.P. Coutinho, *Measurement and Prediction of the Speed of Sound of Biodiesel Fuels.* Fuel 2013. vol. 103: p. 1018-1022.
198. Freitas, S.V.D., Â. Santos, M.-L.C.J. Moita, L.A. Follegatti-Romero, T.P.V.B. Dias, A.J.A. Meirelles, J.-L. Daridon, Á.S. Lima, and J.A.P. Coutinho, *Measurement and prediction of speeds of sound of fatty acid ethyl esters and ethylic biodiesels.* Fuel. 2013. vol. 108 (0): p. 840-845.
199. Freitas, S.V.D., D.L. Cunha, R.A. Reis, Á.S. Lima, J.L. Daridon, J.A.P. Coutinho, and M.L.L. Paredes, *Application of the Wada's Group Contribution method to the prediction of the speed of sound of biodiesel.* Energ Fuel. 2013. vol. 27 (3): p. 1365-1370

200. Hoekman, S.K. and C. Robbins, *Review of the effects of biodiesel on NOx emissions.* Fuel Processing Technology. 2012. vol. 96 (0): p. 237-249.
201. Szybist, J.P., J. Song, M. Alam, and A.L. Boehman, *Biodiesel combustion, emissions and emission control.* Fuel Processing Technology. 2007. vol. 88 (7): p. 679-691.
202. Tat, M. and J. Van Gerpen, *Speed of sound and isentropic bulk modulus of alkyl monoesters at elevated temperatures and pressures.* Journal of the American Oil Chemists' Society. 2003. vol. 80 (12): p. 1249-1256.
203. Payri, R., F.J. Salvador, J. Gimeno, and G. Bracho, *The effect of temperature and pressure on thermodynamic properties of diesel and biodiesel fuels.* Fuel. 2011. vol. 90 (3): p. 1172-1180.
204. Kegl, B., *Effects of biodiesel on emissions of a bus diesel engine.* Bioresource Technology. 2008. vol. 99 (4): p. 863-873.
205. Benjumea, P., J.R. Agudelo, and A.s.F. Agudelo, *Effect of the Degree of Unsaturation of Biodiesel Fuels on Engine Performance, Combustion Characteristics, and Emissions.* Energy & Fuels. 2010. vol. 25 (1): p. 77-85.
206. Freitas, S.V.D., D.L. Cunha, R.A. Reis, Á.S. Lima, J.L. Daridon, J.A.P. Coutinho, and M.L.L. Paredes, *Application of the Wada's Group Contribution method to the prediction of the speed of sound of biodiesel.* Energ Fuel. 2013. vol. Publishing.
207. Gouw, T. and J. Vlugter, *Physical properties of fatty acid methyl esters. IV. Ultrasonic sound velocity.* Journal of the American Oil Chemists' Society. 1964. vol. 41 (8): p. 524-526.
208. Tat, M.E. and J.H. Van Gerpen. *Measurement of Biodiesel Speed of Sound and Its Impact on Injection Timing: Final Report; Report 4 in a Series of 6*, 2003.
209. Tat, M., J. Van Gerpen, S. Soylu, M. Canakci, A. Monyem, and S. Wormley, *The speed of sound and isentropic bulk modulus of biodiesel at 21°C from atmospheric pressure to 35 MPa.* Journal of the American Oil Chemists' Society. 2000. vol. 77 (3): p. 285-289.
210. Ott, L.S., M.L. Huber, and T.J. Bruno, *Density and Speed of Sound Measurements on Five Fatty Acid Methyl Esters at 83 kPa and Temperatures from (278.15 to 338.15) K.* Journal of Chemical & Engineering Data. 2008. vol. 53 (10): p. 2412-2416.
211. Daridon, J.L., J.A.P. Coutinho, E.H.I. Ndiaye, and M.L.L. Paredes, *Novel data and a group contribution method for the prediction of the speed of sound and isentropic compressibility of pure fatty acids methyl and ethyl esters.* Fuel. 2013. vol. 105: p. 466-470.
212. Oswal, S.L., P. Oswal, R.L. Gardas, S.G. Patel, and R.G. Shinde, *Acoustic, volumetric, compressibility and refractivity properties and reduction parameters for the ERAS and Flory models of some homologous series of amines from 298.15 to 328.15 K.* Fluid Phase Equilibria. 2004. vol. 216 (1): p. 33-45.
213. Huber, M.L., E.W. Lemmon, A. Kazakov, L.S. Ott, and T.J. Bruno, *Model for the Thermodynamic Properties of a Biodiesel Fuel.* Energy & Fuels. 2009. vol. 23 (7): p. 3790-3797.
214. Kumar, S., J.S. Yadav, V.K. Sharma, W. Lim, J.H. Cho, J. Kim, and I. Moon, *Physicochemical Properties of Jatropha Curcas Biodiesel + Diesel Fuel No. 2 Binary Mixture at T = (288.15 to 308.15) K and Atmospheric Pressure.* Journal of Chemical & Engineering Data. 2011. vol. 56 (3): p. 497-501.

215. Ndiaye, E.H.I., M. Habrioux, J.L. Daridon, M.L.L. Paredes, and J.A.P. Coutinho, *Speed of Sound, Density and Derivative Properties of Fatty Acid Methyl and Ethyl Esters Under High Pressure: Ethyl Myristate, Methyl Myristate and Methyl Palmitate.* J. Chem. Eng. Data. 2013. vol. Submitted.
216. Paredes, M.L.L., R.A. Reis, A.A. Silva, R.N.G. Santos, G.J. Santos, M.H.A. Ribeiro, and P.B. Ximango, *Densities, sound velocities, and refractive indexes of (tetralin + n-decane) and thermodynamic modeling by Prigogine–Flory–Patterson model.* The Journal of Chemical Thermodynamics. 2012. vol. 45 (1): p. 35-42.
217. Lampreia, I.M.S., Â.F.S. Santos, M.-L.C.J. Moita, A.O. Figueiras, and J.C.R. Reis, *Ultrasound speeds and molar isentropic compressions of aqueous 1-propoxypropan-2-ol mixtures from T = (283.15 to 303.15) K. Influence of solute structure.* The Journal of Chemical Thermodynamics. 2012. vol. 45 (1): p. 75-82.
218. Lampreia, I.M.S. and C.A. Nieto de Castro, *A new and reliable calibration method for vibrating tube densimeters over wide ranges of temperature and pressure.* The Journal of Chemical Thermodynamics. 2011. vol. 43 (4): p. 537-545.
219. Fortin, T.J., A. Laesecke, M. Freund, and S. Outcalt, *Advanced calibration, adjustment, and operation of a density and sound speed analyzer.* Journal of Chemical Thermodynamics. 2013. vol. 57: p. 276-285.
220. Gardas, R.L. and J.A.P. Coutinho, *Estimation of speed of sound of ionic liquids using surface tensions and densities: A volume based approach.* Fluid Phase Equilibria. 2008. vol. 267 (2): p. 188-192.
221. Auerbach, N., *Experientia 4*. 1948. p. 473-474.
222. Ndiaye, E.H.I., D. Nasri, and J.L. Daridon, *Speed of sound, density, and derivative properties of fatty acid methyl and ethyl esters under high pressure: Methyl caprate and ethyl caprate.* Journal of Chemical and Engineering Data. 2012. vol. 57 (10): p. 2667-2676.
223. Habrioux, M., S.V.D. Freitas, J.A.P. Coutinho, and J.L. Daridon, *High pressure Density and Speed of Sound of two biodiesel fuels: Measurement and prediction.* 2013. vol. accepted.
224. Duncan, A.M., A. Ahosseini, R. McHenry, C.D. Depcik, S.M. Stagg-Williams, and A.M. Scurto, *High-Pressure Viscosity of Biodiesel from Soybean, Canola, and Coconut Oils.* Energy & Fuels. 2010. vol. 24 (10): p. 5708-5716.
225. Duncan, A.M., N. Pavlicek, C.D. Depcik, A.M. Scurto, and S.M. Stagg-Williams, *High-Pressure Viscosity of Soybean-Oil-Based Biodiesel Blends with Ultra-Low-Sulfur Diesel Fuel.* Energy & Fuels. 2012. vol. 26 (11): p. 7023-7036.
226. Robertson, L.X. and C.J. Schaschke, *Combined High Pressure and Low Temperature Viscosity Measurement of Biodiesel.* Energy & Fuels. 2009. vol. 24 (2): p. 1293-1297.
227. Paton, J.M. and C.J. Schaschke, *Viscosity measurement of biodiesel at high pressure with a falling sinker viscometer.* Chemical Engineering Research and Design. 2009. vol. 87 (11): p. 1520-1526.
228. Chhetri, A.B. and K.C. Watts, *Viscosities of canola, jatropha and soapnut biodiesel at elevated temperatures and pressures.* Fuel. 2012. vol. 102 (0): p. 789-794.
229. Ghadge, S.V. and H. Raheman, *Biodiesel production from mahua (Madhuca indica) oil having high free fatty acids.* Biomass Bioenerg. 2005. vol. 28 (6): p. 601-605.
230. Dymond, J.H. and R. Malhotra, *The Tait equation: 100 years on.* Int J Thermophys. 1988. vol. 9 (6): p. 941-951.

231. Halvorsen, J., W. Mammel, and L. Clements, *Density estimation for fatty acids and vegetable oils based on their fatty acid composition.* J Am Oil Chem Soc. 1993. vol. 70 (9): p. 875-880.
232. Rodenbush, C., F. Hsieh, and D. Viswanath, *Density and viscosity of vegetable oils.* J Am Oil Chem Soc. 1999. vol. 76 (12): p. 1415-1419.
233. Zong, L., S. Ramanathan, and C.-C. Chen, *Fragment-Based Approach for Estimating Thermophysical Properties of Fats and Vegetable Oils for Modeling Biodiesel Production Processes.* Ind Eng Chem Res. 2009. vol. 49 (2): p. 876-886.
234. Polling, B.E., J.M. Prausnitz, and J.P. O'connell, *The properties of gases and liquids*. Fifth edition ed. 2000: Mcgraw-Hill.
235. Pàmies, J.C. and L.F. Vega, *Vapor−Liquid Equilibria and Critical Behavior of Heavy n-Alkanes Using Transferable Parameters from the Soft-SAFT Equation of State.* Industrial & Engineering Chemistry Research. 2001. vol. 40 (11): p. 2532-2543.
236. Llovell, F. and L.F. Vega, *Phase equilibria, critical behavior and derivative properties of selected n-alkane/n-alkane and n-alkane/1-alkanol mixtures by the crossover soft-SAFT equation of state.* The Journal of Supercritical Fluids. 2007. vol. 41 (2): p. 204-216.
237. Dias, A.M.A., F. Llovell, J.A.P. Coutinho, I.M. Marrucho, and L.F. Vega, *Thermodynamic characterization of pure perfluoroalkanes, including interfacial and second order derivative properties, using the crossover soft-SAFT EoS.* Fluid Phase Equilibria. 2009. vol. 286 (2): p. 134-143.
238. de Melo, M.J.P., A.M.A. Dias, M. Blesic, L.P.N. Rebelo, L.F. Vega, J.A.P. Coutinho, and I.M. Marrucho, *Liquid–liquid equilibrium of (perfluoroalkane+alkane) binary mixtures.* Fluid Phase Equilibria. 2006. vol. 242 (2): p. 210-219.
239. Andreu, J.S. and L.F. Vega, *Capturing the Solubility Behavior of CO2 in Ionic Liquids by a Simple Model†.* The Journal of Physical Chemistry C. 2007. vol. 111 (43): p. 16028-16034.
240. Pedrosa, N., L.F. Vega, J.A.P. Coutinho, and I.M. Marrucho, *Modeling the Phase Equilibria of Poly(ethylene glycol) Binary Mixtures with soft-SAFT EoS.* Industrial & Engineering Chemistry Research. 2007. vol. 46 (13): p. 4678-4685.
241. Andreu, J.S. and L.F. Vega, *Modeling the Solubility Behavior of CO2, H2, and Xe in [Cn-mim][Tf2N] Ionic Liquids.* The Journal of Physical Chemistry B. 2008. vol. 112 (48): p. 15398-15406.
242. Llovell, F., O. Vilaseca, and L.F. Vega, *Thermodynamic Modeling of Imidazolium-Based Ionic Liquids with the [PF6]− Anion for Separation Purposes.* Separation Science and Technology. 2011. vol. 47 (2): p. 399-410.
243. Vega, L.F., O. Vilaseca, F. Llovell, and J.S. Andreu, *Modeling ionic liquids and the solubility of gases in them: Recent advances and perspectives.* Fluid Phase Equilibria. 2010. vol. 294 (1–2): p. 15-30.
244. Vega, L.F., F.l. Llovell, and F.J. Blas, *Capturing the Solubility Minima of n-Alkanes in Water by Soft-SAFT.* The Journal of Physical Chemistry B. 2009. vol. 113 (21): p. 7621-7630.
245. Florusse, L.J., C.J. Peters, J.C. Pàmies, L.F. Vega, and H. Meijer, *Solubility of hydrogen in heavy n-alkanes: Experiments and saft modeling.* AIChE Journal. 2003. vol. 49 (12): p. 3260-3269.

246. Dias, A.M.A., J.C. Pàmies, J.A.P. Coutinho, I.M. Marrucho, and L.F. Vega, *SAFT Modeling of the Solubility of Gases in Perfluoroalkanes.* The Journal of Physical Chemistry B. 2003. vol. 108 (4): p. 1450-1457.
247. Dias, A.M.A., H. Carrier, J.L. Daridon, J.C. Pàmies, L.F. Vega, J.A.P. Coutinho, and I.M. Marrucho, *Vapor−Liquid Equilibrium of Carbon Dioxide−Perfluoroalkane Mixtures: Experimental Data and SAFT Modeling.* Industrial & Engineering Chemistry Research. 2006. vol. 45 (7): p. 2341-2350.
248. Chapman, W.G., K.E. Gubbins, G. Jackson, and M. Radosz, *SAFT: Equation-of-state solution model for associating fluids.* Fluid Phase Equilibria. 1989. vol. 52 (0): p. 31-38.
249. Gil-Villegas, A., A. Galindo, P.J. Whitehead, S.J. Mills, G. Jackson, and A.N. Burgess, *Statistical associating fluid theory for chain molecules with attractive potentials of variable range.* The Journal of Chemical Physics. 1997. vol. 106 (10): p. 4168-4186.
250. Gross, J. and G. Sadowski, *Perturbed-Chain SAFT: An Equation of State Based on a Perturbation Theory for Chain Molecules.* Industrial & Engineering Chemistry Research. 2001. vol. 40 (4): p. 1244-1260.
251. Felipe J, B. and V. Lourdes F, *Thermodynamic behaviour of homonuclear and heteronuclear Lennard-Jones chains with association sites from simulation and theory.* Molecular Physics. 1997. vol. 92 (1): p. 135-150.
252. Blas, F.J. and L.F. Vega, *Prediction of Binary and Ternary Diagrams Using the Statistical Associating Fluid Theory (SAFT) Equation of State.* Industrial & Engineering Chemistry Research. 1998. vol. 37 (2): p. 660-674.
253. Müller, E.A. and K.E. Gubbins, *Molecular-Based Equations of State for Associating Fluids: A Review of SAFT and Related Approaches.* Industrial & Engineering Chemistry Research. 2001. vol. 40 (10): p. 2193-2211.
254. Economou, I.G., *Statistical Associating Fluid Theory: A Successful Model for the Calculation of Thermodynamic and Phase Equilibrium Properties of Complex Fluid Mixtures.* Industrial & Engineering Chemistry Research. 2001. vol. 41 (5): p. 953-962.
255. Llovell, F., E. Valente, O. Vilaseca, and L.F. Vega, *Modeling Complex Associating Mixtures with [Cn-mim][Tf2N] Ionic Liquids: Predictions from the Soft-SAFT Equation.* The Journal of Physical Chemistry B. 2011. vol. 115 (15): p. 4387-4398.
256. Johnson, J.K., J.A. Zollweg, and K.E. Gubbins, *The Lennard-Jones equation of state revisited.* Molecular Physics. 1993. vol. 78 (3): p. 591-618.
257. Wertheim, M.S., *Fluids with highly directional attractive forces. II. Thermodynamic perturbation theory and integral equations.* Journal of Statistical Physics. 1984. vol. 35 (1-2): p. 35-47.
258. Wertheim, M.S., *Fluids with highly directional attractive forces. IV. Equilibrium polymerization.* Journal of Statistical Physics. 1986. vol. 42 (3-4): p. 477-492.
259. Waals, J.D., *The thermodynamic theory of capillarity under the hypothesis of a continuous variation of density.* Journal of Statistical Physics. 1979. vol. 20 (2): p. 200-244.
260. Cahn, J.W. and J.E. Hilliard, *Free Energy of a Nonuniform System. I. Interfacial Free Energy.* The Journal of Chemical Physics. 1958. vol. 28 (2): p. 258-267.
261. Bongiorno, V., L.E. Scriven, and H.T. Davis, *Molecular theory of fluid interfaces.* Journal of Colloid and Interface Science. 1976. vol. 57 (3): p. 462-475.

262. Vilaseca, O. and L.F. Vega, *Direct calculation of interfacial properties of fluids close to the critical region by a molecular-based equation of state.* Fluid Phase Equilibria. 2011. vol. 306 (1): p. 4-14.
263. Duque, D., J.C. Pamies, and L.F. Vega, *Interfacial properties of Lennard-Jones chains by direct simulation and density gradient theory.* The Journal of Chemical Physics. 2004. vol. 121 (22): p. 11395-11401.
264. Chung, T.H., M. Ajlan, L.L. Lee, and K.E. Starling, *Generalized multiparameter correlation for nonpolar and polar fluid transport properties.* Industrial & Engineering Chemistry Research. 1988. vol. 27 (4): p. 671-679.
265. Doolittle, A.K., *Studies in Newtonian Flow. II. The Dependence of the Viscosity of Liquids on Free-Space.* Journal of Applied Physics. 1951. vol. 22 (12): p. 1471-1475.
266. Allal, A., C. Boned, and A. Baylaucq, *Free-volume viscosity model for fluids in the dense and gaseous states.* Physical Review E. 2001. vol. 64 (1): p. 011203.
267. Llovell, F., R. Marcos, and L.F. Vega, *Free-Volume Theory Coupled with soft-SAFT for Viscosity Calculations: Comparison with Molecular Simulation and Experimental Data.* J. Phys. Chem. B. 2013. vol. in press.
268. Llovell, F. and L.F. Vega, *Prediction of Thermodynamic Derivative Properties of Pure Fluids through the Soft-SAFT Equation of State.* The Journal of Physical Chemistry B. 2006. vol. 110 (23): p. 11427-11437.
269. Outcalt, S.L., *Compressed-Liquid Density Measurements of Methyl Oleate and Methyl Linoleate.* Journal of Chemical & Engineering Data. 2011. vol. 56 (11): p. 4239-4243.
270. Hary Sulistyo., e.a., *Biodiesel Production from high Iodine Number cundle nut oil.* Proceeding of world academy os science, engineering and technology. 2008. vol. 36.
271. Ako, H., N. Kong, and A. Brown, *Fatty acid profiles of kukui nut oils over time and from different sources.* Industrial Crops and Products. 2005. vol. 22 (2): p. 169-174.
272. Kumar Tiwari, A., A. Kumar, and H. Raheman, *Biodiesel production from jatropha oil (Jatropha curcas) with high free fatty acids: An optimized process.* Biomass and Bioenergy. 2007. vol. 31 (8): p. 569-575.
273. Al-Hamamre, Z., S. Foerster, F. Hartmann, M. Kröger, and M. Kaltschmitt, *Oil extracted from spent coffee grounds as a renewable source for fatty acid methyl ester manufacturing.* Fuel. 2012. vol. 96 (0): p. 70-76.
274. Oliveira, L.S., A.S. Franca, R.R.S. Camargos, and V.P. Ferraz, *Coffee oil as a potential feedstock for biodiesel production.* Bioresource Technology. 2008. vol. 99 (8): p. 3244-3250.
275. Berchmans, H.J. and S. Hirata, *Biodiesel production from crude Jatropha curcas L. seed oil with a high content of free fatty acids.* Bioresource Technology. 2008. vol. 99 (6): p. 1716-1721.
276. Ong, H.C., A.S. Silitonga, H.H. Masjuki, T.M.I. Mahlia, W.T. Chong, and M.H. Boosroh, *Production and comparative fuel properties of biodiesel from non-edible oils: Jatropha curcas, Sterculia foetida and Ceiba pentandra.* Energy Conversion and Management. 2013. vol. 73 (0): p. 245-255.
277. Baroutian, S., K. Shahbaz, F.S. Mjalli, M.A. Hashim, and I.M. AlNashef, *Densities and Viscosities of Binary Blends of Methyl Esters + Ethyl Esters and Ternary Blends of Methyl Esters + Ethyl Esters + Diesel Fuel from T = (293.15 to 358.15) K.* Journal of Chemical & Engineering Data. 2012. vol. 57 (5): p. 1387-1395.

278. Kumar, S., V.K. Sharma, W. Lim, J.H. Cho, and I. Moon, *Densities and Speeds of Sound of Jatropha curcas Biodiesel + (C4–C5) Alkan-1-ol Binary Mixtures.* Journal of Chemical & Engineering Data. 2012. vol. 57 (8): p. 2236-2242.

Supporting information

A. Supplementary data/results for Chapter 2

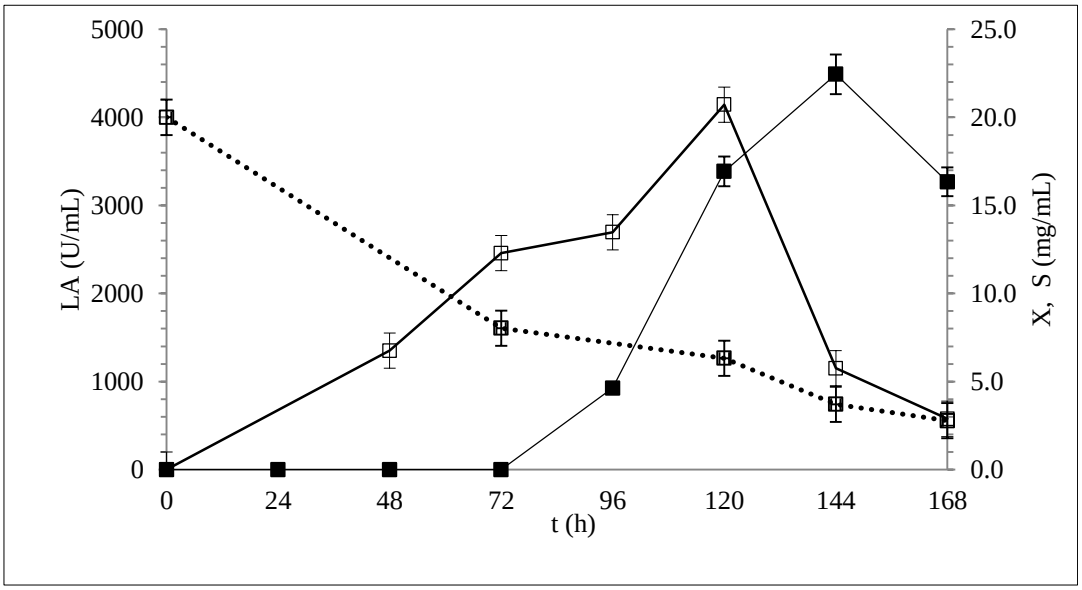

Figure A- 1. Profile of starch, dry cell biomass and lipase activity for the culture of Bacillus sp.ITP-001 at 200 RPM using 20 % C10F18 and 4 % (v/v) of Aleurites moluccana oil. —■— Lipase Activity (LA), —□— Dry cell biomass (X) and ···□··· Starch consumption (S)

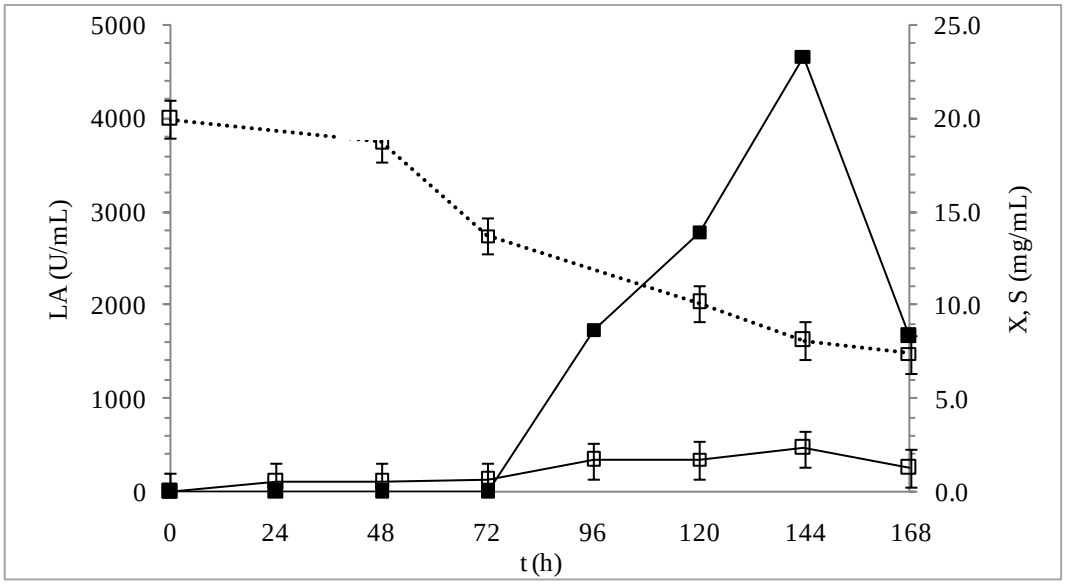

Figure A- 2. Profile of starch, dry cell biomass and lipase activity for the culture of Bacillus sp.ITP-001 at 200 RPM using 20 % C10F18 and 4 % (v/v) of coffee waste oil. —■— Lipase Activity (LA), —□— Dry cell biomass (X) and ···□··· Starch consumption (S)

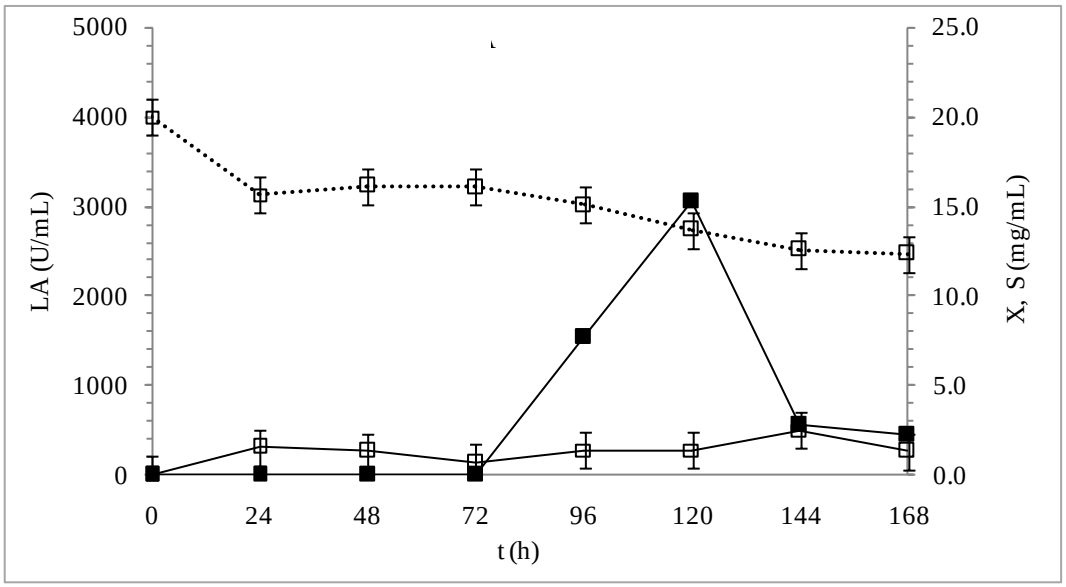

Figure A- 3. Profile of starch, dry cell biomass and lipase activity for the culture of Bacillus sp.ITP-001 at 200 RPM using 20 % C10F18 and 4 % (v/v) of Jatropha curcas oil. —■— Lipase Activity (LA), —□— Dry cell biomass (X) and ···□··· Starch consumption (S)

Table A- 1. Profile of pH for all inducers here studied in presence of perfluorodecaline

Time (h)	Control	Coconut	*AM*	*JC*	CW
0	4.71	4.92	5.08	5.33	5.00
24	5.05	5.41	5.24	5.22	5.02
48	5.46	5.15	5.23	7.72	5.16
72	7.74	5.08	6.75	8.28	4.80
96	7.87	5.06	7.67	6.73	4.69
120	7.87	5.05	7.49	7.44	4.67
144	7.28	4.88	6.55	8.28	4.88
168	5.06	7.88	7.52	8.26	4.88

B. Supplementary data/results for Chapter 3

B.1. Equations for critical properties

Method of Joback's was used to predict the critical properties of fatty esters according to the following equations:

$$T_c(\mathrm{K}) = T_b\left[0.584 + 0.965\left\{\sum_k N_k(tck)\right\} - \left\{\sum_k N_k(tck)\right\}^2\right]^{-1} \quad \text{(B.1.1)}$$

$$P_c\ (\mathrm{bar}) = \left[0.113 + 0.0032N_{\mathrm{atoms}} - \sum_k N_k(pck)\right]^{-2} \quad \text{(B.1.2.)}$$

$$V_c\ (\mathrm{cm^3mol^{-1}}) = 17.5 + \sum_k N_k(vck) \quad \text{(B.1.3)}$$

$$T_b = 198 + \sum_k N_k(tbk) \quad \text{(B.1.4)}$$

$$w = 0.004423\left(ln(3.3063 + \textstyle\sum_k N_k w_k)\right)^{3.651} \quad \text{(B.1.5.)}$$

Table B-1. 1. Parameters for calculations of critical properties

Groups	Tck	Pck	Tbk	Vck	wk
CH3	0.0141	-0.0012	23.58	65	3.4381
CH=	0.0129	-0.0006	24.96	46	3.5129
CH2	0.0189	0	22.88	56	3.4381
COO	0.0481	0.0005	81.1	82	14.439

B.2. Parameters used in the Wada's group contribution methods.

Table B-2. 1. Parameters of Wada's model

	-CH3-	-CH2-	-CH=CH-	CH3COO-	CH2COO-
K_m	5.10E-04	3.52E-04	5.91E-04	1.06E-03	9.06E-04
c	0.000034852				

B.3. High pressure experimental data of speed of sound and density for two biodiesels (S and R)

Table B-3. 1. Experimental values of Speed of Sound c at Temperatures T and Pressures p for both biodiesels S and R[a]

p	*T*	*c*	*T*	*c*	*T*	*c*
MPa	K	$m \cdot s^{-1}$	K	$m \cdot s^{-1}$	K	$m \cdot s^{-1}$
			Biodiesel S			
0.1013	293.15	1414.9	313.15	1342.4	333.15	1276.2
10	293.15	1458.7	313.15	1388.7	333.15	1326.3
20	293.15	1499.4	313.15	1433.6	333.15	1373.9
30	293.15	1539.2	313.15	1474.6	333.15	1417.1
40	293.15	1576.1	313.15	1514.1	333.15	1459.6
50	293.15	1611.5	313.15	1550.9	333.15	1498.4
60	293.15	1643.9	313.15	1586.2	333.15	1535.2
70	293.15	1677.5	313.15	1620.0	333.15	1570.1
80	293.15	1706.9	313.15	1652.5	333.15	1604.2
90	293.15	1737.5	313.15	1683.3	333.15	1635.7
100	293.15	1766.6	313.15	1713.4	333.15	1667.3
120	293.15	1820.8	313.15	1769.0	333.15	1726.2
140	293.15	1873.8	313.15	1822.9	333.15	1781.5
160			313.15	1872.9	333.15	1831.7
180			313.15	1920.9	333.15	1881.5
200			313.15	1965.5	333.15	1927.5
0.1013	353.15	1208.8	373.15	1148.0	-	-
10	353.15	1263.0	373.15	1200.4	393.15	1145.8
20	353.15	1314.3	373.15	1255.0	393.15	1201.8
30	353.15	1360.1	373.15	1304.0	393.15	1251.7
40	353.15	1403.6	373.15	1349.9	393.15	1299.3
50	353.15	1444.1	373.15	1392.7	393.15	1343.6
60	353.15	1482.9	373.15	1432.3	393.15	1384.9
70	353.15	1518.2	373.15	1470.4	393.15	1424.7
80	353.15	1553.9	373.15	1506.4	393.15	1462.2
90	353.15	1586.6	373.15	1540.2	393.15	1497.0
100	353.15	1618.6	373.15	1573.6	393.15	1530.7
120	353.15	1679.3	373.15	1634.1	393.15	1594.8
140	353.15	1735.7	373.15	1692.6	393.15	1652.9
160	353.15	1788.1	373.15	1746.2	393.15	1709.6
180	353.15	1838.5	373.15	1798.8	393.15	1762.2
200	353.15	1886.6	373.15	1847.9	393.15	1811.1
			Biodiesel R			
0.1013	293.15	1414.2	313.15	1343.2	333.15	1279.1
10	293.15	1460.8	313.15	1391.2	333.15	1330.6
20	293.15	1502.4	313.15	1436.2	333.15	1376.8

30	293.15	1541.2	313.15	1477.4	333.15	1421.3
40	293.15	1577.1	313.15	1516.7	333.15	1462.4
50	293.15	1611.3	313.15	1553.9	333.15	1502.0
60	293.15	1647.2	313.15	1589.0	333.15	1538.1
70	293.15	1678.5	313.15	1622.9	333.15	1573.9
80	293.15	1708.6	313.15	1655.1	333.15	1608.5
90	293.15	1737.2	313.15	1685.7	333.15	1639.5
100	293.15	1766.8	313.15	1715.9	333.15	1671.6
120	293.15	1821.1	313.15	1772.9	333.15	1729.7
140	293.15	1872.4	313.15	1825.7	333.15	1785.0
160	293.15	1921.1	313.15	1874.2	333.15	1836.5
180	293.15	1967.5	313.15	1922.8	333.15	1885.3
200	293.15	2012.8	313.15	1968.3	333.15	1931.6
0.1013	353.15	1212.6	373.15	1147.7	-	-
10	353.15	1264.9	373.15	1205.4	393.15	1148.5
20	353.15	1319.5	373.15	1259.1	393.15	1204.8
30	353.15	1363.6	373.15	1308.4	393.15	1255.5
40	353.15	1407.6	373.15	1353.4	393.15	1301.4
50	353.15	1447.7	373.15	1396.5	393.15	1347.5
60	353.15	1486.6	373.15	1436.1	393.15	1389.4
70	353.15	1522.0	373.15	1473.7	393.15	1428.5
80	353.15	1558.0	373.15	1510.9	393.15	1465.9
90	353.15	1591.3	373.15	1544.8	393.15	1501.3
100	353.15	1622.9	373.15	1578.1	393.15	1535.8
120	353.15	1684.2	373.15	1639.8	393.15	1597.9
140	353.15	1739.7	373.15	1697.1	393.15	1657.6
160	353.15	1792.8	373.15	1753.0	393.15	1712.7
180	353.15	1845.9	373.15	1804.6	393.15	1767.5
200	353.15	1890.2	373.15	1851.6	393.15	1815.9

[a] Standard uncertainties *u* are u(*T*) = 0.1 K, *u*(*p*) =0.01 MPa up to 100 MPa, u(p) =0.1 MPa between (100 and 210) MPa and the combined expanded uncertainties *Uc* (level of confidence = 0.95) are *Uc*(*c*) = 0.002 *c* up to 100 MPa, *Uc*(*c*) = 0.003 *c* between (100 and 210)

Table B-3. 2. Values of densities ρ at Temperatures T and Pressures p Measured in Liquid biodiesels S and R by Using U-Tube Densimeter [a]

p	*T*	*ρ*	*T*	*ρ*	*T*	*ρ*	*T*	*ρ*	*T*	*ρ*	*T*	*ρ*
MPa	K	kg·m^{-3}	K	kg·m^{-3}	K	kg·m^{-3}	K	kg·m^{-3}	K	kg·m^{-3}	K	kg·m^{-3}
Biodiesel S												
0.1013	293.15	884.9	303.15	877.6	313.15	870.5	323.15	863.1	333.15	855.8	343.15	848.6
10	293.15	890.9	303.15	883.7	313.15	876.5	323.15	869.4	333.15	862.9	343.15	855.8
20	293.15	896.2	303.15	889.6	313.15	882.6	323.15	875.6	333.15	869.2	343.15	862.4
30	293.15	901.4	303.15	895.1	313.15	888.0	323.15	881.4	333.15	875.1	343.15	868.8

40	293.15	906.7	303.15	899.7	313.15	893.4	323.15	886.5	333.15	880.9	343.15	874.4
50	293.15	910.8	303.15	904.5	313.15	898.1	323.15	892.1	333.15	886.3	343.15	879.9
60	293.15	915.0	303.15	909.3	313.15	902.7	323.15	897.2	333.15	891.5	343.15	885.3
70	293.15	919.4	303.15	913.5	313.15	907.4	323.15	902.1	333.15	896.1	343.15	890.0
80	293.15	923.7	303.15	917.9	313.15	911.8	323.15	906.2	333.15	900.8	343.15	894.7
90	293.15	927.3	303.15	922.2	313.15	915.7	323.15	910.2	333.15	905.4	343.15	899.5
100	293.15	931.3	303.15	925.7	313.15	920.3	323.15	914.5	333.15	908.9	343.15	903.9
0.1013	353.15	841.5	363.15	834.6	373.15	827.0	383.15	819.4	393.15	811.9		
10	353.15	849.2	363.15	842.1	373.15	834.9	383.15	828.2	393.15	821.1		
20	353.15	855.9	363.15	849.4	373.15	843.1	383.15	835.7	393.15	829.6		
30	353.15	862.8	363.15	856.2	373.15	849.4	383.15	843.2	393.15	837.5		
40	353.15	868.6	363.15	862.5	373.15	856.0	383.15	850.0	393.15	844.2		
50	353.15	874.5	363.15	868.2	373.15	862.3	383.15	856.2	393.15	850.7		
60	353.15	879.9	363.15	873.9	373.15	867.9	383.15	862.6	393.15	856.9		
70	353.15	885.1	363.15	879.0	373.15	873.3	383.15	867.7	393.15	862.3		
80	353.15	889.8	363.15	884.1	373.15	878.4	383.15	873.3	393.15	867.9		
90	353.15	894.7	363.15	889.3	373.15	882.9	383.15	877.7	393.15	873.2		
100	353.15	898.8	363.15	893.3	373.15	887.9	383.15	882.9	393.15	878.1		
						Biodiesel R						
0.1013	293.15	884.2	303.15	877.4	313.15	870.3	323.15	862.5	333.15	854.9	343.15	848.3
10	293.15	890.0	303.15	883.5	313.15	875.9	323.15	869.0	333.15	862.0	343.15	855.1
20	293.15	895.2	303.15	888.7	313.15	882.1	323.15	875.5	333.15	868.3	343.15	861.9
30	293.15	900.6	303.15	894.3	313.15	888.0	323.15	880.9	333.15	874.4	343.15	867.9
40	293.15	905.6	303.15	899.1	313.15	893.1	323.15	886.2	333.15	880.3	343.15	873.6
50	293.15	909.9	303.15	903.8	313.15	897.6	323.15	891.5	333.15	885.2	343.15	879.4
60	293.15	914.0	303.15	908.3	313.15	902.1	323.15	896.3	333.15	890.4	343.15	884.8
70	293.15	918.5	303.15	912.8	313.15	906.6	323.15	900.9	333.15	895.2	343.15	889.4
80	293.15	922.9	303.15	917.1	313.15	911.1	323.15	905.2	333.15	899.7	343.15	893.5
90	293.15	926.5	303.15	921.1	313.15	914.8	323.15	909.3	333.15	903.9	343.15	898.5
100	293.15	929.8	303.15	925.2	313.15	919.3	323.15	914.0	333.15	908.1	343.15	903.5
0.1013	353.15	840.7	363.15	833.3	373.15	826.0	383.15	818.5	393.15	810.8		
10	353.15	848.3	363.15	840.8	373.15	834.2	383.15	827.4	393.15	820.0		
20	353.15	854.8	363.15	848.1	373.15	841.3	383.15	834.9	393.15	828.6		
30	353.15	861.7	363.15	854.9	373.15	848.6	383.15	842.4	393.15	836.3		
40	353.15	867.6	363.15	861.1	373.15	855.2	383.15	849.0	393.15	843.0		
50	353.15	873.4	363.15	867.1	373.15	861.3	383.15	855.1	393.15	849.5		
60	353.15	878.6	363.15	872.7	373.15	866.7	383.15	861.6	393.15	855.5		
70	353.15	884.1	363.15	878.0	373.15	872.2	383.15	866.3	393.15	861.1		
80	353.15	888.8	363.15	883.1	373.15	877.5	383.15	871.5	393.15	866.6		
90	353.15	893.4	363.15	887.7	373.15	882.1	383.15	876.7	393.15	871.9		
100	353.15	897.6	363.15	892.5	373.15	886.5	383.15	881.1	393.15	876.7		

[a] Standard uncertainties u are u(T) = 0.1 K, $u(p)$ =0.01 MPa and the combined expanded uncertainties Uc (level of confidence = 0.95) is $Uc(\rho)$ = 0.5 kg·m^{-3}.

C. Supplementary data/results for Chapter 5

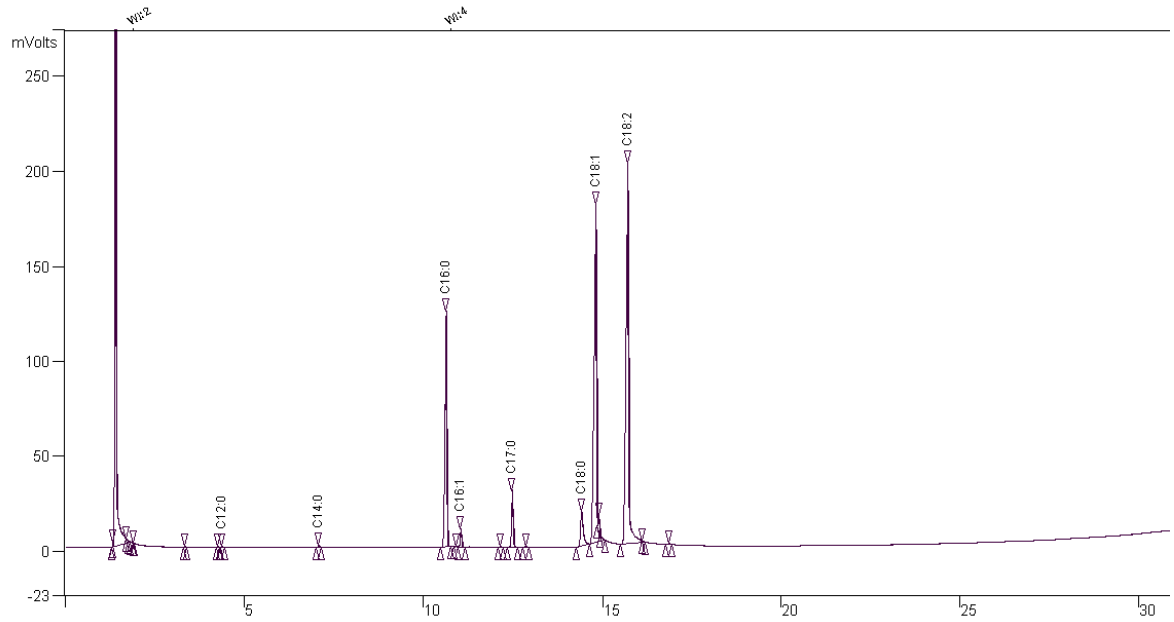

Figure C. 1. Chromatogram of Jc biodiesel

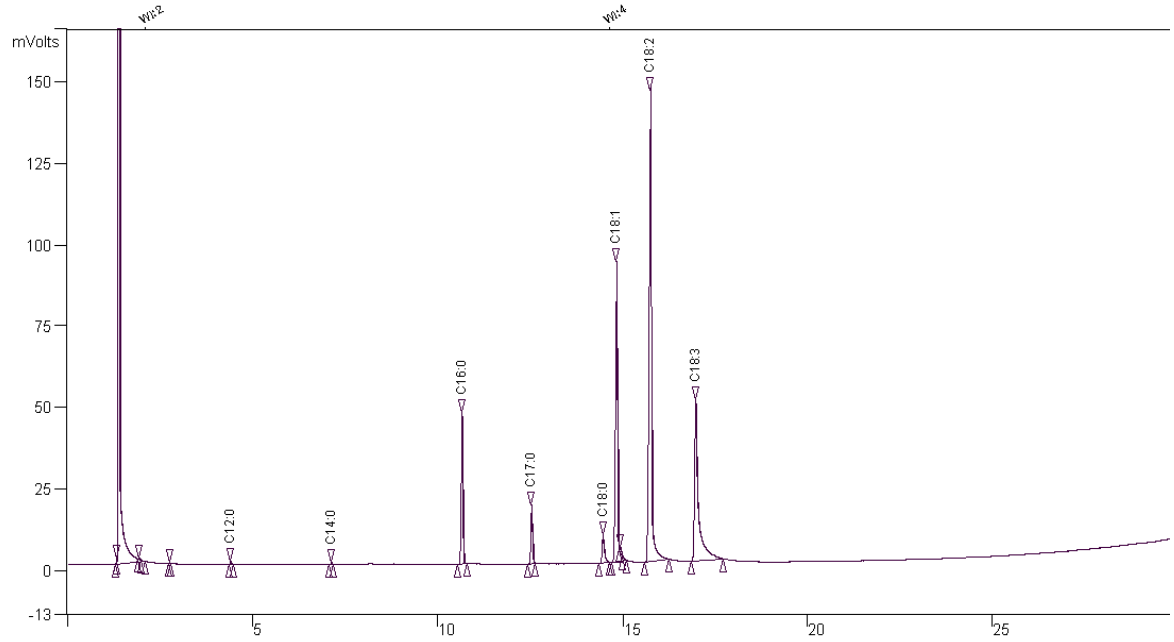

Figure C. 2. Chromatogram of Am biodiesel

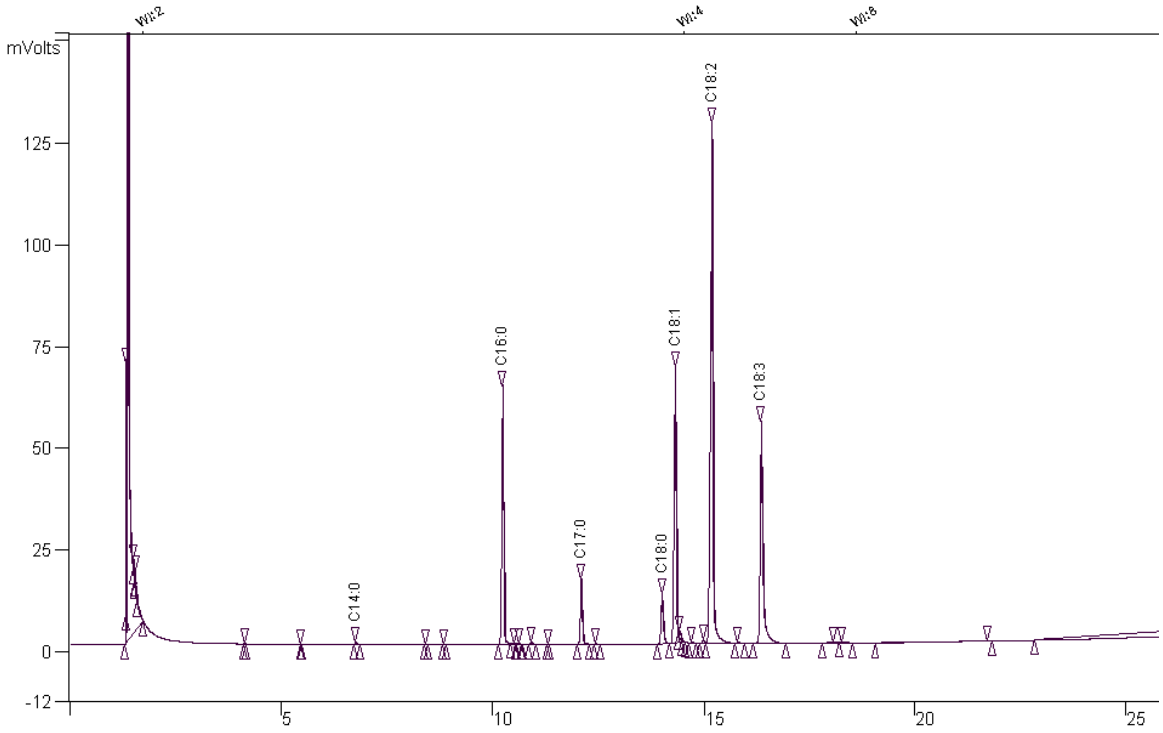

Figure C. 3. Chromatogram of Am+CW biodiesel

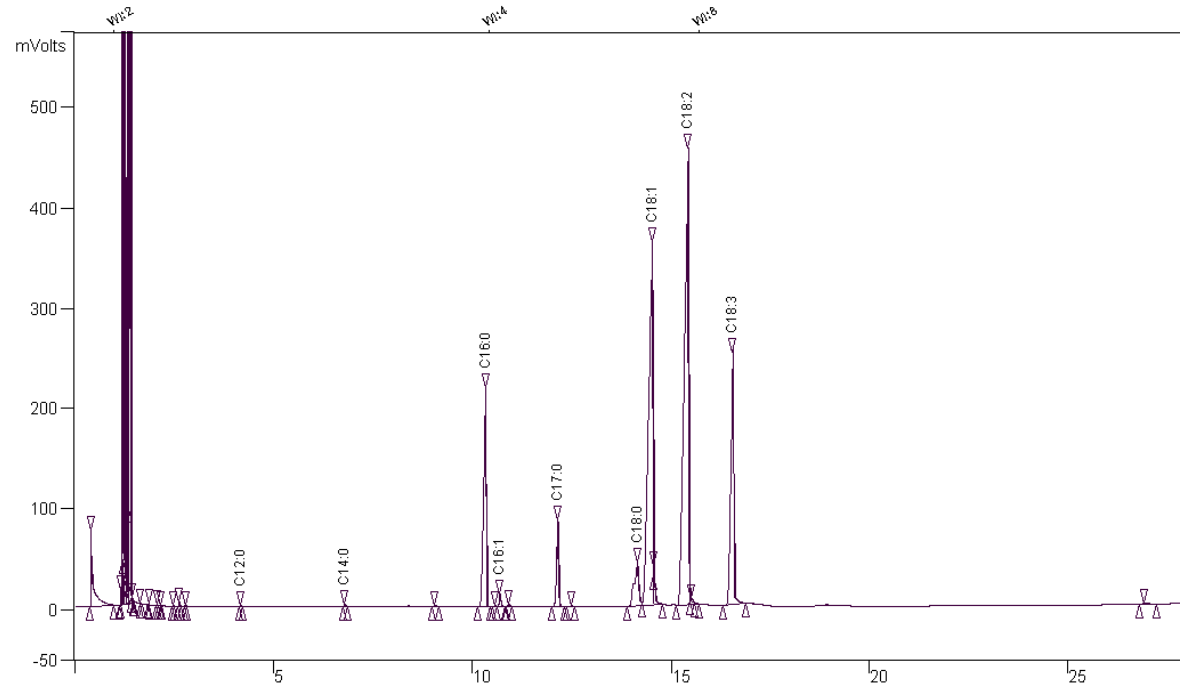

Figure C. 4. Chromatogram of Jc+Am biodiesel